UNIVERSIDADE DE LISBOA

FACULDADE DE MEDICINA DE LISBOA

POST-TRANSCRIPTIONAL REGULATION IN THE DEVELOPING EMBRYO

SARA MARIA FERREIRA FERNANDES

Orientadoras: **Profª Doutora Maria Leonor Tavares Saúde**

Profª Doutora Margarida Henriques da Gama Carvalho

Tese especialmente elaborada para obtenção do grau de Doutor em

Ciências Biomédicas na especialidade de Biologia do Desenvolvimento

2018

UNIVERSIDADE DE LISBOA

FACULDADE DE MEDICINA DE LISBOA

POST-TRANSCRIPTIONAL REGULATION IN THE DEVELOPING EMBRYO

SARA MARIA FERREIRA FERNANDES

Orientadoras: **Profª Doutora Maria Leonor Tavares Saúde**
Profª Doutora Margarida Henriques da Gama Carvalho

Tese especialmente elaborada para obtenção do grau de Doutor em
Ciências Biomédicas na especialidade de Biologia do Desenvolvimento

Júri:

Presidente:

Doutor João Eurico Cortez Cabral da Fonseca, Professor Catedrático e Vice-Presidente do Conselho Científico da Faculdade de Medicina da Universidade de Lisboa

Vogais:

- Doutora Maria Alexandra Marques Moreira Mourão do Carmo, Investigadora Principal do Instituto de Ciências Biomédicas Abel Salazar da Universidade do Porto;
- Doutora Raquel Gláucia Varzielas Pego de Andrade, Professora Auxiliar do Departamento de Ciências Biomédicas e Medicina da Universidade do Algarve;
- Doutora Luísa Maria Ferreira Romão Loison, Investigadora Principal com Habilitação do Instituto Nacional de Saúde Doutor Ricardo Jorge;
- Doutora Solveig Thorsteinsdottir, Professora Associada com Agregação da Faculdade de Ciências da Universidade de Lisboa;
- Domingos Manuel Pinto Henrique, Investigador Auxiliar da Faculdade de Medicina da Universidade de Lisboa;
- Doutora Maria Leonor Tavares Saúde, Professora Auxiliar Convidada da Faculdade de Medicina da Universidade de Lisboa (*Orientadora*).

Fundação para a Ciência e a Tecnologia: SFRH/BD/86371/2012

2018

A impressão desta tese foi aprovada pelo Conselho Científico da Faculdade de Medicina de Lisboa em reunião de 18 de Setembro de 2018.

ABSTRACT

Embryonic development is critically reliant on well-defined spatial and temporal patterns of gene expression. These patterns are often achieved through the regulation of gene expression at the mRNA level. This form of regulation is commonly referred to as post-transcriptional regulation and is frequently mediated by RNA binding proteins (RBPs) and regulatory sequences located in the untranslated regions (UTRs) of the mRNAs.

The mechanisms that underlie these post-transcriptional regulation phenomena have been the focus of an increasing level of attention in recent years. However, their specific roles in embryogenesis, and their relative importance to the different processes that take place in the developing embryo, still require further investigation.

In this thesis we focused our attention on post-transcriptional regulation mechanisms that operate in the developing zebrafish embryo, and investigated their importance to embryogenesis from two perspectives: the perspective of a post-transcriptional regulator – the Quaking A RBP – and the perspective of a set of regulatory sequences – the *fgf8a* alternative 3'UTRs.

Quaking A belongs to the STAR family of RBPs, which has been implicated in several late developmental processes. Using a loss-of-function approach, we uncovered evidence for two previously undescribed functions for Quaking A, namely, in posterior body shaping and in the establishment of internal organ laterality. Furthermore, in our search for potential mRNA targets of Quaking A we came across the cell adhesion molecule Cadherin 11, which also appears to contribute to the establishment of internal organ laterality.

Our investigation of the *fgf8a* alternative 3'UTRs, revealed that the most abundant 3'UTR for this gene mediates a strong translational repression, when compared to a more sparsely used alternative 3'UTR, which supports a higher translation efficiency. By inducing a shift in the selection efficiency of the associated polyadenylation sites, we observed a temporally and spatially specific impact of *fgf8a* 3'UTR usage on embryogenesis, in particular at late stages during sensory

system development. In addition, we identified a previously undescribed role for Fgf signalling in the initial stages of superficial retinal vascularization.

In conclusion, our investigation of Quaking A revealed two previously undescribed roles for this RBP in embryogenesis, thus adding to the current view of STAR proteins, as major regulators of a considerable diversity of developmental processes. In addition, our study of the *fgf8a* alternative 3'UTRs revealed that within the wide range of developmental processes that involve the *fgf8a* gene, only a specific subset appears to rely critically on the regulation of the relative abundances of these 3'UTRs. Overall, these findings highlight the importance of addressing post-transcriptional regulation mechanisms to fully understand gene and pathway functions in embryonic development.

KEYWORDS

Embryonic development; post-transcriptional regulation; alternative polyadenylation; Quaking; Fgf8

RESUMO

O desenvolvimento embrionário depende de uma fina regulação espacial e temporal da expressão génica. Existem vários mecanismos de regulação da expressão génica, entre os quais se encontram os mecanismos de regulação pós-transcricional. A regulação pós-transcricional ocorre ao nível do RNA mensageiro e define fatores como a estabilidade do RNA e a eficiência de tradução. Os mecanismos de regulação pós-transcricional frequentemente envolvem a interação entre moléculas reguladoras e sequências regulatórias da molécula de RNA mensageiro. Estas moléculas reguladoras incluem proteínas de ligação do RNA (RPBs) e as sequências de RNA envolvidas nesta forma de regulação estão frequentemente incluídas nas regiões não traduzidas do RNA mensageiro (UTRs).

A importância da regulação pós-transcricional para o desenvolvimento embrionário é especialmente notória durante as fases iniciais da embriogénese. Durante este período a transcrição zigótica não se encontra ativa, sendo que o desenvolvimento prossegue principalmente devido à presença de RNAs mensageiros maternos e proteínas maternas. Consequentemente, a regulação da estabilidade, eficiência de tradução e localização destes RNAs mensageiros tem uma importância vital, sendo que já foram identificadas várias RBPs com funções documentadas nestes mecanismos de regulação. No entanto, o conhecimento atual acerca da importância da regulação mediada por RBPs para processos mais tardios do desenvolvimento, é substancialmente mais limitado.

Adicionalmente, um dos mecanismos envolvidos na regulação pós-transcricional é a produção de UTRs alternativas na região 3’ da molécula de RNA mensageiro (3’UTRs alternativas). Este mecanismo denomina-se poliadenilação alternativa e é excecionalmente prevalente durante o desenvolvimento embrionário, ocorrendo em aproximadamente 50% dos genes codificantes de modelos vertebrados e invertebrados. No entanto, a importância específica destas 3’UTRs alternativas para o desenvolvimento do embrião carece de elucidação.

Em suma, embora a relevância dos mecanismos de regulação pós-transcricional para o desenvolvimento embrionário e a sua prevalência no embrião se estejam a tornar cada vez mais evidentes, as funções específicas destes mecanismos e a sua

importância relativa para os diferentes aspetos da embriogénese permanecem, em grande parte, por esclarecer.

Este estudo foca-se em dois mecanismos de regulação pós-transcricional, e no impacto que estes têm no desenvolvimento embrionário. Nomeadamente, analisámos a regulação pós-transcricional no embrião sob a perspetiva de um regulador – a RBP *Quaking A* – e sob a perspetiva de um conjunto de regiões do RNA mensageiro com funções regulatórias – as 3'UTRs alternativas do gene *fgf8a* (*fibroblast growth factor 8a*).

A primeira secção deste trabalho foca-se na RBP *Quaking A* (Capítulo II). *Quaking A* pertence a uma das poucas famílias de RBPs que apresentam várias funções descritas nas fases mais tardias do desenvolvimento embrionário – a família STAR (*Signal Transduction and Activation of RNA*). No entanto, o papel destas proteínas em processos como o desenvolvimento do coração e a formação dos sómitos requerem esclarecimento adicional.

Utilizando o peixe zebra como modelo animal do desenvolvimento embrionário em vertebrados, procedemos ao estudo das funções do gene *Quaking A* através de uma abordagem de perda de função (*morfolino antisense*). Esta abordagem revelou uma potencial função para *Quaking A* na morfogénese da região caudal do embrião. Adicionalmente, observámos que tanto a depleção de *Quaking A* como a sobre-expressão de *Quanking A* potenciam defeitos no posicionamento lateral dos órgãos internos do embrião. Especificamente, o coração, o fígado e o pâncreas. Neste contexto, *Quaking A* aparenta contribuir para o estabelecimento da lateralidade dos órgãos internos ao nível da transmissão do sinal que define a lateralidade, entre tecidos, nomeadamente entre a vesícula de *Kupffer* e a mesoderme lateral esquerda.

Uma vez que *Quaking A* pertence a uma família de RBPs (STAR) com várias funções documentadas na regulação pós-transcricional da expressão génica, procedemos então à procura de potenciais alvos de *Quaking A* cuja regulação pudesse estar subjacente às funções deste gene no desenvolvimento. Neste contexto identificámos a molécula de adesão Caderina 11. Embora sejam necessários estudos adicionais para esclarecer uma potencial função de *Quaking A* na regulação pós-transcricional da Caderina 11, os nossos resultados revelaram

que a Caderina 11 também aparenta exercer uma função no posicionamento lateral dos órgãos internos.

A identificação de uma função para *Quaking A* no processo de estabelecimento das assimetrias esquerda-direita no embrião constitui a primeira indicação de que um membro da família STAR contribui para este processo. Adicionalmente, o potencial envolvimento da Caderina 11 no estabelecimento destas assimetrias tem particular interesse uma vez que, até à data, muito poucas moléculas de adesão foram implicadas neste processo.

A segunda secção deste trabalho foca-se na poliadenilação alternativa do gene *fgf8a* (Capítulo III). O gene *fgf8a* codifica um fator de crescimento que pertence à via de sinalização Fgf. Esta via é globalmente reconhecida como uma das principais vias de sinalização implicadas na embriogénese, sendo que o gene *fgf8a* e seus ortólogos têm múltiplas funções documentadas ao longo de toda a extensão temporal do desenvolvimento do embrião. No peixe zebra o gene *fgf8a* apresenta sete 3'UTRs alternativas, no entanto os mecanismos de regulação pós-transcricional mediados por estas UTRs e a sua importância relativa para o desenvolvimento não tinham sido previamente elucidados.

O nosso estudo das 3'UTRs do gene *fgf8a* revelou que a 3'UTR mais abundante no embrião de peixe zebra (*fgf8aM*) está associada a uma forte repressão da tradução do transcrito, quando comparada à segunda mais abundante (*fgf8aS*). Esta observação é particularmente importante tendo em vista que a 3'UTR *fgf8aM* apresenta uma abundância relativa aproximadamente quatro a cinco vezes superior à da 3'UTR *fgf8aS*.

Uma vez que estas 3'UTRs são produzidas através de um processo de poliadenilação alternativa, procedemos então à utilização de um *morfolino antisense* para interferir com este processo. Neste contexto, observámos uma alteração nas abundâncias relativas das 3'UTRs *fgf8aS* e *fgf8aM*, com favorecimento da produção da 3'UTR *fgf8aS* e uma concomitante sobreativação da via de sinalização Fgf.

Sob um ponto de vista fenotípico, a perturbação deste mecanismo de regulação teve um impacto seletivo no desenvolvimento embrionário. Especificamente, observámos perturbações na especificação e maturação de neuroblastos do

gânglio estatoacústico, na formação da comissura anterior e na fase inicial da formação da vasculatura superficial da retina. No entanto, processos do desenvolvimento mais precoces e mais caudais, nos quais o gene *fgf8a* tem funções documentadas, não foram afetados. Nomeadamente, a gastrulação, a especificação dos progenitores da mesoderme caudal, a formação dos sómitos e o desenvolvimento do organizador ístmico permaneceram inalterados. Estes resultados indicam que, neste contexto, a poliadenilação alternativa contribui maioritariamente para a regulação fina dos níveis de expressão do gene *fgf8a* em resposta às necessidades celulares.

Adicionalmente, a nossa abordagem de interferência com a poliadenilação alternativa do gene *fgf8a* permitiu gerar uma sobreativação da via Fgf sem indução simultânea da expressão ectópica do gene. Tal, por sua vez, permitiu a identificação de uma função previamente desconhecida para a via de sinalização Fgf, nomeadamente na fase inicial da formação da vasculatura superficial da retina.

Em conclusão, os resultados obtidos no estudo do gene *Quaking A* não só contribuem para uma melhor compreensão dos papéis da família STAR no desenvolvimento cardíaco, mas também reforçam a perceção atual destas proteínas como reguladores importantes de uma larga gama de processos do desenvolvimento embrionário. Adicionalmente, os resultados obtidos no estudo das 3'UTRs do gene *fgf8a* revelaram que, de entre a larga gama de funções que este gene desempenha no desenvolvimento, apenas algumas são criticamente dependentes da regulação da poliadenilação alternativa do gene.

Globalmente, os resultados obtidos neste estudo enfatizam a importância da investigação dos mecanismos de regulação pós-transcricional que contribuem para o desenvolvimento embrionário e das suas implicações específicas para os diferentes processos da embriogénese.

PALAVRAS-CHAVE

Desenvolvimento embrionário; Regulação pós-transcricional; Poliadenilação alternativa; Quaking; Fgf8

AGRADECIMENTOS

Gostaria de agradecer às minhas orientadoras Leonor Saúde e Margarida Gama Carvalho, por me terem apresentado esta temática híbrida e desafiante, por me terem dado a oportunidade de explorar as ramificações que dela surgiram, e pelo acompanhamento e orientação que ofereceram ao longo desta extensa, e por vezes tumultuosa, jornada.

Gostaria também de agradecer a todos os atuais membros e ex-membros de ambos os laboratórios, com os quais tive o prazer de trabalhar.

Deixo um agradecimento particular à Rita Fior, que não só contribuiu para a génese e evolução deste trabalho, mas também teve um papel importante na minha formação científica. Agradeço ao Francisco Pinto pelas suas contribuições para este trabalho e à Ana Margarida pelo apoio, boa disposição e disponibilidade para lidar com as urgências. Agradeço também ao João Pereira, Raquel Mendes, Susana Pascoal, Sara Matos, Isabel Peixeiro, Ana Ribeiro e Isaura Martins.

Gostaria também de agradecer à Dalila Silva e ao José Leitão pelas suas contribuições para este trabalho, com uma atenção especial à minha primeira pupila "oficial" Dalila por ter sido uma estudante empenhada, atenciosa e simplesmente fantástica. Agradeço também aos estudantes "não-oficiais" Margarida Figueira e José Santos.

Á minha parceira de PhD Rita Pinto agradeço o valiosíssimo feedback, a empatia e o apoio nos momentos de desespero, o bom humor e o companheirismo nos momentos de distração. Não tenho dúvidas que todo este processo teria sido para mim, muito menos tolerável, se não estivéssemos ambas a fazê-lo em paralelo. O mesmo se aplica à minha parceira de PhD do piso de cima, Filipa Marques, à qual agradeço o otimismo crónico, as extensas discussões científicas (e não só), a boa disposição, os momentos de distração e a ocasional reposição do stock de nicotina.

Um agradecimento muito especial às meninas da Fish Facility – Lara Carvalho e Aida Barros – às quais reconheço e agradeço (entre muitas outras coisas) a paciência infindável, a perpétua disponibilidade para ajudar, o serviço de apoio psicológico grátis (com bónus ocasional de embryo-staging) e o inabalável sentido de humor.

Agradeço ao António Temudo, Ana Margarida Nascimento e José Rino da unidade de Bioimagem do iMM todo o apoio técnico dado no contexto da microscopia. À Unidade de Histologia do iMM e à Ana Farinho da Histology Facility do CEDOC agradeço o apoio dado na realização de cortes histológicos.

Agradeço também à Evguenia Bekman, Pedro Prudêncio, Noélia Custódio, Lara Carvalho e Filipa Dias pelas suas contribuições para o processo de revisão do manuscrito. Em particular, gostaria de agradecer o tempo e esforço investidos por Evguenia Bekman e Pedro Prudêncio na realização de RNase Protection Assays no contexto desta revisão, apesar de estes infelizmente não terem sido incluídos nesta dissertação. Agradeço também novamente à Lara Carvalho, Rita Pinto e Dalila Silva, pelo tempo e esforço dedicados às tentativas de otimização das experiências com lipophilic tracers, anticorpos e sondas que infelizmente não foram incluídas nesta dissertação.

Gostaria de agradecer ao meu comité de tese, Domingos Henrique, Isabel Palmeirim e Sérgio de Almeida pela disponibilidade, pelos comentários e consequentemente pelo impacto positivo que tiveram no rumo deste projeto.

À Verónica, à Ana Luísa e à Loira agradeço o facto de ao longo destes anos terem estado sempre presentes quando é preciso. Agradeço todo o apoio, a paciência, as conversas, os momentos de distração e as alegrias. Obrigada às três, e novamente à Lara e à Aida, por me terem ajudado a manter não só a sanidade, mas também a perseverança.

Aos meus pais e aos meus avós, por terem criado as condições que me permitiram seguir este rumo, por acreditarem em mim, por me apoiarem em tudo e por serem uma perpetua fonte de inspiração e afeto, agradeço.

TABLE OF CONTENTS

LIST OF FIGURES

LIST OF TABLES

LIST OF ABBREVIATIONS

A

ace – *acerebellar*
alt3'UTR – Alternative 3' untranslated region
APA – Alternative polyadenylation
ASE – Asymmetric enhancer
aus – *aussicht*

B

BMP – Bone morphogenetic protein

C

Cdh11 – Cadherin 11
cdh11MO – splice blocking morpholino
CDS – Coding sequence
CDS – Coding Sequence
Cpsf6 – Cleavage and Polyadenylation Specificity Factor subunit 6
CRISPR – Clustered regularly interspaced short palindromic repeats
Ctr^{MO} – Standard control morpholino oligo

D

D Loop – Dextral loop

E

eGFP – enhanced Green fluorescent protein
ENU – N-ethyl-N-nitrosourea

F

$fa3ui^{MO}$ - *fgf8a* alt3'UTR interference morpholino oligo
FACS – Fluorescence activated cell sorting
FGF – Fibroblast growth factor
FGFR – FGF receptor

G

GLD-1 – Defective in Germ Line Development
GSG – GRP33, SAM68 and GLD-1

H

Her – hairy and enhancer of split-related
Hes – hairy and enhancer of split
HH – Hedgehog
HOW - Held Out Wing
hpf – Hours post fertilization
hpi – Hours post injection
HS-GAG – heparan sulphate glycosaminoglycan chains

K

KV – Kupffer's Vesicle

L

L Loop – Left loop
LPM – Lateral plate mesoderm
LROs – Left-Right organizers
LSE – Left-side enhancer

M

Mbp – Myelin basic protein
MHB – Midbrain-hindbrain boundary
miR – microRNA
MM – Minimal motif
mRNA – messenger ribonucleic acid
MZT – Maternal to zygotic transition

P

p53^{MO} – *p53* translation blocking morpholino oligo
PAS – Polyadenylation signal
PCR – Polymerase chain reaction
PSM – Presomitic mesoderm

Q

QKI – Quaking I
qkia – Quaking A
qkia$^{ATG\text{-}MO}$ – *qkia* translation blocking morpholino oligo
QRE – Quaking response element

R

RA – Retinoic acid
RBP – RNA binding protein
Rock – Rho kinase
RT-qPCR – Real time quantitative PCR

S

SAG – Statoacoustic ganglion
SAV – Superficial annular vessel.
SF-1 – Splicing Factor 1
SHH – Sonic Hedgehog
Spaw – Southpaw
ss – Somite stage
STAR – Signal Transduction and Activation of RNA

T

TALEN – Transcription activator-like effector nucleases
TGF-β – Transforming growth factor beta

U

UTR – Untranslated region

V

VEGF – Vascular endothelial growth factor

W

WISH – Whole-mount *in situ* hybridization
Wnt – *Wingless*

X

Xqua – Xenopus Quaking

LIST OF PUBLICATIONS

Fernandes, S.F., Fior, R., Pinto, F., Gama-Carvalho, M. and Saúde, L. (2018) 'Fine-tuning of *fgf8a* expression through alternative polyadenylation has a selective impact on Fgf-associated developmental processes', BBA Gene Regulatory Mechanisms, 1861(9), pp. 783-793.

CHAPTER I

Introduction

I.1 EMBRYONIC DEVELOPMENT

Throughout the animal kingdom, there is a remarkable variety in the morphogenetic processes that take place during embryonic development. However, for most species, the patterns of early embryogenesis tend to follow a common sequential thread.

After fertilization, embryonic development begins with the cleavage phase. During this phase, a series of rapid cell divisions takes place giving rise to a substantial increase in cell number. By the end of the cleavage phase these cells, termed blastomeres, are generally arranged in a sphere known as the blastula (Fig. I.1a) (Gilbert, 2003).

The initial stages of animal development occur in the absence of *de novo* transcription. During this period, the progression of embryogenesis relies entirely on maternally inherited mRNAs and proteins. As early development progresses, maternal mRNAs and proteins are gradually degraded, and zygotic transcription is activated, thus progressively diminishing the maternal influence over embryogenesis. This gradual shift from maternal to zygotic control is known as the Maternal to Zygotic Transition (MZT). The MZT spans the period from the onset of maternal mRNA degradation to the first major developmental requirement for zygotic transcripts. For instance, in the zebrafish the MZT begins at fertilization, spanning the entire cleavage and blastula phases and coming to an end during the gastrula phase (Fig. I.1a,b) (Langley et al., 2014, Tadros and Lipshitz, 2009).

The gastrula phase begins after the rate of cell divisions has diminished, and is characterized by extensive cell rearrangements. These highly coordinated cell movements are termed gastrulation. Gastrulation is accompanied by a series of specification and patterning events which enable the establishment of a multi-layered body plan containing three germ layers: the outer ectoderm, the inner endoderm, and the interstitial mesoderm (Fig. I.1c) (Gilbert, 2003, Solnica-Krezel, 2005).

Although the patterns of cell rearrangement during the gastrula phase vary throughout the animal kingdom, there are four evolutionarily conserved gastrulation movements: internalization, epiboly, convergence and extension. Internalization

movements carry prospective mesoderm and endoderm cells inward, beneath the prospective ectoderm. Epiboly movements lead to an expansion and thinning of the germ layers. Convergence and extension movements narrow the germ layers medio-laterally and elongate the embryo from head to tail (Fig. I.1c) (Solnica-Krezel, 2005).

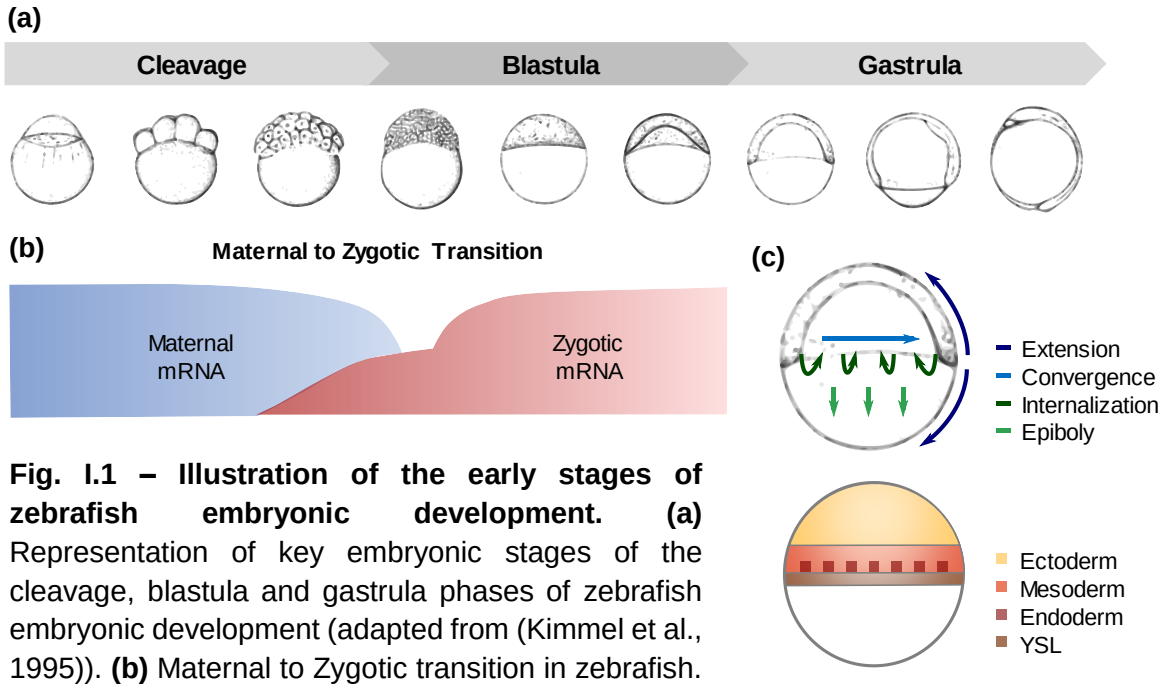

Fig. I.1 – Illustration of the early stages of zebrafish embryonic development. (a) Representation of key embryonic stages of the cleavage, blastula and gastrula phases of zebrafish embryonic development (adapted from (Kimmel et al., 1995)). **(b)** Maternal to Zygotic transition in zebrafish. The blue curve represents the degradation profiles of destabilized maternal transcripts. The red curve illustrates the minor and major waves of zygotic genome activation (adapted from (Tadros and Lipshitz, 2009)). **(c)** Representation of the gastrulation movements and process of germ layer specification in the zebrafish embryo. YSL, yolk syncytial layer (adapted from (Solnica-Krezel, 2006, Kimelman, 2006)).

In vertebrate embryos the final stages of gastrulation are either accompanied with, or followed by, the onset of neurulation – the formation of the neural tube – and segmentation – the formation of the somites. The neural tube is formed from ectodermal precursors situated above a rod-shaped mesodermal structure termed notochord, which demarcates the anterior-posterior embryonic body axis. The somites are spherical mesodermal structures which form on both sides of the notochord, and contain the precursors of the vertebrae, skeletal muscles, and dermis (Wolpert, 2002) (Fig. I.2a,b).

Embryonic development subsequently progresses to the organogenesis phase, during which, extensive cell rearrangement, differentiation and specialization

processes take place to form the different tissues and organs of the embryo (Fig. I.2a). During this phase, the ectoderm will give rise to the epidermis, nervous system and pigmented cells. The endoderm will contribute to the gastrointestinal, urinary and respiratory systems, as well as several endocrine glands. The mesoderm will give rise to the heart, kidneys, gonads, axial skeleton, cartilage, connective tissue, trunk muscles and blood cells. In addition, the formation of various organs will involve interactions between the different germ layers (Gilbert, 2003, Kiecker et al., 2016).

The next subchapter will focus on two critical developmental processes: the elongation and segmentation of the anterior-posterior axis; and the establishment of internal organ asymmetry along the left-right axis. In addition, it will address the specific contributions of the fibroblast growth factor (FGF) signalling pathway to different aspects of embryonic development.

I.1.1 Posterior body elongation and Somitogenesis

The first morphogenetic events that define the shape of the embryonic body are thought to take place during the gastrula phase, as a result of convergence and extension movements. However, this process carries on after gastrulation, with posterior body elongation and segmentation presenting as two major aspects of vertebrate development (McMillen and Holley, 2015, Bénazéraf and Pourquié, 2013).

I.1.1.1 Posterior body elongation

The development and elongation of the posterior body is achieved through the progressive deposition of cells from a posterior growth zone in the embryo. This posterior leading edge of the growing embryo, named tailbud, contains the progenitors of the musculature, axial skeleton, vasculature, spinal cord and blood (McMillen and Holley, 2015, Beck, 2015).

Interestingly, studies done in chick and zebrafish embryos have found that posterior body elongation is primarily driven by cell migration rather than cell proliferation, with tailbud musculoskeletal progenitors exhibiting only a modest level of proliferation during posterior body elongation (Bouldin et al., 2014, Kanki and Ho, 1997, Bénazéraf et al., 2010, McMillen and Holley, 2015). In these organisms, instantaneous cell velocities are greater in the posterior tailbud, with posterior growth occurring as these highly motile progenitors lessen their motility and assimilate into more anterior tissues, namely the paraxial mesoderm (Lawton et al., 2013, Dray et al., 2013, Mara et al., 2007, Bénazéraf et al., 2010, Delfini et al., 2005).

For instance, during zebrafish posterior body elongation, the progenitor cells of the dorsal medial tailbud dive ventrally as a coherent posterior flow. At the posterior ventral tailbud there is a loss in cell flow coherence which leads to an increase in cell mixing (Lawton et al., 2013, Dray et al., 2013). These mesodermal progenitors subsequently lose velocity as they enter the posterior paraxial mesoderm, concomitantly with the assembly of an extracellular matrix composed primarily of Fibronectin and Laminin (Dray et al., 2013, Latimer and Jessen, 2010, McMillen and Holley, 2015).

The entry of these tailbud cells into the paraxial mesoderm territory appears to include a process of convergence and extension, akin to what is observed during gastrulation, with this process being regarded as an important contributing factor to posterior body elongation (Steventon et al., 2016, Kanki and Ho, 1997).

Furthermore, paraxial mesoderm assembly is accompanied by the formation of the notochord from axial mesoderm precursors. The vacuolation and rearrangement of the notochord cells has also been proposed as a contributing factor to the progression of posterior body elongation (McMillen and Holley, 2015, Kanki and Ho, 1997, Dray et al., 2013).

I.1.1.2 Somitogenesis

As posterior body elongation progresses, the paraxial mesoderm, also known as presomitic mesoderm (PSM), is subdivided into metameric structures, termed somites. In vertebrates, somites form sequentially along the anterior-posterior

embryonic axis, budding off in bilateral pairs from the unsegmented PSM. Each somite presents as a spherical cell mass surrounded by an epithelial sheet, and contains the precursors of the vertebrae, skeletal muscles, and dermis (Fig. I.2a,b) (Yabe and Takada, 2016).

The process of somite formation – somitogenesis – is tightly regulated, both spatially and temporally, with the frequency of somite formation and the total number of somites formed being species-specific traits. For instance, in zebrafish a new pair of somites is formed every 25 minutes until a total of approximately 33 somite pairs is reached, whereas in mice a new somite pair is formed every 2 hours resulting in the formation of approximately 65 somite pairs (Yabe and Takada, 2016, Hubaud and Pourquié, 2014).

To account for this spatiotemporal regulation of somitogenesis, a theoretical model termed “Clock and Wavefront model” was proposed. In this model, rhythmic and sequential somite formation is achieved by two regulatory mechanisms: a segmentation clock and a wavefront of differentiation. The cyclic activation of the segmentation clock provides temporal information, which is integrated with the spatial information provided by the continuous regression of the wavefront that results from posterior body elongation. A consequence of this model is that the size of each newly formed somite is fixed by the distance travelled by the wavefront during one period of the segmentation clock (Fig. I.2b) (Cooke and Zeeman, 1976, Yabe and Takada, 2016, Hubaud and Pourquié, 2014).

Since the Clock and Wavefront model was proposed, several genes have been associated with the establishment of the segmentation clock and wavefront mechanisms.

I.1.1.2.1 The segmentation clock

Regarding the segmentation clock, the first gene to be implicated in this mechanism was the chicken *HAIRY1*. In the chick PSM, *HAIRY1* is expressed cyclically in the PSM, with a frequency of expression that is consistent with the frequency of chick somite formation. This gene belongs to the hairy and enhancer of split (*Hes*)/ HES-

related (*her*) family of transcription factors that act mainly as Notch pathway effectors (Palmeirim et al., 1997, Cooke, 1998).

Subsequent studies have implicated multiple members of the Notch, Wingless (Wnt) and FGF pathways in the segmentation clock (Krol et al., 2011, Dequéant et al., 2006, Hubaud and Pourquié, 2014). However, of all the gene families identified to date in connection with the clock, the *Hes/her* family appears to be the most conserved contributor, with *Hes/her* cyclic genes having been identified in mouse, chick, zebrafish, medaka and *Xenopus* (Krol et al., 2011, Dequéant et al., 2006, Elmasri et al., 2004, Li et al., 2003a).

In line with this, the segmentation clock has been proposed to rely heavily on a *Hes/her*-based negative-feedback loop. This loop is thought to drive gene expression oscillations via a mechanism of delayed transcriptional repression (Bessho et al., 2003, Lewis, 2003). For instance, the *her1 and her7* genes are widely regarded as the pacemakers of the zebrafish segmentation clock (Henry et al., 2002, Holley et al., 2002, Oates and Ho, 2002, Gajewski et al., 2003). Her1 and Her7 have been shown to act as transcriptional repressors, inhibiting their own transcription, and that of the Notch ligand DeltaC, in the posterior PSM (Giudicelli et al., 2007). Mathematical modelling has shown that this Her1/Her7 autoinhibition has the potential to generate a delayed negative feedback loop, which could underlie the oscillating expression of these genes. The concomitant cyclical inhibition of DeltaC is thought to coordinate gene expression oscillations between neighbouring cells (Lewis, 2003). It follows from this model that this negative-feedback driven gene expression oscillation frequency would provide the temporal information required to set the pace of the segmentation clock (Fig. I.2b) (Pais-de-Azevedo et al., 2018, Hubaud and Pourquié, 2014).

Interestingly, this model postulates that the production of stable oscillations in gene expression is predicated on several conditions, one of which being the instability of the *her7*, *her1* and *deltaC* mRNAs (Lewis, 2003). This instability was further confirmed by *in situ* hybridisation and fluorescent reporter experiments, which revealed that the mRNAs of these genes have very short half-lives, specifically 6.1-8.1 minutes (Giudicelli et al., 2007, Gajewski et al., 2003). Regarding the mechanisms that mediate this instability, recent studies conducted in zebrafish,

mouse and chick suggest that a Pnrc2-Upf1 complex and the microRNA mir-125a-5p operate as negative regulators of the stability of the cyclic *her1* and *lunatic fringe* mRNAs, respectively (Gallagher et al., 2017, Riley et al., 2013, Wahi et al., 2017).

I.1.1.2.2 The wavefront

The wavefront was originally defined by Cooke and Zeeman as a front of rapid cell change moving slowly in a posterior direction along the axis of the embryo (Cooke and Zeeman, 1976). Subsequent studies have identified the position of this conceptual wavefront (also known as the determination front) as the virtual frontier between the posterior PSM – where the paraxial mesoderm cells have yet to acquire their somitic identity – and the anterior PSM – where cells are already committed to their somitic fate. Furthermore, the clock and wavefront model proposes that the wavefront corresponds to the level at which PSM cells become responsive to a signal from the segmentation clock that potentiates the definition of the future segmental domain, and thus, the size of the formed somites (Fig. I.2b) (Hubaud and Pourquié, 2014, Yabe and Takada, 2016, Cooke and Zeeman, 1976, Dequéant and Pourquié, 2008).

Three major signalling gradients have been implicated in defining the position of the wavefront: a posterior-to-anterior FGF gradient, a posterior-to-anterior Wnt gradient, and an anterior-to-posterior Retinoic Acid (RA) gradient (Fig. I.2b).

Studies done in chick, zebrafish and mouse have shown that both upregulation and downregulation of FGF signalling in the PSM leads to a disruption of somitogenesis, specifically regarding somite boundary positioning (Dubrulle et al., 2001, Sawada et al., 2001, Wahl et al., 2007, Naiche et al., 2011). This wavefront activity appears to be primarily mediated by the *fgf8a* gene in zebrafish embryos, whereas mouse embryos appear to rely on both FGF8 and FGF4 ligands for this process (Akiyama et al., 2014, Naiche et al., 2011).

Interestingly, Dubrulle and Pourquié reported that in the chick and mouse PSM, *Fgf8* transcription is restricted to the growing posterior tip of the embryo. As posterior body elongation progresses, *Fgf8* mRNA is gradually degraded in the newly formed tissues leading to the establishment of the observed posterior-to-anterior *Fgf8*

mRNA gradient. Considering that the process of posterior body elongation is relatively slow, these results indicate that a certain degree of *Fgf8* mRNA stability must be present to enable FGF8 gradient formation, and consequently, wavefront establishment (Dubrulle and Pourquié, 2004).

The role of the Wnt gradient in wavefront establishment was first identified in mouse, where an upregulation of Wnt signalling in the PSM lead to a disruption of paraxial mesoderm maturation and somite boundary positioning (Aulehla et al., 2008, Dunty et al., 2008). Evidence for the conservation of this function comes from studies done in zebrafish, where temporally-controlled modulations of Wnt signalling led to alterations in somite size (Bajard et al., 2014).

In contrast to the FGF and Wnt gradients, which display higher morphogen concentrations at the posterior tip of the embryo, the RA gradient displays higher concentration levels in the somites and anterior PSM (Rossant et al., 1991, Shimozono et al., 2013). In line with this, the RA gradient was proposed to function as an antagonist of the FGF signalling gradient, with FGF8 and RA contributing to wavefront position establishment through a mechanism of mutual inhibition (Diez del Corral et al., 2003, Vermot et al., 2005, Moreno and Kintner, 2004).

In addition, RA has also been implicated in the maintenance of the lateral symmetry of the somites. In this context, it has been proposed that during the period of development when the asymmetric position of internal organs such as the heart, liver and pancreas is being established, RA functions as a buffer in the somites, ensuring that somitogenesis remains refractory to asymmetry-inducing mechanisms (Kawakami et al., 2005, Vermot and Pourquié, 2005, Sirbu and Duester, 2006).

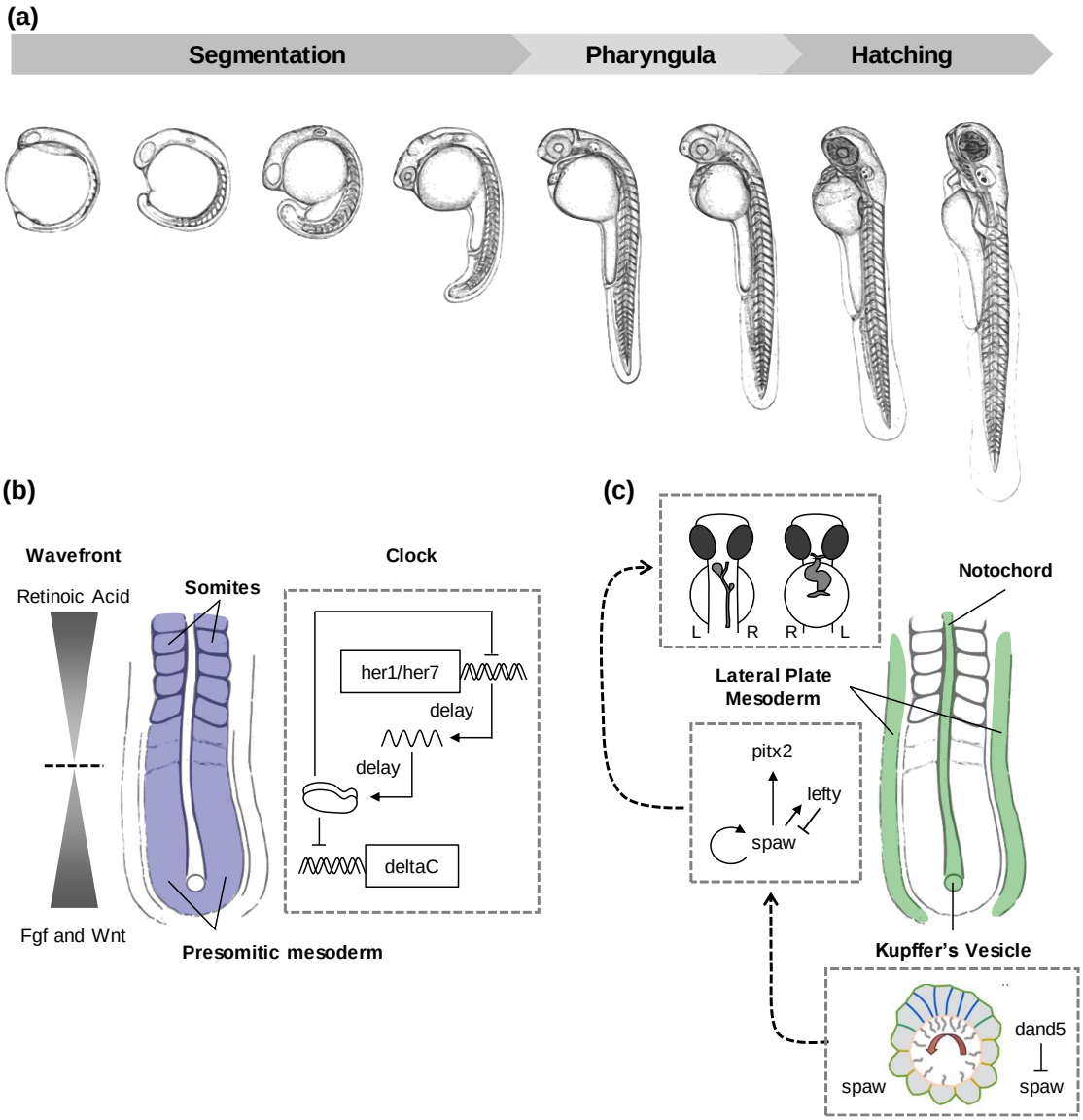

Fig. I.2 – Illustration of the late stages of zebrafish embryonic development.
(a) Representation of key embryonic stages of late zebrafish embryogenesis, specifically, the segmentation, pharyngula and hatching periods (adapted from (Kimmel et al., 1995)). **(b)** The somitogenesis process in zebrafish. Representation of the Clock and Wavefront model, according to which, two mechanisms control the activation of the somitogenesis programme: the Clock (right) and the Wavefront (left). The frequency of the Clock is thought to rely on a delayed negative feedback loop established by the *her1* and *her7* genes. The position of the wavefront is defined by three gradients: A Retinoic Acid gradient, a FGF signalling gradient and a Wnt signalling gradient. According to this model, the frequency of somite formation and the size of the formed somites are determined by the interplay between these two mechanisms (partially adapted from (Giudicelli et al., 2007)). **(c)** Internal organ laterality establishment in zebrafish. The process of Left-Right patterning is initiated by motile cilia present in the KV, which rotate in a counter-clockwise manner creating a leftward extracellular fluid flow. This flow induces the establishment of the first asymmetric cues which, in zebrafish, include the right-side specific expression of the *spaw* inhibitor *dand5*. Asymmetric gene expression in the KV functions as a laterality signal which is transmitted to the LPM and triggers asymmetric gene expression in the left LPM, namely the *nodal-lefty-pitx2* cascade. This in turn determines the correct lateral positioning of the visceral and cardiac organs (partially adapted from (Wang et al., 2012)).

I.1.2 Left-Right organ asymmetry

Embryonic morphogenesis takes place along three orthogonal axes: The Anterior-Posterior axis, the Dorsal-Ventral axis and the Left-Right axis. When it comes to the Left-Right axis, most vertebrates have a largely symmetrical body-plan, with this symmetry being broken by the asymmetric placement of several internal organs, such as the heart, gut, liver, spleen and stomach. Furthermore, paired organs such as the lungs and brain tend to develop asymmetrically, presenting morphological and/or functional differences between the left and right sides (Grimes and Burdine, 2017).

I.1.2.1 The Left-Right organizer

In vertebrates, the establishment of Left-Right asymmetry is widely believed to begin in transient midline structures, which appear at the posterior end of the notochord during early somitogenesis stages and are known as Left-Right organizers (LROs) (Fig. I.2c) (Grimes and Burdine, 2017, Amack, 2014).

In mouse the LRO is termed Node, in zebrafish and medaka the LRO is known as the Kupffer's Vesicle (KV), the *Xenopus* LRO is the Gastrocoel Roof Plate and the rabbit LRO is the posterior notochord. Studies conducted in these organisms have shown that a largely conserved feature of the LRO is the presence of motile cilia which display a posterior tilt and rotate in a clockwise manner, when observed ventrally (Okada et al., 2005, Nonaka et al., 2005, Kramer-Zucker et al., 2005, Okabe et al., 2008, Schweickert et al., 2007). These motility features allow the cilia to generate an extracellular unidirectional leftward fluid flow within the organizer, with this flow being perceived as a crucial aspect of Left-Right asymmetry establishment (Fig. I.2c) (Cartwright et al., 2004, Okada et al., 2005, Kramer-Zucker et al., 2005, Essner et al., 2005, Hojo et al., 2007, Schweickert et al., 2007, Blum et al., 2009).

There are many factors known to influence the LRO fluid flow, one of which is the cellular architecture and morphology of the LRO. Features such as the size and shape of the LRO, as well as the number of ciliated cells and their spatial

organization within the organizer, vary significantly between vertebrate species (Amack, 2014, Blum et al., 2009, Lee and Anderson, 2008, Shook et al., 2004, Wang et al., 2011). However, studies in mouse and zebrafish have shown that the disruption of these specie-specific LRO architectures has a detrimental effect on Left-Right asymmetry establishment (Beckers et al., 2007, Lee et al., 2010, Pulina et al., 2011, Sutherland et al., 2013, Arrington et al., 2013, Oteiza et al., 2010, Wang et al., 2011, Wang et al., 2012, Ablooglu et al., 2010, Matsui et al., 2011).

For instance, the zebrafish Kupffer's Vesicle is a spherical structure, with a higher concentration of ciliated epithelial cells in the anterior side of the dorsal surface of its lumen (Fig. I.2c) (Kreiling et al., 2007). This dorsal anterior cluster of motile cilia is formed through a process called KV remodelling, whereby the most anterior cells become elongated with tight apical surfaces, and the most posterior cells adopt a cuboid shape with larger apical surfaces (Wang et al., 2012). This process appears to be regulated by the Rho kinase (Rock) 2b-Myosin pathway, with disruptions of this pathway leading to alterations in KV morphology, fluid flow, and ultimately internal organ laterality (Wang et al., 2011, Wang et al., 2012). In mouse the RHO family member RAC1 has also been implicated in LRO morphogenesis, and in *Xenopus*, *rock2* knockdown has been linked to Left-Right patterning defects, thus raising the possibility of a conserved role for this pathway in LRO architecture establishment (Migeotte et al., 2011, Fakhro et al., 2011).

Additional proteins with an apparent involvement in mouse LRO architecture establishment, and consequently Left-Right organ asymmetry, include the transcription factors NOTO and ZIC3, the cytoskeletal-associated protein EPB4.1l5, the extracellular matrix component Fibronectin and its receptor Integrin α5β1 (Beckers et al., 2007, Lee et al., 2010, Pulina et al., 2011, Sutherland et al., 2013). The latter has also been implicated in Left-Right organ asymmetry establishment in the zebrafish (Pulina et al., 2011). Furthermore, several genes and signalling pathways have been implicated in different aspects of zebrafish KV morphogenesis, and consequently internal organ laterality establishment. These include Wnt11- and Prickle1a-mediated planar cell polarity signalling, the Integrin subunits αV and β1b, the adhesion molecule Cadherin1, and the transmembrane heparan sulfate proteoglycan Syndecan 2 (Sdc2), with the last two exerting their functions through

interactions with the FGF signalling pathway (Arrington et al., 2013, Oteiza et al., 2010, Ablooglu et al., 2010, Matsui et al., 2011).

I.1.2.2 Asymmetric gene expression in the LRO

In most vertebrate species, the leftward fluid flow generated in the LRO precedes and is widely believed to induce asymmetric gene expression (Fig. I.2c). Despite the extensive work that has been conducted in the field, and the many conserved aspects of Left-Right asymmetry establishment, the mechanisms that effectively detect and translate the LRO fluid flow into an asymmetric signalling pathway remain unknown (Grimes and Burdine, 2017).

The most widely accepted models to address the nature of these mechanisms are the morphogen model and the two-cilia model. The morphogen model proposes that a morphogen, or a series of vesicular parcels (termed “nodal vesicular parcels”) containing morphogens such as Sonic Hedgehog or Retinoic Acid, are transported to the left side of the LRO by the fluid flow. Once these morphogens reach the left LRO, they induce a release of Ca^{2+}, which in turn triggers left side specific gene expression (Nonaka et al., 1998, Tanaka et al., 2005). The two-cilia model proposes that the LRO contains two different populations of cilia: motile cilia and immotile sensory cilia. According to this model, while the motile cilia generate the fluid flow, the immotile cilia sense the flow on the left side of the LRO and trigger the release of Ca^{2+}, which in turn induces left side specific gene expression (McGrath et al., 2003). Note that these models are not mutually exclusive, thus both mechanisms can exist simultaneously in the LRO.

Left side specific gene expression has been identified in several vertebrate organisms, with the major players in asymmetric signalling belonging to the Nodal pathway. The *Nodal* genes are members of the Transforming Growth Factor beta (TGFβ) superfamily and have a highly conserved role as left side determinants. While humans, mice and chick have a single *Nodal* gene, *Xenopus* have five NODAL-related proteins (Xnr1, 2, 4, 5 and 6) and zebrafish have three (Cyclops, Squint and Southpaw (Spaw)) (Shen, 2007, Schier, 2009).

In mouse, *Nodal* expression is transiently enhanced on the left side of the LRO at the 4-5 somite stage (ss), whereas in zebrafish *nodal* expression is always symmetric in the LRO (Collignon et al., 1996, Long et al., 2003). However, studies done in mouse have shown that NODAL activity is higher on the left side of the LRO, even during stages when *Nodal* expression is symmetric. This was proposed to arise from the asymmetric expression of the NODAL inhibitor CERL2 on the right side of the LRO (Kawasumi et al., 2011). A similar mechanism is thought to be present in the zebrafish, with the Nodal inhibitor Dand5 also displaying an asymmetric expression pattern favouring the right side of the LRO (Fig. I.2c) (Lopes et al., 2010).

CERL2 and Dand5 are members of the DAN family of cysteine-rich extracellular proteins that can block Nodal signalling by interacting directly with the NODAL proteins (Shen, 2007, Schier, 2009). In the mouse, CERL2 expression is initially symmetric in the LRO, becoming asymmetric at the onset of LRO ciliary flow (Pearce et al., 1999, Marques et al., 2004). This shift from symmetric to asymmetric expression was proposed to rely on the targeted degradation of *Cerl2* mRNA in the apical and left-sided region of the LRO (Nakamura et al., 2012). Regarding zebrafish, *dand5* expression is also initially symmetrical in the LRO and at the 8 somite stage, with the onset of ciliary flow, becomes asymmetrically positioned on the right side of the LRO, although the mechanisms that regulate this shift in zebrafish are currently unknown (Lopes et al., 2010).

I.1.2.3 Asymmetric gene expression in the LPM

After the first asymmetry cues are established in the LRO, in the form of an asymmetric activation of the Nodal pathway, these cues are transmitted to the left Lateral Plate Mesoderm (LPM) (Fig. I.2c). The process through which left side specific NODAL activity in the LRO translates into left side specific *Nodal* expression in the LPM is still not fully understood. However, several lines of evidence suggest that NODAL exhibits a long-range activity, traveling directly from the left side of the LRO towards the left lateral plate mesoderm, through an intra-embryonic route. The efficiency of this transport appears to rely on interactions between NODAL and

Sulfated Glycosaminoglycans (Oki et al., 2007, Marjoram and Wright, 2011, Shiratori and Hamada, 2014).

Once the NODAL signal reaches the left LPM, it triggers the activation of the *Nodal-Lefty-Pitx2* gene expression cassette. This cassette contains three remarkably conserved Nodal pathway target genes: *Nodal* itself, the Nodal Inhibitor *Lefty*, and *Pitx2* (Fig. I.2c) (Shen, 2007, Schier, 2009).

Evidence supporting the auto-activation of Nodal came from studies done in mouse, where two NODAL-responsive enhancers have been identified in the *Nodal* gene, the left-side enhancer (LSE) and the asymmetric enhancer (ASE). The combined action of these two enhancers is thought to drive *Nodal* expression in the left LPM (Adachi et al., 1999, Norris and Robertson, 1999, Saijoh et al., 2000, Saijoh et al., 2005). This auto-activation of *Nodal* results in the rapid spread of *Nodal* expression throughout the left LPM, as well as the induction of *Lefty* and *Pitx2* expression.

Lefty proteins are Nodal target genes which establish a negative feedback loop with Nodal. Most vertebrates have only one Lefty protein with the exception of mouse and zebrafish, which have two, LEFTY1 and LEFTY2 (Schier, 2009, Shiratori and Hamada, 2014). *Lefty2* expression is activated by NODAL in the left LPM, where it downregulates NODAL activity thus regulating the spread of *Nodal* expression. Nodal signalling also activates *Lefty1* expression in the axial midline, LEFTY1 is therefore thought to function as a molecular barrier that prevents leakage of the Nodal signal from the left to the right side. This mechanism of self-enhancement and lateral inhibition has been proposed to ensure the propagation of NODAL signals throughout the left LPM, while simultaneously inhibiting their activation on the right LPM (Schier, 2009, Shiratori and Hamada, 2014, Nakamura et al., 2006, Saijoh et al., 2000, Meno et al., 1998, Yamamoto et al., 2003).

Much like *Nodal*, *Pitx2* is a highly conserved left-side specific gene, being expressed in the left LPM of all the vertebrate species studied to date (Shiratori and Hamada, 2014, Burdine and Schier, 2000). In addition, *Pitx2* also possesses a left-side specific ASE enhancer, which is responsive to NODAL and required for *Pitx2* expression in the left LPM. In this context, NODAL appears to induce *Pitx2* expression in the left LPM, through the ASE enhancer, with the maintenance of LPM *Pitx2* expression being independent of NODAL and relying instead on the homeobox

transcription factor NKX-2.5 (Shiratori et al., 2001). *Pitx2* expression in the left LPM therefore functions as a readout of Nodal signalling and is thought to contribute to the following stage of Left-Right patterning during which positional information is transferred to the developing internal organs.

I.1.2.4 Asymmetric internal organ placement

There are several lines of evidence supporting the theory that asymmetric gene expression in the LPM conditions the asymmetric placement of internal organs such as the gut, liver, pancreas (also known as visceral organs) and the heart (Fig. I.2c). However, the specific requirements for Nodal-Pitx2 asymmetric signalling and the precise contribution of this pathway to organ laterality establishment require further elucidation.

During gut development, the first break from symmetry occurs when portions of the gut are displaced laterally from the midline, in a process termed gut looping. In zebrafish gut looping occurs when the region that will give rise to the liver and intestinal bulb moves to the left of the midline. The mechanisms that drive gut looping appear to be largely reliant on neighbouring tissues. Specifically, in zebrafish gut asymmetries are driven by the asymmetric migration of the LPM, and in amniotes the initial chirality of gut looping relies on asymmetries in the cellular architecture of the associated dorsal mesentery (Horne-Badovinac et al., 2003, Davis et al., 2008, Kurpios et al., 2008). Importantly, Nodal signalling has been identified as an upstream regulator of asymmetric LPM migration in zebrafish and left-sided *Nodal-Pitx2* expression was shown to instruct asymmetric cellular architecture establishment in the amniote dorsal mesentery (Grimes and Burdine, 2017, Horne-Badovinac et al., 2003, Davis et al., 2008, Kurpios et al., 2008).

Consistent with this is the observation that mouse mutants lacking left-sided *Pitx2* expression exhibit laterality defects in most visceral organs (Shiratori et al., 2006). Furthermore, in zebrafish *nodal* mutants the lateral positions of the visceral organs are randomized (Noël et al., 2013). However, zebrafish *pitx2* mutants do not present laterality defects in the visceral organs, raising the possibility that additional Nodal

signalling effectors can contribute to the establishment of visceral organ laterality in the fish (Ji et al., 2016).

In zebrafish, cardiac symmetry breaking can be divided into two steps: a Jogging step and a Looping step. The Jogging step is characterized by a leftwards and cranial displacement of atrial cardiomyocytes and simultaneous involution of ventricular myocardial cells, which generates a leftward pointing cardiac tube. The Looping step involves the repositioning of the atrium in a caudal direction and the repositioning of the ventricle in an anterior direction, which generates a coiled cardiac tube with well-defined inner and outer curvatures. In wildtype conditions the direction of heart tube Jogging (Left jog) prefigures the direction of cardiac Looping (Dextral loop) (Campione and Franco, 2016).

Noticeably, in zebrafish *nodal* mutant embryos, normal Dextral looping is still observable in approximately 70% of the mutant population (Noël et al., 2013). Furthermore, heart tubes isolated from these embryos and cultivated *in vitro*, retain the capacity to undergo Dextral looping (Noël et al., 2013). These results raise the possibility that nascent cardiomyocytes possess an intrinsic laterality bias, with robust cardiac asymmetry establishment likely resulting from the integration of this intrinsic program with the laterality signals provided by the Nodal pathway.

Furthermore, *Pitx2* has been implicated in several aspects of asymmetric cardiac morphogenesis, with *Pitx2* loss-of-function experiments leading to atrial isomerism, impaired atrioventricular remodelling, atrial and ventricular septal defects and morphological defects arising from an impairment of the alignment and rotation of the outflow tract relative to the ventricles (Campione and Franco, 2016). However, while *PITX2* seems to be required to establish cardiac looping directionality in the chick, this requirement appears to be absent in zebrafish and mouse (Shiratori et al., 2006, Lu et al., 1999, Gage et al., 1999, Kitamura et al., 1999, Lin et al., 1999, Ji et al., 2016, Yu et al., 2001, Campione and Franco, 2016). Further reinforcing the possibility that additional mechanisms, outside the scope of the Nodal pathway, contribute to the establishment of cardiac laterality.

I.1.3 FGF signalling in embryonic development

Embryonic development relies on short- and long-distance cellular communication, with this communication often involving the secretion of signalling molecules and the activation of signalling pathways in response to these secreted signals. Extensive research into the major morphogenetic events that take place during embryogenesis has revealed that a surprisingly small number of signalling pathways appear to regulate the vast majority of developmental programs. One of these major regulators of embryonic development is the FGF signalling pathway (Perrimon et al., 2012).

Fgf ligands are small secreted polypeptides with a partially conserved core of 120–130 amino acids. The majority of Fgf ligands operate as paracrine signalling molecules, forming a tripartite complex with Fgf receptors (Fgfrs) and heparan sulphate glycosaminoglycan chains (HS-GAG). Fgfrs are receptor tyrosine kinases which are activated by Fgf/HS-GAG binding. Fgfr activation results in receptor dimerization and triggers the activation of intracellular signal transduction pathways, including the RAS-MAPK (Ras – Mitogen activated protein kinase), PI3K-AKT (Phosphoinositide 3 kinase - Protein kinase B), PLCγ (phospholipase-Cγ), and STAT (Signal transducer and activator of transcription) pathways. In most cases, the activation of these pathways ultimately affects the transcriptional program of the cell, with genes which are differentially expressed in response to FGF signalling being commonly referred to as Fgf target genes (Pownall and Isaacs, 2010, Ornitz and Itoh, 2015).

During embryonic development, several Fgf ligands and receptors have been implicated in embryonic patterning, progenitor cell maintenance, growth, differentiation and survival. Furthermore, FGF signalling appears to influence embryogenesis from its earliest stages and throughout the entire organogenesis phase (Pownall and Isaacs, 2010, Ornitz and Itoh, 2015). The next sections will focus on highlighting some of the key functions of the FGF signalling pathway during embryonic development, with a special emphasis on the developmental roles of the zebrafish ligand *fgf8a* and its orthologues – the *Fgf8* genes.

I.1.3.1 FGF signalling in gastrulation and posterior body development

In the early stages of embryonic development, the FGF pathway has been shown to contribute to multiple aspects of the gastrulation process, with disruptions of FGF signalling in zebrafish, amniote, fly and frog embryos leading to severe defects in gastrula development (Griffin et al., 1995, Yamaguchi et al., 1994, Deng et al., 1994, Amaya et al., 1991, Isaacs et al., 1994, Beiman et al., 1996, Gisselbrecht et al., 1996).

Several lives of evidence point to a role for the FGF pathway in the coordination of cell movements during gastrulation. In particular, studies done in chimeric mice containing *Fgfr1* mutant cells and in homozygous *Fgf8* mice mutants have reported an accumulation of cells in the primitive streak during gastrulation, and a subsequent disruption of mesoderm and endoderm-derived tissue development (Ciruna et al., 1997, Ciruna and Rossant, 2001, Sun et al., 1999). In addition, FGF8 and FGF4 have been implicated in the coordination of gastrulation movements in the chick, where these ligands were found to act as a chemorepellent and a chemoattractant, respectively, and their combined action was proposed to function as a guide for cell ingression and cell migration away from the primitive streak (Yang et al., 2002). Furthermore, two *Fgf8*-like *Drosophila* genes – *thisbe* and *pyramus* – as well as the *Drosophila Fgfr2* gene – *heartless* – have been implicated in mesoderm cell migration during gastrulation (Gryzik and Müller, 2004, Beiman et al., 1996, Gisselbrecht et al., 1996).

In addition to its role in the coordination of gastrulation cell movements, the FGF signalling pathway has also been implicated in the specification of the dorsal-ventral axis in gastrulating *Xenopus* and zebrafish embryos. In *Xenopus*, FGF appears to achieve this patterning function by contributing to the specification of the animal-vegetal axis, which prefigures the dorsal-ventral axis in this organism (Kumano and Smith, 2000, Kumano et al., 2001, Kumano and Smith, 2002). Several lines of evidence indicate that FGF signalling contributes to dorsal-ventral specification by promoting dorsal fates and inhibiting ventral fates. For instance in zebrafish, Fgf8a was shown to contribute to dorsal fate specification by cooperating with the dorsal fate-associated gene *chordin* and inhibiting the expression of the ventral fate-associated bone morphogenetic proteins (BMPs) in the dorsal mesoderm, thus

restricting BPM expression to the ventral mesoderm (Fürthauer et al., 1997, Fürthauer et al., 2004).

Furthermore, studies done in *Xenopus*, zebrafish, chick and mouse have shown that the FGF signalling pathway is required for the formation of the mesodermal germ layer during the gastrula phase (Slack et al., 1987, Amaya et al., 1991, Amaya et al., 1993, Griffin et al., 1995, Mitrani et al., 1990, Burdsal et al., 1998). In this context FGF signalling does not appear to function as an instructive inducer of the mesodermal fate *per se*. Instead, Fgfs are thought to function primarily as competence factors granting the cells the ability to respond to other mesoderm inducers, such as TGFβs (Mathieu et al., 2004, Cornell and Kimelman, 1994, LaBonne and Whitman, 1994). In addition, FGF signalling also contributes to mesoderm formation by positively regulating the expression of the T-box transcription factor *Brachury*, with this regulation involving a mechanism of positive feedback between FGF and *Brachury* (Isaacs et al., 1994, Schulte-Merker and Smith, 1995, Ciruna and Rossant, 2001, Griffin et al., 1995, Kiecker et al., 2016).

Interestingly, the role of FGF signalling in mesoderm induction appears to extend beyond the gastrula phase, specifically during posterior body development. This was highlighted in a recent study done in zebrafish which found that FGF cooperates with Wnt signalling to induce paraxial mesoderm fates from tailbud neuromesodermal progenitors. The authors propose that this process involves a two-step epithelial to mesenchymal transition event in which Wnt signalling initiates the transition and FGF signalling promotes its completion. Contrary to the gastrulation context, in the tailbud context FGF signalling appears to induce the paraxial mesoderm fate, in part, by indirectly repressing the expression of the zebrafish *brachyury* gene *ta* (Goto et al., 2017).

The specific ligands and receptors involved in the FGF pathway's functions in mesoderm formation have yet to be fully identified. However, studies in *Xenopus* have implicated the *fgf4* and *fgf8* genes in these processes, with the *fgf8* splicing isoform *fgf8b* appearing to have a more prominent role in mesoderm formation than the *fgf8a* isoform (Isaacs et al., 1994, Schulte-Merker and Smith, 1995, Fletcher et al., 2006, Fletcher and Harland, 2008). In zebrafish, posterior mesoderm formation appears to require the combined activity of the Fgf8a and Fgf24 ligands, and

evidence from chick implicates FGFR1 in the process of mesoderm cell fate specification (Draper et al., 2003, Ciruna and Rossant, 2001).

In addition to its role in paraxial mesoderm induction, FGF signalling in the tailbud was shown to contribute to the maintenance of the progenitors of the spinal cord, and is known to operate during posterior body elongation by promoting proper cell migration in the tailbud and paraxial mesoderm (Mathis et al., 2001, Akai et al., 2005, Lawton et al., 2013, Steventon et al., 2016). Lastly, FGF signalling in the paraxial mesoderm is involved in the establishment of the somitogenesis wavefront. As previously noted, this wavefront activity appears to be mediated by the Fgf8a ligand in zebrafish and the FGF4 and FGF8 ligands in mouse, and plays a fundamental role in somite formation (Section I.1.1.2.2).

I.1.3.2 FGF signalling in anterior body and sensory system development

I.1.3.2.1 The midbrain-hindbrain boundary

One of the most important developmental functions of FGF signalling, and the Fgf8a ligand in particular, is in the formation of the midbrain-hindbrain boundary (MHB), also known as the isthmic organizer. The MHB presents morphologically as a constriction in the developing neural tube at the interface between the midbrain and hindbrain neuromeres. Molecularly, the MHB is known to function as a signalling centre responsible for patterning cell fates anteriorly in the midbrain and posteriorly in the cerebellum (Gibbs et al., 2017).

A critical aspect of MHB development is the establishment of an FGF/Wnt signalling interface, with progenitors of the posterior mesencephalon expressing Wnt ligands and progenitors of the anterior rhombencephalon expressing Fgf ligands. In mouse, both homozygous *Wnt1* mutants and homozygous *Fgf8* mutants fail to develop the entire midbrain-hindbrain region (McMahon and Bradley, 1990, Chi et al., 2003). In zebrafish, loss of *wnt3a*, *wnt1* and *wnt10b* produces a similar phenotype and the zebrafish *fgf8a* mutant *acerebellar* (*ace*) lacks a cerebellum, lacks MHB constriction and displays defects in midbrain polarization (Buckles et al., 2004, Reifers et al., 1998, Picker et al., 1999, Gibbs et al., 2017).

The FGF/Wnt signalling interface is first established during late gastrula to early somitogenesis stages and is believed to function initially by reinforcing the positioning of the MHB (Gibbs et al., 2017, Rhinn and Brand, 2001). However, the main function of this interface, and *fgf8a* in particular, appears to be the maintenance of the MHB genetic program. For instance, in zebrafish *ace* mutants the expression of *wnt1* and other patterning genes such as *her5*, *pax2a*, *en2a* and *en2b* is initially activated in the MHB, but fades during early- to mid-somitogenesis stages (Reifers et al., 1998). This failure to maintain the MBH genetic program is mirrored morphologically, with *fgf8a* morphants initiating the process of constriction which then fails to mature properly (Gibbs et al., 2013). It follows from these studies that Fgf8a is necessary for the maintenance of the molecular and mechanical microenvironments required for MHB morphogenesis.

I.1.3.2.2 The inner ear

FGF signalling is also a major player in inner ear development, with its contributions to this process including fate specification, patterning and regulation of neural development. The process of inner ear development begins with the specification of the otic placode, a region of specialised ectoderm lying adjacent to the developing hindbrain. The cells in this otic region subsequently integrate both external and internal signals, which not only drive tissue invagination and subsequent formation of the otic vesicle, but also trigger the specification of the different cell types and spatial identities of the emerging inner ear (Ladher, 2017).

In zebrafish, FGF signalling appears to function, between the late gastrula and early somitogenesis stages, as an early inducer of the otic placodal fate, with this function being mediated by the combined activity of the Fgf8a and Fgf3 ligands (Phillips et al., 2001, Maroon et al., 2002, Léger and Brand, 2002, Liu et al., 2003). The FGF8 and FGF3 ligands have also been implicated in early otic fate induction in chick and mouse, along with the chick FGF19 ligand and the mouse FGF10 ligand (Wright and Mansour, 2003, Ladher et al., 2005, Alvarez et al., 2003, Domínguez-Frutos et al., 2009, Zelarayan et al., 2007, Freter et al., 2008). Following placodal fate induction,

FGF signalling has also been shown to trigger some of the morphological changes underlying the invagination process (Sai and Ladher, 2008).

Furthermore, during late placode and early otic vesicle stages FGF signalling contributes to the anterior-posterior specification of otic fates. In zebrafish, this process takes place at mid-somitogenesis stages and FGF signalling operates in this context by instructing anterior identity, with posterior identity being specified by Hedgehog signalling. The Fgf3 ligand has been shown to be partially responsible for mediating this FGF signalling function (Hammond and Whitfield, 2011).

In addition, FGF signalling has been implicated in otic neuroblast development in chick and zebrafish (Alsina et al., 2004, Vemaraju et al., 2012). For instance, between the mid-somitogenesis and pharyngula stages of zebrafish embryogenesis, FGF signalling regulates several steps of neuronal development in the statoacoustic ganglion (SAG). In the initial phases of SAG development, a moderate level of Fgf8a and Fgf3 promotes neuroblast specification within the otic vesicle. As SAG development progresses, neuroblasts differentiate into mature SAG neurons which express Fgf5, leading to a gradual increase in FGF signalling. When the combined levels of Fgf8a, Fgf3 and Fgf5 exceed a threshold value, FGF signalling terminates specification of new neuroblasts and slows differentiation of progenitors into mature neurons (Vemaraju et al., 2012). This mechanism is thought to enable the maintenance of a stable progenitor pool in the SAG, in which growth and differentiation are evenly balanced.

I.1.3.2.3 The anterior and post optic commissures

The functions of Fgf signalling in sensory system-associated neural development also include an important role in commissure formation. Commissures are axonal connections between the left and right sides of the nervous system, which play critical roles in lateralized sensory-motor functions. For instance, in zebrafish, the post optic and the anterior commissures are formed during the early stages of the pharyngula period. The post optic commissure includes bilateral axons that connect the preoptic area with the hypothalamus, as well as telencephalic and thalamic fibers that project to the hypothalamic region. The anterior commissure connects

the olfactory bulbs, pallial and sub-pallial areas to their contralateral homotopic structures (Suárez et al., 2014, Barresi et al., 2005).

A key function of Fgf signalling in commissural development is in the early dorsoventral patterning events that lead to the subdivision of the commissural plate. Studies in mouse and chick have shown that these patterning events involve the morphogenic activity of BMP/Wnt and Sonic Hedgehog (SHH), which establish the pallial and subpallial territories respectively, with FGF signalling, and the FGF8 ligand in particular, operating primarily in the refinement of the subpallium into septal and preoptic regions (Ohkubo et al., 2002, Shimogori et al., 2004, Storm et al., 2006, Suárez et al., 2014).

Following the patterning of the commissural plate, growing commissural axons are guided toward and across the midline, by several glial cell populations, to form the commissures (Suárez et al., 2014). Although the precise role of FGF signalling in commissure formation remains to be elucidated, studies conducted in FGFR1 deficient mice have shown that FGF signalling is essential for the formation of the major commissures. These studies also proposed that FGF signalling functions in this context, in part, by contributing to the formation of the midline glial structures that guide commissural axon crossing (Smith et al., 2006, Tole et al., 2006).

In line with this, zebrafish *ace* mutants display abnormal cell morphology and altered gene expression patterns in the midline. These embryos also present axon pathfinding defects of varying severities, in the establishment of the anterior and post optic commissures, with the majority of *ace* embryos failing to form one or both commissures (Shanmugalingam et al., 2000). In addition, *aussicht* (*aus*) mutants, in which the expression of *fgf8a* is upregulated, exhibit patterning defects in the midline and pretectal areas, as well as a delay in anterior and post optic commissure formation (Heisenberg et al., 1999). Furthermore, a study done in *fgf8a* and *fgf3* zebrafish morphants revealed that anterior commissure formation is abnormal in the absence of either Fgf3 or Fgf8a, with depletion of both ligands leading to more severe defects in commissure formation (Walshe and Mason, 2003). Taken together these studies provide evidence for a clear contribution of FGF signalling to the commissure formation process, with the zebrafish Fgf8a and Fgf3 ligands exhibiting partially redundant roles in this context.

I.1.3.2.4 The retina

In line with the previously described functions of FGF signalling in sensory system-associated neural development, this pathway has also been implicated in both neurogenesis and patterning of the developing vertebrate retina.

In the vertebrate retina, FGF signalling has been proposed to function primarily as an important organizing center for retinal neurogenesis. In this capacity, data from chick and zebrafish have shown that the concerted activity of FGF8 and FGF3 ligands appears to be both necessary and sufficient to coordinate the differentiation of the retinal ganglion cells, with these cells constituting the first population of retinal neurons to form in the vertebrate embryo (Martinez-Morales et al., 2005). Furthermore, FGF signalling was shown to promote retinal differentiation by activating SHH signalling. In this context, the Fgf8/Fgf3 signalling center appears to promote the initiation of *shh* expression in the ventral-nasal region of the retina, with the Fgf19 ligand subsequently contributing to the propagation of *shh* expression through the retina (Vinothkumar et al., 2008).

An additional aspect of retinal development, which appears to be under the control of Fgf signalling to a considerable extent, is the process of retinal nasal-temporal patterning. This patterning process is a crucial aspect of eye development because it ensures that retinal ganglion cell axonal projections later map onto the correct regions of the brain. Studies in zebrafish have shown that a combined Fgf8a/Fgf3/Fgf24 signal, emanating from neighbouring tissues during the segmentation phase, appears to regulate retinal patterning by confining the expression of nasal and temporal marker genes to the dorsal and ventral halves of the evaginating optic vesicle, respectively (Picker et al., 2009, Picker and Brand, 2005). The process of nasal and temporal marker regionalization was proposed to rely on a balance between FGF signalling and SHH signalling, which appear to have opposing actions in the optic vesicle, with loss of FGF signalling leading to compromised specification of nasal identity and loss of SHH signalling leading to compromised specification of temporal identity (Hernández-Bejarano et al., 2015, Picker et al., 2009). In addition, one of the nasal markers involved in this process is

the *foxg1* gene, which in the presence of FGF signalling appears to enhance cell cohesion in the future nasal compartment through a currently unknown mechanism (Picker et al., 2009). Therefore, the Fgf8a, Fgf3 and Fgf24 ligands appear to function in concert, not only during the early nasal-temporal patterning of the retina, but also during optic vesicle morphogenesis.

I.1.3.2.5 Vascularization

One of the most well recognized functions of the FGF signalling pathway is the regulation of vessel formation. In this context Fgf ligands generally exert pro-angiogenic activities by interacting with various endothelial cell surface receptors, with these interactions being further modulated by a variety of free and extracellular matrix-associated molecules. Interestingly, even though the roles of Fgf ligands have been extensively studied in tumour vascularization, neovascularization and adult angiogenesis contexts, the specific functions of endogenous Fgfs in embryonic vasculature development still require further elucidation (Presta et al., 2005, Murakami and Simons, 2008).

Nevertheless, roles for this pathway in embryonic vascularization have been reported in zebrafish, chick and mouse. In particular, during zebrafish intersomitic vessel assembly FGF signalling was shown to influence vessel integrity to a considerable extent, and vessel guidance and outgrowth to a moderate extent. In this system, FGF signalling was proposed to function primarily by ensuring the formation of proper cell-cell junctions between endothelial cells, while also displaying a certain inductive control over vessel sprouting (De Smet et al., 2014).

A role for FGF signalling in intersomitic vessel development was also observed in cultured mouse embryos expressing a dominant-negative form of FGFR1 in endothelial cells. These authors report that targeted inhibition of FGF signalling leads to incomplete intersomitic vessel formation, defects in yolk sack vasculature assembly, and heart septation (Lee et al., 2000). Furthermore, combined inactivation of the mouse FGFR1 and FGFR2 receptors in endothelial cells brought about defects in coronary vessel formation (Lavine et al., 2006).

Transgenic mice overexpressing a truncated form of the FGFR1 specifically in the developing eye, also display vascularization defects. In particular, transgene activation lead to an inhibition of angiogenesis in a superficial layer of the retinal vasculature, termed choroidal vasculature. Furthermore, these authors observed defects in the assembly of the inner layer of retinal vessels which begins to develop at birth in mice (Rousseau et al., 2003).

Lastly, studies done in chick have identified the FGF2 ligand as an important stimulator of angiogenesis in the chorioallantoic membrane, with this extraembryonic membrane constituting an important gas exchange surface during avian development (Ribatti and Presta, 2002).

I.2 POST-TRANSCRIPTIONAL REGULATION IN EMBRYONIC DEVELOPMENT

Embryonic development is a highly regulated process both spatially and temporally, with many of the genes that coordinate embryogenesis being expressed for short periods of time and/or in well-defined spatial domains. These patterns of gene expression are not only required to specify cellular identities but also to direct the complex morphogenetic processes that potentiate the formation of a multicellular organism. Precise control over gene expression patterns is often achieved through the regulation of the multiple steps in the pathway from RNA to protein.

The regulation of gene expression at the RNA level, between the initiation of transcription and the translated protein phase, is typically referred to as post-transcriptional regulation, and encompasses different mechanisms. These mechanisms include alternative RNA splice-site selection, control of 5'-capping, control of 3'-end formation by cleavage and polyadenylation, RNA editing, control of mRNA transport from the nucleus to the cytosol, localization of mRNA to specific sub-cellular regions, control of translation efficiency and regulation of mRNA stability. Among these mechanisms, splice-site selection, control of 5'-capping and control of 3'-end formation, generally take place concomitantly with the transcription process and are thus specifically referred to as co-transcriptional regulation mechanisms (Fig. I.3) (Alberts, 2002).

The importance of post-transcriptional regulation mechanisms to the developing embryo is evident in key developmental processes such as vertebrate segmentation and *Drosophila* axis establishment. As previously noted, the process of vertebrate segmentation, or somitogenesis, is governed by two mechanisms – a molecular clock and a wavefront of differentiation – both of which are thought to rely on a tight post-transcriptional control of mRNA stability (Section I.1.1.2) (Hubaud and Pourquié, 2014, Cooke and Zeeman, 1976). In particular, the clock is composed of cyclically expressed genes, with current models postulating that these genes need to be unstable at the mRNA level to produce sustained transcriptional oscillations (Lewis, 2003). Conversely, the establishment of the wavefront of differentiation was show to partially rely on an FGF8 gradient which is produced by the slow degradation of the *Fgf8* mRNA (Dubrulle and Pourquié, 2004). In *Drosophila*,

extensive research has shown that during the early stages of development, asymmetric protein expression and mRNA localization are critical to the establishment of the Anterior-Posterior and Dorsal-Ventral axis. These axis specification events are mediated by several patterning genes, such as *Hunchback*, *Nanos*, *Oskar*, *Caudal* and *Bicoid*. The expression of these genes in precise spatial and temporal patterns is primarily achieved through post-transcriptional mechanisms, particularly the regulation of translation efficiency and mRNA localization (Kuersten and Goodwin, 2003, de Moor et al., 2005, Colegrove-Otero et al., 2005).

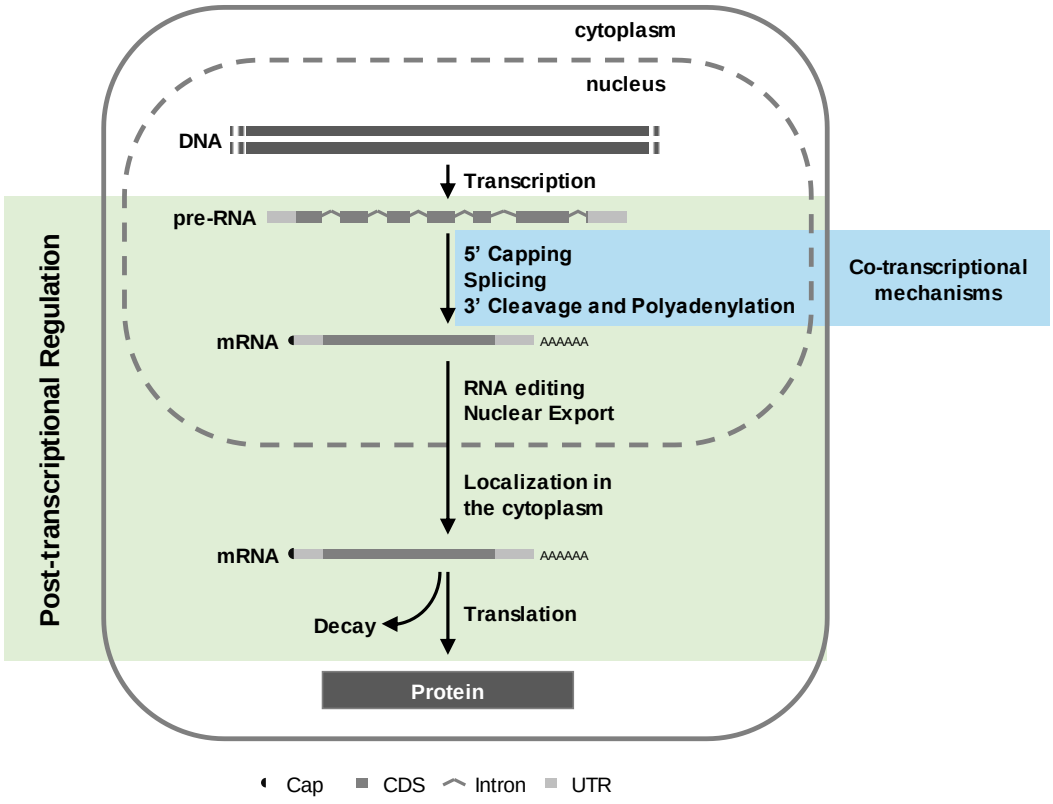

Fig. I.3 – Gene expression regulation at the post-transcriptional level. Illustration of the different steps in the pathway from transcription to protein which can be subjected to post-transcriptional regulation. The pre-RNA processing mechanisms highlighted in blue generally take place concomitantly with the transcription process and thus their regulation can be referred to as co-transcriptional.

A large majority of post-transcriptional regulation mechanisms involve the recognition of specific sequence or structural motifs in the RNA molecule under regulation, by either regulatory proteins or regulatory RNAs. These regulatory motifs

are often found in the untranslated regions (UTRs) of the mRNA molecules, with the 3'UTRs in particular, frequently displaying important roles in different forms of post-transcriptional regulation. Furthermore, these regulatory proteins, also referred to as RNA binding proteins (RBP), have long been recognized as important regulators of embryogenesis, with their functions being especially critical during the earliest stages of development (Matoulkova et al., 2012, Colegrove-Otero et al., 2005).

The next sections will focus on 3'UTR-mediated and RBP-mediated post-transcriptional regulation of gene expression in the developing embryo, with a special emphasis on a specific co-transcriptional mechanism of gene expression regulation – alternative polyadenylation – and a specific family of RBPs – the Signal Transduction and Activation of RNA (STAR) protein family.

I.2.1 The 3'UTRs

The untranslated regions of the mRNA molecule have long been associated with gene expression regulation at the post-transcriptional level, and 3'UTR sequences in particular, are notably conserved among vertebrates. Although 3'UTRs are generally less conserved than protein coding regions, their degree of conservation supersedes that of other non-coding regions, such as promoters, introns and 5'UTRs (Matoulkova et al., 2012, Duret et al., 1993).

As previously stated, post-transcriptional regulation events are often mediated by elements located in the 3'UTRs. However, unlike DNA-based regulatory elements which operate through their primary structure, RNA-based regulatory motifs can exert their regulatory activity either through their primary structure, their secondary structure, or through a combination of both. These sequence and structural elements in the 3'UTRs have been shown to influence mRNA stability, transport and translation efficiency primarily through interactions with regulatory RNAs and RBPs (Fig. I.4a) (Matoulkova et al., 2012).

The most widely recognized group of regulatory RNAs to function in this context is a class of noncoding RNAs termed microRNAs (miRs). As the name suggests microRNAs are small RNA molecules that bind to short sequence motifs (6–8 nucleotides) known as miR binding sites (Matoulkova et al., 2012, Fabian et al.,

2010). miR-3'UTR interactions typically lead to an inhibition of protein production, with miRs functioning either by blocking translation or by inducing mRNA degradation (Fig. I.4a) (Matoulkova et al., 2012, Fabian et al., 2010).

Interactions between 3'UTRs and RBPs are typically mediated by regulatory motifs in the 3'UTR termed RPB binding sites, with the sequence and structural features of these binding sites varying considerably between RBPs. RBP-3'UTR interactions can bring about either a stimulation or an inhibition of protein production, with different RBPs exerting different effects over mRNA stability and translation efficiency, in a context-dependent manner (Matoulkova et al., 2012, Glisovic et al., 2008). Furthermore, RBP-3'UTR interactions can facilitate mRNA transport and thus enable transcript localization to the correct subcellular compartment (Fig. I.4a) (Eliscovich et al., 2013).

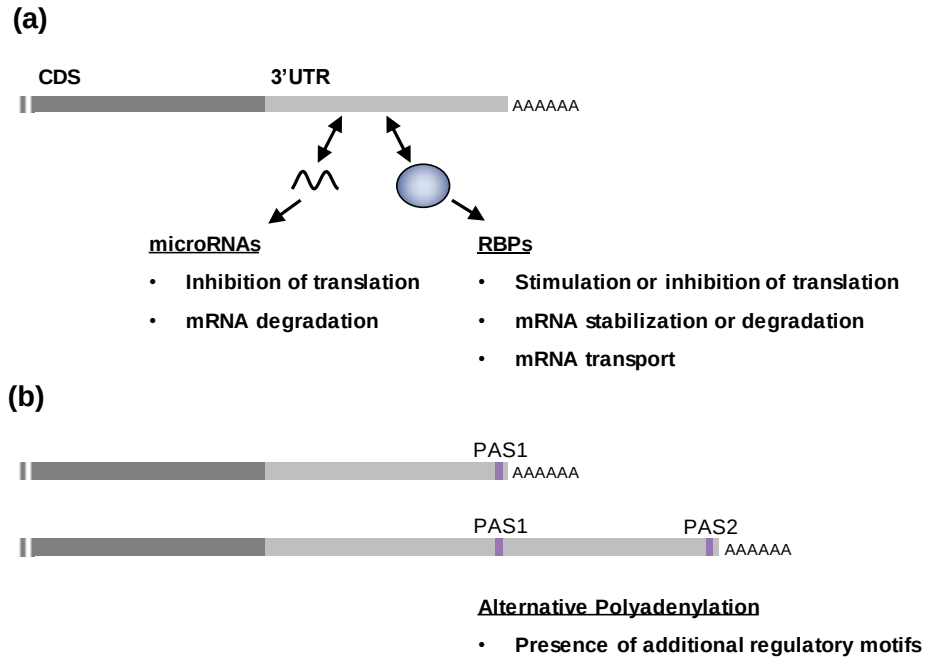

Fig. I.4 – The 3′ untranslated region (3′UTR) and associated mechanisms of post-transcriptional regulation. (a) 3′UTRs contribute to gene expression regulation via multiple mechanisms, two of which are illustrated: microRNA binding and RNA-binding protein (RBP) binding. MicroRNAs typically interact with microRNA binding sites in the 3′UTR to either block translation or promote mRNA degradation. RBPs interact with RBP binding sites in the 3′UTR and regulate mRNA translation, turnover and/or transport. **(b)** Alternative Polyadenylation (APA) is a regulatory mechanism that takes place when multiple alternative polyadenylation signals (PAS) are present. APA in the 3'UTR determines the length of the 3′UTR, and consequently, dictates the number and type of regulatory motifs (e.g. microRNA and RBP binding sites) that are available to regulate transcript expression.

Lastly, 3’UTRs have been implicated in membrane protein localization through the formation of scaffolds and have been proposed to function during the termination of translation to stabilize the ribosomal complexes and support ribosome recycling (Berkovits and Mayr, 2015, Pánek et al., 2016).

I.2.1.1 Alternative polyadenylation

An additional level of complexity associated with post-transcriptional regulation ties in with the fact that a considerable number of genes give rise to mRNAs with alternative 3’UTRs (alt3’UTRs), through a process termed alternative polyadenylation (APA) (Fig. I.4b).

The mRNA polyadenylation process is generally concomitant with transcription and is triggered by a sequence motif termed polyadenylation signal (PAS). The recognition of this signal by the polyadenylation machinery leads to the endonucleolytic cleavage of the precursor mRNA in the polyadenylation site, located 10-30 nucleotides downstream of the polyadenylation signal, and subsequent addition of the polyA tail. Alternative polyadenylation occurs when more than one PAS is present. In most cases these alternative PASs are located in the 3’UTR, with 3’UTR-APA therefore leading to the production of alternative transcripts which differ exclusively in the length of their 3'UTRs. These 3’UTRs are naturally referred to as alternative 3’UTRs (Fig. I.4b) (Chen et al., 2017a, Tian and Manley, 2017, Tian et al., 2005).

Therefore, the selection of alternative PASs determines the sequence content of the 3’UTR and thus the landscape of regulatory motifs in the mRNA that are available to interact with miRs and RBPs. Since longer 3’UTRs tend to have additional regulatory motifs, their regulatory potential is greater than that of shorter 3’UTRs, and thus APA can have a substantial impact on gene expression (Fig. I.4b) (Chen et al., 2017a, Tian and Manley, 2017).

Furthermore, APA has recently been appreciated as highly conserved and widespread mechanism of gene expression regulation, with approximately half of

protein coding genes in the human, mouse, zebrafish, *Drosophila* and *C. elegans* producing alternative 3′UTRs through APA (Tian et al., 2005, Shepard et al., 2011, Lianoglou et al., 2013, Smibert et al., 2012, Jan et al., 2011, Mangone et al., 2010, Ulitsky et al., 2012, Li et al., 2012).

I.2.1.2 APA dynamics during embryonic development

The prevalence of APA is particularly noteworthy during embryonic development, as shown in several large-scale studies conducted in zebrafish, mouse and *Drosophila*. Moreover, these studies revealed that alternative PAS selection can be regulated in both a tissue dependent and a developmental stage dependent manner.

For instance, during zebrafish development, two studies have shown that between 43% and 55% of expressed protein coding genes display alternative 3'UTRs. Furthermore, average alt3'UTR lengths tend to be shorter during early development, specifically during the cleavage period, and subsequently undergo a pronounced lengthening after 4 hours post fertilization (hpf), during the blastula stages. This 3'UTR lengthening event was correlated with a potential role for APA during the maternal to zygotic transition (MZT) (Li et al., 2012, Ulitsky et al., 2012). Furthermore, 3'UTR lengthening appears to continue during the gastrula period and for the duration of embryonic development. The authors also report that two families of regulatory sequence elements, namely miR-430 target sites and U-Rich elements, are enriched in the 3'UTRs of genes that undergo these shifts in 3'UTR length, in a stage specific manner (Li et al., 2012). Overall these studies point to a role for APA in a stage specific modulation of the post-transcriptional mechanisms that affect gene expression.

Similar findings were reported in the mouse, with murine genes displaying a progressive 3'UTRs lengthening trend that accompanies the entire course of embryonic development. Furthermore, these authors observed that the 3'UTR lengthening trend is not only observable at the whole embryo level, but also at a tissue specific level. In particular, mRNAs expressed in murine brain tissues tend to have progressively longer 3'UTRs throughout embryonic and post-natal

developmental stages (Ji et al., 2009). Indeed, subsequent studies have shown that several mouse genes produce transcripts with longer 3'UTRs specifically in the developing and adult brain (Miura et al., 2013). The selective expression of these extended 3'UTR sequences in neural tissues is highly indicative of a potential role for APA in brain development.

Studies in *Drosophila* have further substantiated a potential role for APA in neural development. Consistently with the observations made in mouse and zebrafish, *Drosophila* embryogenesis also appears to be accompanied by a progressive 3'UTR lengthening trend. However, in *Drosophila* it has been shown that a substantial component of this lengthening trend consists of the tissue-specific extension of 3'UTRs in the nervous system (Sanfilippo et al., 2017, Hilgers et al., 2011, Smibert et al., 2012).

The mechanisms responsible for the production of these neural-specific alt3'UTRs have not been fully characterized, however, the *Drosophila* pan-neuronal RBP ELAV (embryonic lethal abnormal visual system) was identified as an important factor in the regulation of neural-specific APA (Hilgers et al., 2012). In addition, the specific implications of neuronal APA to gene expression also require further elucidation. However, one way in which these neural-specific UTRs could function is illustrated by the *Drosophila Ultrabithorax* gene. The longer neural-specific alt3'UTR of the *Ultrabithorax* gene contains an additional set of miR target sites, when compared to the shorter alt3'UTR. Therefore, in this case 3'UTR APA was proposed function by regulating target mRNA visibility to miRs according to developmental context (Thomsen et al., 2010).

I.2.1.3 Importance of APA to embryonic development

Despite the prevalence of 3'UTR APA in the developing embryo the specific functional implications of this co-transcriptional regulation mechanism to the different aspects of embryonic development remain largely unknown. Most of the studies conducted so far on this issue have focused on the developmental impact of interfering with the expression or activity of proteins that are involved in the APA process.

For instance, in mouse, the transcription factor NKX2-5 was shown to control the 3'UTR length of a set of genes involved in cardiac development. This transcription factor, which had previously been identified as a coordinator of the transcriptional networks involved in heart development, was proposed to function in APA as well, through an interaction with the exonuclease XRN2. Simultaneous suppression of NKX2-5 and XRN2 activity was shown to bring about defects in cardiac development. Therefore, the function of NKX2-5 as an APA regulator, and the control of 3'UTR length in this context, was proposed to play a significant role in heart development (Nimura et al., 2016).

Furthermore, repression of the RBPs MBNL1 and MBNL2 (Muscleblind-like1 and 2) has been associated with the development of congenital myotonic dystrophy. These proteins have been implicated in several aspects of RNA processing, including alternative splicing and mRNA transport, and were recently shown to mediate the regulation of thousands of alternative polyadenylation events during embryonic development (Batra et al., 2014, Thomas et al., 2017). These studies highlight the importance of understanding the dynamics of pre-RNA processing and APA that take place during embryonic development.

In addition, the medaka recessive homozygous embryonic lethal mutation *naruto* was shown to interfere with the expression of the Cleavage and Polyadenylation Specificity Factor subunit 6 (Cpsf6). The Cpsf6 is a component of the Cleavage Factor Im complex which plays a key role in pre-RNA 3' cleavage and polyadenylation, and importantly, Cpsf6 appears to contribute to the regulation of PAS selection for several genes. The *naruto* mutant embryos display gross morphological abnormalities, including defects in primordial germ cell migration, enlarged brain ventricles, curved trunks, enlarged pericardial spaces, thin hearts, compromised blood circulation and homozygous embryos die before hatching. Whether or not the functions of Cpsf6 as an APA regulator are tissue or developmental stage specific remains to be clarified. Furthermore, the full scope of genes that present APA defects in these mutants, and their contributions to the *naruto* mutant's morphological defects, require further elucidation (Sasado et al., 2017). Much like the previous studies, the *naruto* mutant highlights the importance of APA regulation to the progression of embryonic development.

However, the previous studies fail to address the particular roles of individual gene-specific alternative 3'UTRs formed through APA, and their overall importance to embryonic development.

To the extent of my knowledge, the only study to address the phenotypic impact of gene-specific 3'UTR APA in a developmental context was conducted by Pinto et al., 2011. In this study the authors focused on the *Drosophila* cell-cycle gene *polo*, which produces two alt3'UTRs through APA. In flies carrying a deletion of one of the *polo* polyadenylation signals, *polo* protein expression is compromised. As a result, the authors observed defects in the proliferation of the precursor cells of the abdominal epidermis during the metamorphosis stage. In particular, these cells – termed histoblasts – are correctly formed in mutants during embryogenesis and develop normally until the larvae stage, with proper *polo* APA being especially required for normal *Drosophila* development and survival beyond the late third instar larval stage (Pinto et al., 2011).

Importantly, the formation of alt3'UTRs through APA has been reported for a multitude of additional genes, including genes known to function as major regulators of embryonic development. For instance, the *Fgf8* genes are among the most extensively studied ligands of the FGF signalling pathway, and their functions throughout development are extensive (Section I.1.3) (Pownall and Isaacs, 2010). Evidence that the post-transcriptional regulation of the *Fgf8* genes has a critical role during development comes from the observation that, in chick and mouse embryos, *Fgf8* mRNA stability is crucial for the establishment of a signalling gradient required for somite formation (Section I.1.1.2.2) (Dubrulle and Pourquié, 2004, Dubrulle et al., 2001). For the zebrafish *Fgf8* orthologue – the *fgf8a* gene – seven distinct alt3'UTRs have been reported, a number paralleled only by *fgf12b* among the other 32 Fgf ligands of the fish (Ulitsky et al., 2012, You et al., 2015). However, the post-transcriptional regulation events mediated by these *fgf8a* alt3'UTRs and their functional importance to different aspects of embryonic development have, thus far, remained unaddressed.

I.2.2 RNA binding proteins

RNA binding proteins (RBPs) have a central role in the post-transcriptional regulation of gene expression. As previously noted, RBPs typically interact with specific sequence and/or structural motifs in the mRNA molecule, which are often located in the 5' or 3' UTRs (Glisovic et al., 2008).

The interactions between RBPs and mRNAs can have a variety of regulatory outcomes. During mRNA biogenesis alternative splicing, polyadenylation, mRNA export to the cytoplasm and the subcellular localization of the mRNA are all processes which critically rely on RBPs. Furthermore, RBPs can function as regulators of mRNA stability, by either triggering the recruitment of the mRNA degradation machinery or by protecting the mRNA molecule from it. RBPs can also affect gene expression by interfering with the translation initiation process, thus regulating the efficiency of protein production. The interaction of an RBP with an mRNA molecule can also function by promoting or hindering additional interactions between the mRNA molecule and other regulatory factors. Lastly, several RBPs can recognize and interact with different regions of their target mRNA molecules, and thus contribute to more than one mechanism of post-transcriptional regulation (Glisovic et al., 2008).

The importance of RBPs to embryonic development is particularly noteworthy during the earliest stages of embryogenesis, specifically throughout the cleavage phase, prior to zygotic genome activation. During this phase, development is almost entirely reliant on maternal mRNAs and proteins. Therefore, the regulation of maternal mRNA translation and cellular localization is critical to the progression of development, with numerous RBP families having been implicated in these regulatory events (Colegrove-Otero et al., 2005). However, the importance of RBP-mediated post-transcriptional regulation to later stages of embryonic development, has only began to garner attention in recent years.

I.2.2.1 The STAR protein family

The Signal Transduction and Activation of RNA (STAR) protein family, also known as the GSG (GRP33, SAM68 and GLD-1) protein family, is one of the few families of RBPs that has been implicated in several aspects of post-MZT embryonic development. These include mesoderm invagination and spreading, muscle fiber maturation, cardiac tube formation, cardiovascular development and visceral endoderm function (Volk and Artzt, 2010, Lobbardi et al., 2011).

Members of the STAR family have been identified in various eukaryotes including zebrafish, worms, flies and mice. The STAR family can be divided into three subfamilies: Sam68 related proteins, SF-1 (*Splicing Factor 1*) related proteins and Quaking related proteins. The most well studied STAR proteins are members of the Quaking-related subfamily, specifically the murine Quaking, the *Drosophila* HOW (*Held Out Wing*) and the *C. elegans* GLD-1 (*defective in Germ Line Development*) proteins (Fig. I.5a) (Biedermann et al., 2010).

The characteristic feature of the STAR family is a highly conserved domain of approximately 200 amino acids. This domain typically consists of a maxi-KH RNA binding domain and two flanking QUA domains (QUA1 and QUA2). The only exception to this domain organization is SF-1, which lacks the QUA1 domain (Fig. I.5b) (Liu et al., 2001). The specific functions of these domains, especially the QUA2 domain, present a certain variability between STAR family members and still require further characterization (Teplova et al., 2013, Feracci et al., 2016, Chen et al., 1997). Nonetheless, in the majority of STAR proteins, the QUA1 domain appears to contribute primarily to protein dimerization, while the KH and QUA2 domains appear to contribute primarily to RNA binding (Fig. I.5b) (Beuck et al., 2010, Beuck et al., 2012, Teplova et al., 2013, Chen and Richard, 1998, Ryder et al., 2004, Meyer et al., 2010, Feracci et al., 2016, Liu et al., 2001, Chen et al., 1997, Lin et al., 1997, Daubner et al., 2014).

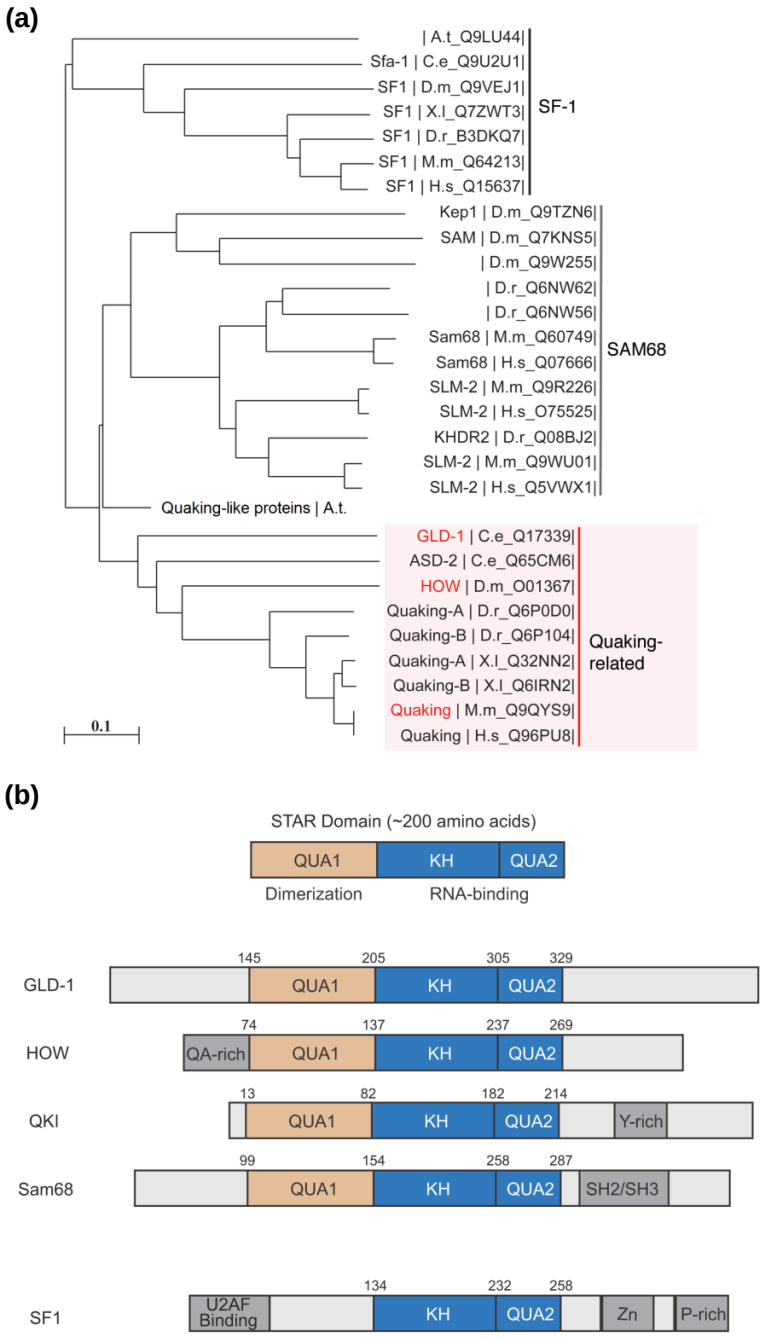

Fig. I.5 – The STAR protein family and the STAR domain.
(a) Phylogenetic tree of the STAR protein family. This family can be subdivided into three subfamilies SF-1, Sam68 and Quaking-related. The best characterized Quaking-related proteins (worm GLD-1, fly HOW and murine Quaking) are highlighted in red. Scale: relative distance; H.s, *Homo sapiens*; M.m, *Mus musculus*; X.l, *Xenopus laevis;* D.r, *Danio rerio;* D.m, *Drosophila melanogaster;* C.e, *Caenorhabditis elegans*; A.t, *Arabidopsis thaliana.* (adapted from (Biedermann et al., 2010)). **(b)** STAR domain structure for the STAR family members GLD-1, HOW, QKI, Sam68 and SF-1. The STAR domain typically consists of a maxi-KH RNA binding domain and two flanking QUA domains (QUA1 and QUA2). An exception to this organization is found in SF-1, which lacks a QUA1 domain. For most STAR proteins, the QUA1 domain (orange) contributes primarily to protein dimerization, and the KH and QUA2 domains (blue) contribute primarily to RNA binding. The approximate limits of each domain are denoted. Other notable domains are illustrated in gray (adapted from (Ryder and Massi, 2010)).

The mammalian Quaking proteins are thought to function primarily as homodimers, and several other STAR proteins appear to form homodimers as well (Chen and Richard, 1998, Beuck et al., 2012, Teplova et al., 2013, Chen et al., 1997). However, these proteins also have the capacity to form heterodimers. For instance, in mouse, the different splicing isoforms of the *Quaking I* gene, named QKI-5, QKI-6 and QKI-7 have been shown to associate with each other (Wu et al., 1999). Furthermore, the STAR proteins QKI and GLD-1 have the capacity to interact with one another, with the same being true for the GRP33 and Sam68 proteins (Chen et al., 1997). The Sam68 protein, in particular, appears to be especially prone to form heterodimers and hetero-multimers, with both STAR family members and several proteins involved in signal transduction (Di Fruscio et al., 1999, Najib et al., 2005). Lastly, the SF-1 and BBP1 (*branchpoint binding protein 1*) proteins appear to establish interactions with several proteins involved in spliceosome assembly (Rymond, 2010).

Regarding the RNA binding specificity of the STAR proteins, specific consensus binding sequences vary between individual STAR family members. However, the majority of the STAR proteins studied to date require, at minimum, the presence of an hexameric consensus sequence to bind the RNA molecule with high-affinity. For certain STAR proteins, the presence of an additional partial or full consensus sequence, either upstream or downstream of the core binding site, was proposed to provide a further contribution to high-affinity binding. A possible explanation for these bipartite binding sites is that two binding sequences may allow for both protomers of the STAR dimer to interact with the RNA molecule. The majority of STAR family proteins do not appear to exhibit secondary structure binding requirements, with the exception of the *Drosophila* HOW protein which was shown to bind a consensus sequence embedded within a loop secondary structure (Table I.1) (Feracci et al., 2014).

Table I.1 – Consensus binding sequences of STAR family proteins. Overview of the consensus RNA binding sequences reported for members of the STAR family.

Protein	Consensus		Reported by
QKI	5'-NA(A>C)U(A>>C)A-3'		(Ryder and Williamson, 2004)
	5'-NACUAA(C/U)-3' (core site) spacer:1-20nts	5'-UAA(C/U)-3' (half site)	(Galarneau and Richard, 2005) (Hafner et al., 2010)
GLD-1	5'-UACU(C/A)A-3' (conservative) 5'-(U>G>C/A)A(C>A)U(C/A>U)A-3' (relaxed)		(Ryder et al., 2004)
	5'-UACU(C/A)A-3' (core site)	5'- UAAU-3' (half site)	(Galarneau and Richard, 2009)
HOW	5'-NA(C>A)UAA-3' (embedded within a loop secondary structure)		(Israeli et al., 2007)
Sam68	5'-UAAA-3'		(Lin et al., 1997)
	5'-U(U/A)AA-3' repeats		(Galarneau and Richard, 2009)
SLM-2	5'-U(U/A)AA-3' repeats, spacer: 3-25nts		(Galarneau and Richard, 2009)
BBP, SF-1	5'-UACUAAC-3'		(Berglund et al., 1997)
SF-1	5'-UACUAAC-3'		(Peled-Zehavi et al., 2001) (Liu et al., 2001)
ASD-2	5'-UA(A>C)U(A>>C)A-3'		(Carmel et al., 2010)

I.2.2.1.1 Functions of STAR proteins in post-transcriptional regulation

The molecular functions of STAR proteins in post-transcriptional regulation are remarkably diverse, with STAR proteins having been implicated in alternative splicing, mRNA transport and localization, mRNA stability and translation efficiency (Volk and Artzt, 2010).

For instance, the mouse Quaking I proteins have been implicated in the regulation of multiple steps of mRNA metabolism in connection with brain development and myelination. The QKI-5 protein was shown to affect the splicing of the myelin-associated glycoprotein *Mag* (Wu et al., 2002). Furthermore, the QKI proteins have been associated with the regulation of the nuclear retention of the myelin basic protein (*Mbp*) mRNA and its transport to the myelinating membranes (Li et al., 2000, Larocque et al., 2002). A role was also proposed for QKI in the stabilization of the *Mbp* mRNA through an interaction with a QKI RNA-binding element (also known as a Quaking Response Element (QRE)) found in the *Mbp* 3'UTR (Zhang and Feng, 2001, Li et al., 2000). Additional targets of QKI-mediated mRNA stabilization include the Cyclin-dependent kinase (CDK)-inhibitor 1 (*p27Kip1*) and the Microtubule-

associated protein 1B (*Map1b*), which have been implicated in oligodendroglia development (Larocque et al., 2005, Zhao et al., 2006, Artzt and Wu, 2010).

A role for STAR proteins in the regulation of translation efficiency was first uncovered in *C. elegans*, when the GLD-1 protein was shown to function as a translational repressor of the sex determination gene *tra-2*, through an interaction with the *tra-2* 3'UTR (Jan et al., 1999). Later studies revealed that a similar mechanism is present in mouse, with the QKI-6 protein functioning as a translational repressor of the *tra-1* homologue *Gli1* (Lakiza et al., 2005, Saccomanno et al., 1999, Artzt and Wu, 2010).

As previously noted, the mouse Quaking I gene gives rise to different proteins formed through alternative splicing, with the most well studied being QKI-5, QKI-6 and QKI-7, which differ only in their C-terminal domains. Similarly, the *Drosophila* HOW gene also produces at least two splicing isoforms, termed HOW(L) and HOW(S), with differing C-terminal domains (Nabel-Rosen et al., 1999, Kondo et al., 1999). The HOW(L) and HOW(S) proteins are particularly noteworthy because they have been shown to mediate opposite forms of gene expression regulation, when interacting with the same 3'UTR sequence. In particular, during *Drosophila* tendon cell differentiation, the HOW proteins function by regulating the expression of two splicing isoforms of the *Stripe* gene, StripeA and StripeB, which are key factors in tendon cell specification and differentiation (Frommer et al., 1996, Volk, 1999). In immature tendon cells StripeB activates the expression of HOW(L), which in turn binds to the *Stripe* 3'UTR and promotes its degradation. This negative feedback loop is thought to ensure a reduced expression of StripeB in tendon precursors which contributes to the maintenance of the immature state (Nabel-Rosen et al., 1999, Nabel-Rosen et al., 2002). Conversely the HOW(S) protein was shown to function both by promoting the splicing of the StripeA isoform, and by binding the *Stripe* 3'UTR and protecting the mRNA from degradation. This regulation is thought to lead to a stimulation of StripeA expression which contributes to tendon cell maturation (Volohonsky et al., 2007, Nabel-Rosen et al., 2002). Therefore, the progression of *Drosophila* tendon cell differentiation appears to rely on a balance between the relative amounts of the repressor isoform, HOW(L), and the activator isoform, HOW(S). A similar regulatory mechanism was also proposed for the QKI-mediated regulation of *Krox20* expression in Schwann cells, with the QKI-5 isoform

functioning as the repressor isoform and the QKI-6 and QKI-7 isoforms functioning as the activator isoforms, in this context (Nabel-Rosen et al., 2002).

I.2.2.1.2 Functions of STAR proteins in development

STAR proteins are widely expressed during embryogenesis and have been shown to function in various developmental processes. A great deal of what is currently known about STAR protein functions came from the study of several spontaneous mutations, N-ethyl-N-nitrosourea (ENU)-induced point mutations and knockout alleles of the mouse Quaking I gene.

The viable alleles of QKI have revealed a critical role for this protein in nervous system development and function. In particular, QKI appears to be required for myelination in both the central and peripheral nervous systems. In this context, QKI has been implicated in the proliferation, differentiation and maturation of oligodendrocyte progenitor cells and Schwann cells, which are responsible for myelin formation, as well as in the actual ensheathment of axons by the specialized myelin membrane (Ehrmann et al., 2016, Bockbrader and Feng, 2008, Volk and Artzt, 2010).

However, from a developmental standpoint, the QKI ENU-induced alleles and knockout allele have proven more informative. Specifically, the diverse range of phenotypes observed using these alleles include impaired vascular development, heart defects, abnormal somites, disorganized anterior-posterior axis, defects in neural tube development, cranial abnormalities and defects in smooth muscle cell differentiation (Justice and Bode, 1988, Cox et al., 1999, Li et al., 2003b, Noveroske et al., 2002, Bohnsack et al., 2006, Justice and Hirschi, 2010).

I.2.2.1.2.1 STAR proteins in cardiovascular development

During embryogenesis STAR proteins, and the mouse QKI protein in particular, have been shown to function as critical regulators of cardiovascular development. The importance of QKI to cardiovascular development is best illustrated in the

mouse ENU-induced point mutations, qk^{l-1} and qk^{k2} and the qkI knockout deletion allele, as these alleles when homozygous, cause embryonic death at mid gestation from apparent cardiovascular failure (Noveroske et al., 2002, Bohnsack et al., 2006, Li et al., 2003b, Justice and Hirschi, 2010).

To a considerable extent, the vascular insufficiency observed under QKI depletion appears to stem from defects in yolk sac and embryonic vascular remodelling. These defects have been partially attributed to compromised visceral endoderm function. The visceral endoderm of the extraembryonic yolk sac is required for the production of junctional proteins, serum proteins, metabolic enzymes and growth factors that modulate vascular development (Bohnsack and Hirschi, 2004). QKI appears to function in this context by regulating visceral endoderm function through the modulation of local retinoic acid synthesis and the subsequent control of endothelial cell proliferation, matrix production, and visceral endoderm survival (Bohnsack et al., 2006). In addition, QKI was proposed to promote vascular remodelling by controlling the recruitment and/or differentiation of smooth muscle cells, which are required for the stabilization of the blood vessel structures and modulation of their functions (Li et al., 2003b).

Furthermore, analysis of the QKI ENU and knockout alleles revealed morphological defects in the heart, specifically enlarged hearts, less compact hearts, pericardial effusion and defects in the outflow tract (Justice and Hirschi, 2010, Cox et al., 1999, Justice and Bode, 1988, Noveroske et al., 2002, Li et al., 2003b). Consistent with these observations, QKI5 protein expression was detected in the endocardium of the common atrium, outflow tract and sinus venosus of the developing mouse heart (Justice and Hirschi, 2010). However, the precise role of QKI in heart development requires further elucidation, especially considering that in qk^{k2} homozygous mutants, cardiac differentiation and myocardial contractile function do not appear to be compromised, despite the morphological abnormalities observed (Noveroske et al., 2002).

A role for STAR proteins in heart development was also identified in *Drosophila*, with HOW mutant embryos displaying a reduced heart beat rate, weakened myocardial contractile function and defects in cardiac dorsal vessel morphology (Baehrecke, 1997, Zaffran et al., 1997). HOW has been shown to be part of the

genetic pathway that controls cardiac lumen formation during heart tube morphogenesis, together with the extracellular matrix protein *Slit*, its receptor *Roundabout* and *Dystroglycan* (Medioni et al., 2008). In addition, a recent study raised the possibility that HOW may also function in this context by modulating the expression of genes involved in muscle sarcomerization (Nir et al., 2012).

Lastly, the zebrafish Quaking A (*qkia*), the *Xenopus* Quaking (*Xqua*) and the mouse Sam68 genes are expressed in the developing heart, however their potential contributions to cardiac development and function have not been assessed (Tanaka et al., 1997, Zorn and Krieg, 1997, Richard et al., 2005, Thisse et al., 2001).

Taken together these studies indicate that STAR proteins are likely important contributors to both vascular development and heart development. However, the specific targets and functions of these proteins in heart development remain largely unknown, especially in vertebrate models.

I.2.2.1.2.2 STAR proteins in mesoderm and muscle development

In addition to the previously discussed importance of STAR proteins to cardiac development these proteins have also been implicated in several other aspects of mesoderm establishment and differentiation, including the formation of this germ layer during gastrulation, the formation of the somites and the differentiation of muscle cells.

In the *Drosophila* gastrula, the HOW protein has a critical role in the morphogenetic processes underlying the formation of the mesoderm germ layer, with embryos lacking both maternal and zygotic HOW exhibiting defects in mesoderm invagination and spreading. During the mesoderm invagination process HOW was proposed to function by facilitating the mRNA turnover of the mitotic activator *String* (also known as Cell division control 25 (Cdc25)). This inhibition of *String* contributes to the temporary arrest of mesodermal cell divisions, which is required to ensure that the invagination process proceeds in a timely and synchronized manner (Nabel-Rosen et al., 2005, Grosshans and Wieschaus, 2000). During the subsequent mesoderm spreading process HOW was shown to function by inhibiting the stability of the mRNA of several genes, including *falten*, *lap* and *miple1*. The repression of *miple1*

expression in particular, is thought to contribute to correct mesoderm spreading by restricting the domain of MAPK activation to the most dorsal row of mesodermal cells (Toledano-Katchalski et al., 2007).

The mouse QKI ENU mutant alleles also revealed an apparent role for QKI in somite formation. In particular, abnormal somites and the absence of somites have been reported in connection with the qk^{k2}, qk^{kt1} and qk^{kt4} alleles (Justice and Bode, 1988, Cox et al., 1999). In addition, the zebrafish *qkia* gene is expressed in the PSM and in the somites, however a potential involvement of this gene in PSM differentiation and somitogenesis has not been explored (Tanaka et al., 1997, Thisse et al., 2001). Taken together these observations argue in favour of a potential role for Quaking proteins in vertebrate somitogenesis, which requires further investigation.

Lastly, studies in zebrafish, *Drosophila* and mouse have revealed a prominent contribution of STAR proteins to the process of somatic muscle development. In zebrafish, loss of *qkia* function leads to defects in fast muscle fiber maturation as well as HH-induced muscle derivative specification and morphogenesis. In this context Qkia was proposed to function, at least in part, by positively regulating *gli2a* expression through an interaction with the *gli2a* 3'UTR (Lobbardi et al., 2011). Furthermore, the zebrafish Qkia and Qkic proteins were shown regulate the early steps of myofibril assembly by interacting with the 3'UTR of *tropomyosin-3* and promoting the accumulation of its mRNA (Bonnet et al., 2017).

In *Drosophila*, the HOW protein has been implicated in the late stages of somatic muscle development. In particular, flies that lack HOW function present defects indicative of a function for this gene in myotube migration and/or myotube attachment to the epidermis, during both the embryogenesis and metamorphosis phases (Baehrecke, 1997, Zaffran et al., 1997). Additional studies revealed that HOW contributes to muscle sarcomerization, at least in part, by targeting the *sallimus* (*kettin/D-titin, sls*) gene in a phosphorylation-dependent manner (Schnorrer et al., 2010, Nir et al., 2012).

Studies in cultured mouse myoblasts have also shown that QKI functions as a global regulator of splicing during myoblast differentiation. In this context, the splicing regulatory network of QKI overlaps considerably with that of the PTB (polypyrimidine tract-binding) protein, suggesting that these two regulators are critical players in

establishing the gene expression programs associated with muscle cell differentiation (Hall et al., 2013).

In conclusion, STAR proteins appear to exhibit crucial roles in embryonic development, with these functions being particularly noteworthy in regard to the development of mesoderm derivatives. However, the full extent and mechanistic nature of these roles is still largely unknown, with potential functions for the Quaking proteins in developmental processes such as cardiac development and somite formation requiring further elucidation.

I.3 THE GOAL OF THIS THESIS

Embryonic development is critically reliant on well-defined spatial and temporal gene expression patterns. Precise control of gene expression is often achieved through post-transcriptional regulation mechanisms, which are frequently mediated by RBPs and/or 3'UTR sequences. However, the specific functional impact of these post-transcriptional regulation mechanisms on the different processes that take place in the developing embryo still requires further investigation.

In particular, the STAR RBPs appear to contribute to developmental processes such as cardiac development and somite formation however, the full extent and mechanistic aspects of these roles are still largely unknown (Section I.2.2.1.2). Furthermore, alternative 3'UTR production through APA is a remarkably prevalent phenomena during embryogenesis, with major developmental regulators such as the *fgf8a* gene producing several alternative 3'UTRs. However, the post-transcriptional regulation events mediated by these *fgf8a* alt3'UTRs and their functional importance to different aspects of embryonic development have, thus far, remained unaddressed (Sections I.2.1.2 and I.2.1.3).

The main goal of the present work was to investigate two specific facets of the post-transcriptional regulation program that operates during embryogenesis, namely:

- The roles of the zebrafish STAR protein Quaking A in the processes of somite formation and heart development.
- The functions of the alternative 3'UTRs of the zebrafish *fgf8a* gene during embryogenesis.

Our investigation of Quaking A involved both loss-of-function and gain-of-function approaches and a subsequent analysis of the resulting effects on the aforementioned developmental processes. As detailed in Chapter II, our results revealed an unexpected role for this RBP in the establishment of the laterality of the heart and visceral organs.

As detailed in Chapter III, our assessment of the *fgf8a* alternative 3'UTRs functions was based on a morpholino-mediated interference with the APA process, which produced a temporally and spatially selective impact on the late development of the

anterior sensory system. Furthermore, this analysis led to the identification of a novel role for the Fgf signalling pathway in superficial retinal vascularization.

CHAPTER II

The RNA binding protein Quaking A is involved in the establishment of internal organ laterality

Sara F. Fernandes, Dalila Silva, José Leitão, Rita Pinto, Rita Fior, Margarida Gama-Carvalho and Leonor Saúde

D.S. performed the experiments and analysed the data pertaining to the cardiac laterality of *cdh11* mutants (Fig. II.6c,f) and the expression of laterality markers in *cdh11* morphants (Fig. II.7).

J.L. performed the experiments and analysed the data pertaining to the gut laterality of *cdh11* mutants (Fig. II.6i) and the assessment of *cdh11* expression in FACS sorted *sox17*:GFP cells (Fig. II.8h-j).

R.P. performed the WISHs shown in Fig. II.3 and several WISHs for *myl7* during the course of this work.

S.F.F., R.P. and D.S. contributed to the assessment of the *cdh11* expression pattern by WISH (Fig. II.8a-g).

S.F.F. performed the remaining experiments and data analysis and wrote this chapter.

S.F.F., R.F., M.G-C. and L.S. conceived the project and contributed to the analysis and interpretation of the data.

II.1 INTRODUCTION

RNA binding proteins (RBPs) have a central role in the post-transcriptional regulation of gene expression. These proteins typically interact with specific sequence motifs in the mRNA, often located in the 5' or 3' untranslated regions (UTR), and can influence mRNA biogenesis, stability, translation, transport and cellular localization (Glisovic et al., 2008).

The importance of RBPs to embryonic development is particularly remarkable during the cleavage phase, prior to zygotic genome activation. During this phase, development is almost entirely reliant on the regulation of maternal mRNA translation and cellular localization, with several RBPs having been identified as major regulators of these mechanisms (Colegrove-Otero et al., 2005). However, the importance of post-transcriptional regulation to later stages of development has only began to garner attention in recent years, with the contribution of RBPs to these later processes remaining poorly understood.

The process of somite formation, in particular, is thought to be especially reliant on a tight post-transcriptional regulation of mRNA stability. Somite formation (also known as somitogenesis) is governed by two mechanisms – a molecular clock and a wavefront of differentiation (Dequéant and Pourquié, 2008). The clock is composed of cyclically expressed genes, with current models postulating that these genes need to be unstable at the mRNA level to produce sustained transcriptional oscillations (Lewis, 2003). Conversely, the wavefront is partially established by an FGF8 gradient, which stems from the slow degradation of the *Fgf8* mRNA (Dubrulle and Pourquié, 2004). Nonetheless, little is known about the post-transcriptional mechanisms that operate during somitogenesis (Gallagher et al., 2017, Riley et al., 2013, Wahi et al., 2017).

One RBP family which could be involved in the post-transcriptional regulation of somitogenesis is the Signal Transduction and Activation of RNA (STAR) family. Members of this family have been implicated in mesoderm invagination and spreading in *Drosophila*, as well as somatic muscle development in zebrafish, *Drosophila* and mouse (Volk and Artzt, 2010, Lobbardi et al., 2011, Bonnet et al.,

2017, Baehrecke, 1997, Zaffran et al., 1997, Hall et al., 2013). Furthermore, both abnormal somites and the absence of somites have been reported in connection with the qk^{k2}, qk^{kt1} and qk^{kt4} mutant alleles of the mouse STAR family member Quaking I (QKI) (Justice and Bode, 1988, Cox et al., 1999). Lastly, the zebrafish QKI orthologue – *quaking a* (*qkia*) – is expressed in the presomitic mesoderm (PSM) and in the somites during somitogenesis stages, however a potential function for this gene in somite formation has not been addressed (Thisse et al., 2001). Taken together, these studies point to a potentially significant but as of yet unexplored role for STAR proteins in the post-transcriptional regulation of somite formation.

In addition, several lines of evidence point to an important role for STAR family members, like the mouse QKI and the *Drosophila* HOW (*Held Out Wing*) proteins, in the development of another mesoderm derivative, the heart. In particular, mouse QKI mutants display morphological defects in the heart, namely enlarged hearts, less compact hearts, pericardial effusion and defects in the outflow tract (Justice and Hirschi, 2010, Cox et al., 1999, Justice and Bode, 1988, Noveroske et al., 2002, Li et al., 2003b). Furthermore, *Drosophila* HOW mutant embryos display a reduced heart beat rate, weakened myocardial contractile function and defects in cardiac dorsal vessel morphology (Baehrecke, 1997, Zaffran et al., 1997). The HOW protein in particular, has been associated with the genetic pathway that controls cardiac lumen formation during heart tube morphogenesis, which could partially account for the observed mutant phenotypes (Medioni et al., 2008). Lastly, the mouse STAR protein Sam68, the zebrafish *qkia* gene and the *Xenopus quaking* (*Xqua*) gene are all expressed in the developing heart, however their contributions to cardiac development and function have not been assessed (Tanaka et al., 1997, Zorn and Krieg, 1997, Richard et al., 2005, Thisse et al., 2001). Overall, despite these strong indicators of an important role for STAR proteins in cardiac development, the specific targets and specific functions of these proteins in the process of cardiac morphogenesis remain largely unknown, especially in vertebrate models.

In this chapter, we conducted a functional study of the zebrafish *qkia* gene, specifically focusing on a potential role for this gene in the processes of somitogenesis and heart development. It is important to note that the zebrafish *qkia* gene is expected to produce two protein isoforms– Qkia1 and Qkia2 – as a result of alternative splicing, however, their specific functions and individual expression

patterns remain to be elucidated (Lobbardi et al., 2011). In this study, we resorted to gain-of-function and loss-of-function approaches that target both isoforms. For purposes of discussion, these isoforms will be collectively referred to as the Qkia protein.

Even though we found no clear evidence to support a role for *qkia* in the somitogenesis process, our results indicate that *qkia* appears to be involved in the establishment of posterior body morphology. In addition, we identified an unexpected function for *qkia* in heart development, namely in the establishment of heart tube laterality. Further analysis led to the observation that both Qkia depletion and overexpression potentiate a disruption of visceral organ laterality, which is strongly indicative of a role for this gene in the mechanisms of Left-Right patterning and internal organ laterality establishment.

The current paradigm of organ laterality establishment postulates that this process is initiated by motile cilia present in the Kupffer's Vesicle (KV). These cilia rotate in a counter-clockwise manner creating a leftward extracellular fluid flow that promotes a left-side specific activation of Nodal signalling. Asymmetric Nodal signalling in the KV functions as a laterality signal which is transmitted to the lateral plate mesoderm (LPM) and induces asymmetric Nodal signalling in the LPM. This in turn is thought to determine the correct lateral positions of the visceral and cardiac organs (Grimes and Burdine, 2017). Our results indicate that *qkia* is likely to function in this process at the level of laterality signal transmission from the KV to the LPM.

As a post-transcriptional regulator, Qkia is expected to function in development by modulating the expression of its target transcripts. Therefore, we also sought to identify candidate targets of *qkia*, which could act as mediators of its roles in embryogenesis. In this context, we identified the adhesion molecule Cadherin 11 (Cdh11), as a potential target of Qkia-mediated post-transcriptional regulation, with our results also indicating that *cdh11* has a role in the establishment of organ laterality.

II.2 RESULTS

II.2.1 *qkia* knockdown leads to defects in posterior body morphology

To assess the functional importance of *qkia* to embryonic development we resorted to a translation blocking morpholino oligo (*qkia*$^{ATG\text{-}MO}$). This morpholino is expected to induce a knockdown of both *qkia* splicing isoforms - *qkia1* and *qkia2* (Fig. II.M1a,b) and was co-injected into 1-cell stage wildtype embryos with a morpholino against *p53* (*p53*^{MO}) to counteract the pro-apoptotic effects of the *qkia*$^{ATG\text{-}MO}$.

To address a potential role for *qkia* in the somitogenesis process we began by analysing the effects of Qkia depletion on somite morphology through live imaging. In morphant embryos, we observed a mediolateral enlargement (29µm, equivalent to 29%, Fig. II.1a) and an anterior-posterior shortening (29µm, equivalent to 15%, Fig. II.1a) of the somites, relative to control embryos. These results indicate that the knockdown of *qkia* leads to a disruption of somite morphology. We next sought to determine if these morphological abnormalities were restricted to the somites, or rather reflected a more widespread disruption of the overall shape of the posterior body. To address this, we evaluated the impact of Qkia depletion on PSM morphology by performing triple Whole-Mount *In Situ* Hybridization (WISH) for the somite marker *myoD*, the wavefront marker *mesp-ab* and the tailbud progenitor marker *tbx16* (Fig. II.1b). We observed that *qkia* morphants also displayed a mediolateral enlargement (87µm, equivalent to 28%, Fig. II.1b) and an anterior-posterior shortening (46µm, equivalent to 13%, Fig. II.1b) of the PSM relative to control embryos. These results show that Qkia depletion does not lead to a somite-specific phenotype, but instead leads to an overall disruption of the shape of the posterior body. This in turn indicates that *qkia* is likely to be involved in the morphogenetic processes that define the shape of the caudal region of the embryo.

The morphogenetic events that define posterior body shape are thought to begin during the gastrulation phase, as a result of convergence and extension movements, and carry through into the somitogenesis phase via the process of

posterior body elongation (Yin et al., 2009, Kanki and Ho, 1997, Solnica-Krezel, 2005).

To determine if Qkia depletion disrupted the gastrulation process, we examined the position and shape of the prechordal plate relative to the anterior edge of the neural plate, and the length and width of the notochord, at bud stage. These features were assessed by performing WISHs for the notochord marker *ta,* the neural plate marker *dlx3* and the prechordal plate marker *ctslb* (Fig. II.1c,d). We observed no clear difference in prechordal plate position or notochord morphology between *qkia* morphants and control embryos (Fig. II.1c,d.). Therefore, these results indicate that Qkia depletion does not disrupt convergence and extension, and consequently that the *qkia* gene is more likely to contribute to the establishment of posterior body shape by influencing the process of posterior body elongation.

In conclusion, we found no clear evidence to support a specific role for *qkia* in the somitogenesis process, with our results indicating that *qkia* is more likely to function in the establishment of caudal morphology by contributing to posterior body elongation.

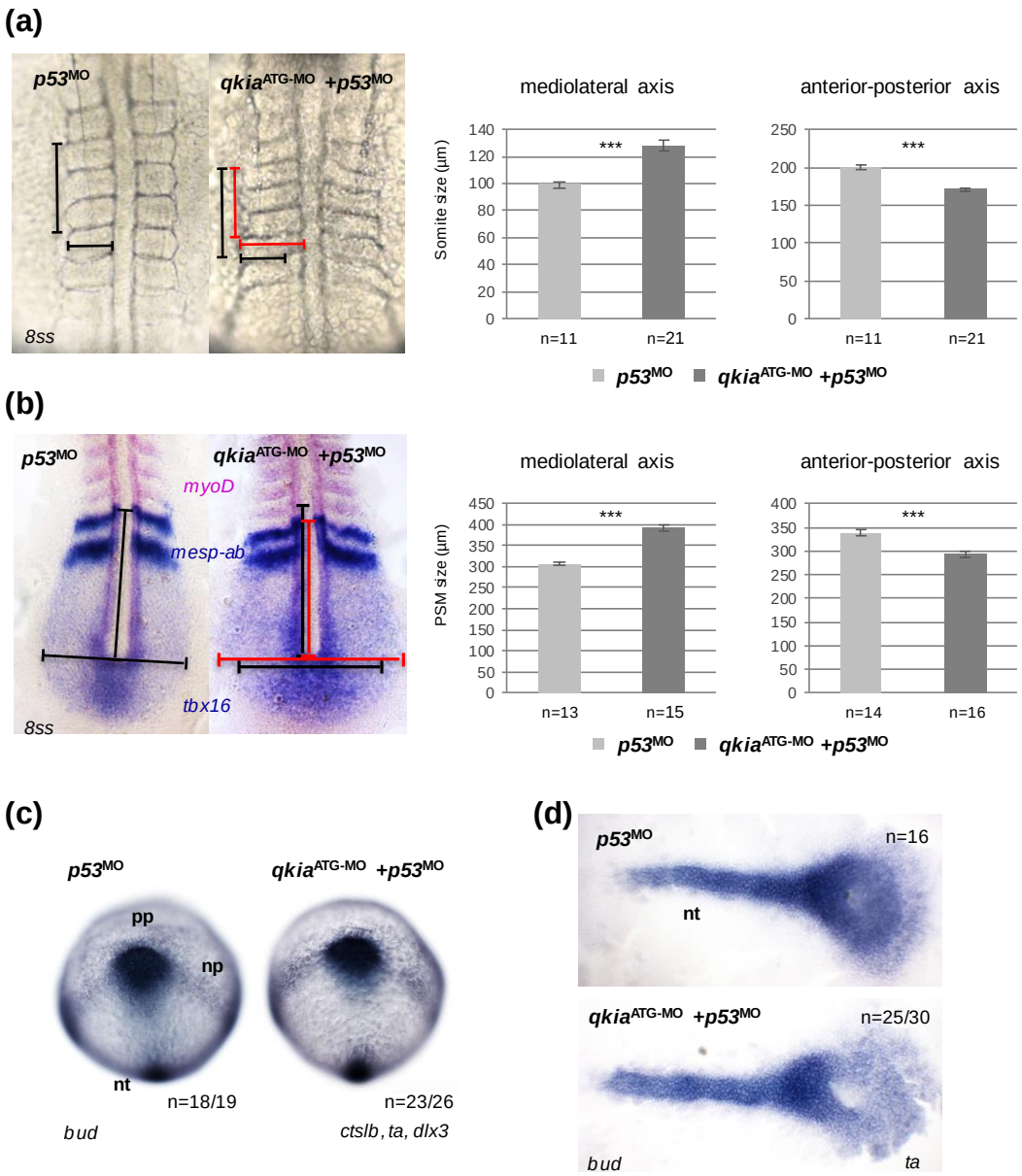

Fig. II.1 – *qkia* knockdown affects posterior body morphology.
(a) Analysis of mediolateral and anterior-posterior somite size in live *qkia* morphants and control embryos at the 8 ss. Anterior-posterior measurements correspond to the combined length of somites 3 to 5 and mediolateral measurements correspond to the width of somite 6, as illustrated. **(b)** Analysis of mediolateral and anterior-posterior PSM size in *qkia* morphants and control embryos following triple WISH for *myoD, mesp-ab* and *tbx16* at the 8 ss. Anterior-posterior measurements correspond to the distance between the anterior stripe of *mesp-ab* expression and the posterior edge of the notochord, identified through *tbx16* and *myod* expression. Mediolateral measurements were performed at the posterior edge of the notochord, as illustrated. **(a,b)** Data shows mean size ± SEM. Statistical analysis was done using Student's t-test (***p<0.001). **(c)** Triple WISH for *ctslb, ta* and *dlx3* in bud stage *qkia* morphant and control embryos. Showing the position of the prechordal plate (pp), through *ctslb* expression, the anterior border of the neural plate (np), through *dlx3* expression, and the relative position of the notochord (nt), through *ta* expression. **(d)** WISH for *ta* in bud stage *qkia* morphant and control embryos, showing the width and length of the notochord.

II.2.2 *qkia* is involved in Left-Right patterning

We next set out to determine if the *qkia* gene is involved in cardiac development, by conducting WISHs for the cardiac marker *myl7* in *qkia* morphant embryos. Interestingly the results obtained were not indicative of defects in heart tube formation, but instead revealed a disruption of the lateral placement of the heart tube. In particular, in control conditions zebrafish heart tubes display a left jog at 30 hpf and a dextral loop at 48 hpf, whereas in *qkia* morphants 57% of the embryos displayed unjogged hearts and 34% displayed unlooped hearts (Fig. II.2a,b,e,f). Similar looping defects were observed when using a previously described *qkia*^{t31954} mutant line ((Lobbardi et al., 2011) and Fig. II.M1a,b), with 27% of homozygous *qkia* mutant embryos displaying unlooped hearts (Fig. II.2a,c). These results indicate that *qkia* is required for the establishment of cardiac laterality.

To determine if this requirement for *qkia* in laterality establishment was restricted to the heart or extended to other asymmetric internal organs, the lateral positions of the liver and pancreas were evaluated in *qkia* morphants and control embryos, using a *sox17*:GFP transgenic line, which labels endoderm-derived organs.

In *qkia* morphants we observed that the lateral positions of the liver and pancreas were reversed in a small percentage of embryos (19%), at 48 hpf. Specifically, the liver was positioned on the right side and the pancreas on the left, in contrast with the control situation where the liver was on the left and the pancreas on the right (Fig. II.2h,i). This phenotype was rescued by the co-microinjection of the *qkia*$^{ATG\text{-}MO}$ with *in vitro* synthesised RNA coding for the *qkia2* isoform of the *qkia* gene (Fig. II.2h,j). These results indicate that *qkia* is also required for the establishment of liver and pancreas laterality.

To determine if an overexpression of *qkia* would be sufficient to bring about laterality defects, we microinjected zebrafish embryos, at the 1-cell stage, with *in vitro* synthesised RNA coding for both Qkia splicing isoforms – *qkia1* and *qkia2* – and evaluated the resulting effects on organ laterality.

In the *qkia* overexpression context, we observed the same heart tube laterality defects encountered in *qkia* morphants but in a lower percentage of embryos (7%

unlooped; 13% unjogged) (Fig. II.2a,d,e,g). In addition, following *qkia* overexpression the lateral positions of the liver and pancreas were affected in a similar manner to that observed in the morphant situation, with 14% of *qkia* overexpressing embryos displaying reversed liver and pancreas positions (Fig. II.2h,k).

Taken together these results indicate that *qkia* is involved in the establishment of internal organ laterality, with both Qkia depletion and overexpression leading to laterality defects in the heart, liver and pancreas.

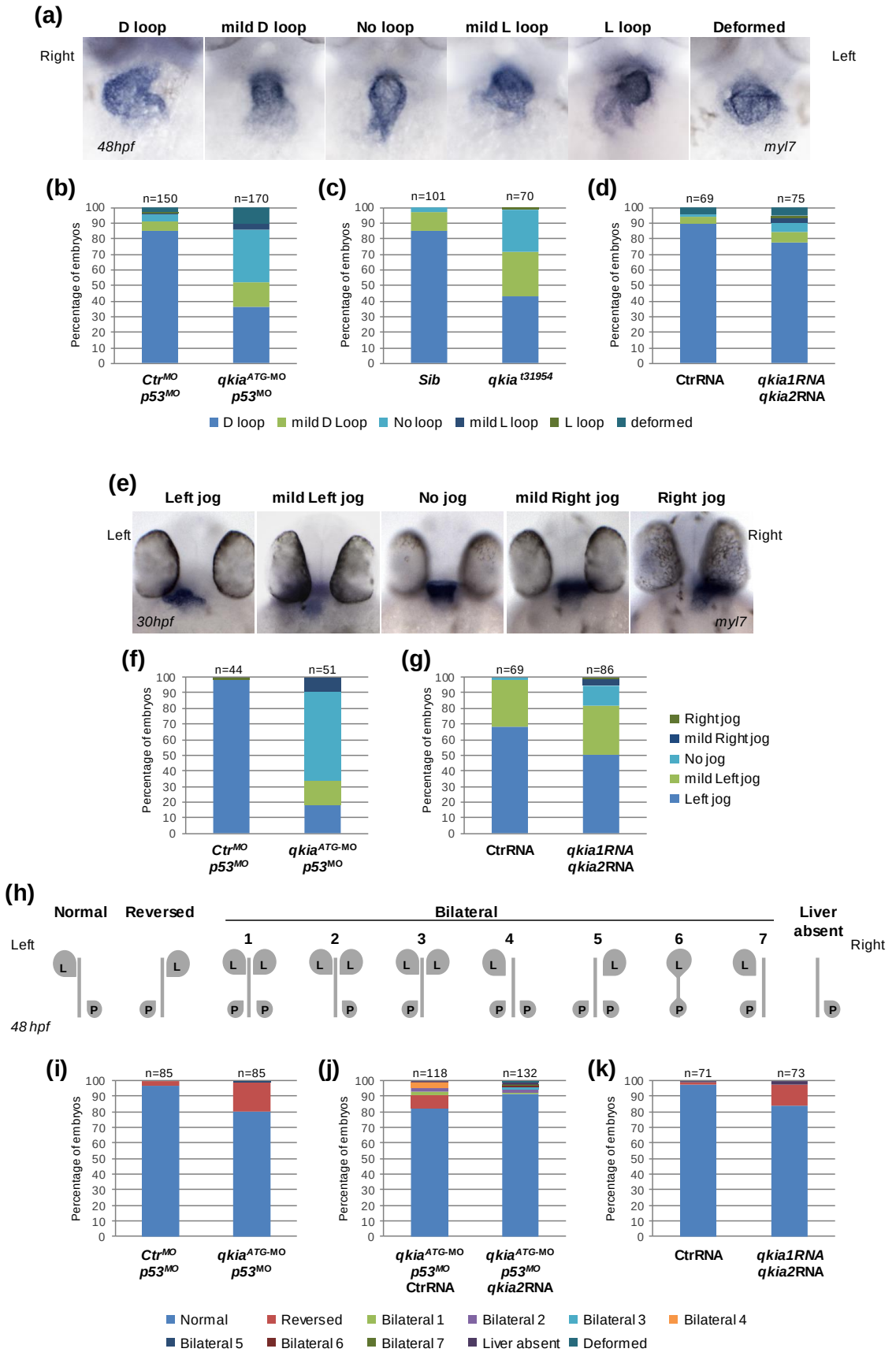

Fig. II.2 – *qkia* loss-of-function and gain-of-function affect organ laterality.
(Figure legend on the next page)

Fig. II.2 – *qkia* loss-of-function and gain-of-function affect organ laterality.
(a) Ventral views of representative embryos illustrating the different heart laterality phenotypes observed at 48 hpf after WISH for *myl7*. **(b-d)** Quantification of the heart laterality phenotypes observed under **(b)** *qkia* knockdown conditions (*qkia*$^{ATG\text{-}MO}$ *p53*^{MO}), **(c)** *qkia* mutant conditions (*qkia*^{t31954}*)* and **(d)** *qkia* gain-of-function conditions (*qkia1*RNA *qkia2*RNA). The respective control conditions are indicated. **(e)** Dorsal views of representative embryos illustrating the different heart laterality phenotypes observed at 30 hpf after WISH for *myl7*. **(f,g)** Quantification of the heart laterality phenotypes observed under **(f)** *qkia* knockdown conditions (*qkia*$^{ATG\text{-}MO}$ *p53*^{MO}), **(g)** *qkia* gain-of-function conditions (*qkia*1RNA *qkia*2RNA). The respective control conditions are indicated. **(h)** Schematic representation of the different phenotypes observed regarding the laterality of the Liver (L) and Pancreas (P). Organ laterality was assessed in *sox17*:GFP embryos at 48 hpf. **(i-k)** Quantification of the liver and pancreas laterality phenotypes observed under **(i)** *qkia* knockdown conditions (*qkia*$^{ATG\text{-}MO}$ *p53*^{MO}), **(j)** *qkia* knockdown rescue conditions (*qkia*$^{ATG\text{-}MO}$ *p53*^{MO} *qkia2*RNA) and **(k)** *qkia* gain-of-function conditions (*qkia1*RNA *qkia2*RNA). The respective control conditions are indicated.

To determine if the observed organ laterality defects derived from a disruption of asymmetric Nodal signalling, we analysed the expression of the Left-Right patterning genes *spaw*, *pitx2* and *dand5* in *qkia* morphants. Our results show that the majority of morphant embryos did not express the left side specific LPM gene *pitx2* (54%), with an additional 11% displaying bilateral *pitx2* expression and 15% expressing *pitx2* on the right LPM (Fig. II.3a). In addition, *spaw* left side specific LPM expression was completely absent in the morphants, however *spaw* expression in the KV did not appear to be affected by *qkia* knockdown (Fig. II.3b). The expression of *dand5* in the KV was mostly unaffected in *qkia* morphants which exhibited only a slight tendency for asymmetric left side expression, unlike control embryos which expressed *dand5* primarily on the right side of the KV between the 8 and 10 somite stages (Fig. II.3c). These results indicate that Qkia depletion affects Left-Right patterning gene expression primarily in the LPM, with the establishment of early asymmetric cues in the KV being largely unaffected.

In conclusion, our results indicate that *qkia* is involved in the establishment of liver, pancreas and heart laterality, and is likely to affect Left-Right patterning at the level of asymmetric signal transmission from the KV to the LPM.

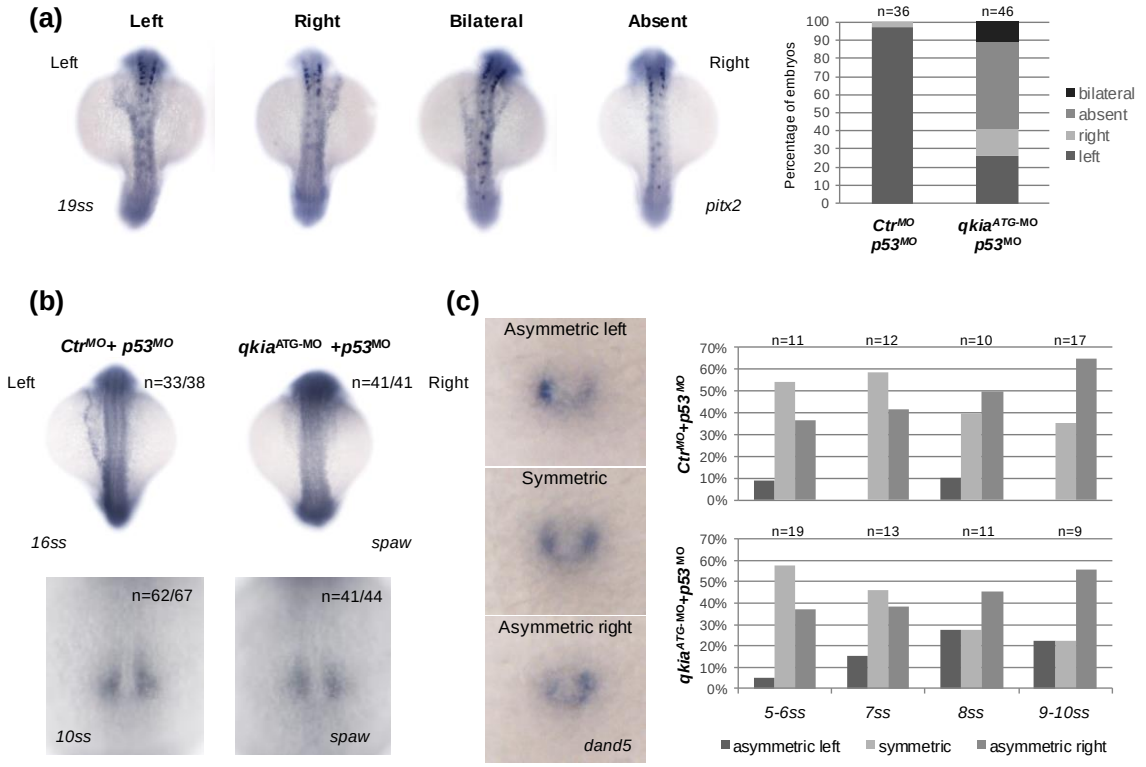

Fig. II.3 – Expression of Left-Right patterning genes is affected in *qkia* morphants.
(a) WISH analysis of *pitx2* expression in the lateral plate mesoderm of 19 ss control and *qkia* morphant embryos. **(b)** WISH analysis of *spaw* expression in control and *qkia* morphant embryos, in the LPM at the 16 ss and in the KV at the 10 ss. **(c)** WISH analysis of *dand5* expression in the KV of control embryos and *qkia* morphants at the 5-6, 7, 8 and 9-10 somite stages.

II.2.3 *cdh11* - a candidate target of Qkia-mediated post-transcriptional regulation

To further dissect the role of *qkia* in embryonic development we set out to identify a candidate target of Qkia-mediated post-transcriptional regulation, which could act as a mediator of one or more of its developmental functions.

The adhesion molecule Cdh11 was considered as a good candidate target of Qkia for the following reasons. Firstly, zebrafish *cdh11* morphant embryos were reported to have somite morphology defects which resembled those observed in *qkia* morphants ((Clendenon et al., 2009) and Fig. II.1a). Secondly, the zebrafish *cdh11* gene has been implicated in the process of otolith formation in the developing inner ear ((Clendenon et al., 2009) and Fig. II.4b), a process which we also found to be

affected by *qkia* knockdown (Fig. II.4a). Thirdly, the mouse QKI protein was previously shown to interact with the 3'UTR of the murine *Cdh11* (Galarneau and Richard, 2005). Lastly, we identified two sequence motifs near identical to the mouse QKI binding motif – termed Quaking Response Element (QRE) (Galarneau and Richard, 2005) – in the 3'UTR of the zebrafish *cdh11* gene (Fig. II.5a).

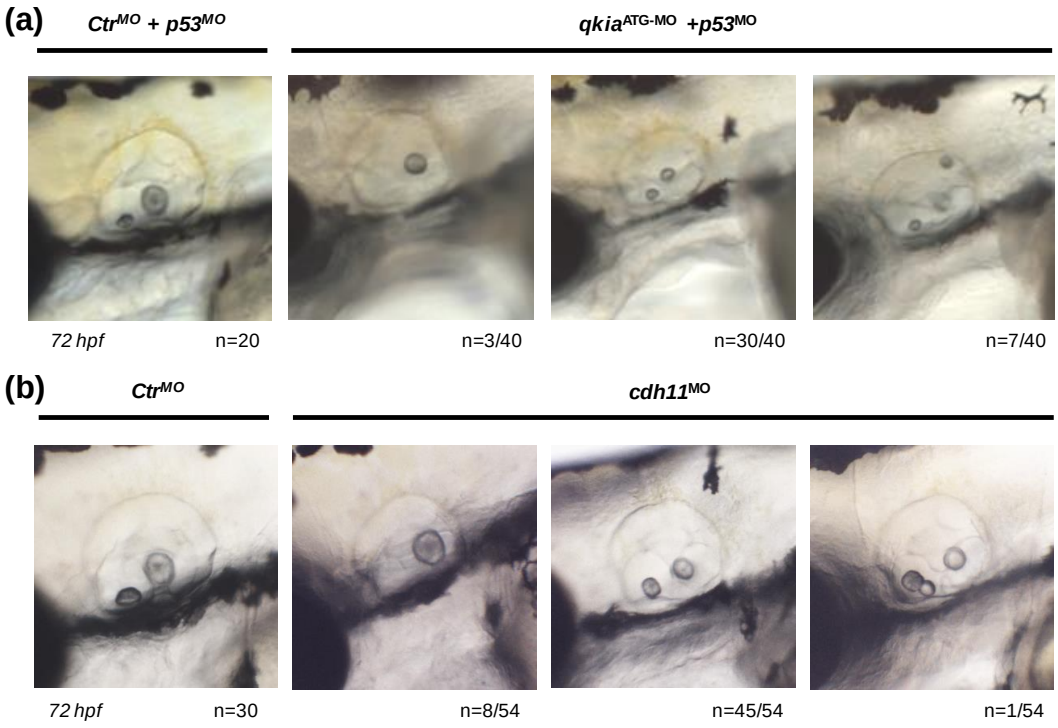

Fig. II.4 – *qkia* knockdown and *cdh11* knockdown affect otolith formation.
(a,b) Representative images of the number of otoliths formed at 72 hpf in **(a)** *qkia* morphants (*qkia*$^{ATG\text{-}MO}$ *p53*^{MO}), **(b)** *cdh11* morphants (*cdh11*^{MO}), and in the respective control conditions.

To determine if Qkia could act as a post-transcriptional regulator of *cdh11* we began by assessing the effects of Qkia depletion on the expression of an eGFP reporter fused to the 3'UTR of *cdh11*. Reporter transcripts, termed *eGFP-cdh113'UTR*, were produced by *in vitro* transcription and co-injected into 1-cell stage zebrafish embryos, with either control or *qkia*$^{ATG\text{-}MO}$. mCherry mRNA was used as an injection control and the resulting mean fluorescence intensities were measured at 15 hours post-injection (hpi) (Fig. II.5b). In this context, we observed that Qkia depletion led to an increase in eGFP expression, suggesting that Qkia could act as post-transcriptional repressor of *cdh11* through interactions with its 3'UTR (Fig. II.5c).

To determine if the previously observed effect was mediated by direct interactions between Qkia and the QREs identified in the *cdh11* 3'UTR, we resorted to site-directed mutagenesis to modify the *eGFP-cdh113'UTR* reporter. The two core QRE sites were removed from the *cdh11* 3'UTR, and the resulting reporter was termed *eGFP-cdh113'UTR_QREdel*. The expression of this reporter under Qkia depletion conditions was assessed as described previously (Fig. II.5b). We observed that the increase in reporter expression brought about by Qkia depletion was not abolished by the removal of the QREs from the 3'UTR (Fig. II.5d). This indicates that the effect of Qkia on reporter expression does not rely on the QRE binding motifs, and therefore, that Qkia is unlikely to interact directly with the QREs identified in the 3'UTR of *cdh11*.

We performed an additional set of reporter experiments with the *eGFP-cdh113'UTR* reporter under *qkia* overexpression conditions, to determine if an increase in Qkia levels was sufficient to repress reporter expression (Fig. II.5e). We did not detect a significant difference in reporter fluorescence between the control and *qkia* overexpression conditions (Fig. II.5f), suggesting that other factors may be involved in this regulation.

Taken together our results indicate that Qkia may act as a negative post-transcriptional regulator of *cdh11*. However, this regulation does not appear to be mediated by the QREs identified in the *cdh11* 3'UTR and is likely to involve additional regulatory factors.

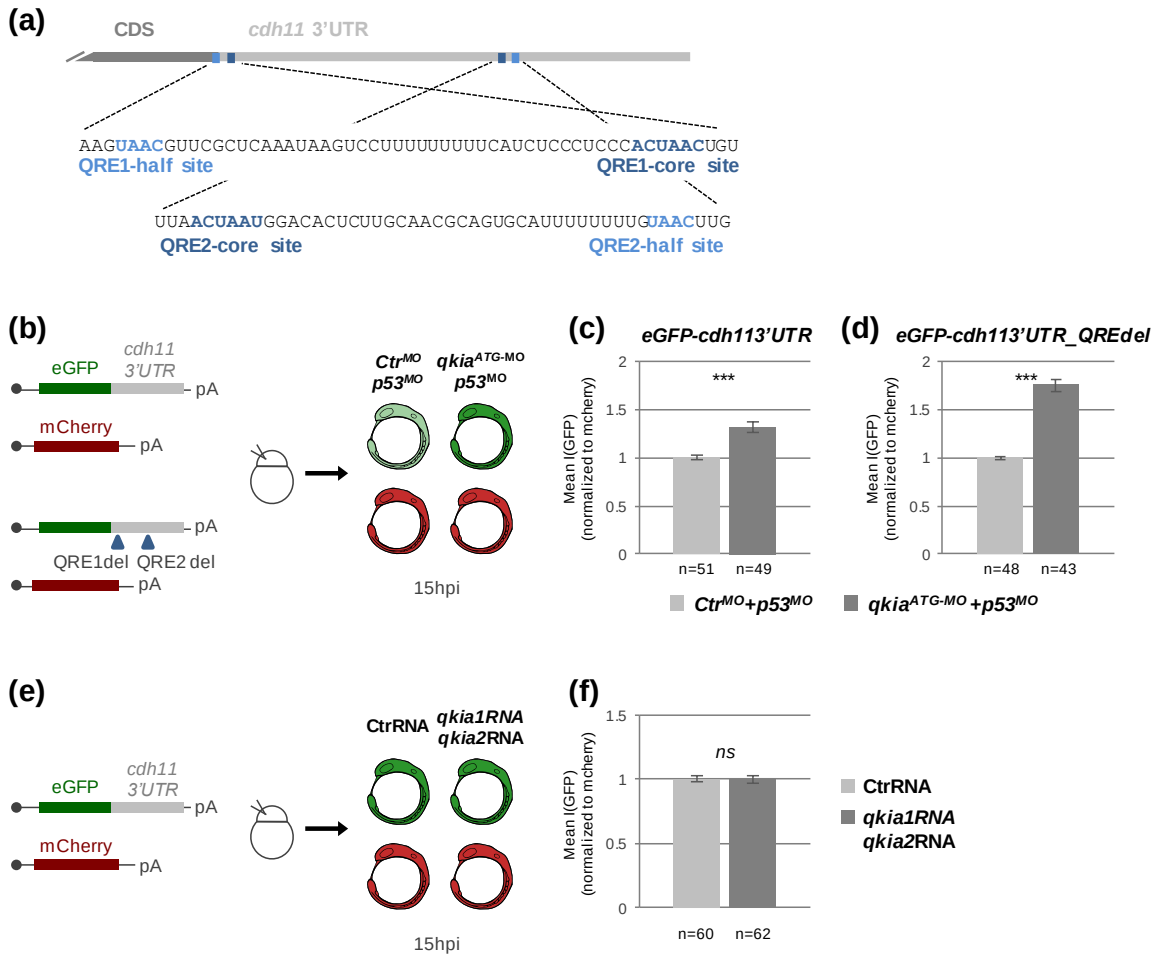

Fig. II.5 – Effect of *qkia* knockdown and overexpression on *cdh11* 3'UTR-mediated regulation of reporter expression.

(a) Quaking Response Elements (QREs) identified in the zebrafish *cdh11* 3'UTR sequence. For each QRE, the core site and the half site are shown. **(b,e)** Schematic representations of the experimental setups. **(b,c)** RNA encoding eGFP fused to the *cdh11* 3'UTR was injected, together with either *qkia*$^{ATG\text{-}MO}$ or *Ctr*^{MO} into 1-cell stage embryos. mCherry RNA was used as an injection control. Fluorescence intensities were measured at 15hours post injection (hpi). **(b,d)** The same experimental procedure was carried out using an eGFP reporter fused to a *cdh11* 3'UTR QREdel, which had both QRE core sites removed via site-directed mutagenesis. **(e,f)** The same experimental procedure was carried out under *qkia* overexpression conditions, using the eGFP reporter fused to the wildtype *cdh11* 3'UTR, and CtrRNA and a mixture of *qkia1*RNA and *qkia2*RNA instead of the control and *qkia* morpholinos. **(c,d,f)** Data shows mean normalized fluorescence intensities ±SEM, for the indicated conditions. Statistical analysis was done using Student's t-test (***p<0.001).

II.2.4 *cdh11* knockdown leads to Left-Right patterning defects

To determine if *cdh11* could act as a potential mediator of Qkia's function in Left-Right patterning, we next analysed the effect of Cdh11 depletion on organ laterality. We used a previously described splice blocking morpholino (*cdh11*^{MO}) (Clendenon et al., 2009) and a homozygous *cdh11* mutant line carrying the *cdh11*^{sa14413} allele. This allele contains a premature stop codon upstream of the *cdh11* transmembrane and intracellular domain coding region, and therefore is not expected to produce a functional protein (Fig. II.M1c,d).

In regard to cardiac laterality, we observed that 37% of *cdh11* morphants had unlooped heart tubes and 11% had reversely looped heart tubes (L loop) at 48-50 hpf (Fig. II.6a,b). Additionally, at 30 hpf, 19% of *cdh11* morphants displayed unjogged heart tubes and 13% displayed reversely jogged heart tubes (Right jog) (Fig. II.6d,e). However, no significant laterality defects were detected in the heart tubes of *cdh11* mutants, both at 48-50 hpf and at 30 hpf (Fig. II.6a,c,d,f). In *cdh11* morphant embryos we also observed that the lateral positions of the liver and pancreas were reversed in a small percentage of embryos (17%) (Fig. II.6g,h). However, as with the heart tube, no significant laterality defects were observed in the liver and pancreas of *cdh11* mutant embryos (Fig. II.6g,i).

Taken together these results indicate that the establishment of heart, liver and pancreas laterality is compromised under *cdh11* knockdown conditions, but not under *cdh11* knockout conditions.

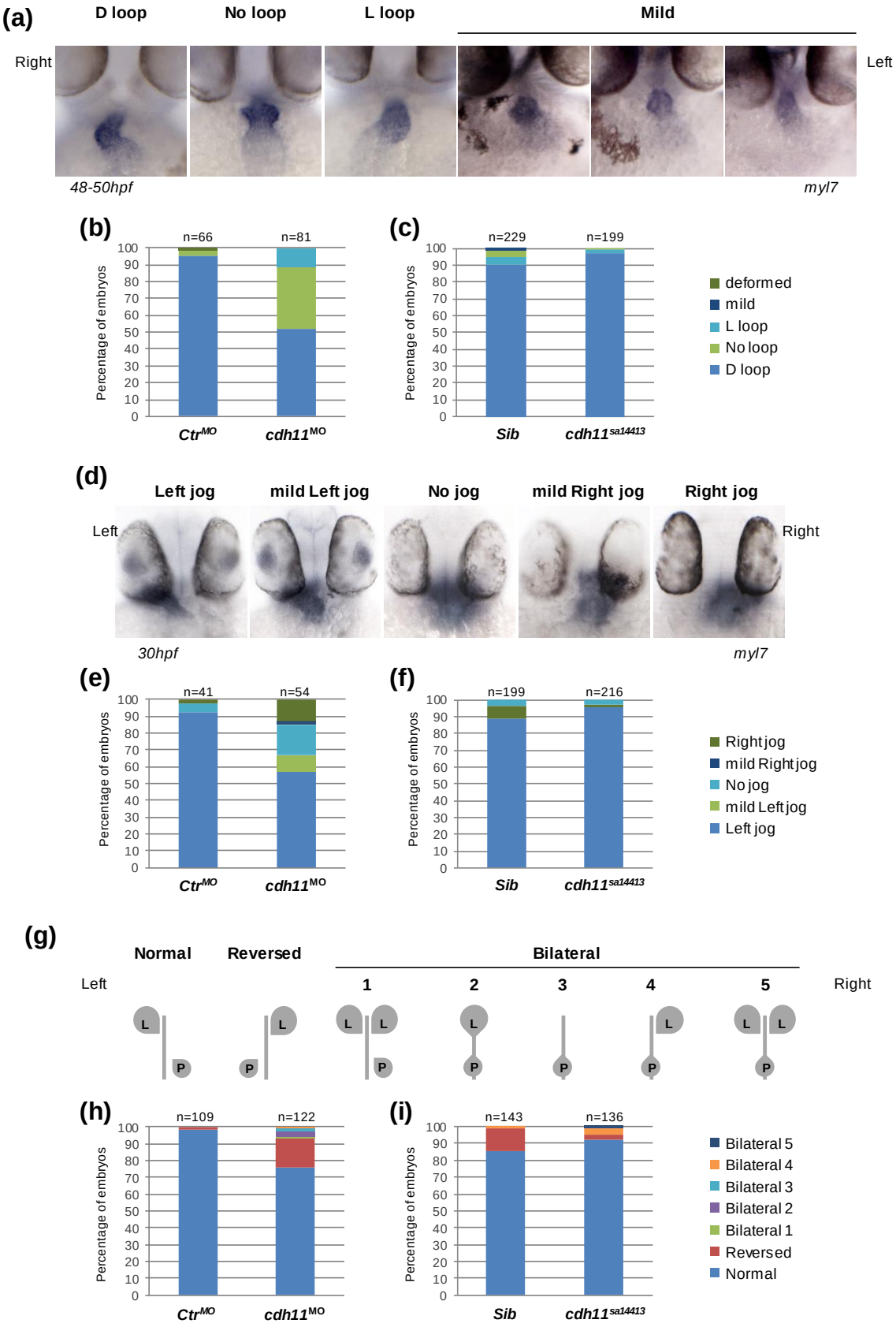

Fig. II.6 – *cdh11* morphants, but not *cdh11* mutants, display organ laterality defects.
(Figure legend on the next page)

Fig. II.6 – *cdh11* morphants, but not *cdh11* mutants, display organ laterality defects. **(a)** Ventral views of representative embryos illustrating the different heart laterality phenotypes observed at 48-50 hpf after WISH for *myl7*. **(b,c)** Quantification of the heart tube laterality phenotypes observed **(b)** under *cdh11* knockdown conditions (*cdh11*^{MO}) and **(c)** in *cdh11* mutant embryos (*cdh11*^{sa14413}). The respective control conditions are indicated. **(d)** Dorsal views of representative embryos illustrating the different heart laterality phenotypes observed at 30 hpf after WISH for *myl7*. **(e,f)** Quantification of the heart laterality phenotypes observed under **(e)** *cdh11* knockdown conditions (*cdh11*^{MO}) and **(f)** in *cdh11* mutant embryos (*cdh11*^{sa14413}). The respective control conditions are indicated. **(g)** Schematic representation of the different phenotypes observed regarding the laterality of the Liver (L) and Pancreas (P). Visceral organ laterality was assessed **(h)** in *sox17*:GFP embryos at 48 hpf, **(i)** after WISH for *foxa3* at 50 hpf. **(h,i)** Quantification of the liver and pancreas laterality phenotypes observed **(h)** under *cdh11* knockdown conditions (*cdh11*^{MO}) and **(i)** in *cdh11* mutant embryos (*cdh11*^{sa14413}). The respective control conditions are indicated.

To determine if the organ laterality defects observed in *cdh11* morphants derived from a disruption of asymmetric Nodal signalling, we analysed the expression of the laterality associated genes *spaw* and *pitx2* in the LPM of *cdh11* morphants. The left side specific LPM expression of *pitx2a* appeared to be randomized in *cdh11* morphants, with 33% of embryos displaying right side expression, 24% displaying either bilateral expression or no expression in the LPM and 43% displaying left side expression (Fig. II.7a). Similarly, expression of the left side specific LPM gene *spaw* was randomized in *cdh11* morphant embryos, with 40% of morphants displaying right side expression, 20% displaying either bilateral expression or no expression in the LPM and the remaining 40% displaying left side expression (Fig. II.7b). These results indicate that the *cdh11* morphant phenotype stems from a disruption upstream of LPM Nodal signalling, probably at the level of asymmetric signal establishment in the KV.

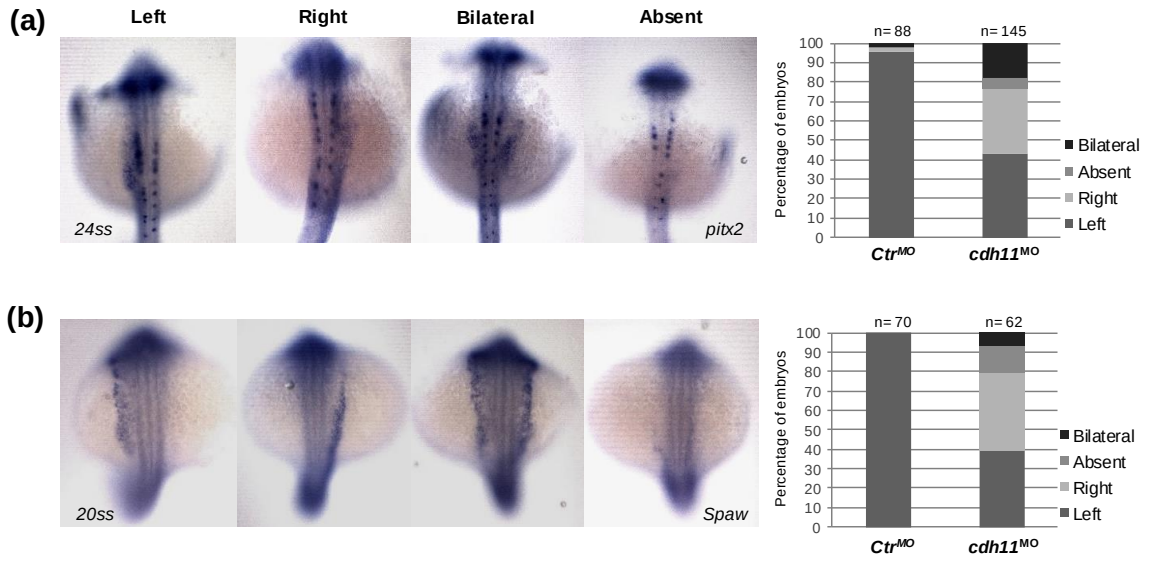

Fig. II.7 – Expression of Left-Right patterning genes is affected in the LPM of *cdh11* morphants.
(a) WISH analysis of *pitx2* expression in the lateral plate mesoderm of 24 ss control and *cdh11* morphant embryos. **(b)** WISH analysis of *spaw* expression in the lateral plate mesoderm of 20 ss control and *cdh11* morphant embryos.

To ascertain if *cdh11* could influence Left-Right patterning by contributing to asymmetric signal establishment in the KV, we next set out to determine if *cdh11* is expressed in this organ. Through WISH we were able to verify the previously reported expression of *cdh11* in the intermediate mesoderm and neural tube at the 8 ss, as well as in the otic vesicle and inner ear at the 20 ss and 24 hpf, respectively (Fig. II.8a-g) (Franklin and Sargent, 1996, Clendenon et al., 2009). However, this technique did not enable a clear detection of *cdh11* expression in tissues with a known involvement in Left-Right patterning, specifically, the KV at the 8ss and the LPM at the 20ss and at 24hpf (Fig. II.8a-g).

To account for a potentially reduced sensitivity of the WISH method to low levels of gene expression, we resorted to a complementary approach to determine if *cdh11* is expressed in the KV. Specifically, we performed fluorescence activated cell sorting (FACS) of 8 ss *sox17*:GFP transgenic embryos, which label the KV and the endoderm at this developmental stage. Total RNA was subsequently extracted from the sorted cells and, following reverse transcription, the expression of *cdh11* was detected by PCR amplification. The expression of *dand5* was also analysed and used as a marker for KV cells. This approach allowed us to detect *cdh11* expression

in cells sorted for high levels of GFP expression (GFP++), with these cells also expressing *dand5* (Fig. II.8h,i,j). Therefore, even though further experiments are required to validate this expression, the results obtained suggest that *cdh11* is expressed in KV cells at the 8 ss.

Taken together, our results reveal that under *cdh11* knockdown conditions internal organ laterality is compromised, most likely due to a disruption of the establishment of early asymmetric cues in the KV.

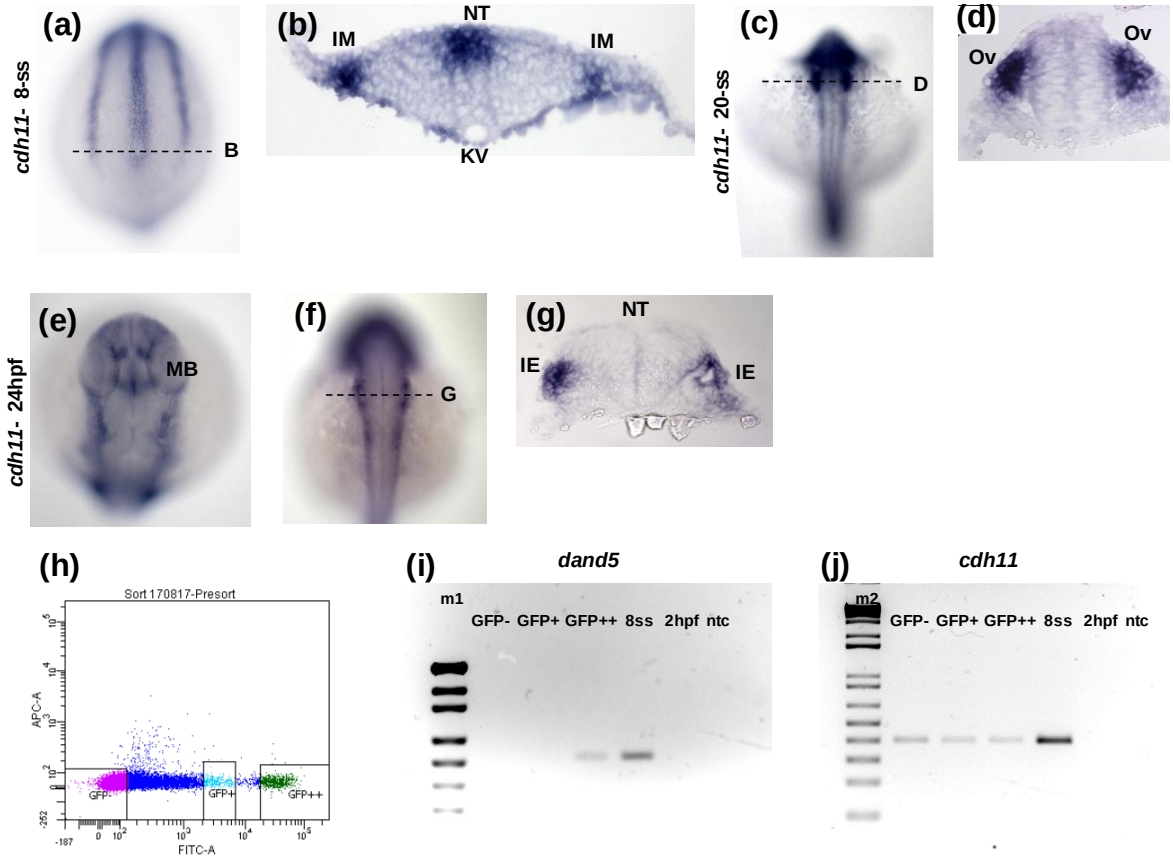

Fig. II.8 – *cdh11* expression in wildtype embryos and FACS sorted *sox17*:GFP cells. **(a-g)** WISH for *cdh11* in wildtype embryos **(a,b)** at the 8 ss, **(c,d)** at the 20 ss and **(e,f,g)** at 24 hpf. **(a,c,e,f)** Whole-mount embryos, dorsal view, anterior to top. **(b)** Transversal section at the KV level (B). **(d)** Transversal section at the otic vesicle level (D). **(g)** Transversal section at the inner ear level (G). **(b,d,g)** Dorsal to top. **(a-g)** IM, Intermediate mesoderm; NT, Neural Tube; KV, Kupffer's vesicle; Ov, Otic vesicle; MB, Midbrain; IE, Inner Ear. **(h)** FACS profile for *sox17*:GFP 8 ss embryos. Cells were sorted based on GFP levels. **(i)** PCR detection of *dand5* in samples obtained from *sox17*:GFP cell sorting, 8 ss whole embryos and 2 hpf whole embryos. **(j)** PCR detection of *cdh11* in samples obtained from *sox17*:GFP cell sorting, 8 ss whole embryos and 2 hpf whole embryos. **(i,j)** The 8 ss whole embryo condition was used as a positive control and the 2 hpf whole embryo condition was used as a negative control for both *cdh11* and dand5 expression. ntc, no template control; m1, pUC19 DNA/MspI (HpaII) Marker 23 (Thermo Fisher); m2, 1 Kb Plus DNA Ladder (Invitrogen).

II.3 DISCUSSION

In this study, we have uncovered evidence for two potential functions of the *qkia* gene during embryonic development, namely, in posterior body shaping and in the establishment of internal organ laterality.

The results shown concerning the role of *qkia* in the establishment of posterior body morphology indicate that *qkia* operates at post-gastrulation stages, and is likely to influence the shape of the posterior body through a role in the process of posterior body elongation (Fig. II.1). Previous studies have shown that even though several mechanisms contribute to posterior body elongation, the primary driving force of this process appears to be cell migration in the posterior PSM (Bouldin et al., 2014, Kanki and Ho, 1997, McMillen and Holley, 2015, Lawton et al., 2013, Dray et al., 2013, Steventon et al., 2016). To explore a potential role for *qkia* in this process future experiments can be carried out using an experimental setup, previously implemented in our lab, that utilizes a photoconvertible fluorescent reporter to track individual cell movements in the posterior PSM (Fior et al., 2012). In addition, to show a specific role for *qkia* in cell movement and morphogenesis, rescue experiments can be carried out by co-injection of *qkia* mRNA with the *qkia*$^{ATG\text{-}MO}$.

Regarding the role of *qkia* in the establishment of organ laterality, we have shown that both Qkia depletion and overexpression affect the lateral positions of the heart, liver and pancreas (Fig. II.2). Our analysis of Left-Right patterning gene expression, under Qkia depletion conditions, revealed that *qkia* appears to operate primarily at the level of laterality signal transmission from the KV to the LPM (Fig. II.3). These results therefore suggest that the role of *qkia* in the establishment of Left-Right asymmetry could be mediated by its expression in the PSM, which is located between these two laterality-associated tissues (Thisse et al., 2001).

To gain a better understanding of the role of *qkia* in Left-Right patterning, future experiments can focus on a more in-depth analysis of this process in the *qkia* mutant line. In addition, previous studies have shown that distinct STAR protein splicing isoforms can have different sub-cellular localizations and different functions on RNA metabolism (Artzt and Wu, 2010, Volk, 2010). Therefore, since the knockdown and

overexpression tools used in this study target both Qkia isoforms (Fig. II.M1a,b), it would be interesting to dissect the individual roles of each Qkia isoform in Left-Right patterning.

Considering that Qkia is an RNA binding protein, it is expected to function in development through its roles as a post-transcriptional regulator. In this study, we identified a potential target of Qkia-mediated regulation, *cdh11*. At this time, we cannot conclusively claim that *cdh11* is a direct target of Qkia, however the results obtained in this study under Qkia depletion conditions indicate that Qkia could act as a post-transcriptional repressor of *cdh11* expression (Fig. II.5b,c). We have also observed that this potential regulation is independent of the two QREs identified in the 3'UTR of *cdh11* (Fig. II.5a,b,d). As previously noted, the *cdh11* QREs were identified considering the consensus binding sequences proposed for the mouse QKI protein (Galarneau and Richard, 2005). However, discrete variations in preferential consensus binding motifs have been reported for different members of the STAR family (Table I.1) (Carmel et al., 2010, Ryder and Williamson, 2004, Hafner et al., 2010, Ryder et al., 2004, Galarneau and Richard, 2009, Israeli et al., 2007, Lin et al., 1997, Berglund et al., 1997, Peled-Zehavi et al., 2001, Liu et al., 2001). It is therefore possible that the zebrafish Qkia displays different binding preferences when compared to the mouse ortholog.

In addition, our results show that *qkia* overexpression is not sufficient to repress *eGFP-cdh113'UTR* reporter expression, suggesting that other factors could be involved in this regulation (Fig. II.5e,f). Previous studies have revealed that, even though the mammalian Quaking proteins typically function as homodimers, STAR family members can operate as heterodimers, associate with other KH domain proteins, and function as adaptor proteins in a signal transduction context (Beuck et al., 2012, Teplova et al., 2013, Wu et al., 1999, Rymond, 2010, Chen et al., 1997, Di Fruscio et al., 1999, Najib et al., 2005). It is therefore conceivable that a post-transcriptional regulation of *cdh11* mediated by Qkia could involve additional RBPs.

Nevertheless, further studies are required to conclusively determine if the Qkia protein interacts with the endogenous *cdh11* transcripts and to characterize the resulting effects on *cdh11* expression and embryonic development.

We have also uncovered a potential role for *cdh11* in the establishment of Left-Right organ asymmetry. In particular, we observed that in *cdh11* morphants the lateral positions of the heart, liver and pancreas are compromised (Fig. II.6a,b,d,e,g,h). These defects, however, were not phenocopied in *cdh11* mutants (Fig. II.6a,c,d,f,g,i). These phenotypic differences could stem from the activation of a genetic compensation program in *cdh11* mutant conditions, which is not triggered by morpholino mediated knockdown. Mechanisms of this nature were shown to underlie the phenotypic differences observed between mutants and morphants of the *egfl7* and *vegfaa* genes, and were proposed as an explanation for some of the widely observed phenotypical inconsistencies between knockdown and knockout strategies (Rossi et al., 2015). To determine if a compensation program is active in *cdh11* mutant embryos large scale approaches, such as microarrays or RNAseq, can be employed as described by (Rossi et al., 2015). In addition, future work should focus on addressing the specificity of the *cdh11*^{MO}-induced laterality phenotype.

Our analysis of the role of Cdh11 in Left-Right patterning revealed that this protein is likely to operate at the KV level, in asymmetric signal establishment (Fig. II.7 and Fig. II.8). To further elucidate this mechanism, it is necessary to determine if the expression of *spaw* and *dand5* is affected in the KV of *cdh11* morphants, and to perform a more definitive characterization of the expression pattern of *cdh11*. Nevertheless, considering that Cdh11 is an adhesion molecule, our results raise the possibility that it may function in this context by contributing to the establishment of proper KV morphology. Previous studies have shown that the cellular architecture of the KV is asymmetric along the anterior-posterior axis, with disruptions of this, and other aspects of KV morphology, affecting fluid flow and consequently compromising organ laterality (Wang et al., 2011, Wang et al., 2012, Kreiling et al., 2007, Arrington et al., 2013, Oteiza et al., 2010, Matsui et al., 2011, Ablooglu et al., 2010). However, despite the extensive work that has been conducted in the field thus far, only a small number of cell adhesion molecules have been implicated in the process of KV morphogenesis (e.g. Integrin subunits αV and β1b and Cadherin1) with the specific proteins involved in the establishment of KV anterior-posterior asymmetry remaining largely unknown (Matsui et al., 2011, Ablooglu et al., 2010, Wang et al., 2011, Wang et al., 2012). Future approaches can therefore focus

on determining if Cdh11 influences the establishment of organ laterality by contributing to KV morphogenesis.

Even though a more in-depth analysis is required to clarify the mechanisms through which *cdh11* and *qkia* operate in Left-Right patterning, our results also seem to indicate that *cdh11* and *qkia* contribute to different phases of organ laterality establishment. Specifically, while *cdh11* appears to function upstream, at the KV level, *qkia* appears to function further downstream, at the level of asymmetric signal transmission to the LPM (Fig. II.3 and Fig. II.7). Therefore, our results indicate that *cdh11* is unlikely to mediate *qkia*'s function in organ laterality.

In conclusion, our results reveal an apparent role for *qkia* in posterior body shaping and Left-Right patterning. These findings are therefore incremental to the current view of STAR proteins as important regulators of a considerable diversity of developmental processes (Volk and Artzt, 2010).

The observation that Qkia is involved in the establishment of internal organ laterality constitutes, to the extent of our knowledge, the first time that a STAR protein has been implicated in this developmental process. In addition, this observation serves to further our current understanding of STAR protein functions in cardiac development and opens the door for future studies aimed at assessing its conservation.

Lastly, our results are indicative of a potential function for Cdh11 in KV morphogenesis which, upon further dissection, could contribute to our understanding of the mechanisms that govern the formation and structural integrity of this organ.

II.4 MATERIALS AND METHODS

II.4.1 Zebrafish lines

Adult zebrafish and embryos were maintained and bred under standard laboratory conditions (Westerfield, 2000). Embryonic staging was done according to (Kimmel et al., 1995).

This work was carried out using AB wildtype strains, a transgenic Tg(*sox17*:GFP)^{s870} strain (Chung and Stainier, 2008) and two mutant strains, *qkia*^{t31954} (Lobbardi et al., 2011) and *cdh11*^{sa14413}.

The transgenic line Tg(*sox17*:GFP)^{s870} labels the endoderm and was used to visualize the gut, liver and pancreas, and as a KV/endodermal marker for FACS. Transgenic Tg(*sox17*:GFP)^{s870} embryos were obtained by outcrossing either homozygous, or heterozygous adults with wildtype AB fish.

The *qkia*^{t31954} allele displays a T to A missense mutation in position +467 relative to the ATG start codon, which leads to an Ile to Asn substitution (Fig. II.M1a,b) (Lobbardi et al., 2011). Paraformaldehyde fixed homozygous *qkia*^{t31954} mutant embryos, and the respective siblings, were provided by F.M. Rosa.

The *cdh11*^{sa14413} allele displays a T to A nonsense mutation at position +1361 relative to the ATG start codon, which generates a premature stop codon (Fig. II.M1c,d). Heterozygous fish obtained from the European Zebrafish Resource Center (EZRC), were incrossed to generate a homozygous *cdh11*^{sa14413} mutant line and a control wildtype line. Carriers were identified by PCR amplification of the corresponding genomic region and sanger sequencing (Stavbida), using the following primers Fw 5'-CCTTTATGGCTCCCAGCTAC-3', Rv 5'-AGGTTTACCGAGTGCCTTGAT-3'.

A schematic representation of the *qkia*^{t31954} and *cdh11*^{sa14413} alleles, and expected protein products, is presented in Fig. II.M1.

II.4.2 Morpholino oligonucleotides

The antisense morpholino oligonucleotides used in this study were obtained from Gene Tools.

qkia knockdown experiments were performed using the translation blocking morpholino oligo *qkia*$^{ATG\text{-}MO}$ 5'-CACCTCCATCTCCCCGACCATCATC-3'. The *qkia*$^{ATG\text{-}MO}$ was injected into 1-cell stage embryos with the *p53* morpholino (*p53*^{MO}) 5'-GCGCCATTGCTTTGCAAGAATTG-3' to counteract the pro-apoptotic effects of the *qkia*$^{ATG\text{-}MO}$. Control experiments were done by injecting sibling embryos with either *p53*^{MO} or a mixture of *p53*^{MO} and standard control morpholino (*Ctr*^{MO}) 5'-CCTCTTACCTCAGTTACAATTTATA-3'. The *qkia*$^{ATG\text{-}MO}$ and the *Ctr*^{MO} were injected at 1.7ng/embryo and the *p53*^{MO} was injected at 2.5ng/embryo, using an injection volume of 1.4nL/embryo.

cdh11 knockdown experiments were performed using a previously described splice blocking morpholino oligo *cdh11*^{MO} 5'-TGTCACGCACCTCTGTTGTCCTTGA-3' (Clendenon et al., 2009). Control experiments were done by injecting sibling embryos with *Ctr*^{MO}. The *cdh11*^{MO} and the *Ctr*^{MO} were injected into 1-cell stage embryos at 2.3ng/embryo, using an injection volume of 1.4nL/embryo.

A schematic representation of the *qkia*$^{ATG\text{-}MO}$ and *cdh11*^{MO} binding sites, and expected effects on protein synthesis, is presented in Fig. II.M1.

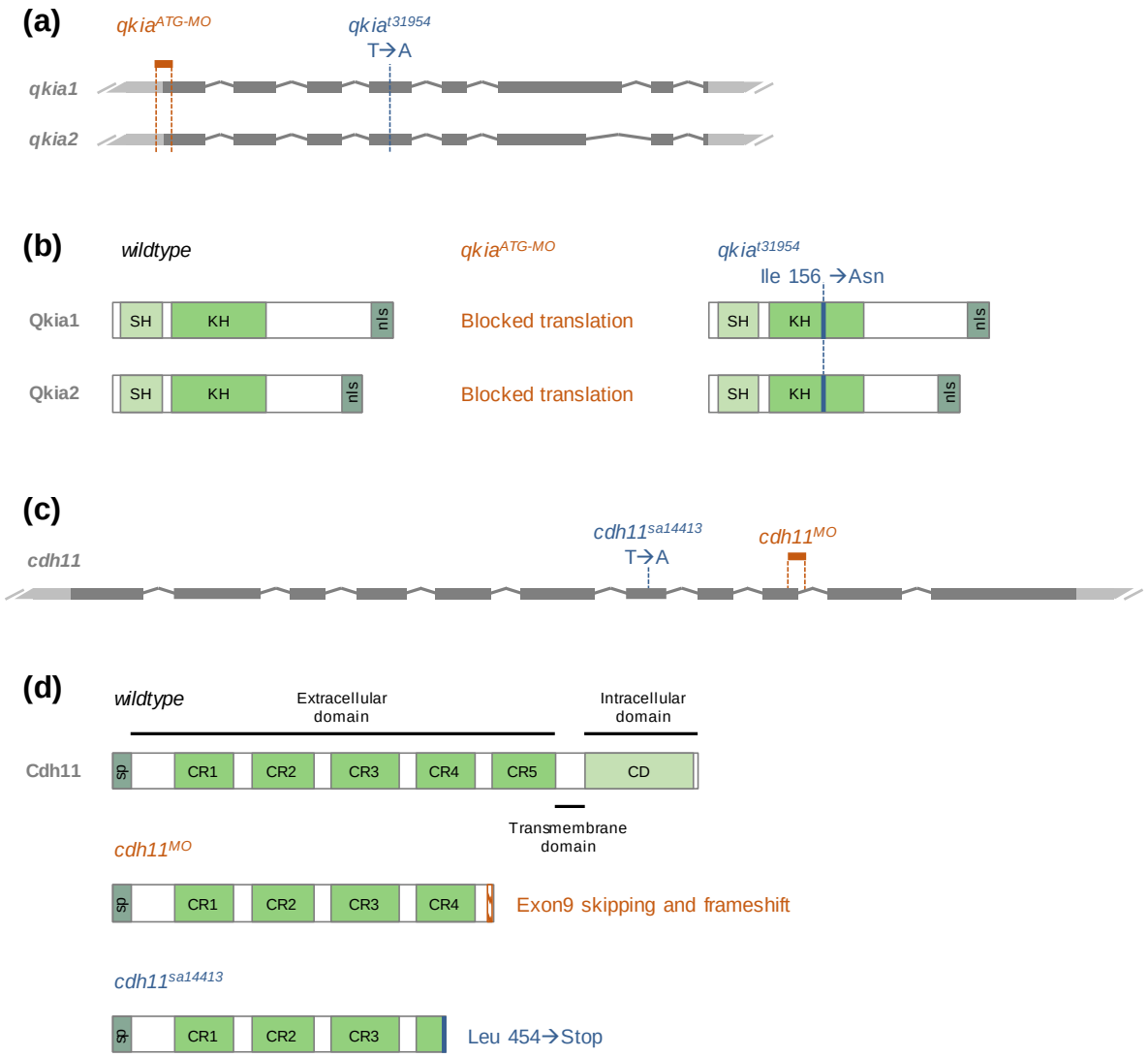

Fig. II.M1 – *qkia* and *cdh11* morpholino oligos and mutant alleles used in this work. **(a)** Schematic representation of the *qkia1* and *qkia2* splicing isoforms of the zebrafish *qkia* gene. Illustration of the *qkia*$^{ATG\text{-}MO}$ binding site and the relative position of the *qkia*^{t31954} mutation. **(b)** Expected outcomes of the *qkia*$^{ATG\text{-}MO}$ interference and the *qkia*^{t31954} mutation, at the protein level. The *qkia*$^{ATG\text{-}MO}$ is expected to block translation of both *qkia* isoforms. The *qkia*^{t31954} mutation leads to a substitution of a highly conserved Ile in the KH domain, which is expected to lead to misfolding (Lobbardi et al., 2011). Relevant protein domains are indicated. SH, STAR protein homodimerization region; KH, K homology Domain; nls, putative nuclear localization signal. **(c)** Schematic representation of the zebrafish *cdh11* gene and illustration of the *cdh11*^{MO} binding site and the relative position of the *cdh11*^{sa14413} mutation. **(d)** Expected outcomes of the *cdh11*^{MO} interference and the *cdh11*^{sa14413} mutation, at the protein level. The most likely outcome of *cdh11*^{MO} interference is exon 9 skipping, accompanied by a frameshift in exon 10 leading to a premature stop codon and consequent production of a truncated protein (illustrated) (Clendenon et al., 2009). However, if intronic or exonic cryptic splice sites are present, this morpholino can also give rise to partial or total intron 9 inclusion, or to only a partial exclusion of exon 9. The *cdh11*^{sa14413} mutation generates a premature stop codon in the CR4 domain coding region. If transcripts with this mutation escape nonsense-mediated decay, they are expected to lead to the production of a truncated protein. Relevant protein domains are indicated. sp, signal peptide; CR1-5, Cadherin extracellular repeats; CD, Cadherin cytoplasmic domain.

II.4.3 Cloning and site directed mutagenesis

In the following cloning procedures, PCR amplifications were performed using Phusion High-Fidelity DNA Polymerase (Thermo Fisher) and DNA ligation reactions were done using T4 DNA Ligase (NEB).

In the following mutagenesis reactions, amplification was done using either KOD Hot Start DNA Polymerase (Novagen) or PfuTurbo DNA Polymerase (Agilent) and digestion of template DNA was done with DpnI (Thermo Fisher).

All the constructs produced were sequenced by Stabvida to verify the efficiency and accuracy of each cloning procedure.

The *qkia1* and *qkia2* isoforms are annotated under the ENSDART00000169708.1 and ENSDART00000170462.1 accession numbers, respectively. The *cdh11* sequence is annotated under the ENSDART00000002279.7 accession number (Aken et al., 2017).

II.4.3.1 qkia constructs

Wildtype zebrafish embryos between the 6 and 10 somite stages were dechorionated and microdissections were performed using a fine pointed scalpel to isolate the caudal portions of each embryo, which included all tissues posterior to the last formed somite. Total RNA was extracted from these samples using TRIzol (Invitrogen), according to the manufacturers' instructions, and cDNA was synthesized using the MMLV-Reverse Transcriptase kit (Promega).

The cDNA sample obtained was used as a template to amplify the coding sequence (CDS) of *qkia* with primers *qkia_CDS_Fw* and *qkia_CDS_Rv* (Table II.M1). We obtained two PCR amplification products, corresponding to the previously described alternative splicing isoforms of the *qkia* gene: *qkia1* and *qkia2* (Fig. II.M1a) (Lobbardi et al., 2011). These amplification products were cloned into the *pCS2+* vector after restriction digestion with BamHI (NEB) and ClaI (NEB). The resulting constructs were termed *pCS2-qkia1-CDS* and *pCS2-qkia2-CDS*.

The *pCS2-qkia1-CDS* and *pCS2-qkia2-CDS* constructs were used as templates to amplify and subsequently clone the *qkia1* and *qkia2* coding sequences in reverse orientation into the *pCS2*+ vector. PCR amplification was done using primers *qkia_antiCDS_Fw* and *qkia_antiCDS_Rv* (Table II.M1) and restriction digestions were done with BamHI (NEB) and ClaI (NEB). The resulting constructs were named *pCS2-antiqkia1-CDS* and *pCS2-antiqkia2-CDS*.

An additional set of constructs was produced in which an HA tag was added upstream of the *qkia1* and *qkia2* coding sequences. This was done by PCR amplification using the *pCS2-qkia1-CDS* and *pCS2-qkia2-CDS* constructs as templates and primers *qkia_HA-CDS_Fw* and *qkia_CDS_Rv* (Table II.M1). The *pCS2*+ vector was digested with StuI (Thermo Fisher) and the PCR amplification products were blunt-end cloned into the vector. The constructs obtained in which the amplification products were inserted in the forward orientation were termed *pCS2-HA-qkia1* and *pCS2-HA-qkia2*. The constructs in which insertion occurred in the reverse orientation were termed *pCS2-antiHA-qkia1* and *pCS2-antiHA-qkia2*.

The *pCS2-HA-qkia1* and *pCS2-HA-qkia2* constructs were subjected to site directed mutagenesis to introduce five silent substitutions in the region of the CDS predicted to interact with the $qkia^{ATG\text{-}MO}$. Mutagenesis was done using primers *qkia_mut1* and *qkia_mut2* (Table II.M1), and the resulting constructs were named *pCS2-HA-mutqkia1* and *pCS2-HA-mutqkia2*.

II.4.3.2 cdh11 constructs

The 3'UTR of *cdh11* was amplified from the cDNA sample described previously (Section II.4.3.1) by PCR using primers *cdh11_3UTR_Fw* and *cdh11_3UTR_Rv* (Table II.M1). After restriction digestion with StuI (Thermo Fisher) and XhoI (NEB) the amplification product was cloned into a pCS2+eGFP vector (Lopes et al., 2010). This procedure lead to the insertion of the *cdh11* 3'UTR downstream of the eGFP coding sequence.

In the previous construct, a section of the vector's multiple cloning site was present between the 3'end of the eGFP CDS and the 5'end of the *cdh11* 3'UTR. In order to replicate the endogenous zebrafish *cdh11* QRE1 half site (Fig. II.5a), this section of

the vector was removed by site directed mutagenesis, thus fusing the eGFP coding sequence with the *cdh11* 3'UTR. Mutagenesis was done using primers *cdh11_3UTRfus_Fw* and *cdh11_3UTRfus_Rv* (Table II.M1) and the resulting construct was termed *pCS2-eGFP-cdh113'UTR*. Because the primers used in this mutagenesis protocol are in back-to-back orientation, a ligation step was done after DpnI digestion, using T4 DNA Ligase (NEB).

An additional construct was produced, by removing the two QRE core sites located in the *cdh11* 3'UTR from the *pCS2-eGFP-cdh113'UTR* construct. This was done in two sequential site directed mutagenesis steps. The first step targeted the QRE1 core site, and was done with primers *QRE1del_Fw* and *QRE1del_Rv* (Table II.M1). The second step targeted the QRE2 core site and was done with primers *QRE2del_Fw* and *QRE2del_Rv* (Table II.M1). The resulting construct was named *pCS2-eGFP-cdh113'UTR_QREdel.*

To generate a control reporter construct, the CDS of mCherry was subcloned from a *pKS-mCherry* vector, provided by the D. Henrique Lab, into a *pCS2+* backbone. Subcloning was done after digestion with XhoI (Thermo Fisher) and XbaI (Thermo Fisher), and the resulting construct was named *pCS2-mCherry*.

To produce a template construct for *cdh11* ISH probe synthesis, total RNA was extracted from wildtype 8 somite stage whole embryos using TRIzol (Invitrogen) and cDNA was synthesized using the MMLV-Reverse Transcriptase kit (Promega). PCR was done with primers *cdh11_CDS-ISH_Fw* and *cdh11_CDS-ISH_Rv* (Table II.M1), which amplify the sequence between positions +947 and +1524 relative to the ATG start codon of the *cdh11* CDS. After restriction digestion with BamHI (NEB) and EcoRI (NEB) the amplification product was cloned into the pCS2+ vector. The resulting construct was termed *pCS2-cdh11-ISH*.

Table II.M1 – Primers used in the *qkia* and *cdh11* cloning procedures. Underlined sequences correspond to restriction sites. The sequence highlighted in green codes for an HA tag. Nucleotides highlighted in blue correspond to silent substitutions introduced through mutagenesis. Asterisks indicate mutagenesis primers designed in back-to-back orientation, the remaining mutagenesis primers were designed in overlapping orientation.

Primer name	Sequence (5'→3')
qkia_CDS_Fw	ACAGGATCCATGATGGTCGGGGAGATGGAGGT
qkia_CDS_Rv	ATCATCGATTTAGTTGCCGGTGGCGGCTCTGT
qkia_antiCDS_Fw	ATCATCGATATGATGGTCGGGGAGATGGAGGT
qkia_antiCDS_Rv	ACTGGATCCTTAGTTGCCGGTGGCGGCTCTGT
qkia_HA-CDS_Fw	ACAGGATCCATGTACCCTTACGACGTCCCTGATTATGCAATG ATGGTCGGGGAGATGGAGGT
qkia_mut1	GCAATGATGGTGGGCGAAATGGAAGTCAAGGAGAGACCGA GGCC
qkia_mut2	GGCCTCGGTCTCTCCTTGACTTCCATTTCGCCCACCATCATT GC
cdh11_3UTR_Fw	AGTAGGCCTCGTTCGCTCAAATAAGTCCT
cdh11_3UTR_Rv	ACGCTCGAGTCAAAGTTTTTTGCTTCTTAGATTGA
*cdh11_3UTRfus_Fw **	CGTTCGCTCAAATAAGTCCTTT
*cdh11_3UTRfus_Rv **	TTACTTGTACAGCTCGTCCATGC
QRE1del_Fw	CATCTCCCTCCCTGTGTGTTTTGTGAAG
QRE1del_Rv	CTTCACAAAACACACAGGGAGGGAGATG
QRE2del_Fw	GCTCAAAAAACGCCTTAGGACACTCTTGCAACG
QRE2del_Rv	CGTTGCAAGAGTGTCCTAAGGCGTTTTTTGAGC
cdh11_CDS-ISH_Fw	ATCGGATCCTAGAGGGAGACGGCATGAAC
cdh11_CDS-ISH_Rv	ATCGAATTCACATTCTCACAGACCAGCACTT

II.4.4 *In vitro* transcription and mRNA microinjections

DNA templates for *in vitro* transcription were prepared by NotI (NEB) digestion of the indicated constructs. *In vitro* transcriptions were performed using the SP6 mMessage mMachine kit (Ambion) and followed by in-tube Turbo DNAseI (Ambion) digestion of the template DNAs. The transcript samples were purified using illustra ™ MicroSpin™ G-50 Columns (GE Healthcare) prior to microinjection.

The following microinjection procedures were done at the 1-cell stage, with an injection volume of 1.4nL/embryo and the morpholino concentrations used are indicated in Section II.4.2.

II.4.4.1 qkia^{ATG-MO} rescue and qkia overexpression

The transcripts used for the *qkia^{ATG-MO}* laterality phenotype rescue experiments were *in vitro* transcribed from the following constructs: *pCS2-HA-mutqkia1*, *pCS2-HA-mutqkia2, pCS2-antiHA-qkia1* and *pCS2-antiHA-qkia2* (Section II.4.3.1) and termed *HA-mutqkia1*, *HA-mutqkia2*, *antiHA-qkia1* and *antiHA-qkia2*, respectively.

Optimization of the rescue experiments was done, using *sox17:*GFP embryos, by microinjection of the *qkia^{ATG-MO} p53^{MO}* mix with either *HA-mutqkia1*, *HA-mutqkia2*, or a 1:1 molar ratio of *HA-mutqkia1* and *HA-mutqkia2*. Control experiments were done using sibling *sox17:*GFP embryos by microinjection of the *qkia^{ATG-MO} p53^{MO}* mix with the corresponding antisense transcripts (*antiHA-qkia1, antiHA-qkia2* or both). Several transcript concentrations were tested for each rescue condition, and the resulting laterality phenotypes we assessed by live fluorescent imaging. The condition that produced the most efficient rescue of the *qkia^{ATG-MO}* liver and pancreas laterality phenotype was the microinjection of *qkia^{ATG-MO}, p53^{MO}* and 20pg/embryo of *HA-mutqkia2*. In the corresponding control experiment, sibling embryos were injected with *qkia^{ATG-MO}*, *p53^{MO}* and 20pg/embryo of *antiHA-qkia2*.

The transcripts used for *qkia* overexpression were *in vitro* transcribed from the following constructs: *pCS2-qkia1-CDS*, *pCS2-qkia2-CDS, pCS2-antiqkia1-CDS*

and *pCS2-antiqkia2-CDS* (Section II.4.3.1) and named *qkia1-CDS*, *qkia2-CDS, antiqkia1-CDS* and *antiqkia2-CDS,* respectively.

Overexpression of *qkia* was done by microinjection of a mixture of *qkia1-CDS* and *qkia2-CDS*, in a 1:1 molar ratio, corresponding to 70pg/embryo of *qkia1-CDS* and 64pg/embryo of *qkia2-CDS,* into wildtype embryos. In the respective control experiments, sibling embryos were injected with 70pg/embryo of *antiqkia1-CDS* and 64pg/embryo of *antiqkia2-CDS.*

II.4.4.2 Fluorescent reporters

The transcripts used for the fluorescent reporter experiments were *in vitro* transcribed from the *pCS2-eGFP-cdh113'UTR, pCS2-eGFP-cdh113'UTR_QREdel* and *pCS2-mCherry* constructs (Section II.4.3.2). The transcript samples obtained were termed *eGFP-cdh113'UTR, eGFP-cdh113'UTR_QREdel* and *mCherry*, respectively.

The *eGFP-cdh113'UTR* and *eGFP-cdh113'UTR_QREdel* samples were used at 100pg/embryo and the *mCherry* sample was used at 50pg/embryo.

To determine the effect of Qkia depletion on reporter expression, two experiments were carried out. One was done by microinjection of *eGFP-cdh113'UTR* with *mCherry*, $qkia^{ATG\text{-}MO}$ and $p53^{MO}$ into wildtype embryos. The other was done by microinjection of *eGFP-cdh113'UTR_QREdel* with *mCherry*, $qkia^{ATG\text{-}MO}$ and $p53^{MO}$ into wildtype embryos. The respective control experiments were done in sibling embryos using Ctr^{MO} instead of $qkia^{ATG\text{-}MO}$.

To determine the effect of *qkia* overexpression on reporter expression, *eGFP-cdh113'UTR* was microinjected with *mCherry* and a 1:1 molar ratio of *qkia1-CDS* and *qkia2-CDS,* into wildtype embryos. The respective control experiments were done in sibling embryos using *antiqkia1-CDS* and *antiqkia2-CDS* instead of *qkia1-CDS* and *qkia2-CDS*. The sense and antisense *qkia* transcript samples were used at the previously indicated concentrations (Section II.4.4.1).

II.4.5 Fluorescent reporter assays

Production and microinjection of reporter transcripts was done as described in Section II.4.4 and Section II.4.4.2. Following microinjection, the embryos were kept at 28ºC for 15 hours until imaging.

Prior to imaging, experimental and control embryos were mounted, in chorion, on a glass-base petri dish. Imaging was done with a Zeiss Axiovert 200M widefield fluorescence microscope, using a 20x magnification. For eGFP exposure was set to 100ms and for mCherry exposure was set to 50ms.

Image processing was done using ImageJ 1.44p (Schneider et al., 2012). Average pixel intensities were measured, for each channel and each embryo, in a circular section of the tailbud. The average background pixel intensities were measured using an identical section, in an area adjacent to the embryo. The background values were subtracted from those obtained for the tailbud. The resulting intensity values obtained for eGFP were normalized to those obtained for mCherry in each embryo. The mean normalized fluorescence intensities were calculated for each experimental condition, and the values shown are relative to the indicated control condition. Statistical analysis was done using Student's t-test.

II.4.6 Whole-mount *in situ* hybridization and histology

The antisense RNA WISH probes used in this study were *in vitro* transcribed from the respective DNA templates following construct linearization. The restriction enzymes, RNA polymerases and constructs used for probe production in this study are indicated in Table II.M2.

With the exception of the *myoD* probe, which was labelled with Fluorescein (Fluo RNA labelling mixture, Roche), all the probes used in this study were labelled with Digoxigenin (DIG RNA labelling mixture, Roche).

WISH experiments were done according to the protocol described by (Thisse and Thisse, 2008), with the modifications described below.

In the triple WISH experiments, namely the *myoD, mesp-ab, tbx16* WISH and the *ctslb, ta, dlx3* WISH, probe hybridizations were done using a mixture of the indicated probes.

In the triple WISH for *myoD, mesp-ab* and *tbx16* two antibody incubation steps were carried out. In the first step, the embryos were incubated overnight with anti-Fluo-AP antibody (Roche, working dilution 1:10,000), washed in PBS, 0.1% Tween, washed in Tris 0.1M, pH8 and staining was done with Fast Red (Roche). After this step antibody inactivation was done by incubation in a Glycine 0.1M, 0.1% Tween20, pH2.2 solution, for 15minutes, followed by a TBS, 0.1% Tween (TBST) wash and subsequent incubation in TBST at 70ºC for 30min. The blocking step was repeated and the second antibody incubation was done with anti-DIG-AP (Roche, working dilution 1:5,000), as described in (Thisse and Thisse, 2008).

In the WISH experiments done with DIG labelled probes, staining was performed using BM purple AP substrate (Roche), with the exception of the experiments done with the *foxa3* probe, in which staining was done as described in (Thisse and Thisse, 2008).

Table II.M2 – WISH probes used in this study. For each probe, the restriction enzyme required for DNA template linearization, and the RNA polymerase required for *in vitro* transcription are indicated, along with the sources of the respective template constructs used.

Probe	Restriction Enzyme	RNA Polymerase	Template
myoD	BamHI	T7	(Weinberg et al., 1996)
mesp-ab	NotI	T3	(Cutty et al., 2012)
tbx16	EcoRI	T7	(Ruvinsky et al., 1998)
ta	HindIII	T7	(Amack and Yost, 2004)
dlx3	EcoRV	T7	(Akimenko et al., 1994)
ctslb	XhoI	T3	(Thisse et al., 1994)
myl7	NotI	T7	(Yelon et al., 1999)
pitx2	SpeI	T7	(Essner et al., 2000)
spaw	SpeI	T7	(Long et al., 2003)
dand5	BamHI	T3	(Hashimoto et al., 2004)
foxa3	XhoI	T3	(Odenthal and Nüsslein-Volhard, 1998)
cdh11	HindIII	T7	(Section II.4.3.2)

To characterize the *cdh11* expression pattern, following WISH for this gene, embryos were gelatin embedded and cryosectioned transversely, with a section thickness of 16-18µm. The embedding and sectioning procedures were done by the Histology Facility of the Chronic Diseases Research Center (CEDOC).

Image acquisition was done using a Leica Z6 PRO stereoscope and a Leica DM2500 bright-field microscope.

II.4.7 Fluorescence activated cell sorting and *cdh11* detection

To determine if *cdh11* is expressed in the KV we resorted to the *sox17*:GFP transgenic line, which labels the endoderm, the dorsal forerunner cells and the KV (Chung and Stainier, 2008). Heterozygous *sox17*:GFP embryos were obtained by outcrossing homozygous Tg(*sox17*:GFP)^{s870} male adults with wildtype AB female adults. Embryo disaggregation was done at the 8 ss as described in (Tavares et al., 2017).

Fluorescence activated cell sorting (FACS) was performed with a FACSAria bench top High Speed Cell Sorter (Becton Dickinson), with a 100µm nozzle, a 0-16-0 mask, and a sheath fluid pressure of 20psi. GFP excitation was done using a 488nm (Blue) laser and detection was done using 502LP 530/30nm filters.

Total RNA extractions were done using TRIzol (Invitrogen). The extracted RNA was subsequently treated with DNase I (Promega) and purified with the RNA clean and concentrator kit (Zymo Research). RNA was extracted from GFP negative cells (GFP-) and two sets of GFP positive cells (GFP+ and GFP++), illustrated in Fig. II.8h. In addition, total RNA was extracted from whole embryos at the 8 ss and at 2 hpf.

cDNA was synthetized using the ProtoScript® II First Strand cDNA Synthesis Kit (NEB), with random hexamer primers, and PCR amplifications were done using the Phusion High-Fidelity DNA Polymerase (Thermo Fisher).

cdh11 and *dand5* expression was detected using the following primers,
Cdh_Fw 5'-ACGTGGGAAATCAAATCCAGTGAGG-3',
Cdh_Rv 5'-GGGATCTGGGCCTGTGTACTCC-3',
Dand5_Fw 5'-CCGCAATCCTGACCCATAGCAA-3',
Dand5_Rv 5'-CTCCTCCGTTATGCGCTGTGTA-3'.

In these experiments, the 8 ss whole embryo condition was used as a positive control for *cdh11* and *dand5* expression and the 2 hpf whole embryo condition was used as a negative control for *cdh11* and *dand5* expression. *dand5* expression was used as a marker for KV cells.

CHAPTER III

Fine-tuning of *fgf8a* expression through alternative polyadenylation has a selective impact on Fgf-associated developmental processes

Sara F. Fernandes, Rita Fior, Francisco Pinto, Margarida Gama-Carvalho and Leonor Saúde

S.F.F. performed all the experiments and analyzed the data.

F.P. built the mathematical model and performed its analysis.

S.F.F., R.F., M.G.-C. and L.S. conceived the project and contributed to the analysis and interpretation of the data.

S.F.F., R.F., F.P., M.G.-C. and L.S. were involved in writing this chapter.

III.1 INTRODUCTION

Alternative polyadenylation (APA) is a mechanism of gene expression regulation that involves the formation of alternative mRNA 3′ ends through pre-mRNA cleavage and polyadenylation at different sites. It results from the use of different polyadenylation signals (PASs) and, in the 3' untranslated region (UTR), leads to the formation of alternative 3'UTRs (alt3'UTRs). The presence of longer 3'UTRs formed through APA can provide additional binding sites for microRNAs (miRs) and RNA binding proteins (RBPs), enabling more complex forms of post-transcriptional regulation (Tian and Manley, 2017).

APA is a widespread phenomenon, having been associated with both physiological and disease contexts (Tian and Manley, 2017, Chen et al., 2017a). In particular, genome-wide studies have revealed that high levels of APA occur throughout embryonic development. Widespread 3'UTR lengthening and shortening events have been shown to take place during early zebrafish development (Ulitsky et al., 2012, Li et al., 2012) and a 3'UTR lengthening trend accompanies the progression of mouse embryogenesis (Ji et al., 2009). In addition, several mouse and *Drosophila* genes undergo neural-specific 3'UTR elongation during development (Miura et al., 2013, Hilgers et al., 2011). These studies provide evidence of a tight temporal and spatial control of APA dynamics throughout embryogenesis. However, the functional importance of gene-specific APA events to embryonic development has been largely unaddressed.

Fibroblast growth factors (FGFs) represent a large family of secreted signalling molecules that has been implicated in the regulation of multiple processes of embryonic development (Pownall and Isaacs, 2010). Evidence that the post-transcriptional regulation of *Fgf* genes has a critical role during development comes from a study done in chick and mouse embryos, where the authors showed that *Fgf8* mRNA stability is crucial for the establishment of a signalling gradient required for somite formation (Dubrulle and Pourquié, 2004, Dubrulle et al., 2001). For the zebrafish *Fgf8* orthologue – the *fgf8a* gene – seven distinct alt3'UTRs have been reported, a number paralleled only by *fgf12b* among the other 32 *fgf* genes of the fish (Ulitsky et al., 2012, You et al., 2015). However, the post-transcriptional regulatory events mediated by these *fgf8a* alt3'UTRs and their functional importance

to different aspects of embryonic development have, thus far, remained unaddressed.

During embryonic development, multiple processes are known to be regulated by Fgf8a (Pownall and Isaacs, 2010). For instance, early on Fgf8a contributes to gastrulation (Griffin et al., 1995, Reifers et al., 1998, Fürthauer et al., 1997, Fürthauer et al., 2004), during tail and trunk development, *fgf8a* contributes to mesodermal progenitor specification (Griffin et al., 1995, Mathieu et al., 2004, Goto et al., 2017, Draper et al., 2003) and somite formation (Akiyama et al., 2014, Sawada et al., 2001). In anterior regions *fgf8a* is required for midbrain-hindbrain boundary (MHB) patterning (Reifers et al., 1998) and contributes to several aspects of sensory organ development. These include neurogenesis in the statoacoustic ganglion (Vemaraju et al., 2012), anterior and postoptic commissure formation (Shanmugalingam et al., 2000), neuronal differentiation and nasal-temporal patterning in the retina (Martinez-Morales et al., 2005, Picker et al., 2009).

Here we perform the first functional characterization of the *fgf8a* alt3'UTRs. Our results show that the *fgf8a* alt3'UTR with the highest reported abundance mediates a strong translational repression, in contrast with the second most abundant alt3'UTR, which is much more sparsely used, but supports a higher translation efficiency. By inducing a shift in the usage of the two corresponding PASs we observed a specific impact on late developmental processes associated with the sensory system. Furthermore, this modulation of Fgf signalling enabled the identification of a previously undescribed role for this pathway in the early stages of superficial retinal vascularization.

III.2 RESULTS

III.2.1 *fgf8a* alt3'UTRs mediate distinct effects on translation efficiency

To address the significance of APA to the regulation of *fgf8a* expression during embryonic development, we began by analysing the usage patterns of its alternative PASs. Data from two independent genome-wide poly(A) event profiling studies of embryonic development revealed seven alternative PASs for the zebrafish *fgf8a* gene (Ulitsky et al., 2012, You et al., 2015) (Table III.S1, altUTRs 1 to 7). A predominant PAS is used in 65.9-74.3% of *fgf8a* transcripts and generates a 3'UTR with 797 nucleotides (nt) which we termed *fgf8aM* (altUTR-4). The PAS with the second highest usage frequency, considering the data obtained in both studies, is used in 12.5-18.7% of transcripts. The resulting 3'UTR is 728nt long and was named *fgf8aS* (altUTR-3). Three additional PASs (altUTR-5, -6 and -7) were identified distal to the *fgf8aM* PAS, with a reported combined usage frequency of 4.5-7.4%. The remaining two PASs (altUTR-1 and -2) are proximal to *fgf8aS* PAS and have a combined usage frequency of 2.5-14.2% (Ulitsky et al., 2012, You et al., 2015) (Table III.S1).

Given the distinctive expression patterns of the *fgf8a* gene during embryogenesis (Fig. III.1a) (Thisse et al., 2001), we set out to determine if the *fgf8a* alternative PASs displayed different usage preferences in different embryonic tissues and developmental timepoints. We considered two developmental stages, 8-somite stage (8 ss) and 24 hours post fertilization (24 hpf), and performed microdissections to isolate the head, somites/anterior presomitic mesoderm (PSM) and posterior PSM at the 8 ss, along with the anterior-half and posterior-half of 24 hpf embryos (Fig. III.1b). All samples were analysed by RT-qPCR using primers that specifically recognize different subsets of *fgf8a* alt3'UTRs (Fig. III.1c). We observed no significant variations in relative alt3'UTR abundance between these conditions (Fig. III.1d-f), indicating that *fgf8a* PAS usage preferences are largely conserved across the embryonic tissues and developmental stages analysed. Therefore, we focused on the alt3'UTRs with the highest reported abundance - *fgf8aM* and *fgf8aS*.

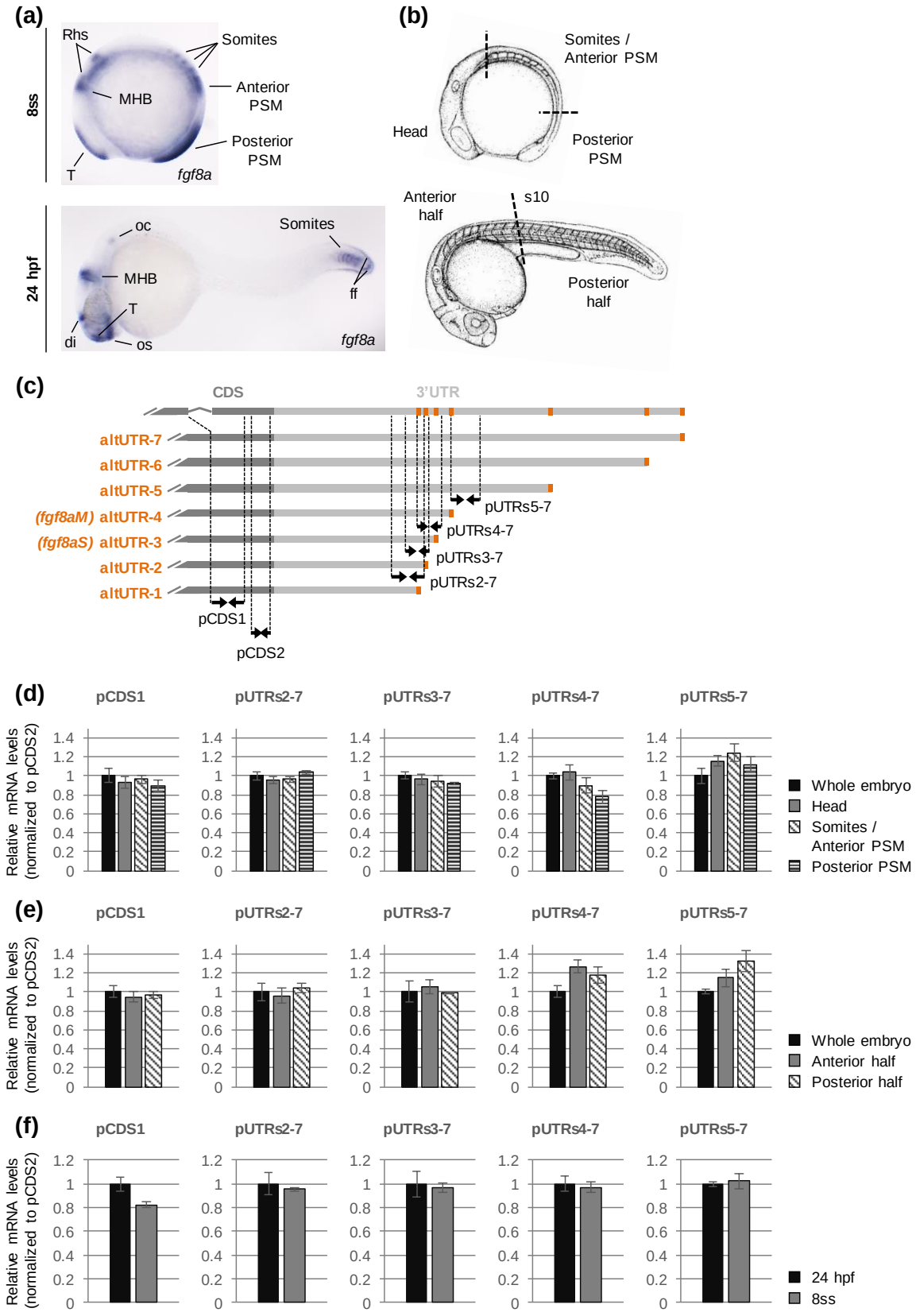

Fig. III.1 – Alternative *fgf8a* 3'UTR usage in the developing embryo.
(Figure legend on the next page)

Fig. III.1 – Alternative *fgf8a* 3'UTR usage in the developing embryo.
(a) Representative images of the wildtype expression pattern of the zebrafish *fgf8a* gene at the 8 somite stage (8 ss) and at 24 hours post fertilization (hpf). Images obtained following Whole-mount *In Situ* Hybridization (WISH) for the coding sequence of *fgf8a*. T, telencephalon; Rhs, rhombomeres 2 and 4; MHB, midbrain-hindbrain boundary; PSM, presomitic mesoderm; oc, otic capsule; os, optic stalks; di, diencephalon; ff, dorsal and caudal fin fold. **(b)** Illustration of the microdissection procedures performed on 8 ss and 24 hpf zebrafish embryos. s10, position of the 10th somite. **(c)** Schematic representation of the alt3'UTRs previously reported for *fgf8a* and primers used for RT-qPCR (pUTRs, pCDS). The alt3'UTRs amplified by each primer pair are indicated by the dashed lines. The pCDS1 and pCDS2 primer pairs both recognize the *fgf8a* coding sequence, with pCDS1 targeting the exon4-exon5 junction. The pUTRs2-7 primer pair recognizes all *fgf8a* transcripts, except those with the altUTR-1. The pUTRs3-7 primer pair recognizes transcripts with the *fgf8aS* UTR, the *fgf8aM* UTR and the longer alt3'UTRs-5 to 7. The pUTRs4-7 primer pair recognizes transcripts with the *fgf8aM* UTR and the longer alt3'UTRs-5 to 7. The pUTRs5-7 primer pair only recognizes transcripts with the longer alt3'UTRs-5 to 7. **(d-f)** Relative RT-qPCR quantification of the endogenous levels of *fgf8a* transcript and indicated alt3'UTRs **(d)** in 8 ss whole embryos and microdissected tissue samples, **(e)** in 24 hpf whole embryos and microdissected tissue samples, **(f)** in 24 hpf and 8 ss whole embryos. **(d-f)** All the results shown are relative to the indicated control conditions, namely, **(d,e)** the whole embryo condition, **(f)** the 24 hpf condition. **(d-f)** Data show mean ± SEM. Statistical analysis was done using two-tailed t-test, and all comparisons were deemed not statistically significant ($p>0.05$).

To assess the impact of the *fgf8aM* and *fgf8aS* 3'UTRs on translation efficiency and mRNA stability, we generated a set of reporters in which the eGFP coding sequence was fused to each 3'UTR. Reporter constructs were *in vitro* transcribed, and the resulting mRNAs were co-injected with control mCherry mRNA into wildtype 1-cell stage embryos. mCherry was used, in this context, to account for microinjection variability. eGFP-3'UTR fluorescence intensities and mRNA abundances were quantified 24 hours post injection, normalized to mCherry, and compared to those obtained with control eGFP mRNA. (Fig. III.2a). We found that the *fgf8aM* 3'UTR induced a 72% reduction in reporter fluorescence (Fig. III.2b,d) in contrast to the *fgf8aS* 3'UTR which had a mild effect on reporter fluorescence (10% reduction) (Fig. III.2b,d). No clear tissue-specific variations in reporter fluorescence were identified in these assays (Fig. III.2d), suggesting that the effect of these 3'UTRs on reporter expression is spatially conserved. Furthermore, both 3'UTRs mediated a reduction in reporter mRNA levels, of 45% and 29% for *fgf8aM* and *fgf8aS*, respectively (Fig. III.2c). Taken together, these results indicate that, while both 3'UTRs have a moderate impact on mRNA stability, the *fgf8aM* 3'UTR mediates a strong translational repression when compared to the *fgf8aS* 3'UTR.

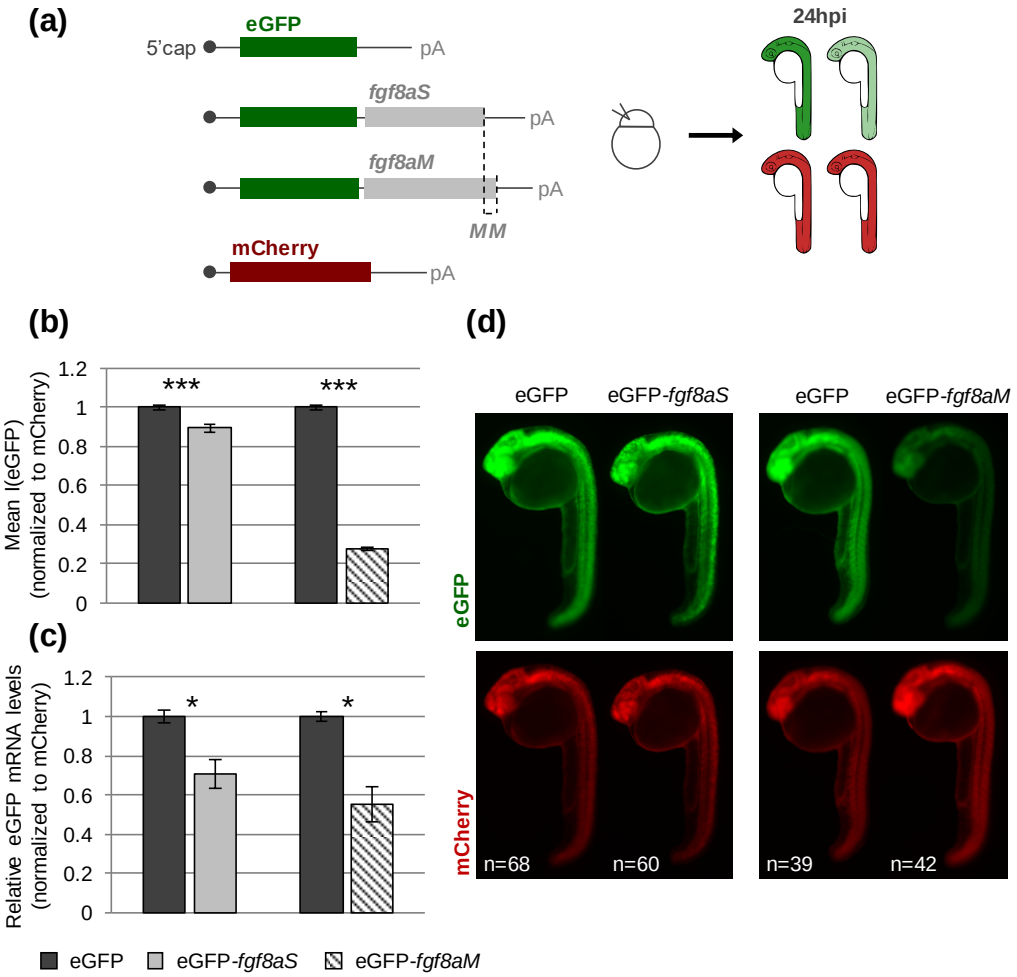

Fig. III.2 – Alt3'UTRs *fgf8aM* and *fgf8aS* mediate different effects on post-transcriptional regulation.
(a) Schematic representation of the experimental setup. eGFP mRNAs with and without the *fgf8aS* or *fgf8aM* 3'UTRs were co-injected with *mCherry* mRNA at the 1-cell stage. At 24 hours post-injection (hpi) fluorescence intensities were measured and relative reporter mRNA levels determined by RT-qPCR. pA, SV40 polyadenylation signal; MM, Minimal Motif. **(b)** Mean eGFP fluorescence intensities, normalized to mCherry fluorescence intensities, obtained for the indicated reporters. **(c)** Relative eGFP mRNA levels, normalized to mCherry mRNA levels, obtained for the indicated reporters. **(d)** Representative images of embryos injected with each reporter. **(b,c)** Data show mean ±SEM (*p<0.05; ***p<0.001).

To gain a better understanding of the *fgf8a* post-transcriptional regulation dynamics, we established a system of differential equations to simulate the translation and decay of the eGFP-*fgf8aS* and eGFP-*fgf8aM* reporters during a 24 hour period and estimate their respective rate constants based on the observed mRNA and protein abundances. To account for the experimental observations, the best fitting model parameters require a 3 fold lower translation rate for the eGFP-*fgf8aM* mRNA than

for the eGPF-*fgf8aS* mRNA, and a relatively small difference in the respective mRNA decay constants (k_M-k_S=0.010 h^{-1}) (Section III.5.1 - Supplemental Text - Analysis of the reporter system).

Interestingly, the *fgf8aM* and *fgf8aS* 3'UTRs differ only in a 71nt sequence (Fig. III.2a and Fig. III.3a). To assess the relative importance of this sequence to the *fgf8aM*-mediated regulation of transcript stability and translation efficiency, we compared the fluorescence intensities and relative transcript levels of an eGFP reporter fused to this sequence to those obtained with the eGFP-*fgf8aM* reporter. We found that both the fluorescence intensities and the relative transcript levels of the eGFP reporter fused to this sequence were equivalent to those obtained with the eGFP-*fgf8aM* reporter (Fig. III.3b,c,d). Therefore, this 71nt sequence, which we termed Minimal Motif (MM), appears to be both necessary and sufficient to mediate the post-transcriptional regulation associated with the *fgf8aM* 3'UTR.

To understand the mechanisms underlying this regulation, we analysed the MM sequence for the presence of post-transcriptional regulatory elements. The TargetScanFish6.2 database reports a binding site for dre-miR-2187 in the central region of the MM (Fig. III.3a) (Lewis et al., 2005, Grimson et al., 2007, Ulitsky et al., 2012). Furthermore, the available miRBase expression data indicates that this miR is expressed during development, in particular at 24 hpf (Kozomara and Griffiths-Jones, 2014). This prediction therefore suggests that the dre-miR-2187 could be involved in the MM-mediated post-transcriptional regulation.

In conclusion, our results reveal a significant impact of the presence of the MM sequence on mRNA expression. Therefore, even though the endogenous levels of the *fgf8aS* 3'UTR are much lower than those of the *fgf8aM* 3'UTR, transcripts with the *fgf8aS* 3'UTR are likely to contribute significantly to Fgf8a protein synthesis due to the absence of the MM.

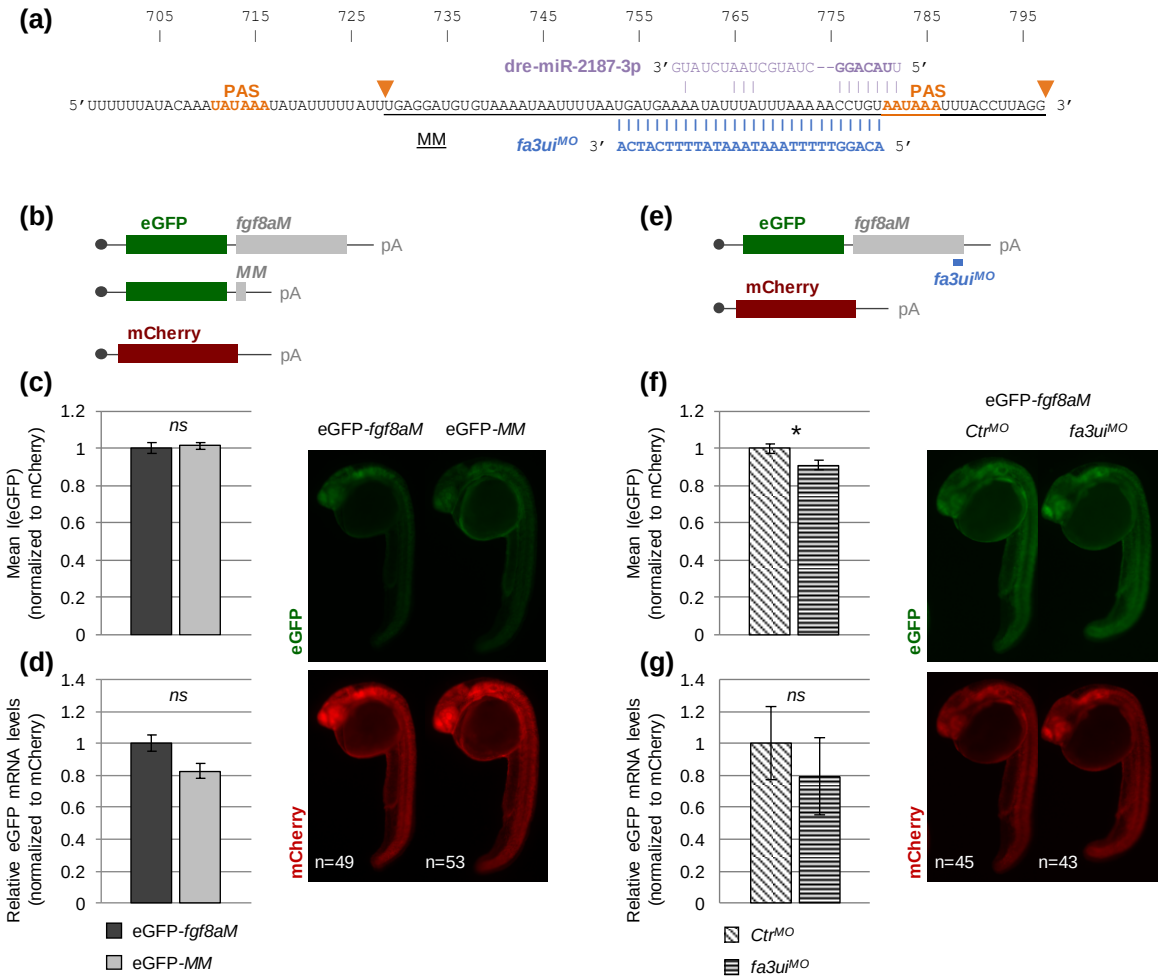

Fig. III.3 – The MM is necessary and sufficient to mediate the *fgf8aM*-associated post-transcriptional regulation and this regulation is not substantially affected by the *fa3ui*^{MO}.

(a) Illustration of the MM sequence, the *fgf8aS* and *fgf8aM* PASs and polyadenylation sites (arrowheads), the predicted miR-2187 binding site and the *fa3ui*^{MO} binding site. **(b)** Schematic representation of the experimental setup. *eGFP* mRNAs with either *fgf8aM* or *MM* were co-injected with *mCherry* mRNA at the 1-cell stage. At 24 hpi **(c)** fluorescence intensities were measured and **(d)** relative reporter mRNA levels determined by RT-qPCR. **(e)** Schematic representation of the experimental setup. eGFP-*fgf8aM* mRNA was co-injected with *mCherry* mRNA and either *Ctr*^{MO} or *fa3ui*^{MO} at the 1-cell stage. At 24 hpi **(f)** fluorescence intensities were measured and **(g)** relative reporter mRNA levels determined by RT-qPCR. **(c,f)** Mean eGFP fluorescence intensities, normalized to mCherry fluorescence intensities. **(d,g)** Relative eGFP mRNA levels normalized to mCherry mRNA levels. **(c,d,f,g)** Data show mean ±SEM (*p<0.05). Representative images of embryos for each condition are shown.

III.2.2 Interference with alternative PAS usage potentiates Fgf signalling

To investigate the functions of the *fgf8aS* and *fgf8aM* 3'UTRs, we used TALEN and CRISPR/Cas9 technologies to modify relevant sequences in the MM, with no success (Section III.4.1.2). We believe this was due to the low GC-content of this genomic region, a sequence feature which has been previously shown to be associated with ineffective mutagenesis (Liu et al., 2016, Wang et al., 2014, Doench et al., 2014, Gagnon et al., 2014).

Therefore, to address the functional relevance of the *fgf8aS* and *fgf8aM* 3'UTRs we designed a morpholino oligo against the central region of the MM, which we termed *fgf8a* alt3'UTR interference morpholino (*fa3ui*^{MO}) (Fig. III.3a). By targeting the MM, our aim was to disrupt either the post-transcriptional regulation mediated by the *fgf8aM* 3'UTR or the alternative PAS selection process.

Morpholino oligonucleotides have been previously used, as target protector molecules, to disrupt post-transcriptional regulation events. In their capacity as target protectors, morpholinos bind to regulatory RNA elements blocking their interaction with post-transcriptional regulators (e.g. miRs or RBPs), and thus protect the transcript from the resulting regulation of mRNA stability and/or translation efficiency (Choi et al., 2007, Staton et al., 2011, Cibois et al., 2010).

The *fa3ui*^{MO} was designed to protect the predicted miR-2187 target site (Fig. III.3a) and its effect on the *fgf8aM*-mediated post-transcriptional regulation was assessed by co-injecting the *fa3ui*^{MO} with eGFP-*fgf8aM* mRNA and analysing the resulting effects on reporter fluorescence and relative reporter mRNA levels. We would expect that if the predicted miR-2187-*fgf8aM* interaction had a significant contribution to the post-transcriptional repression mediated by this 3'UTR, the *fa3ui*^{MO} would disrupt this interaction and thus bring about an increase in eGFP-*fgf8aM* reporter fluorescence and/or relative transcript levels. However, we found that the presence of the *fa3ui*^{MO} had a minor effect on eGFP-*fgf8aM* reporter fluorescence (9% reduction) (Fig. III.3e,f) and did not affect the relative transcript levels of the eGFP-*fgf8aM* reporter (Fig. III.3e,g). These results therefore argue against a role for the miR-2187 in the regulation of *fgf8a* expression.

In addition, the observation that the *fa3ui*^{MO} had a negligible impact on eGFP-*fgf8aM* reporter expression, both at the mRNA and at the protein level (Fig. III.3f,g), indicates that this morpholino does not interfere substantially with either the stability or with the translation efficiency of transcripts with the *fgf8aM* 3'UTR. Therefore, we conclude that the *fa3ui*^{MO} does not effectively disrupt these post-transcriptional regulation mechanisms.

Considering that the *fa3ui*^{MO} target sequence is directly upstream of the *fgf8aM* polyadenylation signal (Fig. III.3a), we next sought to determine if the *fa3ui*^{MO} could be used to interfere with the endogenous *fgf8a* alternative PAS selection process.

To address this question, we assessed the impact of *fa3ui*^{MO} injection on the endogenous *fgf8a* transcript and alt3'UTR levels, using the previously described RT-qPCR approach (Fig. III.1c). At 24 hpf, using primers that target the coding sequence we observed that the presence of the *fa3ui*^{MO} led to a 2.5 fold increase in total *fgf8a* mRNA levels, (Fig. III.4a, pCDS2). A similar increase (2.7 fold) was observed when using primers that detect both the *fgf8aS* and *fgf8aM* 3'UTRs (Fig. III.4a, pUTRs3-7). However, when using primers that detect the *fgf8aM* 3'UTR, but not the *fgf8aS* 3'UTR, we observed a smaller increase in transcript levels (1.8 fold) in *fa3ui*^{MO} morphants (Fig. III.4a, pUTRs4-7). A similar trend was observed in *fa3ui*^{MO} morphants at the 8 ss (Fig. III.4b), albeit with less pronounced fold changes in transcript levels when using the pCDS2 (1.3 fold) and pUTRs3-7 (1.4 fold) primers and no significant difference in relative transcript levels when using the pUTRs4-7 primers.

Furthermore, while the relative abundance of the longer 3'UTRs (altUTRs-5 to -7) did not change at 24 hpf (Fig. III.4a, pUTRs5-7), a significant reduction was detected at the 8 ss in *fa3ui*^{MO} morphants (Fig. III.4b, pUTRs5-7). However, given the low abundance of these longer 3'UTRs in the developing embryo (4.5-7.4%, Table III.S1), their contribution to the system is negligible and therefore we did not consider them in the global analysis of *fgf8* expression.

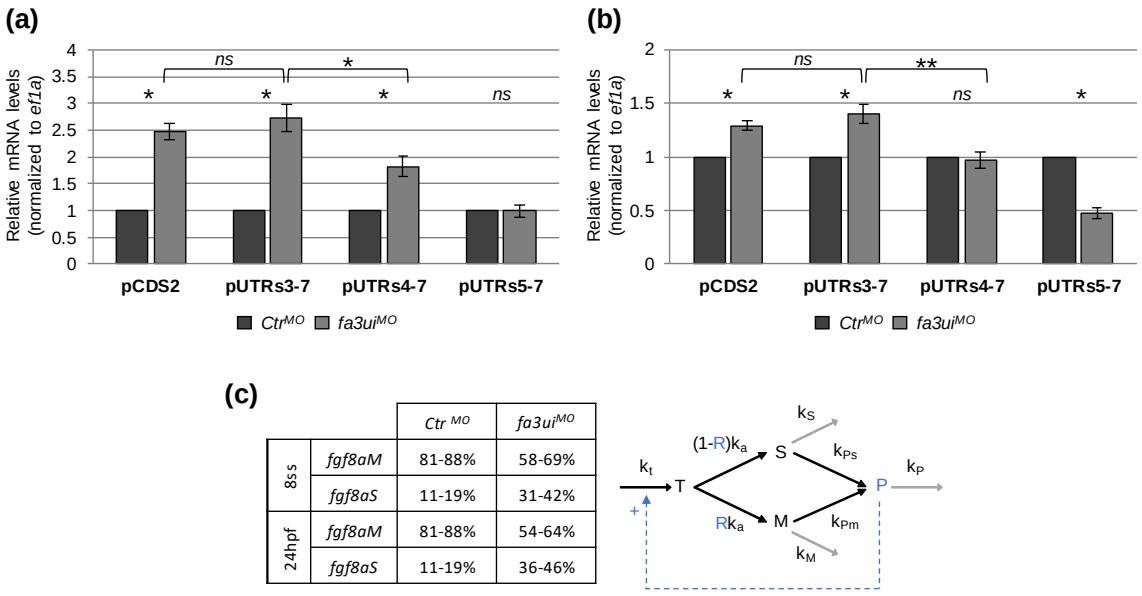

(c)

		Ctr^{MO}	$fa3ui^{MO}$
8ss	*fgf8aM*	81-88%	58-69%
	fgf8aS	11-19%	31-42%
24hpf	*fgf8aM*	81-88%	54-64%
	fgf8aS	11-19%	36-46%

Fig. III.4 – *fa3ui*^{MO} morphants display a shift in PAS usage preferences.
(a,b) RT-qPCR quantification of the relative endogenous *fgf8a* transcript and indicated alt3'UTR levels in *Ctr*^{MO} and *fa3ui*^{MO} morphants **(a)** at 24 hpf and **(b)** at the 8 ss. **(a,b)** The pCDS2 primer pair recognizes the *fgf8a* coding sequence. The pUTRs3-7 primer pair recognizes transcripts with the *fgf8aS* UTR, the *fgf8aM* UTR and the longer alt3'UTRs -5 to -7. The pUTRs4-7 primer pair recognizes transcripts with the *fgf8aM* UTR and the longer alt3'UTRs -5 to -7, but not transcripts with the *fgf8aS* UTR. The pUTRs5-7 primer pair only recognizes transcripts with the longer alt3'UTRs -5 to -7. Data show mean ±SEM (*p<0.05; ** p<0.01). **(c)** Estimated relative percentages of the *fgf8aM* and *fgf8aS* 3'UTRs under *Ctr*^{MO} and *fa3ui*^{MO} morphant conditions at the 8 ss and at 24 hpf and schematic representation of the mathematical model. Black arrows represent transcription, APA and translation. Grey arrows represent mRNA and protein decay. Parameters in blue highlight key points of the *fa3ui*^{MO}-mediated interference. For more details see Section III.5.1 - Supplemental text.

From these results we conclude that there is a differential increase in the relative levels of the *fgf8aS* 3'UTR compared to the *fgf8aM* 3'UTR in the presence of *fa3ui*^{MO} (pUTRs3-7 and pUTRs4-7 in Fig. III.4a,b). The simplest explanation for these observations is that the *fa3ui*^{MO} interferes with the endogenous PAS selection process, leading to a more pronounced usage of the *fgf8aS* PAS. However, this intuitive interpretation is limited by the fact that we are only quantifying the change in transcript abundance between the control and *fa3ui*^{MO} injected embryos for each primer pair, and the fact that the signal from the primer pair pUTRs3-7 represents the sum of both the *fgf8aS* and *fgf8aM* 3'UTRs. Furthermore, these results reveal an overall increase in total *fgf8a* transcript levels (pCDS2 in Fig. III.4a,b), which was not expected to emerge from the proposed shift in PAS usage.

Therefore, to gain a better understanding of the *fa3ui*^{MO}-mediated interference with PAS selection and address the nature of the observed increase in total *fgf8a* transcript levels, we resorted to mathematical modelling of the kinetics of *fgf8a* expression (Section III.5.1 - Supplemental Text). The data obtained in the fluorescent reporter assays (Fig. III.2) were used to estimate the mRNA decay and translation rate constants imposed by the *fgf8aS* and *fgf8aM* 3'UTRs (Section III.5.1 - Supplemental Text - Analysis of the Reporter system). In addition, the model incorporates the RT-qPCR data assessing the impact of the *fa3ui*^{MO} on the endogenous target expression (Fig. III.4a,b and Section III.5.1 - Supplemental Text - Model of endogenous *fgf8a* expression). This approach allowed us to integrate the results obtained using the reporter constructs and endogenous targets, into a comprehensive model of the endogenous *fgf8a* gene-to-protein pathway (Fig. III.4c).

We began by using the mathematical model to calculate the relative fractions of transcripts produced with each 3'UTR in control and *fa3ui*^{MO} conditions. This analysis estimates that in control conditions 11-19% of transcripts are produced with the *fgf8aS* 3'UTR, whereas in the presence of the *fa3ui*^{MO} this percentage increases to 36-46% at 24 hpf and 31-42% at the 8 ss (Fig. III.4c and Section III.5.1 - Supplemental Text). The model can simulate this change in UTR abundance by altering the parameter defining the selection of the polyadenylation site (Section III.5.1 - Supplemental Text). This supports the conclusion that the presence of the *fa3ui*^{MO} stimulates the usage of the *fgf8aS* PAS. Furthermore, the similarity between the values obtained for 24 hpf and 8 ss indicates that the effect of the *fa3ui*^{MO} on PAS usage is consistent between both developmental stages.

Interestingly, since the *fgf8aS* 3'UTR supports a higher translation efficiency (Fig. III.2b), the model predicts that the *fa3ui*^{MO}-induced increase in *fgf8aS* PAS usage would lead to a 40-60% increase in Fgf8a protein levels (Section III.5.1 - Supplemental Text).

Furthermore, our model revealed that this shift in PAS usage, on its own, would not be sufficient to account for the observed increase in total *fgf8a* transcript levels in *fa3ui*^{MO} morphants. The simplest way to mathematically account for this increase is to accompany the shift in PAS usage with an increase in *fgf8a* transcription (Section

III.5.1 - Supplemental Text). To address this increase in *fg8a* transcription, we propose the presence of a direct or indirect positive feedback element. In essence, the enhanced production of the *fgf8aS* 3'UTR is predicted to lead to an increase in Fgf8a protein levels (Section III.5.1 - Supplemental Text and Fig. III.2b), which in turn is expected to induce an overactivation of Fgf signalling. By introducing a feedback element whereby this overactivation of Fgf signalling leads to a positive modulation of the transcription of the *fgf8a* gene, we were able to accurately reproduce the observed increase in *fgf8a* mRNA levels in the mathematical model as an indirect response to the shift in PAS usage (Section III.5.1 - Supplemental Text and Fig. III.4c).

Taken together, our results indicate that the *fa3ui*^{MO} induces a shift in PAS selection preferences, favouring *fgf8aS* PAS usage, along with an increase in total *fgf8a* transcript levels which could emerge from feedback-based mechanisms.

We next evaluated if the increase in *fgf8a* mRNA levels in the presence of the *fa3ui*^{MO} was spatially uniform in the embryo. Using whole-mount *in situ* hybridization (WISH), we observed a greater increase in *fgf8a* mRNA levels in the optic stalks and diencephalon than in the MHB (Fig. III.5a). Additionally, using RT-qPCR, we showed that in *fa3ui*^{MO} morphants the increase in total *fgf8a* transcript levels was more pronounced in anterior (2.4 fold) than in posterior (2.0 fold) tissues (Fig. III.5b). These results reveal the presence of tissue-specific responses to the *fa3ui*^{MO}. Since the Fgf pathway interacts with varied signalling pathways in different tissues (Pownall and Isaacs, 2010), these tissue-specific responses could arise from tissue-specific differences in the mechanisms underlying the previously proposed feedback element.

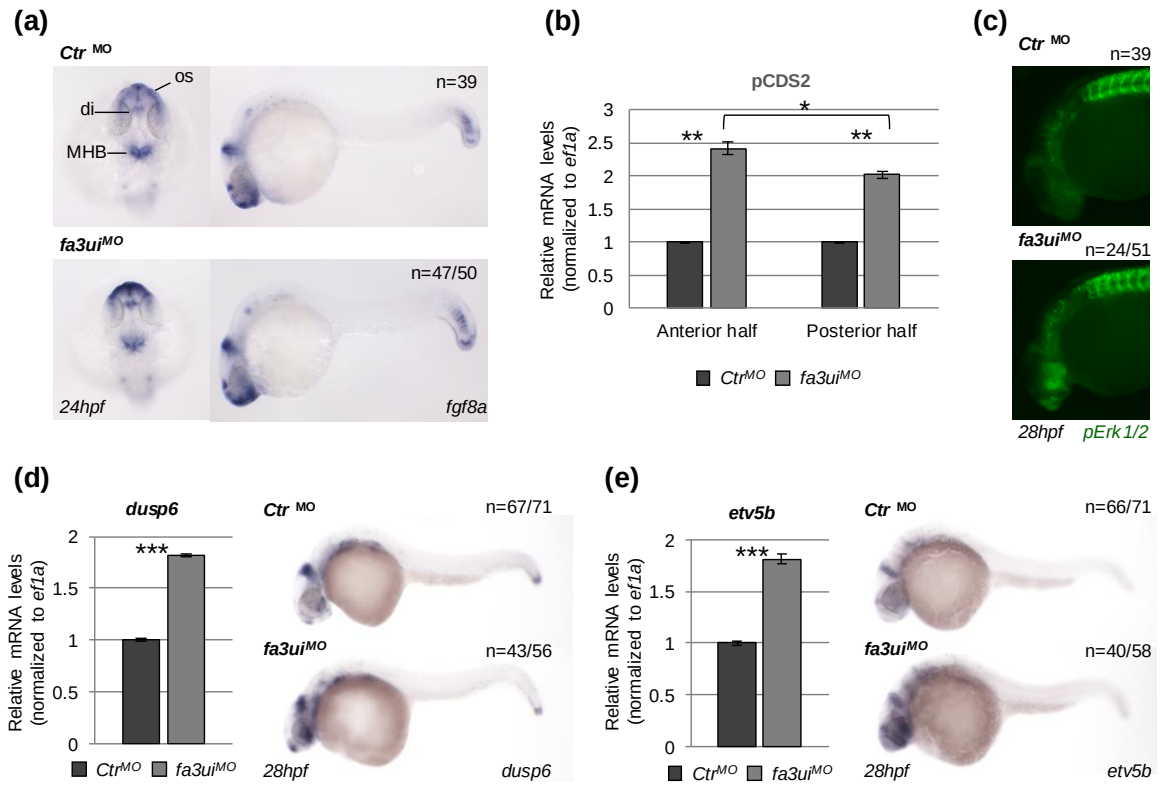

Fig. III.5 – *fa3ui*^{MO} morphants display an increase in Fgf signalling.
(a) WISH for the coding sequence of *fgf8a* at 24 hpf in *Ctr*^{MO} and *fa3ui*^{MO} morphants. os, optic stalks; di, diencephalon; MHB, midbrain-hindbrain boundary. **(b)** RT-qPCR quantification of the endogenous relative *fgf8a* transcript levels in microdissected anterior and posterior tissues of 24 hpf *Ctr*^{MO} and *fa3ui*^{MO} injected embryos. For an Illustration of the microdissection procedures performed see Fig. III.1b. **(c)** Immunohistochemistry for pErk1/2 (Phospho-p44/42MAPK) at 28 hpf in *Ctr*^{MO} and *fa3ui*^{MO} morphants. **(d,e)** WISH (28 hpf) and RT-qPCR quantification (24 hpf) of the relative mRNA levels of **(d)** *dusp6* and **(e)** *etv5b* in *Ctr*^{MO} and *fa3ui*^{MO} morphants. **(b,d,e)** Data show mean ±SEM (*p<0.05; ** p<0.01;***p<0.001).

To determine if the overall effects of the *fa3ui*^{MO} on *fgf8a* at the transcript level effectively led to a modulation of Fgf signalling we analysed the phosphorylation of Erk1/2, an effector of Fgf signalling, and the expression of the Fgf downstream targets *dusp6* and *etv5b* in *fa3ui*^{MO} morphants. We found an increase in the activated forms of Erk1/2, primarily in the eye-field (Fig. III.5c) and, using RT-qPCR and WISH, we observed an increase in the expression levels of *dusp6* and *etv5b* (Fig. III.5d,e). These results show that the *fa3ui*^{MO} mediates an activation of Fgf signalling.

III.2.3 Interference with *fgf8a* PAS usage selectively affects sensory system development

We next took advantage of the *fa3ui*^{MO}-induced shift in *fgf8a* PAS usage to address the impact of interfering with this process on embryonic development. We began by focusing on developmental processes that are known to be dependent on, or affected by, Fgf8a.

In the otic vesicle, we observed that *fa3ui*^{MO} morphants showed a downregulation of *neurog1* in the statoacoustic ganglion, indicating an impairment of neuroblast specification (Fig. III.6a). Furthermore, we observed a reduction in *isl1* expression, which suggests an inhibition of neuronal maturation (Fig. III.6b). Both observations are consistent with previous studies conducted in the context of a strong activation of *fgf8a* expression at 24 hpf using a heat-shock promoter (Vemaraju et al., 2012).

In the forebrain, *fa3ui*^{MO} morphants presented defects in axon guidance in the anterior commissure (Fig. III.6c). This is consistent with the defects observed in commissure formation in *ace* and *aus* mutants, which display a depletion and overexpression of *fgf8a*, respectively (Shanmugalingam et al., 2000, Heisenberg et al., 1999).

Interestingly, earlier developmental processes known to involve Fgf8a, were not compromised in *fa3ui*^{MO} morphants. Namely, we did not observe noticeable gastrulation defects, alterations in the tailbud mesodermal progenitor population (Fig. III.6d) or defects in somite formation (Fig. III.6e). Furthermore, MHB patterning also appeared to be unaffected in *fa3ui*^{MO} morphants (Fig. III.6f,g).

These results reveal that the *fa3ui*^{MO} mediated interference with *fgf8a* PAS selection affects primarily developmental processes taking place at later stages of development and in more anterior tissues associated with the sensory system. This is in line with our observation that *fgf8* transcript levels were more substantially affected by the *fa3ui*^{MO} at later (24 hpf) than earlier stages (8 ss), with different tissues displaying different magnitudes of this effect (Fig. III.4a,b and Fig. III.5a,b). These spatially and temporally specific responses to the *fa3ui*^{MO} likely reflect the distinct mechanisms involved in the different functions of Fgf8a throughout development (Pownall and Isaacs, 2010).

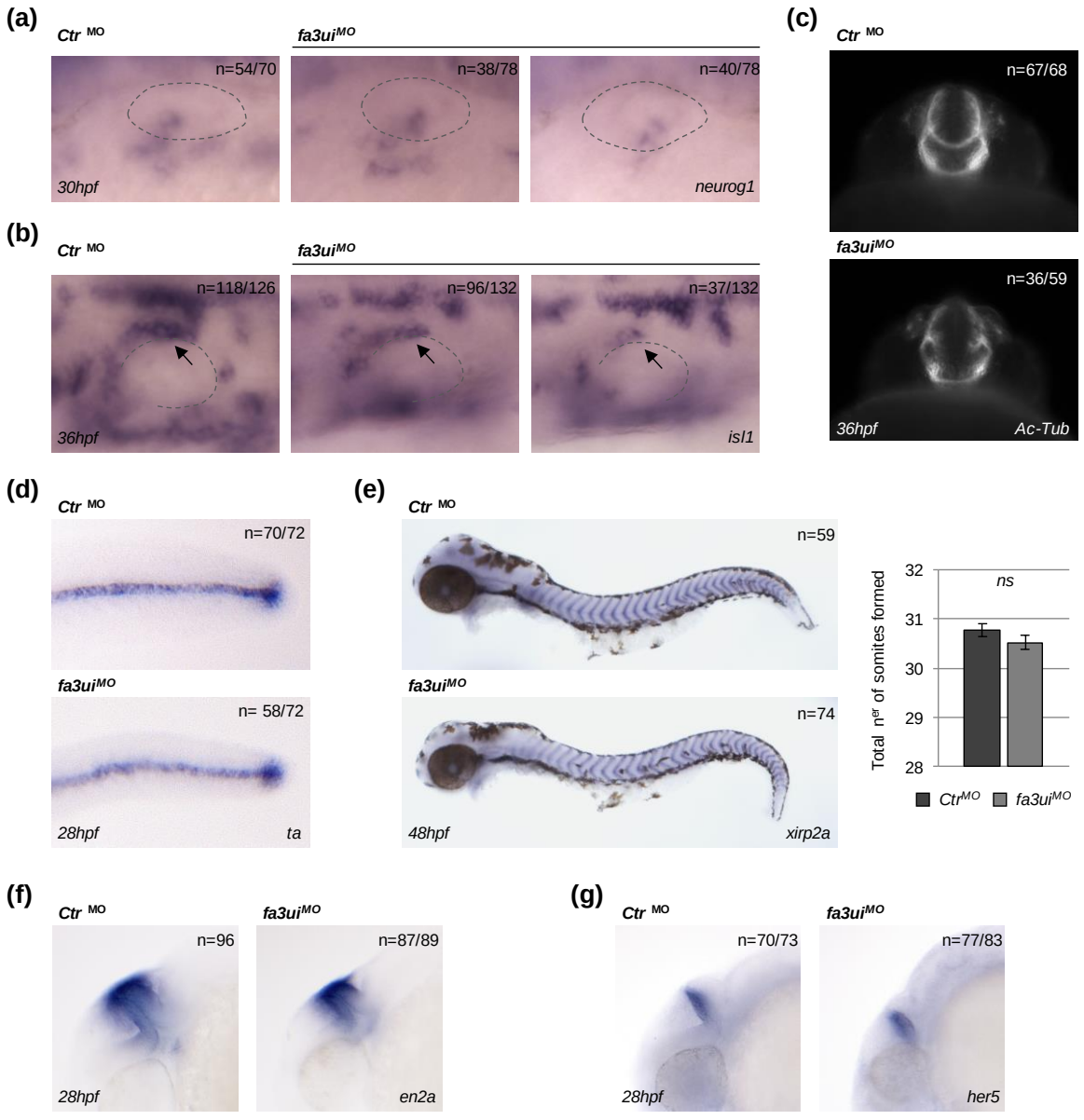

Fig. III.6 – Assessment of *fgf8a*-associated developmental processes in *fa3ui*^{MO} morphants.

(a) WISH for *neurog1* at 30 hpf in *Ctr*^{MO} and *fa3ui*^{MO} morphants. **(b)** WISH for *isl1* at 36 hpf in *Ctr*^{MO} and *fa3ui*^{MO} morphants. Arrows indicate the mature neuronal population of the statoacoustic ganglion. **(a,b)** Dorsolateral views, anterior to the left. The otic vesicle is outlined. **(c)** Immunohistochemistry for acetylated-tubulin at 36 hpf in *Ctr*^{MO} and *fa3ui*^{MO} morphants. **(d-g)** WISH in *Ctr*^{MO} and *fa3ui*^{MO} morphants for **(d)** the tailbud progenitor marker *ta*, **(e)** the somite boundary marker *xirp2a*, mean ±SEM number of somites for each condition, **(f)** the MHB markers *en2a* and **(g)** *her5*, **(d,f,g)** at 28 hpf, **(e)** at 48 hpf.

We additionally observed abnormalities in *fa3ui*^{MO} morphants regarding the formation of the superficial ocular vasculature (Kaufman et al., 2015). Using a *kdrl*:mCherry transgenic line, which labels endothelial cells, we found that *fa3ui*^{MO} morphants displayed an increased number of superficial ocular radial vessels when compared to control embryos (Fig. III.7a,c). This increase was partially rescued by a mild activation of the dominant-negative form of Fgfr1 (Fig. III.7b,c), suggesting an involvement of Fgf signalling in superficial ocular vascularization.

To determine the effect of Fgf signalling depletion on the formation of this vascular system, we analysed the ocular vasculature of *ace* mutant embryos and embryos expressing the hs:*dnfgfr1* transgene. We found no noticeable difference in the number of radial vessels formed in these conditions, relative to controls. However, both *ace* mutants and hs:*dnfgfr1*+/- embryos showed a delay in the formation of the superficial annular vessel (SAV) at 48 hpf (Fig. III.7f,i, arrows in Fig. III.7d,g). By 72 hpf, *ace* mutants recovered from this delay while hs:*dnfgfr1*+/- embryos still presented an incomplete SAV (Fig. III.7f,i,e, arrow in Fig. III.7h). Furthermore, we detected morphological abnormalities, primarily an increase in the width of the SAV vessel, in hs:*dnfgfr1*+/- embryos but not in *ace* mutants (Fig. III.7i, arrowheads in Fig. III.7g,h).

Taken together these results reveal a previously undescribed role for Fgf signalling in the early stages of superficial ocular vascularization.

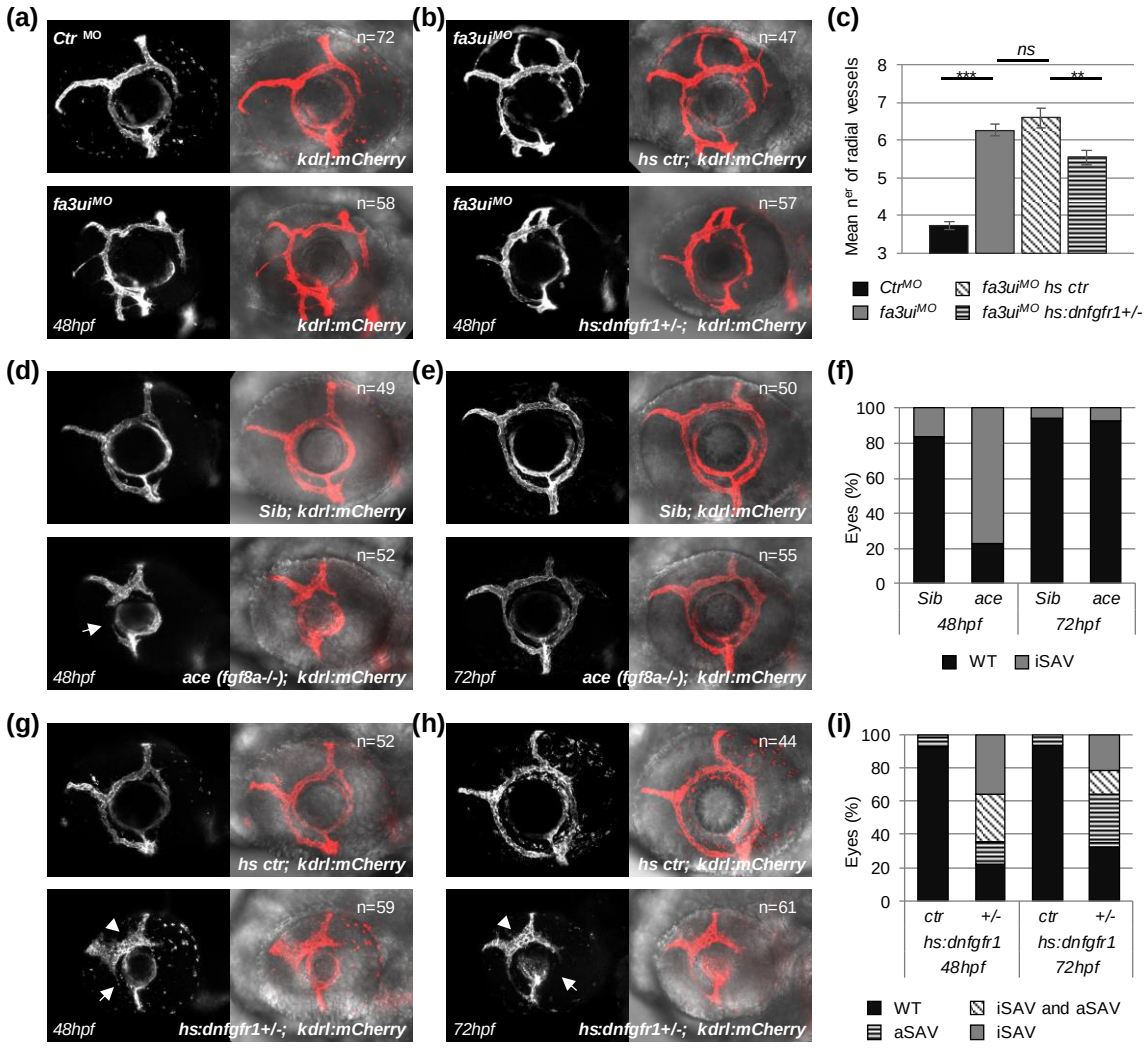

Fig. III.7 – Fgf signalling is involved in the early stages of superficial retinal vascularization.

(a-c) Superficial ocular vasculature of 48 hpf *kdrl*:mCherry embryos **(a)** injected with *Ctr*^{MO} or *fa3ui*^{MO} **(b)** injected with *fa3ui*^{MO} with and without the hs:*dnfgfr1*+/- transgene, under mild heat-shock conditions. **(c)** Mean number of ocular radial vessels ±SEM (**p<0.01; ***p<0.001). **(d-i)** Superficial ocular vasculature of **(d,e)** *ace*(*fgf8a*-/-), *kdrl*:mCherry embryos and siblings **(g,h)** hs:*dnfgfr1*+/-, *kdrl*:mCherry embryos and siblings under strong heat-shock conditions **(d,g)** at 48 hpf **(e,h)** at 72 hpf **(f,i)** Percentage of eyes with wildtype SAV, incomplete SAV formation (iSAV, Arrows) and abnormal SAV morphology (aSAV, Arrowheads).

III.3 DISCUSSION

Alternative polyadenylation in the 3'UTR is remarkably prevalent during embryonic development, with studies in zebrafish revealing that approximately half of all expressed protein-coding genes undergo 3'UTR APA during embryogenesis (Ulitsky et al., 2012, Li et al., 2012). However, the functional relevance of individual APA events has remained largely unaddressed. While investigating the 3'UTR-dependent regulation of *fgf8a* expression during embryonic development we came across multiple alternative 3'UTRs reported in different databases and transcriptome profiling datasets (Table III.S1). This study was focused on assessing the impact of the two most abundant *fgf8a* alt3'UTRs on gene expression, and addressing their functional relevance to embryonic development.

The emerging picture for the post-transcriptional regulation of *fgf8a* expression is somewhat distinct from the trends reported by large scale studies of gene expression control and alternative polyadenylation. Firstly, a study conducted in mouse fibroblast cells revealed that alternative 3'UTRs tend to have a limited impact on mRNA stability and protein translation (i.e., <20%) (Spies et al., 2013). Here we demonstrate that the most abundant alt3'UTR - *fgf8aM* - is associated with a strong inhibition of protein synthesis (Fig. III.2b,d), with the source of this differential post-transcriptional regulation residing in a 71nt sequence motif, termed minimal motif (MM) (Fig. III.3b,c,d). Furthermore, we observed that a shift from distal to proximal PAS usage has a significant impact on Fgf signalling levels (Fig. III.4 and Fig. III.5). Secondly, genome wide studies report that average 3'UTR lengths tend to vary throughout the progression of embryonic development (Li et al., 2012, Ulitsky et al., 2012, Ji et al., 2009, Sanfilippo et al., 2017, Mangone et al., 2010), with several genes also displaying tissue-specific alternative PAS usage preferences (Ulitsky et al., 2012, Sanfilippo et al., 2017, Hilgers et al., 2011, Miura et al., 2013). In contrast, our results indicate that, for the *fgf8a* gene, endogenous alternative PAS usage seems to remain relatively stable across the tissues and developmental stages analysed (Fig. III.1). Therefore, we propose that in this specific case, APA can act to fine-tune overall protein levels within each cell.

To address the functions of the *fgf8aS* and *fgf8aM* 3'UTRs we initially resorted to TALEN and CRISPR/Cas9 technologies, to modify relevant sequences in the MM,

with no success (Section III.4.1.2). Both CRISPR/Cas9 and TALEN technologies have been previously used successfully in our lab (Ribeiro et al., 2017, Pinto et al., 2018). We believe that in this case, site directed mutagenesis was unsuccessful due to the very low G/C content of the MM sequence. As previously shown, mutagenesis efficiency is dependent on the G/C content of the target sequence, with guide RNAs targeting regions with either very low or very high G/C contents, being less efficient (Liu et al., 2016, Wang et al., 2014, Doench et al., 2014, Gagnon et al., 2014). An additional sequence-specific factor, known to influence mutagenesis efficiency, which could have contributed to our inability to generate a stable mutant line is the local chromatin structure (Chen et al., 2017b, Wu et al., 2014, Kuscu et al., 2014). The *fa3ui*^{MO} was therefore used in this study, to address the functional importance of the *fgf8a* alt3'UTRs.

Sequence analysis of the *fgf8aM* alt3'UTR using the TargetScanFish algorithm revealed a predicted binding site for dre-miR-2187 in the MM region (Fig. III.3a). miRs have well-established roles in the post-transcriptional regulation of gene expression, through the modulation of translation efficiency and mRNA decay, in several model organisms (Fabian et al., 2010, Alvarez-Garcia and Miska, 2005). In this study, the *fa3ui*^{MO}, which directly targets the predicted miR-2187 binding site, was used as a target protector morpholino, to address the potential significance of this predicted miR-MM interaction. However, as shown in Fig. III.3e,f,g, the expression levels of the eGFP reporter containing the *fgf8aM* alt3'UTR were not restored by co-injection of the *fa3ui*^{MO}. This result indicates that the dre-miR-2187 is unlikely to be involved in the MM-associated regulation, and consequently, that this predicted miR-MM interaction does not have a meaningful role in the regulation of *fgf8a* expression *in vivo*. Therefore, the mechanism that underlies the post-transcriptional regulation associated with the *fgf8aM* 3'UTR remains to be elucidated.

Furthermore, the observation that the *fa3ui*^{MO} had a negligible impact on the expression of the eGFP-*fgf8aM* reporter, both at the mRNA and at the protein levels (Fig. III.3e,f,g), indicates that this morpholino does not interfere markedly with the regulation of *fgf8a* expression at the post-transcriptional level (e.g. mRNA stability and translation efficiency). Therefore, we set out to determine if the *fa3ui*^{MO} could

be used to interfere with the regulation of *fgf8a* expression at the co-transcriptional level (e.g. APA).

In particular, the *fa3ui*^{MO} targets the sequence directly upstream of the *fgf8aM* polyadenylation signal (Fig. III.3a), thus raising the possibility that it could interfere with the endogenous *fgf8a* polyadenylation. In agreement with this, we observed that the *fa3ui*^{MO} induced a shift in PAS selection, favouring *fgf8aS* PAS usage (Fig. III.4a,b). The increase in *fgf8aS* PAS usage was accompanied by an increase in total *fgf8a* transcript levels, which seemed difficult to explain considering the small differences in transcript stability conferred by the two alt3'UTRs (Fig. III.4a,b and Fig. III.2c). To address this issue, we built a mathematical model that integrates the distinct kinetic parameters of *fgf8a* gene expression, from transcription to protein turn-over (Section III.5.1 - Supplemental Text). The aim of this modelling approach was to understand if, given the dynamics of the process underlying the biogenesis of transcripts with the *fgf8aS* and *fgf8aM* 3'UTRs and the actual experimental measurements obtained in our system, the observed results could be explained by a shift in polyadenylation efficiency between the *fgf8aS* and *fgf8aM* PASs. Furthermore, such a modelling approach allowed us to estimate the relative abundance of each mRNA species.

Analysis of this model confirmed that our experimental observations imply a 2 to 4 fold increase in the selection of the proximal PAS in the presence of the *fa3ui*^{MO}, whereas the observed increase of total mRNA levels could only be efficiently reproduced with the inclusion of a feedback-based mechanism in the mathematical model (Section III.5.1 - Supplemental Text and Fig. III.4c). In conclusion, this modelling approach demonstrates that our experimental observations are well described by a simple model where the sequence targeted by the *fa3ui*^{MO} is important for polyadenylation site selection and an overactivation of Fgf signalling can, directly or indirectly, positively regulate *fgf8a* transcription. The presence of such feedback mechanisms fits into a model of regulation of *fgf8a* gene expression in which alternative polyadenylation is part of a fine-tuning system that coordinates protein expression levels with cellular needs.

The shift in PAS usage preferences brought about a spatially and temporally specific impact on embryonic development (Fig. III.6). These responses to the *fa3ui*^{MO} likely

reflect the complex mechanisms and inter-pathway crosstalk events involved in the different functions of Fgf8a during development (Pownall and Isaacs, 2010). For instance, previous work done in mouse has shown that, during commissural plate patterning, a reciprocal induction loop is present between Fgf8 and Sp8 in the forebrain, with Sp8 acting as a transcriptional activator of *Fgf8* (Sahara et al., 2007). Therefore, the presence of an analogous positive feedback element in the zebrafish forebrain, could underlie the enhanced response to the *fa3ui*^{MO} observed in these tissues at 24 hpf (Fig. III.5a), and the subsequent disruption of commissure formation (Fig. III.6c).

In addition, by targeting this mechanism of *fgf8a* expression fine-tuning, we generated a late-onset overexpression of *fgf8a* without inducing *fgf8a* missexpression, which enabled the identification of a previously undescribed Fgf signalling function in the early stages of superficial ocular vascularization (Fig. III.7). In this context, the greater severity of the vascular phenotype observed in hs:*dnfgfr1*+/- embryos, when compared to *ace* mutants (Fig. III.7d-i), indicates that Fgf8a has a non-essential role in the process, with other Fgfs being likely involved. Indeed, concerted actions between Fgf ligands were previously reported in the context of zebrafish ocular development. In particular, Fgf8 and Fgf3 are both necessary and sufficient to initiate neuronal differentiation in the retina (Martinez-Morales et al., 2005), and the combined action of Fgf8a, Fgf3 and Fgf24 is required to fully control nasal-temporal patterning of the neural retina (Picker et al., 2009). A potential role for these Fgfs in the vascularization of the zebrafish retina remains to be explored.

The morphological abnormalities observed in the SAV vessels of hs:*dnfgfr1*+/- embryos (Fig. III.7i and arrowheads in Fig. III.7g,h) might derive from an impaired capacity to maintain vessel integrity. In fact, Fgf signalling has been shown to play an important role in the maintenance of intersomitic vascular integrity in zebrafish embryos (De Smet et al., 2014). In addition, a study done in mouse described a role for FGF signalling at later stages of superficial ocular vascularization, specifically during choroidal angiogenesis (Rousseau et al., 2003). In light of this, our results are strongly indicative of an earlier requirement for Fgf signalling, specifically in the initial stages of superficial retinal vasculature assembly, with this pathway appearing

to contribute, not only to the timely induction of superficial vessel formation, but also to the structural integrity of this vascular system (Fig. III.7g-i).

Interestingly, the Vascular Endothelial Growth Factor (VEGF) and Hedgehog signalling pathways have also been implicated in the formation of the superficial ocular vasculature in the zebrafish embryo (Weiss et al., 2017). Various synergistic effects and pathway crosstalk events have been described, between the FGF and VEGF pathways, in multiple angiogenic contexts (Presta et al., 2005). Therefore, a potential synergy between these pathways may underlie the especially enhanced response to the *fa3ui*^{MO} observed in the eye field (Fig. III.5c) and contribute to the observed vascular phenotype (Fig. III.7a,c). Future studies are required to determine if FGF-VEGF crosstalk mechanisms are present in this context.

In conclusion, to the extent of our knowledge, this is the first study to address the functional impact of the 3'UTR APA of a regulator of vertebrate embryonic development.

By inducing a shift in *fgf8a* PAS usage preferences we brought about a spatially and temporally specific impact on embryonic development. In addition, this approach enabled the identification of a previously undescribed role for Fgf signalling in the early stages of zebrafish ocular vascularization.

These findings highlight the importance of addressing gene expression fine-tuning mechanisms, and 3'UTR APA in particular, to fully understand gene and pathway functions in embryonic development.

III.4 MATERIALS AND METHODS

The fibroblast growth factor 8a gene is listed in the National Center for Biotechnology Information (NCBI) under the Gene ID 30538, and in the Zebrafish Information Network (ZFIN) under the identifier ZFIN:ZDB-GENE-990415-72.

III.4.1 Zebrafish lines

Adult zebrafish and embryos were maintained and bred under standard laboratory conditions (Westerfield, 2000). Embryonic staging was done according to (Kimmel et al., 1995).

III.4.1.1 Transgenic and mutant lines

This work was carried out using AB wildtype strains, a transgenic Tg(hsp70l:*dnfgfr1*-EGFP) (Lee et al., 2005) line, a transgenic Tg(*kdrl*:Hsa.HRAS-mCherry) (Chi et al., 2008) line and a mutant *fgf8a*^{ti282a} (Reifers et al., 1998) line.

The hs:*dnfgfr1* transgene codes for a heat-shock inducible dominant negative form of the *fgfr1* gene (Lee et al., 2005) and the *kdrl:*mCherry line labels endothelial cells (Chi et al., 2008). hs:*dnfgfr1* and *kdrl:*mCherry transgenic embryos were generated from outcrosses of heterozygous adults.

The *fgf8a*^{ti282a} allele has a G to A mutation in the 5' splice donor site following exon 4, which leads to exon 4 skipping, and a consequent frameshift in exon 5. This frameshift is predicted to lead to a premature stop codon (Reifers et al., 1998). *fgf8a*$^{ti282a/ti282a}$ (*ace*) embryos were generated from outcrosses of *fgf8a*$^{ti282a/+}$ adults with *fgf8a*$^{ti282a/+}$, *kdrl*:mCherry$^{+/-}$ adults.

For the heat-shock experiments performed on *fa3ui*^{MO} injected morphants, embryos were raised at 28ºC and heat-shocked at 24 hpf at 38ºC for 5 minutes. For the remaining heat-shock experiments, embryos were raised at 28ºC and heat-shocked at 20 hpf at 39ºC for 5 minutes.

Imaging of transgenic embryos was done using Zeiss LSM 880 and Zeiss LSM 710 confocal point-scanning microscopes. Representative images are maximum intensity projections of confocal z-stacks.

III.4.1.2 TALEN and Crispr mutagenesis

To investigate the functions of the *fgf8aS* and *fgf8aM* 3'UTRs we set out to generate zebrafish mutant lines carrying mutations in the MM, *fgf8aS* PAS and *fgf8aM* PAS.

We designed two CRISPR guide RNAs and one TALEN pair against the *fgf8aM* PAS (Fig. III.M1a,b). An additional TALEN pair was produced against the *fgf8aS* PAS (Fig. III.M1c), and lastly, two TALEN pairs were designed against the *fgf8aS and fgf8aM* polyadenylation sites which flank the MM sequence (Fig. III.M1d). The last two TALEN pairs were used in conjunction with the aim of excising the full MM sequence.

CRISPR guide RNA design was done as described in (Talbot and Amacher, 2014) and *pCS2nCas9n* was a gift from Wenbiao Chen (Addgene plasmid # 47929) (Jao et al., 2013). Guide RNA and Cas9 mRNA production was done as described in (Gagnon et al., 2014).

TALEN design was done using the TAL Effector Nucleotide Targeter 2.0 and Paired Target Finder web tools as described in (Doyle et al., 2012). TALEN construct assembly and TALEN mRNA production was done using the golden gate approach described in (Cermak et al., 2011, Dahlem et al., 2012).

Microinjection procedures were done at the 1-cell stage using AB wildtype zebrafish embryos and an injection volume of 1.4nL/embryo. Each guide RNA was co-injected with Cas9 mRNA, and for each TALEN pair a 1:1 molar ratio of each TALEN mRNA in the pair was used. Several RNA concentrations were tested for each mutagenesis strategy.

To assess mutagenesis efficiency, genomic DNA was extracted from pools of microinjected embryos, between 24 hpf and 48 hpf, using the HotShot protocol (Meeker et al., 2007). The genomic region targeted was PCR amplified using the following primers Fw 5'-TCGCAGGTTTCCTACCGTG-3', Rv 5'-ATGTACTTTTCATTTTGTTCCACAG-3'. The presence of mutations was evaluated using Sanger sequencing (Stabvida) and the T7 Endonuclease I method (Reyon et al., 2012). All the mutagenesis strategies carried out in this study were inefficient.

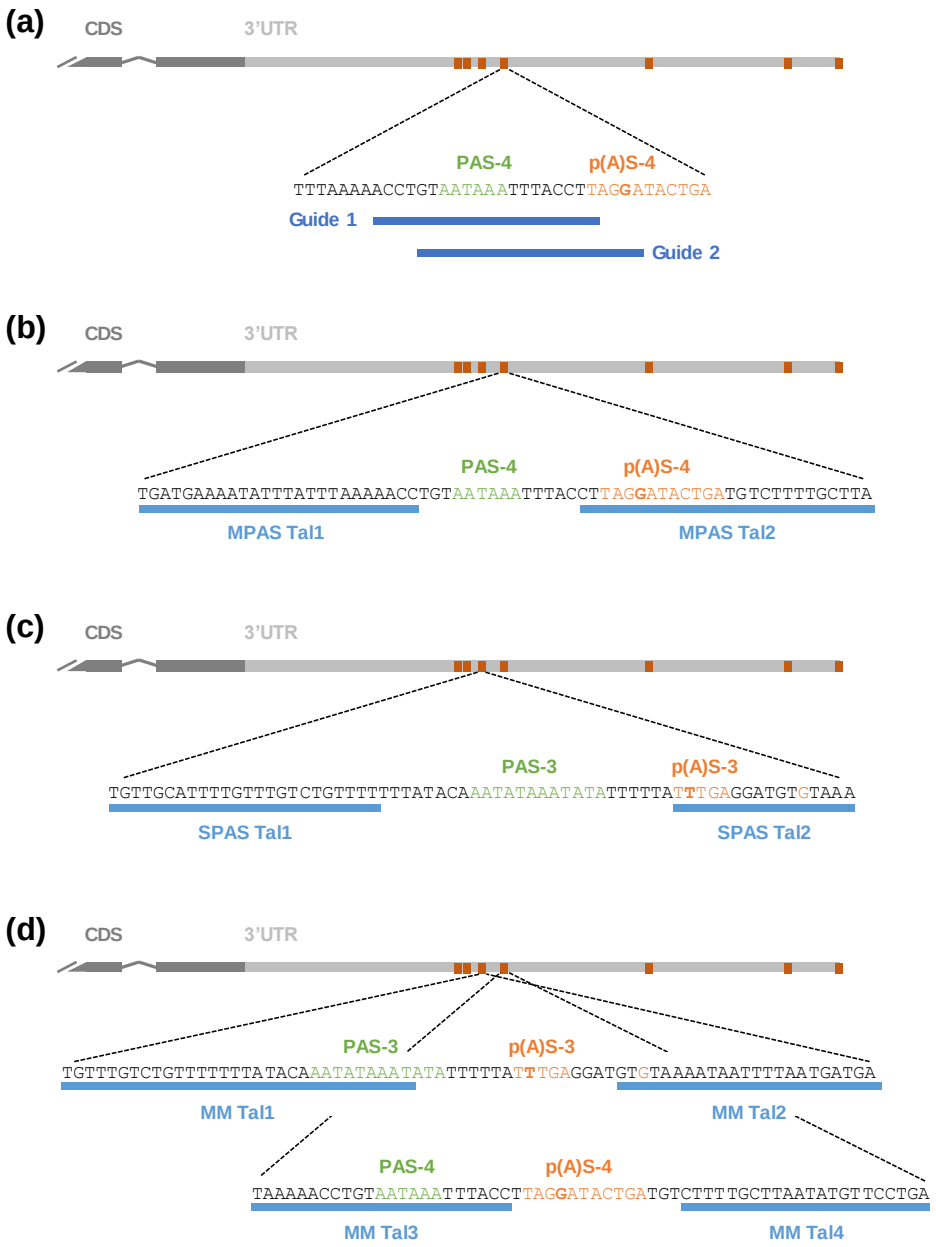

Fig. III.M1- Schematic representation of the mutagenesis strategies used in this work. **(a)** Illustration of the sequences targeted by the guide RNAs used in this work (blue). **(b,c,d)** Illustration of the sequences targeted by the TALEN pairs used in this work (blue). **(a-d)** Sequences highlighted in green correspond to the *fgf8aS* (PAS-3) and *fgf8aM* (PAS-4) polyadenylation signals; Sequences highlighted in orange correspond to the *fgf8aS* (p(A)S-3) and *fgf8aM* (p(A)S-4) polyadenylation sites.

Since we were unable to generate germline mutations in the MM, *fgf8aS* PAS or *fgf8aM* PAS, we adopted a morpholino-based approach to assess the functional relevance of these sequences (Section III.4.2).

III.4.2 Morpholino oligonucleotides

The antisense morpholino oligonucleotides used in this study were obtained from Gene Tools.

To investigate the functions of the *fgf8aS* and *fgf8aM* 3'UTRs we used the following *fgf8a* alt3'UTR interference morpholino (*fa3ui*^{MO}):
5'-ACAGGTTTTTAAATAAATATTTTCATCA-3'.

Control experiments were done by injecting sibling embryos with standard control morpholino (*Ctr*^{MO}):
5'-CCTCTTACCTCAGTTACAATTTATA-3'.

The *fa3ui*^{MO} and the *Ctr*^{MO} were injected into 1-cell stage embryos at 6ng/embryo, using an injection volume of 1.4nL/embryo.

A schematic representation of the *fa3ui*^{MO} binding site is presented in Fig. III.3a.

III.4.3 RT-qPCR

Microdissections were performed on dechorionated embryos, in Leibovitz's L-15 medium (Invitrogen) with 0.016% (w/v) of ethyl 3-aminobenzoate (tricaine), using a fine pointed scalpel and tungsten needle. The microdissection procedures carried out in this study are illustrated in Fig. III.1b.

At least three biological replicates were collected per experimental condition, from different breeders. For the conditions where whole embryos were used, each biological replicate corresponds to a pool of 20 to 40 embryos. For the conditions where microdissected 24 hpf tissue samples were used, each biological replicate corresponds to a pool of 30 to 40 individual tissue samples. For the conditions where microdissected 8 ss tissue samples were used, each biological replicate corresponds to a pool of 70 individual tissue samples.

Total RNA extractions were done using TRIzol (Invitrogen), according to the manufacturers protocol. In the experimental conditions where whole embryos were used, RNA extractions were done using 0.5-1mL of TRIzol per 20 embryos. In the

experimental conditions where microdissected tissue samples were used, RNA extractions were done using 1mL of TRIzol per 10 tissue samples.

Following RNA extraction an in-tube DNAseI digestion (Zymo Reseach) step was carried out to remove residual genomic DNA, followed by an RNA purification step using the RNA Clean & Concentrator™-5 kit (Zymo Reseach).

cDNA was synthetized from the purified total RNA samples using either the DyNAmo cDNA Synthesis Kit (Thermo) or the ProtoScript® II First Strand cDNA Synthesis Kit (NEB). For the fluorescent reporter experiments a random hexamer primer mix was used, and for the remaining experiments an oligo(dT) primer mix was used.

RT-qPCR reactions were performed using Power SYBR® Green PCR Master Mix (Applied Biosystems) and the primers used are listed in Table III.M1.

For the fluorescent reporter experiments (Fig. III.2c and Fig. III.3d,g), the primers used were designed to specifically target the coding sequences of eGFP and mCherry. For the pUTR and pCDS primer sets, primer design was done as illustrated in Fig. III.1c and detailed in the corresponding figure legend. For these sets of primers, primer concentrations and annealing temperatures were optimized using 24 hpf and 8 ss wildtype whole embryo cDNA. All relative fold changes in transcript levels were determined using the standard curve method (Pfaffl, 2001).

For the experiments done using wildtype whole embryo and microdissected tissue samples (Fig. III.1d-f), the standard curves were done using serial dilutions of a DNA template. This template was amplified from wildtype genomic DNA with the following primers Fw: 5'-ATTGGCAAGAAAAATGGTCTGGGAAAAGACTG-3' and Rv: 5'-ATCTTGGCTTTCGGCTCCTT-3'. In this set of experiments quantities were normalized to pCDS2. The results shown are relative to the whole embryo condition, except in comparisons between 8 ss whole embryo and 24 hpf whole embryo (Fig. III.1f) where values are relative to the 24 hpf whole embryo condition.

For the experiments done with *fa3ui*^{MO} and *Ctr*^{MO} injected whole embryo and microdissected tissue samples (Fig. III.4a,b and Fig. III.5b,d,e), the standard curves were done using serial dilutions of wildtype cDNA from the respective tissue sources. In this set of experiments quantities were normalized to *ef1a*, and the results shown are relative to the *Ctr*^{MO} condition.

For the fluorescent reporter experiments shown in Fig. III.2c and Fig. III.3d, the standard curves were done using serial dilutions of cDNA obtained from wildtype embryos injected with eGFP and mCherry mRNA. For the experiment shown in Fig. III.3g, standard curves were done using serial dilutions of cDNA from the indicated control condition. In this set of experiments (Fig. III.2c and Fig. III.3d,g) quantities were normalized to mCherry, and the results shown are relative to the indicated control conditions.

For each experimental condition, the results shown represent the mean of three biological replicates, with the exception of the results shown in Fig. III.3g which represent the mean of five biological replicates per experimental condition.

Table III.M1 - Primers used for RT-qPCR.

Target	Forward primer (5'->3')	Reverse primer (5'->3')
pCDS1	TGGCAAGAAAAATGGTCTGGGA	GCCTGGTTTTGGAGCCCTTG
pCDS2	GCCCAAGGGACACCAAATC	GGTGCGTTTAGTCCGTCTGTT
pUTRs2-7	ACACGGTTAAAGCAAACAGAGC	AGCTTTTTCCTACAGTCCATACAA
pUTRs3-7	ATTATCGCAGGTTTCCTACCG	CAAAATGCAACAAAGAACAAAAGC
pUTRs4-7	TGCATTGTATGGACTGTAGG	TATTTTACACATCCTCAAATAAAAAT
pUTRs5-7	CTTAGGATACTGATGTCTTTTGCTT	ACCCCATAGACTTTCATTGTGTTT
eGFP	GGACGACGGCAACTACAAGA	TTCAGCTCGATGCGGTTCA
mCherry	GCCGACATCCCCGACTACTT	GTAGATGAACTCGCCGTCCT
dusp6	GTTCGAGAATGCCGGGGAG	GTCCACGGGCCTCATCAATAAA
etv5b	TGGTGAGGGTTTTGGGTATGA	CCTTCGCTGATATGGAGGGC
ef1a (Azevedo et al., 2011)	ACGCCCTCCTGGCTTTCACCC	TGGGACGAAGGCAACACTGGC

III.4.4 Fluorescent reporter assays

III.4.4.1 Cloning and microinjections

The *fgf8a* alt3'UTR and MM sequences were amplified from wildtype genomic DNA using the primers indicated in Table III.M2, and cloned into *pCS2+eGFP* (Lopes et al., 2010), downstream of the eGFP coding sequence, using the indicated restriction

enzymes (Table III.M2). PCR amplifications were performed using Phusion High-Fidelity DNA Polymerase (Thermo Fisher) and DNA ligation reactions were done using T4 DNA Ligase (NEB).

All the constructs produced were sequenced by Stabvida to verify the efficiency and accuracy of each cloning procedure.

Table III.M2 – Primers and restriction enzymes used for alt3'UTR and MM cloning.

Amplicon	Forward primer (5'->3')	Reverse primer (5'->3')	Restriction Enzymes
fgf8S	TGTAATCGATAGAGTGAAG CCAGAGAAAAG	TGTTCTCGAGTCAAATAAAAATA TATTTATATTTGTATAA	XhoI (Promega) StuI (NEB)
fgf8M	TGTAATCGATAGAGTGAAG CCAGAGAAAAG	TGTTCTCGAGATCCTAAGGTAA ATTTATTACA	XhoI (Promega) StuI (NEB)
MM	GAGGATGTGTAAAATAATTT	TGTTCTCGAGATCCTAAGGTAA ATTTATTACA	StuI (NEB)

The *pCS2-eGFP-fgf8aS, pCS2-eGFP-fgf8aM, pCS2-eGFP-MM* and *pCS2-mCherry* constructs were linearized with NotI (NEB). *In vitro* transcriptions were performed using the SP6 mMessage mMachine kit (Ambion) and followed by in-tube Turbo DNAseI (Ambion) digestion of the template DNAs. The transcript samples were purified using illustra™ MicroSpin™ G-50 Columns (GE Healthcare) prior to microinjection.

mCherry mRNA was co-injected with mRNA from each of the *eGFP* reporters in a 1:1 molar ratio, into 1-cell stage zebrafish embryos. mRNAs from each reporter were microinjected at 0.3fmol/embryo for the experiments shown in Fig. III.2 and Fig. III.3b,c,d, and at 0.15fmol/embryo when co-injected with the $fa3ui^{MO}$ or Ctr^{MO} (Fig. III.3e,f,g), using an injection volume of 1.4nL/embryo. In the latter set of experiments these quantities equate to a 1:4267 molar ratio of reporter mRNA to $fa3ui^{MO}$.

III.4.4.2 Image acquisition and processing

Embryos were kept at 28ºC for 24 hours after injection, until imaging. Experimental and control embryos were dechorionated, anesthetised with 0.016% (w/v) ethyl 3-aminobenzoate (tricaine) and mounted in 1.5% (w/v) low melting agarose on a glass-base petri dish for imaging.

Imaging was done with a Zeiss Axiovert 200M widefield fluorescence microscope, using a 10x magnification. For the experiments shown in Fig. III.2a,b,d and Fig. III.3b,c eGFP exposure was set to 100ms, and mCherry exposure was set to 100ms. For the experiments done with the *fa3ui*^{MO} and *Ctr*^{MO} (Fig. III.3e,f) eGFP exposure was set to 200ms, and mCherry exposure was set to 200ms.

Image processing was done using ImageJ 1.44p (Schneider et al., 2012). Average pixel intensities were measured, for each channel and each embryo, in a circular section adjacent to the midbrain-hindbrain boundary. The average background pixel intensities were measured using an identical section in an area adjacent to the embryo. The background values were subtracted from those obtained for the embryo. The resulting intensity values obtained for eGFP were normalized to those obtained for mCherry in each embryo. The mean normalized fluorescence intensities were calculated for each experimental condition, and the values shown are relative to the indicated control condition.

III.4.5 Whole-mount *in situ* hybridization and Immunohistochemistry

The antisense RNA WISH probes used in this study were *in vitro* transcribed from the respective DNA templates following construct linearization. The restriction enzymes, RNA polymerases and constructs used for probe production in this study are indicated in (Table III.M3).

The *fgf8a-CDS* probe template in particular was sub-cloned from a construct provided by (Reifers et al., 1998), by restriction digestion with EcoRV (NEB) and ScaI (NEB), into a pGEM-T Easy vector (Promega).

All the probes used in this study were labelled with Digoxigenin (DIG RNA labelling mixture, Roche).

WISH experiments were done according to the protocol described by (Thisse and Thisse, 2008). Staining was performed using BM purple AP substrate (Roche), with the exception of the experiments done with the *dusp6* and *etv5b* probes, in which staining was done as described in (Thisse and Thisse, 2008).

Table III.M3 – WISH probes used in this study. For each probe, the restriction enzyme required for DNA construct linearization, and the RNA polymerase required for *in vitro* transcription, are indicated, along with the sources of the respective template constructs used.

Probe	Restriction Enzyme	RNA Polymerase	Template
fgf8a-CDS	ApaI	SP6	(Section III.4.5)
dusp6	ScaI	T7	(Kawakami et al., 2003)
etv5b	EcoRI	T7	(Roehl and Nüsslein-Volhard, 2001)
neurog1	XhoI	T7	(Blader et al., 1997)
isl1	SacI	T3	(Inoue et al., 1994)
ta	HindIII	T7	(Amack and Yost, 2004)
xirp2a	SalI	T7	(Thisse et al., 2001)
eng2a	XhoI	T7	(Fjose et al., 1992)
her5	XhoI	T3	(Müller et al., 1996)

Immunohistochemistry experiments were done according to the protocol described by (Matsui et al., 2011), with the following alterations. Acetylated tubulin staining was done using a monoclonal anti-acetylated tubulin, clone 6-11B-1 primary antibody (Sigma), at 1:400 working dilution. p-ERK staining was done using a Phospho-p44/42 MAPK (Erk1/2) (Thr202/Tyr204) primary antibody (Cell Signalling Technology), at 1:150 working dilution. Incubations with primary antibodies were done at 4ºC for approximately 40 hours. The secondary antibodies used were Alexa Fluor594 goat anti-Mouse (Invitrogen) and Alexa Fluor488 goat anti-Rabbit (Invitrogen). Both secondary antibodies were used at 1:400 working dilution and incubations with these antibodies were done at 4ºC overnight.

Image acquisition was done using a Leica Z6 PRO stereoscope, a Leica DM2500 bright-field microscope and a Zeiss AxioZoom V16 fluorescence stereo microscope.

III.4.6 Statistical analysis

Statistical analysis were done using two-tailed t-test, for all the results shown, with the exception of the RT-qPCR results shown in Fig. III.4a,b and Fig. III.5b where statistical analysis was done using both two-tailed t-test and 2-way ANOVA.

For the RT-qPCR experiments, three biological replicates were used per experimental condition, with the exception of the experiment shown in Fig. III.3g in which five biological replicates were used per experimental condition.

For the remaining experiments, the number of biological replicates considered per experimental condition is indicated in the corresponding figure panel.

III.5 SUPPLEMENTAL DATA

Table III.S1 – Reported alt3'UTRs for the *fgf8a* gene. Also shown are the relative abundances of each alt3'UTR reported in the indicated studies.

Alternative 3'UTRs	3'UTR length (nts)	Relative polyadenylation site usage (%) [(a)]	Relative polyadenylation site usage (%) [(b)]
altUTR-1	654	-	1.6
altUTR-2	680	14.2	0.9
altUTR-3 *(fgf8aS)*	728	12.5	18.7
altUTR-4 *(fgf8aM)*	797	65.9	74.3
altUTR-5	1242	-	3.7
altUTR-6	1667	5.4	0.8
altUTR-7	1829	2.0	-

[(a)] Pooled data obtained for the following developmental stages: 0 hpf; 4 hpf; 6 hpf; 12 hpf; 24 hpf; 48 hpf; 72 hpf; 120 hpf. Adapted from L. You, J. Wu, Y. Feng, Y. Fu, Y. Guo, L. Long, H. Zhang, Y. Luan, P. Tian, L. Chen, G. Huang, S. Huang, Y. Li, J. Li, C. Chen, Y. Zhang, S. Chen and A. Xu, APASdb: a database describing alternative poly(A) sites and selection of heterogeneous cleavage sites downstream of poly(A) signals, Nucleic Acids Res. 43, 2015, D59–D67.

[(b)] Pooled data obtained for the following samples: Embryos:1.5–2 hpf; 4.5–5.5 hpf; 24 hpf; 72 hpf; Mixed gender adults; Adult tissues: brain, testes, and ovaries. Adapted from I. Ulitsky, A. Shkumatava, C.H. Jan, A.O. Subtelny, D. Koppstein, G.W. Bell, H. Sive and D.P. Bartel, Extensive alternative polyadenylation during zebrafish development, Genome Res. 22, 2012, 2054–2066.

III.5.1 Supplemental Text

Analysis of the reporter system

24 hours-post-injection eGFP-*fgf8aS* mRNA is approximately 1.3 times more abundant than eGFP-*fgf8aM* mRNA (Fig. III.2c). As both molecular species are not produced endogenously, we can assume that they both decay exponentially (equation 1).

$$N(t) = N_0 e^{-k_d t} \quad (1)$$

Therefore, we can compute the ratio between the two quantities for a given time point (equation 2).

$$\frac{N_S}{N_M} = \frac{N_{S0}}{N_{M0}} e^{(k_M - k_S)t} \quad (2)$$

Considering equal initial quantities, we can determine the difference between degradation rate constants k_M and k_S through equation 3.

$$(k_M - k_S) = \ln\left(\frac{N_S}{N_M}\right)/t \quad (3)$$

Applying equation 3 for t=24h we get (k_M-k_S)=0.01 h^{-1}.

The absolute rate constant values vary with the baseline degradation rate constant of one of the forms. Considering that most transcripts have half-lives of between 1 and 30 hours (Milo and Phillips, 2016), in the fastest degradation scenario k_S=0.68 h^{-1} and k_M=0.69 h^{-1} while for the more stable scenario k_S=0.02 h^{-1} and k_M=0.03 h^{-1}.

Additionally, we also observed that, 24 hours-post-injection, the ratio of protein produced by eGFP-*fgf8aS* vs eGFP-*fgf8aM* is approximately 3.4 (Fig. III.2b). To

explain this variation, we analysed a simple dynamical model of protein synthesis including mRNA degradation (but not synthesis, since mRNA was exogenous), protein synthesis and protein degradation (equation 4).

$$\frac{dS}{dt} = -k_S S$$

$$\frac{dM}{dt} = -k_M M$$

$$\frac{dPs}{dt} = k_{Ps} S - k_P Ps$$

$$\frac{dPm}{dt} = k_{Pm} M - k_P Pm \quad (4)$$

S represents eGFP-*fgf8aS* while M is eGFP-*fgf8aM*, the two variant transcripts that code for the proteins Ps and Pm respectively. Although it is the same protein (eGFP), each variant is expressed in a different reporter system, so two different variables are modelled. Being the same protein, both Ps and Pm have the same degradation rate constant k_P. eGFP in zebrafish has an approximate half-life of 24 hours (Thomas et al., 2012), therefore we considered k_P=0.03 h^{-1}.

We simulated the model until 24 hours and computed the ratios Ps/Pm and M/S.

The initial M and S values were 1 (varying these initial values did not change the ratios). All other variables were absent in the beginning of the simulation.

We started by considering k_{Pm}=1 h^{-1} and increased k_{Ps} until Ps/Pm was around 3.4, as observed experimentally. We could reproduce the 3.4 ratio with k_{Ps}=3.15 h^{-1}. If we changed k_{Pm} and k_{Ps} maintaining their ratio (k_{Ps}/k_{Pm}=3.15), both Ps/Pm and M/S values were not affected.

Similarly, we could change k_S and k_P constants, but, if their difference was kept at 0.01 h^{-1}, both Ps/Pm and M/S ratios were constant.

Changing k_P (protein degradation constant) has a slight effect on the ratio P_S/P_M. But even considering k_P=0.7 h^{-1} (half-life of 1h) k_{Ps}/k_{Pm} would have to be 2.75 to reproduce the 3.4 ratio of Ps/Pm.

In conclusion, although we are uncertain about absolute parameter values, having k_M-k_S=0.010 h^{-1} and k_{Ps}/k_{Pm} around 3 are sufficient conditions to support the experimental observations made with the reporter system.

Model of endogenous *fgf8a* expression

Quantification of endogenous expression of different transcript variants in the presence of *fa3ui*^{MO} (Fig. III.4a,b) showed that this morpholino induces a global increase in total transcript (1.4 times increase at 8 ss and 2.7 times at 24 hpf) that is not proportionately distributed among the two main transcript variants.

To enhance the understanding of this system, we developed a dynamical model of endogenous *fgf8a* expression, including the two main transcript variants and the capacity of Fgf signalling to, directly or indirectly, activate *fgf8a* transcription. This feedback element was necessary to allow the model to replicate the increase in total transcript observed in presence of the morpholino.

The model is defined as a set of ordinary differential equations (equation 5).

$$\frac{dT}{dt} = k_t + k_{tP}H(P,P_T) - k_aT \qquad \text{where} \qquad H(P,P_T) = \begin{cases} 0\ if\ P \le P_T \\ 1\ if\ P > P_T \end{cases}$$

$$\frac{dS}{dt} = k_a(1-R)T - k_SS$$

$$\frac{dM}{dt} = k_aRT - k_MM$$

$$\frac{dP}{dt} = k_{Ps}S + k_{Pm}M - k_PP \qquad (5)$$

In this model, T is a common transcript precursor, S is *fgf8aS*, M is *fgf8aM* and P is Fgf8a. k_t is a basal transcription rate constant, k_{tP} is the transcription rate constant associated with the positive feedback, and P_T is the Fgf8a concentration threshold above which this feedback is effective. k_a is the polyadenylation rate constant, while R is the fraction of transcripts that originate the M transcript after polyadenylation. Considering the system evolves to a steady state we can deduce the relation between the ratio M/S, R and f=k_M/k_S (equation 6).

$$\frac{M}{S} = \frac{R}{(1-R)f} \quad (6)$$

According to previous observations (Table III.S1), M/S should be between 4 and 5. According to our analysis of the reporter system, and allowing for large variations in mRNA stability, f can vary between 1.1 and 1.5. This implies that R should vary between 81 and 88%.

When the morpholino is present, we assume that R changes to a lower value R', giving rise to new steady state values of T', M', S' and P'. As we know the observed values of M'/M and of (M'+S')/(M+S), we can deduce the experimental values of M'/S'. Given our uncertainty in the M/S value (that can vary between 4 and 5), at 8 ss M'/S' is between 1.3 and 1.5, while at 24 hpf it is between 1.1 and 1.2. Using equation 6, we can predict that, at 8 ss, R' is between 58 and 69%, while at 24 hpf it is between 54 and 64%.

If there is no positive feedback (k_{tP}=0) and if k_M-k_S=0.010 h^{-1}, k_{Ps}/k_{Pm}= 3 and the previously estimated R and R' were used, the model predicts a ratio P'/P between 1.4 and 1.6, but the ratio (M'+S')/(M+S) is never higher than 1.1. Since the increase in protein levels is significant (between 40 and 60%), the hypothesis that this extra protein can lead to a positive regulation of *fgf8a* expression (positive feedback element) could explain the experimentally observed increase of total transcript in the presence of the morpholino.

Considering the positive feedback and simulating the model until it reached a steady state (keeping k_M-k_S=0.010 h^{-1}, k_{Ps}/k_{Pm}= 3, R between 81-88% and R' between 54-69%), it was possible to vary the remaining parameters and still replicate the observed M/S, (M'+S')/(M+S) and M'/M ratios. This was easily achieved by tuning the values of P_T and k_{TP}. ratios. Several successful parameter sets are presented in the Parameter Table below.

In conclusion, this analysis demonstrates that our experimental observations are well described by a simple model where the sequence targeted by the morpholino is important for polyadenylation site selection and an overactivation of Fgf signalling can, directly or indirectly, positively regulate *fgf8a* expression.

Parameter Table – Sets of parameters that make the dynamical model compatible with the experimental observations.

Parameters	Set 1	Set 2	Set 3	Set 4	Set 5	Set 6	Set 7	Experimental observations	
k_T (h^{-1})	0.50	0.50	0.50	0.50	0.50	0.50	0.50		
k_{TP} (h^{-1})	0.25	0.25	0.25	0.75	0.75	0.75	0.75		
P_T (A.U.)	10	250	40	40	250	10	10		
k_a (h^{-1})	0.50	0.50	0.50	0.50	0.50	0.50	0.50		
R (%)	85	85	85	85	85	85	85		
R' (%)	63	63	59	59	59	59	63		
k_M (h^{-1})	0.12	0.12	0.03	0.03	0.12	0.12	0.12		
k_S (h^{-1})	0.11	0.11	0.02	0.02	0.11	0.11	0.11		
k_{Pm} (h^{-1})	1.00	1.00	1.00	1.00	1.00	1.00	1.00		
k_{Ps} (h^{-1})	3.00	3.00	3.00	3.00	3.00	3.00	3.00		
k_P (h^{-1})	0.70	0.03	0.70	0.70	0.03	0.70	0.70		
Ratios								**8 ss**	**24 hpf**
M/S	5.19	5.19	3.78	3.78	5.19	5.19	5.19	4-5	
M'/S'	1.56	1.56	0.96	0.96	1.32	1.32	1.56	1.3-1.5	1.1-1.2
(M'+S')/(M/S)	1.53	1.53	1.68	2.79	2.56	2.56	2.55	1.4	2.7
M'/M	1.10	1.10	1.00	1.73	1.73	1.73	1.85	1.0	1.8

CHAPTER IV

Discussion and Conclusions

The development of a living organism is critically reliant on a tight spatial and temporal regulation of gene expression. Among the mechanisms involved in this regulation, the ones that operate at the post-transcriptional level have been the focus of an increasing level of attention. However, their specific roles in embryogenesis, and their relative importance to the different processes that take place in the developing embryo, still require further investigation.

For instance, the importance of RNA binding protein (RBP)-mediated post-transcriptional regulation to embryonic development is particularly remarkable, and has been extensively studied, during Maternal to Zygotic Transition stages (Colegrove-Otero et al., 2005). However, less in known about the functional impact of RBP-mediated regulation on later developmental processes. Furthermore, alternative 3'UTR production through alternative polyadenylation (APA) is a remarkably prevalent phenomena during embryogenesis. However, the functional importance of individual APA events to embryogenesis has remained largely unaddressed (Sections I.2.1.2 and I.2.1.3).

In this thesis we set out to investigate the impact of post-transcriptional regulation to zebrafish embryogenesis from two perspectives: the perspective of a post-transcriptional regulator – the Quaking A (Qkia) RBP – and the perspective of a set of regulatory RNA sequences – the fibroblast growth factor 8a (*fgf8a*) alternative 3'UTRs.

In Chapter II, we uncovered evidence for two potential functions for the *qkia* gene during zebrafish embryonic development, namely in posterior body shaping and in the establishment of the lateral positions of the heart, liver and pancreas.

Our results concerning the role of *qkia* in the establishment of the shape of the posterior body indicate that *qkia* operates at post-gastrulation stages, and may influence posterior body morphogenesis during the process of posterior body elongation, most likely through its expression in the paraxial mesoderm (Section II.2.1).

Furthermore, our analysis of the role of *qkia* in internal organ laterality establishment revealed that *qkia* appears to operate in this process at the level of laterality signal

transmission from the Kupffer's vesicle to the lateral plate mesoderm (Section II.2.2). These results therefore suggest that the functions of *qkia* in Left-Right patterning could also be mediated by its expression in the paraxial mesoderm, which is located between these two laterality-associated tissues (Thisse et al., 2001).

Further studies are required to address the specificity of the observed posterior body shaping phenotype and to dissect the mechanisms that underlie these two potential *qkia* functions. In this context, the identification of potential targets of Qkia-mediated post-transcriptional regulation, with a known expression in the paraxial mesoderm, would constitute a logical next step.

Furthermore, previous studies have shown that different STAR protein splicing isoforms can not only influence different facets of RNA metabolism, but can also exert opposite forms of gene expression regulation when interacting with the same target transcript (Section I.2.2.1.1). Therefore, an independent assessment of the specific functions mediated by the two Qkia splicing isoforms in these developmental processes would also be particularly relevant.

In this study we identified a potential target of Qkia-mediated regulation, namely the adhesion molecule Cdh11, with our results indicating that Qkia could function as a negative regulator of Cdh11 expression (Section II.2.3). However, additional studies are required to determine if direct Qkia-*cdh11* interactions take place *in vivo*, and to assess the resulting effects on endogenous Cdh11 expression and embryonic development. Furthermore, we observed that *qkia* overexpression is not sufficient to repress the expression of a reporter fused to the *cdh11* 3'UTR, thus raising the possibility that additional RBPs could be involved in this regulation, and consequently opening the door for future studies aimed at their identification.

Our results also revealed a potential function for the Cdh11 protein in the establishment of internal organ laterality. In particular, we observed that *cdh11* morphants display defects in the lateral positioning of the cardiac and visceral organs, which are not phenocopied in *cdh11* mutants (Section II.2.4). Future approaches can therefore focus on assessing the specificity of the *cdh11* morphant phenotype, and determining if these phenotypic differences stem from the activation of a genetic compensation program in *cdh11* mutants (Rossi et al., 2015).

A more thorough analysis is required to clarify the mechanisms through which *qkia* and *cdh11* operate in Left-Right patterning. However, the results obtained thus far indicate that while *qkia* appears to function at the level of asymmetric signal transmission between the Kupffer's vesicle and the lateral plate mesoderm, *cdh11* is more likely to operate at the level of asymmetric signal establishment in the Kupffer's vesicle (Sections II.2.2 and II.2.4). Future dissection of these mechanisms can therefore, potentially further our understanding of these two facets of Left-Right patterning (Sections I.1.2.1 and I.1.2.3).

Taken together, the results shown in this chapter are incremental to the current view of STAR protein family members as major regulators of a considerable diversity of developmental processes, particularly during the later stages of embryogenesis (Section I.2.2.1.2). Indeed, the observation that Qkia appears to be required for proper Left-Right patterning in the developing zebrafish embryo constitutes, to the extent of our knowledge, the first time that a STAR protein has been implicated in this process. Furthermore, this observation serves to further our current understanding of STAR protein functions in cardiac development and opens the door for future studies aimed at assessing its conservation.

In Chapter III we focused our attention on the analysis of the alternative 3'UTRs of the *fgf8a* gene, with our results supporting a model in which *fgf8a* APA is part of a fine-tuning system that coordinates Fgf8a protein expression levels with cellular needs. In this context previous studies have reported that the most abundant *fgf8a* alternative 3'UTR – *fgf8aM* – is approximately 4 to 5 fold more abundant than the second most abundant alternative 3'UTR – *fgf8aS* – (Ulitsky et al., 2012, You et al., 2015), with our results indicating that endogenous alternative polyadenylation signal (PAS) usage preferences appear to remain relatively stable across the tissues and developmental stages analysed (Section III.2.1). Furthermore, we demonstrate that despite its greater relative abundance, the *fgf8aM* 3'UTR is associated with a strong inhibition of translation, with a shift from *fgf8aM* to *fgf8aS* PAS usage exerting a significant impact on Fgf signalling levels (Sections III.2.1 and III.2.2).

In addition, we determined that the source of the *fgf8aM*-associated post-transcriptional repression resides in a 71nt sequence motif, termed minimal motif (MM) (Section III.2.1). This MM sequence includes a predicted binding site for dre-

miR-2187, however, our results indicate that this predicted miR-MM interaction is unlikely to have a meaningful role in the regulation of *fgf8a* expression *in vivo* (Section III.2.2). Therefore, additional studies are required to identify the mechanism that underlies the post-transcriptional regulation associated with the *fgf8aM* 3'UTR.

Using a morpholino oligo that targets the central region of the MM - *fa3ui*^{MO} - we were able to induce a shift in the relative *fgf8a* alternative 3'UTR abundances, favouring the *fgf8aS* 3'UTR. This increased production of the *fgf8aS* 3'UTR was accompanied by an unexpected increase in total *fgf8a* transcript levels. To address the nature of this increase and to gain a better understanding of the *fa3ui*^{MO}-mediated interference with *fgf8a* PAS selection, we resorted to mathematical modelling (Section III.2.2). Our modelling approach demonstrates that our experimental observations are well described by a model where the sequence targeted by the *fa3ui*^{MO} plays a role in PAS selection, and an overactivation of Fgf signalling can stimulate *fgf8a* transcription through a direct or indirect feedback-based mechanism (Section III.2.2). This proposed positive feedback mechanism is also consistent with a model in which *fgf8a* APA functions as part of a system of Fgf8a protein expression fine-tuning. Future approaches should therefore focus on dissecting the mechanisms that control *fgf8a* alternative PAS usage and addressing the presence of this proposed feedback.

Furthermore, our study showed that this shift in the *fgf8a* PAS usage preferences brought about a spatially and temporally specific impact on embryonic development, namely in late anterior sensory system development (Section III.2.3). These observations likely reflect the complex mechanisms and inter-pathway crosstalk events involved in the different functions of Fgf8a during development (Section I.1.3), and consequently may partially derive from tissue-specific differences in the mechanisms that underlie the previously proposed feedback. Taken together, these findings indicate that, within the wide range of developmental processes that are under the influence of Fgf8a (Section I.1.3), only a specific subset appears to rely critically on the APA-mediated fine-tuning of *fgf8a* expression. Therefore, our results contribute to the current understanding of the functional importance of gene-specific APA events in the progression of embryonic development.

In addition, our investigation of the APA of *fgf8a* led to the identification of a previously undescribed role for the Fgf signalling pathway in the early stages of zebrafish ocular vascularization. Our results are indicative of a requirement for Fgf signalling in the initial stages of superficial retinal vascularization, with this pathway appearing to contribute to the structural integrity of this vascular system and to the timely induction of superficial vessel formation (Section III.2.3). Future work can focus on a more in-depth characterization of this Fgf signalling function. This characterization can include a more detailed analysis of the vessel morphology defects observed, the identification of the downstream mechanisms involved in this function, and the assessment of the precise temporal requirements for Fgf signalling in this process.

Interestingly, our results also indicate that the Fgf8a ligand has a non-essential role in this Fgf pathway function, with other Fgf ligands being likely involved (Section III.2.3). Future studies could therefore focus on the identification of additional Fgf ligands with a potential role in superficial ocular vascularization, and on the assessment of their specific contributions to this process. Furthermore, since previous studies have implicated the VEGF and HH signalling pathways in the early stages of superficial retinal vascularization (Weiss et al., 2017), it would be interesting to determine if inter-pathway cross-talk mechanisms are present between the Fgf, VEGF and HH pathways in this developmental context.

The work described in this chapter constitutes, to the extent of our knowledge, the first study to address the functional impact of modulating the 3'UTR APA of a major regulator of vertebrate embryogenesis. By interfering with the endogenous *fgf8a* PAS usage preferences we brought about a spatially and temporally specific impact on embryonic development, with this approach also leading to the identification of a previously undescribed role for Fgf signalling in the early stages of zebrafish ocular vascularization.

In conclusion, our investigation of these two facets of the post-transcriptional regulation program that operates during zebrafish embryogenesis generated insights into:

- The range of developmental processes that involve STAR protein family members.

- The developmental impact of the APA-mediated regulation of Fgf8a expression.

These findings highlight the importance of addressing post-transcriptional regulation mechanisms, and their specific roles in embryogenesis, to fully understand gene and pathway functions in development.

CHAPTER V

References

Ablooglu, A. J., Tkachenko, E., Kang, J. and Shattil, S. J. (2010) 'Integrin alphaV is necessary for gastrulation movements that regulate vertebrate body asymmetry', *Development,* 137(20), pp. 3449-58.

Adachi, H., Saijoh, Y., Mochida, K., Ohishi, S., Hashiguchi, H., Hirao, A. and Hamada, H. (1999) 'Determination of left/right asymmetric expression of nodal by a left side-specific enhancer with sequence similarity to a lefty-2 enhancer', *Genes Dev,* 13(12), pp. 1589-600.

Akai, J., Halley, P. A. and Storey, K. G. (2005) 'FGF-dependent Notch signaling maintains the spinal cord stem zone', *Genes Dev,* 19(23), pp. 2877-87.

Aken, B. L., Achuthan, P., Akanni, W., Amode, M. R., Bernsdorff, F., Bhai, J., Billis, K., Carvalho-Silva, D., Cummins, C., Clapham, P., Gil, L., Girón, C. G., Gordon, L., Hourlier, T., Hunt, S. E., Janacek, S. H., Juettemann, T., Keenan, S., Laird, M. R., Lavidas, I., Maurel, T., McLaren, W., Moore, B., Murphy, D. N., Nag, R., Newman, V., Nuhn, M., Ong, C. K., Parker, A., Patricio, M., Riat, H. S., Sheppard, D., Sparrow, H., Taylor, K., Thormann, A., Vullo, A., Walts, B., Wilder, S. P., Zadissa, A., Kostadima, M., Martin, F. J., Muffato, M., Perry, E., Ruffier, M., Staines, D. M., Trevanion, S. J., Cunningham, F., Yates, A., Zerbino, D. R. and Flicek, P. (2017) 'Ensembl 2017', *Nucleic Acids Res,* 45(D1), pp. D635-D642.

Akimenko, M. A., Ekker, M., Wegner, J., Lin, W. and Westerfield, M. (1994) 'Combinatorial expression of three zebrafish genes related to distal-less: part of a homeobox gene code for the head', *J Neurosci,* 14(6), pp. 3475-86.

Akiyama, R., Masuda, M., Tsuge, S., Bessho, Y. and Matsui, T. (2014) 'An anterior limit of FGF/Erk signal activity marks the earliest future somite boundary in zebrafish', *Development,* 141(5), pp. 1104-9.

Alberts, B. (2002) *Molecular biology of the cell.* 4th ed / Bruce Alberts [et al.] edn. New York: Garland Science.

Alsina, B., Abelló, G., Ulloa, E., Henrique, D., Pujades, C. and Giraldez, F. (2004) 'FGF signaling is required for determination of otic neuroblasts in the chick embryo', *Dev Biol,* 267(1), pp. 119-34.

Alvarez, Y., Alonso, M. T., Vendrell, V., Zelarayan, L. C., Chamero, P., Theil, T., Bösl, M. R., Kato, S., Maconochie, M., Riethmacher, D. and Schimmang, T. (2003) 'Requirements for FGF3 and FGF10 during inner ear formation', *Development,* 130(25), pp. 6329-38.

Alvarez-Garcia, I. and Miska, E. A. (2005) 'MicroRNA functions in animal development and human disease', *Development,* 132(21), pp. 4653-62.

Amack, J. D. (2014) 'Salient features of the ciliated organ of asymmetry', *Bioarchitecture,* 4(1), pp. 6-15.

Amack, J. D. and Yost, H. J. (2004) 'The T box transcription factor no tail in ciliated cells controls zebrafish left-right asymmetry', *Curr Biol,* 14(8), pp. 685-90.

Amaya, E., Musci, T. J. and Kirschner, M. W. (1991) 'Expression of a dominant negative mutant of the FGF receptor disrupts mesoderm formation in Xenopus embryos', *Cell,* 66(2), pp. 257-70.

Amaya, E., Stein, P. A., Musci, T. J. and Kirschner, M. W. (1993) 'FGF signalling in the early specification of mesoderm in Xenopus', *Development,* 118(2), pp. 477-87.

Arrington, C. B., Peterson, A. G. and Yost, H. J. (2013) 'Sdc2 and Tbx16 regulate Fgf2-dependent epithelial cell morphogenesis in the ciliated organ of asymmetry', *Development,* 140(19), pp. 4102-9.

Artzt, K. and Wu, J. I. (2010) 'STAR trek: An introduction to STAR family proteins and review of quaking (QKI)', *Adv Exp Med Biol,* 693, pp. 1-24.

Aulehla, A., Wiegraebe, W., Baubet, V., Wahl, M. B., Deng, C., Taketo, M., Lewandoski, M. and Pourquié, O. (2008) 'A beta-catenin gradient links the clock and wavefront systems in mouse embryo segmentation', *Nat Cell Biol,* 10(2), pp. 186-93.

Azevedo, A. S., Grotek, B., Jacinto, A., Weidinger, G. and Saúde, L. (2011) 'The regenerative capacity of the zebrafish caudal fin is not affected by repeated amputations', *PLoS One,* 6(7), pp. e22820.

Baehrecke, E. H. (1997) 'who encodes a KH RNA binding protein that functions in muscle development', *Development,* 124(7), pp. 1323-32.

Bajard, L., Morelli, L. G., Ares, S., Pécréaux, J., Jülicher, F. and Oates, A. C. (2014) 'Wnt-regulated dynamics of positional information in zebrafish somitogenesis', *Development,* 141(6), pp. 1381-91.

Barresi, M. J., Hutson, L. D., Chien, C. B. and Karlstrom, R. O. (2005) 'Hedgehog regulated Slit expression determines commissure and glial cell position in the zebrafish forebrain', *Development,* 132(16), pp. 3643-56.

Batra, R., Charizanis, K., Manchanda, M., Mohan, A., Li, M., Finn, D. J., Goodwin, M., Zhang, C., Sobczak, K., Thornton, C. A. and Swanson, M. S. (2014) 'Loss of MBNL leads to disruption of developmentally regulated alternative polyadenylation in RNA-mediated disease', *Mol Cell,* 56(2), pp. 311-322.

Beck, C. W. (2015) 'Development of the vertebrate tailbud', *Wiley Interdiscip Rev Dev Biol,* 4(1), pp. 33-44.

Beckers, A., Alten, L., Viebahn, C., Andre, P. and Gossler, A. (2007) 'The mouse homeobox gene Noto regulates node morphogenesis, notochordal ciliogenesis, and left right patterning', *Proc Natl Acad Sci U S A,* 104(40), pp. 15765-70.

Beiman, M., Shilo, B. Z. and Volk, T. (1996) 'Heartless, a Drosophila FGF receptor homolog, is essential for cell migration and establishment of several mesodermal lineages', *Genes Dev,* 10(23), pp. 2993-3002.

Berglund, J. A., Chua, K., Abovich, N., Reed, R. and Rosbash, M. (1997) 'The splicing factor BBP interacts specifically with the pre-mRNA branchpoint sequence UACUAAC', *Cell,* 89(5), pp. 781-7.

Berkovits, B. D. and Mayr, C. (2015) 'Alternative 3' UTRs act as scaffolds to regulate membrane protein localization', *Nature,* 522(7556), pp. 363-7.

Bessho, Y., Hirata, H., Masamizu, Y. and Kageyama, R. (2003) 'Periodic repression by the bHLH factor Hes7 is an essential mechanism for the somite segmentation clock', *Genes Dev,* 17(12), pp. 1451-6.

Beuck, C., Qu, S., Fagg, W. S., Ares, M. and Williamson, J. R. (2012) 'Structural analysis of the quaking homodimerization interface', *J Mol Biol,* 423(5), pp. 766-81.

Beuck, C., Szymczyna, B. R., Kerkow, D. E., Carmel, A. B., Columbus, L., Stanfield, R. L. and Williamson, J. R. (2010) 'Structure of the GLD-1 homodimerization domain: insights into STAR protein-mediated translational regulation', *Structure,* 18(3), pp. 377-89.

Biedermann, B., Hotz, H. R. and Ciosk, R. (2010) 'The Quaking family of RNA-binding proteins: coordinators of the cell cycle and differentiation', *Cell Cycle,* 9(10), pp. 1929-33.

Blader, P., Fischer, N., Gradwohl, G., Guillemot, F. and Strähle, U. (1997) 'The activity of neurogenin1 is controlled by local cues in the zebrafish embryo', *Development,* 124(22), pp. 4557-69.

Blum, M., Weber, T., Beyer, T. and Vick, P. (2009) 'Evolution of leftward flow', *Semin Cell Dev Biol,* 20(4), pp. 464-71.

Bockbrader, K. and Feng, Y. (2008) 'Essential function, sophisticated regulation and pathological impact of the selective RNA-binding protein QKI in CNS myelin development', *Future Neurol,* 3(6), pp. 655-668.

Bohnsack, B. L. and Hirschi, K. K. (2004) 'Red light, green light: signals that control endothelial cell proliferation during embryonic vascular development', *Cell Cycle,* 3(12), pp. 1506-11.

Bohnsack, B. L., Lai, L., Northrop, J. L., Justice, M. J. and Hirschi, K. K. (2006) 'Visceral endoderm function is regulated by quaking and required for vascular development', *Genesis,* 44(2), pp. 93-104.

Bonnet, A., Lambert, G., Ernest, S., Dutrieux, F. X., Coulpier, F., Lemoine, S., Lobbardi, R. and Rosa, F. M. (2017) 'Quaking RNA-Binding Proteins Control Early Myofibril Formation by Modulating Tropomyosin', *Dev Cell,* 42(5), pp. 527-541.e4.

Bouldin, C. M., Snelson, C. D., Farr, G. H. and Kimelman, D. (2014) 'Restricted expression of cdc25a in the tailbud is essential for formation of the zebrafish posterior body', *Genes Dev,* 28(4), pp. 384-95.

Buckles, G. R., Thorpe, C. J., Ramel, M. C. and Lekven, A. C. (2004) 'Combinatorial Wnt control of zebrafish midbrain-hindbrain boundary formation', *Mech Dev,* 121(5), pp. 437-47.

Burdine, R. D. and Schier, A. F. (2000) 'Conserved and divergent mechanisms in left-right axis formation', *Genes Dev,* 14(7), pp. 763-76.

Burdsal, C. A., Flannery, M. L. and Pedersen, R. A. (1998) 'FGF-2 alters the fate of mouse epiblast from ectoderm to mesoderm in vitro', *Dev Biol,* 198(2), pp. 231-44.

Bénazéraf, B., Francois, P., Baker, R. E., Denans, N., Little, C. D. and Pourquié, O. (2010) 'A random cell motility gradient downstream of FGF controls elongation of an amniote embryo', *Nature,* 466(7303), pp. 248-52.

Bénazéraf, B. and Pourquié, O. (2013) 'Formation and segmentation of the vertebrate body axis', *Annu Rev Cell Dev Biol,* 29, pp. 1-26.

Campione, M. and Franco, D. (2016) 'Current Perspectives in Cardiac Laterality', *J Cardiovasc Dev Dis,* 3(4).

Carmel, A. B., Wu, J., Lehmann-Blount, K. A. and Williamson, J. R. (2010) 'High-affinity consensus binding of target RNAs by the STAR/GSG proteins GLD-1, STAR-2 and Quaking', *BMC Mol Biol,* 11, pp. 48.

Cartwright, J. H., Piro, O. and Tuval, I. (2004) 'Fluid-dynamical basis of the embryonic development of left-right asymmetry in vertebrates', *Proc Natl Acad Sci U S A,* 101(19), pp. 7234-9.

Cermak, T., Doyle, E. L., Christian, M., Wang, L., Zhang, Y., Schmidt, C., Baller, J. A., Somia, N. V., Bogdanove, A. J. and Voytas, D. F. (2011) 'Efficient design and assembly of custom TALEN and other TAL effector-based constructs for DNA targeting', *Nucleic Acids Res,* 39(12), pp. e82.

Chen, T., Damaj, B. B., Herrera, C., Lasko, P. and Richard, S. (1997) 'Self-association of the single-KH-domain family members Sam68, GRP33, GLD-1, and Qk1: role of the KH domain', *Mol Cell Biol,* 17(10), pp. 5707-18.

Chen, T. and Richard, S. (1998) 'Structure-function analysis of Qk1: a lethal point mutation in mouse quaking prevents homodimerization', *Mol Cell Biol,* 18(8), pp. 4863-71.

Chen, W., Jia, Q., Song, Y., Fu, H., Wei, G. and Ni, T. (2017a) 'Alternative Polyadenylation: Methods, Findings, and Impacts', *Genomics Proteomics Bioinformatics,* 15(5), pp. 287-300.

Chen, X., Liu, J., Janssen, J. M. and Gonçalves, M. A. F. V. (2017b) 'The Chromatin Structure Differentially Impacts High-Specificity CRISPR-Cas9 Nuclease Strategies', *Mol Ther Nucleic Acids,* 8, pp. 558-563.

Chi, C. L., Martinez, S., Wurst, W. and Martin, G. R. (2003) 'The isthmic organizer signal FGF8 is required for cell survival in the prospective midbrain and cerebellum', *Development,* 130(12), pp. 2633-44.

Chi, N. C., Shaw, R. M., De Val, S., Kang, G., Jan, L. Y., Black, B. L. and Stainier, D. Y. (2008) 'Foxn4 directly regulates tbx2b expression and atrioventricular canal formation', *Genes Dev,* 22(6), pp. 734-9.

Choi, W. Y., Giraldez, A. J. and Schier, A. F. (2007) 'Target protectors reveal dampening and balancing of Nodal agonist and antagonist by miR-430', *Science,* 318(5848), pp. 271-4.

Chung, W. S. and Stainier, D. Y. (2008) 'Intra-endodermal interactions are required for pancreatic beta cell induction', *Dev Cell,* 14(4), pp. 582-93.

Cibois, M., Gautier-Courteille, C., Vallée, A. and Paillard, L. (2010) 'A strategy to analyze the phenotypic consequences of inhibiting the association of an RNA-binding protein with a specific RNA', *RNA,* 16(1), pp. 10-5.

Ciruna, B. and Rossant, J. (2001) 'FGF signaling regulates mesoderm cell fate specification and morphogenetic movement at the primitive streak', *Dev Cell,* 1(1), pp. 37-49.

Ciruna, B. G., Schwartz, L., Harpal, K., Yamaguchi, T. P. and Rossant, J. (1997) 'Chimeric analysis of fibroblast growth factor receptor-1 (Fgfr1) function: a role for FGFR1 in morphogenetic movement through the primitive streak', *Development,* 124(14), pp. 2829-41.

Clendenon, S. G., Shah, B., Miller, C. A., Schmeisser, G., Walter, A., Gattone, V. H., Barald, K. F., Liu, Q. and Marrs, J. A. (2009) 'Cadherin-11 controls otolith assembly: evidence for extracellular cadherin activity', *Dev Dyn,* 238(8), pp. 1909-22.

Colegrove-Otero, L. J., Minshall, N. and Standart, N. (2005) 'RNA-binding proteins in early development', *Crit Rev Biochem Mol Biol,* 40(1), pp. 21-73.

Collignon, J., Varlet, I. and Robertson, E. J. (1996) 'Relationship between asymmetric nodal expression and the direction of embryonic turning', *Nature,* 381(6578), pp. 155-8.

Cooke, J. (1998) 'A gene that resuscitates a theory--somitogenesis and a molecular oscillator', *Trends Genet,* 14(3), pp. 85-8.

Cooke, J. and Zeeman, E. C. (1976) 'A clock and wavefront model for control of the number of repeated structures during animal morphogenesis', *J Theor Biol,* 58(2), pp. 455-76.

Cornell, R. A. and Kimelman, D. (1994) 'Activin-mediated mesoderm induction requires FGF', *Development,* 120(2), pp. 453-62.

Cox, R. D., Hugill, A., Shedlovsky, A., Noveroske, J. K., Best, S., Justice, M. J., Lehrach, H. and Dove, W. F. (1999) 'Contrasting effects of ENU induced embryonic lethal mutations of the quaking gene', *Genomics,* 57(3), pp. 333-41.

Cutty, S. J., Fior, R., Henriques, P. M., Saúde, L. and Wardle, F. C. (2012) 'Identification and expression analysis of two novel members of the Mesp family in zebrafish', *Int J Dev Biol,* 56(4), pp. 285-94.

Dahlem, T. J., Hoshijima, K., Jurynec, M. J., Gunther, D., Starker, C. G., Locke, A. S., Weis, A. M., Voytas, D. F. and Grunwald, D. J. (2012) 'Simple methods for generating and detecting locus-specific mutations induced with TALENs in the zebrafish genome', *PLoS Genet,* 8(8), pp. e1002861.

Daubner, G. M., Brümmer, A., Tocchini, C., Gerhardy, S., Ciosk, R., Zavolan, M. and Allain, F. H. (2014) 'Structural and functional implications of the QUA2 domain on RNA recognition by GLD-1', *Nucleic Acids Res,* 42(12), pp. 8092-105.

Davis, N. M., Kurpios, N. A., Sun, X., Gros, J., Martin, J. F. and Tabin, C. J. (2008) 'The chirality of gut rotation derives from left-right asymmetric changes in the architecture of the dorsal mesentery', *Dev Cell,* 15(1), pp. 134-45.

de Moor, C. H., Meijer, H. and Lissenden, S. (2005) 'Mechanisms of translational control by the 3' UTR in development and differentiation', *Semin Cell Dev Biol,* 16(1), pp. 49-58.

De Smet, F., Tembuyser, B., Lenard, A., Claes, F., Zhang, J., Michielsen, C., Van Schepdael, A., Herbert, J. M., Bono, F., Affolter, M., Dewerchin, M. and Carmeliet, P. (2014) 'Fibroblast growth factor signaling affects vascular outgrowth and is required for the maintenance of blood vessel integrity', *Chem Biol,* 21(10), pp. 1310-1317.

Delfini, M. C., Dubrulle, J., Malapert, P., Chal, J. and Pourquié, O. (2005) 'Control of the segmentation process by graded MAPK/ERK activation in the chick embryo', *Proc Natl Acad Sci U S A,* 102(32), pp. 11343-8.

Deng, C. X., Wynshaw-Boris, A., Shen, M. M., Daugherty, C., Ornitz, D. M. and Leder, P. (1994) 'Murine FGFR-1 is required for early postimplantation growth and axial organization', *Genes Dev,* 8(24), pp. 3045-57.

Dequéant, M. L., Glynn, E., Gaudenz, K., Wahl, M., Chen, J., Mushegian, A. and Pourquié, O. (2006) 'A complex oscillating network of signaling genes underlies the mouse segmentation clock', *Science,* 314(5805), pp. 1595-8.

Dequéant, M. L. and Pourquié, O. (2008) 'Segmental patterning of the vertebrate embryonic axis', *Nat Rev Genet,* 9(5), pp. 370-82.

Di Fruscio, M., Chen, T. and Richard, S. (1999) 'Characterization of Sam68-like mammalian proteins SLM-1 and SLM-2: SLM-1 is a Src substrate during mitosis', *Proc Natl Acad Sci U S A,* 96(6), pp. 2710-5.

Diez del Corral, R., Olivera-Martinez, I., Goriely, A., Gale, E., Maden, M. and Storey, K. (2003) 'Opposing FGF and retinoid pathways control ventral neural pattern, neuronal differentiation, and segmentation during body axis extension', *Neuron,* 40(1), pp. 65-79.

Doench, J. G., Hartenian, E., Graham, D. B., Tothova, Z., Hegde, M., Smith, I., Sullender, M., Ebert, B. L., Xavier, R. J. and Root, D. E. (2014) 'Rational design of highly active sgRNAs for CRISPR-Cas9-mediated gene inactivation', *Nat Biotechnol,* 32(12), pp. 1262-7.

Domínguez-Frutos, E., Vendrell, V., Alvarez, Y., Zelarayan, L. C., López-Hernández, I., Ros, M. and Schimmang, T. (2009) 'Tissue-specific requirements for FGF8 during early inner ear development', *Mech Dev,* 126(10), pp. 873-81.

Doyle, E. L., Booher, N. J., Standage, D. S., Voytas, D. F., Brendel, V. P., Vandyk, J. K. and Bogdanove, A. J. (2012) 'TAL Effector-Nucleotide Targeter (TALE-NT) 2.0: tools for TAL effector design and target prediction', *Nucleic Acids Res,* 40(Web Server issue), pp. W117-22.

Draper, B. W., Stock, D. W. and Kimmel, C. B. (2003) 'Zebrafish fgf24 functions with fgf8 to promote posterior mesodermal development', *Development,* 130(19), pp. 4639-54.

Dray, N., Lawton, A., Nandi, A., Jülich, D., Emonet, T. and Holley, S. A. (2013) 'Cell-fibronectin interactions propel vertebrate trunk elongation via tissue mechanics', *Curr Biol,* 23(14), pp. 1335-41.

Dubrulle, J., McGrew, M. J. and Pourquié, O. (2001) 'FGF signaling controls somite boundary position and regulates segmentation clock control of spatiotemporal Hox gene activation', *Cell,* 106(2), pp. 219-32.

Dubrulle, J. and Pourquié, O. (2004) 'fgf8 mRNA decay establishes a gradient that couples axial elongation to patterning in the vertebrate embryo', *Nature,* 427(6973), pp. 419-22.

Dunty, W. C., Biris, K. K., Chalamalasetty, R. B., Taketo, M. M., Lewandoski, M. and Yamaguchi, T. P. (2008) 'Wnt3a/beta-catenin signaling controls posterior body development by coordinating mesoderm formation and segmentation', *Development,* 135(1), pp. 85-94.

Duret, L., Dorkeld, F. and Gautier, C. (1993) 'Strong conservation of non-coding sequences during vertebrates evolution: potential involvement in post-transcriptional regulation of gene expression', *Nucleic Acids Res,* 21(10), pp. 2315-22.

Ehrmann, I., Fort, P. and Elliott, D. J. (2016) 'STARs in the CNS', *Biochem Soc Trans,* 44(4), pp. 1066-72.

Eliscovich, C., Buxbaum, A. R., Katz, Z. B. and Singer, R. H. (2013) 'mRNA on the move: the road to its biological destiny', *J Biol Chem,* 288(28), pp. 20361-8.

Elmasri, H., Liedtke, D., Lücking, G., Volff, J. N., Gessler, M. and Winkler, C. (2004) 'her7 and hey1, but not lunatic fringe show dynamic expression during somitogenesis in medaka (Oryzias latipes)', *Gene Expr Patterns,* 4(5), pp. 553-9.

Essner, J. J., Amack, J. D., Nyholm, M. K., Harris, E. B. and Yost, H. J. (2005) 'Kupffer's vesicle is a ciliated organ of asymmetry in the zebrafish embryo that initiates left-right development of the brain, heart and gut', *Development,* 132(6), pp. 1247-60.

Essner, J. J., Branford, W. W., Zhang, J. and Yost, H. J. (2000) 'Mesendoderm and left-right brain, heart and gut development are differentially regulated by pitx2 isoforms', *Development,* 127(5), pp. 1081-93.

Fabian, M. R., Sonenberg, N. and Filipowicz, W. (2010) 'Regulation of mRNA translation and stability by microRNAs', *Annu Rev Biochem,* 79, pp. 351-79.

Fakhro, K. A., Choi, M., Ware, S. M., Belmont, J. W., Towbin, J. A., Lifton, R. P., Khokha, M. K. and Brueckner, M. (2011) 'Rare copy number variations in congenital heart disease patients identify unique genes in left-right patterning', *Proc Natl Acad Sci U S A,* 108(7), pp. 2915-20.

Feracci, M., Foot, J. and Dominguez, C. (2014) 'Structural investigations of the RNA-binding properties of STAR proteins', *Biochem Soc Trans,* 42(4), pp. 1141-6.

Feracci, M., Foot, J. N., Grellscheid, S. N., Danilenko, M., Stehle, R., Gonchar, O., Kang, H. S., Dalgliesh, C., Meyer, N. H., Liu, Y., Lahat, A., Sattler, M., Eperon, I. C., Elliott, D. J. and Dominguez, C. (2016) 'Structural basis of RNA recognition and dimerization by the STAR proteins T-STAR and Sam68', *Nat Commun,* 7, pp. 10355.

Fior, R., Maxwell, A. A., Ma, T. P., Vezzaro, A., Moens, C. B., Amacher, S. L., Lewis, J. and Saúde, L. (2012) 'The differentiation and movement of presomitic mesoderm progenitor cells are controlled by Mesogenin 1', *Development,* 139(24), pp. 4656-65.

Fjose, A., Njølstad, P. R., Nornes, S., Molven, A. and Krauss, S. (1992) 'Structure and early embryonic expression of the zebrafish engrailed-2 gene', *Mech Dev,* 39(1-2), pp. 51-62.

Fletcher, R. B., Baker, J. C. and Harland, R. M. (2006) 'FGF8 spliceforms mediate early mesoderm and posterior neural tissue formation in Xenopus', *Development,* 133(9), pp. 1703-14.

Fletcher, R. B. and Harland, R. M. (2008) 'The role of FGF signaling in the establishment and maintenance of mesodermal gene expression in Xenopus', *Dev Dyn,* 237(5), pp. 1243-54.

Franklin, J. I. and Sargent, T. D. (1996) 'Ventral neural cadherin, a novel cadherin expressed in a subset of neural tissues in the zebrafish embryo', *Dev Dyn,* 206(2), pp. 121-30.

Freter, S., Muta, Y., Mak, S. S., Rinkwitz, S. and Ladher, R. K. (2008) 'Progressive restriction of otic fate: the role of FGF and Wnt in resolving inner ear potential', *Development,* 135(20), pp. 3415-24.

Frommer, G., Vorbrüggen, G., Pasca, G., Jäckle, H. and Volk, T. (1996) 'Epidermal egr-like zinc finger protein of Drosophila participates in myotube guidance', *EMBO J,* 15(7), pp. 1642-9.

Fürthauer, M., Thisse, C. and Thisse, B. (1997) 'A role for FGF-8 in the dorsoventral patterning of the zebrafish gastrula', *Development,* 124(21), pp. 4253-64.

Fürthauer, M., Van Celst, J., Thisse, C. and Thisse, B. (2004) 'Fgf signalling controls the dorsoventral patterning of the zebrafish embryo', *Development,* 131(12), pp. 2853-64.

Gage, P. J., Suh, H. and Camper, S. A. (1999) 'Dosage requirement of Pitx2 for development of multiple organs', *Development,* 126(20), pp. 4643-51.

Gagnon, J. A., Valen, E., Thyme, S. B., Huang, P., Akhmetova, L., Ahkmetova, L., Pauli, A., Montague, T. G., Zimmerman, S., Richter, C. and Schier, A. F. (2014) 'Efficient mutagenesis by Cas9 protein-mediated oligonucleotide insertion and large-scale assessment of single-guide RNAs', *PLoS One,* 9(5), pp. e98186.

Gajewski, M., Sieger, D., Alt, B., Leve, C., Hans, S., Wolff, C., Rohr, K. B. and Tautz, D. (2003) 'Anterior and posterior waves of cyclic her1 gene expression are differentially regulated in the presomitic mesoderm of zebrafish', *Development,* 130(18), pp. 4269-78.

Galarneau, A. and Richard, S. (2005) 'Target RNA motif and target mRNAs of the Quaking STAR protein', *Nat Struct Mol Biol,* 12(8), pp. 691-8.

Galarneau, A. and Richard, S. (2009) 'The STAR RNA binding proteins GLD-1, QKI, SAM68 and SLM-2 bind bipartite RNA motifs', *BMC Mol Biol,* 10, pp. 47.

Gallagher, T. L., Tietz, K. T., Morrow, Z. T., McCammon, J. M., Goldrich, M. L., Derr, N. L. and Amacher, S. L. (2017) 'Pnrc2 regulates 3'UTR-mediated decay of segmentation clock-associated transcripts during zebrafish segmentation', *Dev Biol,* 429(1), pp. 225-239.

Gibbs, H. C., Chang-Gonzalez, A., Hwang, W., Yeh, A. T. and Lekven, A. C. (2017) 'Midbrain-Hindbrain Boundary Morphogenesis: At the Intersection of Wnt and Fgf Signaling', *Front Neuroanat,* 11, pp. 64.

Gibbs, H. C., Dodson, C. R., Bai, Y., Lekven, A. C. and Yeh, A. T. (2013) 'Combined lineage mapping and fate specification profiling with NLOM-OCM using sub-10-fs pulses', ***Op**tical Methods in Developmental Biology,* 8593(85930K 11).

Gilbert, S. F. (2003) *Developmental Biology.* 7th edn. Sunderland, MA: Sinauer Associates Inc.

Gisselbrecht, S., Skeath, J. B., Doe, C. Q. and Michelson, A. M. (1996) 'heartless encodes a fibroblast growth factor receptor (DFR1/DFGF-R2) involved in the directional migration of early mesodermal cells in the Drosophila embryo', *Genes Dev,* 10(23), pp. 3003-17.

Giudicelli, F., Ozbudak, E. M., Wright, G. J. and Lewis, J. (2007) 'Setting the tempo in development: an investigation of the zebrafish somite clock mechanism', *PLoS Biol,* 5(6), pp. e150.

Glisovic, T., Bachorik, J. L., Yong, J. and Dreyfuss, G. (2008) 'RNA-binding proteins and post-transcriptional gene regulation', *FEBS Lett,* 582(14), pp. 1977-86.

Goto, H., Kimmey, S. C., Row, R. H., Matus, D. Q. and Martin, B. L. (2017) 'FGF and canonical Wnt signaling cooperate to induce paraxial mesoderm from tailbud neuromesodermal progenitors through regulation of a two-step epithelial to mesenchymal transition', *Development,* 144(8), pp. 1412-1424.

Griffin, K., Patient, R. and Holder, N. (1995) 'Analysis of FGF function in normal and no tail zebrafish embryos reveals separate mechanisms for formation of the trunk and the tail', *Development,* 121(9), pp. 2983-94.

Grimes, D. T. and Burdine, R. D. (2017) 'Left-Right Patterning: Breaking Symmetry to Asymmetric Morphogenesis', *Trends Genet,* 33(9), pp. 616-628.

Grimson, A., Farh, K. K., Johnston, W. K., Garrett-Engele, P., Lim, L. P. and Bartel, D. P. (2007) 'MicroRNA targeting specificity in mammals: determinants beyond seed pairing', *Mol Cell,* 27(1), pp. 91-105.

Grosshans, J. and Wieschaus, E. (2000) 'A genetic link between morphogenesis and cell division during formation of the ventral furrow in Drosophila', *Cell,* 101(5), pp. 523-31.

Gryzik, T. and Müller, H. A. (2004) 'FGF8-like1 and FGF8-like2 encode putative ligands of the FGF receptor Htl and are required for mesoderm migration in the Drosophila gastrula', *Curr Biol,* 14(8), pp. 659-67.

Hafner, M., Landthaler, M., Burger, L., Khorshid, M., Hausser, J., Berninger, P., Rothballer, A., Ascano, M., Jungkamp, A. C., Munschauer, M., Ulrich, A., Wardle, G. S., Dewell, S., Zavolan, M. and Tuschl, T. (2010) 'Transcriptome-wide identification of RNA-binding protein and microRNA target sites by PAR-CLIP', *Cell,* 141(1), pp. 129-41.

Hall, M. P., Nagel, R. J., Fagg, W. S., Shiue, L., Cline, M. S., Perriman, R. J., Donohue, J. P. and Ares, M. (2013) 'Quaking and PTB control overlapping splicing regulatory networks during muscle cell differentiation', *RNA,* 19(5), pp. 627-38.

Hammond, K. L. and Whitfield, T. T. (2011) 'Fgf and Hh signalling act on a symmetrical pre-pattern to specify anterior and posterior identity in the zebrafish otic placode and vesicle', *Development,* 138(18), pp. 3977-87.

Hashimoto, H., Rebagliati, M., Ahmad, N., Muraoka, O., Kurokawa, T., Hibi, M. and Suzuki, T. (2004) 'The Cerberus/Dan-family protein Charon is a negative regulator of Nodal signaling during left-right patterning in zebrafish', *Development,* 131(8), pp. 1741-53.

Heisenberg, C. P., Brennan, C. and Wilson, S. W. (1999) 'Zebrafish aussicht mutant embryos exhibit widespread overexpression of ace (fgf8) and coincident defects in CNS development', *Development,* 126(10), pp. 2129-40.

Henry, C. A., Urban, M. K., Dill, K. K., Merlie, J. P., Page, M. F., Kimmel, C. B. and Amacher, S. L. (2002) 'Two linked hairy/Enhancer of split-related zebrafish genes, her1 and her7, function together to refine alternating somite boundaries', *Development,* 129(15), pp. 3693-704.

Hernández-Bejarano, M., Gestri, G., Spawls, L., Nieto-López, F., Picker, A., Tada, M., Brand, M., Bovolenta, P., Wilson, S. W. and Cavodeassi, F. (2015) 'Opposing Shh and Fgf signals initiate nasotemporal patterning of the zebrafish retina', *Development,* 142(22), pp. 3933-42.

Hilgers, V., Lemke, S. B. and Levine, M. (2012) 'ELAV mediates 3' UTR extension in the Drosophila nervous system', *Genes Dev,* 26(20), pp. 2259-64.

Hilgers, V., Perry, M. W., Hendrix, D., Stark, A., Levine, M. and Haley, B. (2011) 'Neural-specific elongation of 3' UTRs during Drosophila development', *Proc Natl Acad Sci U S A,* 108(38), pp. 15864-9.

Hojo, M., Takashima, S., Kobayashi, D., Sumeragi, A., Shimada, A., Tsukahara, T., Yokoi, H., Narita, T., Jindo, T., Kage, T., Kitagawa, T., Kimura, T., Sekimizu, K., Miyake, A., Setiamarga, D., Murakami, R., Tsuda, S., Ooki, S., Kakihara, K., Naruse, K. and Takeda, H. (2007) 'Right-elevated expression of charon is regulated by fluid flow in medaka Kupffer's vesicle', *Dev Growth Differ,* 49(5), pp. 395-405.

Holley, S. A., Jülich, D., Rauch, G. J., Geisler, R. and Nüsslein-Volhard, C. (2002) 'her1 and the notch pathway function within the oscillator mechanism that regulates zebrafish somitogenesis', *Development,* 129(5), pp. 1175-83.

Horne-Badovinac, S., Rebagliati, M. and Stainier, D. Y. (2003) 'A cellular framework for gut-looping morphogenesis in zebrafish', *Science,* 302(5645), pp. 662-5.

Hubaud, A. and Pourquié, O. (2014) 'Signalling dynamics in vertebrate segmentation', *Nat Rev Mol Cell Biol,* 15(11), pp. 709-21.

Inoue, A., Takahashi, M., Hatta, K., Hotta, Y. and Okamoto, H. (1994) 'Developmental regulation of islet-1 mRNA expression during neuronal differentiation in embryonic zebrafish', *Dev Dyn,* 199(1), pp. 1-11.

Isaacs, H. V., Pownall, M. E. and Slack, J. M. (1994) 'eFGF regulates Xbra expression during Xenopus gastrulation', *EMBO J,* 13(19), pp. 4469-81.

Israeli, D., Nir, R. and Volk, T. (2007) 'Dissection of the target specificity of the RNA-binding protein HOW reveals dpp mRNA as a novel HOW target', *Development,* 134(11), pp. 2107-14.

Jan, C. H., Friedman, R. C., Ruby, J. G. and Bartel, D. P. (2011) 'Formation, regulation and evolution of Caenorhabditis elegans 3'UTRs', *Nature,* 469(7328), pp. 97-101.

Jan, E., Motzny, C. K., Graves, L. E. and Goodwin, E. B. (1999) 'The STAR protein, GLD-1, is a translational regulator of sexual identity in Caenorhabditis elegans', *EMBO J,* 18(1), pp. 258-69.

Jao, L. E., Wente, S. R. and Chen, W. (2013) 'Efficient multiplex biallelic zebrafish genome editing using a CRISPR nuclease system', *Proc Natl Acad Sci U S A,* 110(34), pp. 13904-9.

Ji, Y., Buel, S. M. and Amack, J. D. (2016) 'Mutations in zebrafish pitx2 model congenital malformations in Axenfeld-Rieger syndrome but do not disrupt left-right placement of visceral organs', *Dev Biol,* 416(1), pp. 69-81.

Ji, Z., Lee, J. Y., Pan, Z., Jiang, B. and Tian, B. (2009) 'Progressive lengthening of 3' untranslated regions of mRNAs by alternative polyadenylation during mouse embryonic development', *Proc Natl Acad Sci U S A,* 106(17), pp. 7028-33.

Justice, M. J. and Bode, V. C. (1988) 'Three ENU-induced alleles of the murine quaking locus are recessive embryonic lethal mutations', *Genet Res,* 51(2), pp. 95-102.

Justice, M. J. and Hirschi, K. K. (2010) 'The role of quaking in mammalian embryonic development', *Adv Exp Med Biol,* 693, pp. 82-92.

Kanki, J. P. and Ho, R. K. (1997) 'The development of the posterior body in zebrafish', *Development,* 124(4), pp. 881-93.

Kaufman, R., Weiss, O., Sebbagh, M., Ravid, R., Gibbs-Bar, L., Yaniv, K. and Inbal, A. (2015) 'Development and origins of zebrafish ocular vasculature', *BMC Dev Biol,* 15, pp. 18.

Kawakami, Y., Raya, A., Raya, R. M., Rodríguez-Esteban, C. and Izpisúa Belmonte, J. C. (2005) 'Retinoic acid signalling links left-right asymmetric patterning and bilaterally symmetric somitogenesis in the zebrafish embryo', *Nature,* 435(7039), pp. 165-71.

Kawakami, Y., Rodríguez-León, J., Koth, C. M., Büscher, D., Itoh, T., Raya, A., Ng, J. K., Esteban, C. R., Takahashi, S., Henrique, D., Schwarz, M. F., Asahara, H. and Izpisúa Belmonte, J. C. (2003) 'MKP3 mediates the cellular response to FGF8 signalling in the vertebrate limb', *Nat Cell Biol,* 5(6), pp. 513-9.

Kawasumi, A., Nakamura, T., Iwai, N., Yashiro, K., Saijoh, Y., Belo, J. A., Shiratori, H. and Hamada, H. (2011) 'Left-right asymmetry in the level of active Nodal protein produced in the node is translated into left-right asymmetry in the lateral plate of mouse embryos', *Dev Biol,* 353(2), pp. 321-30.

Kiecker, C., Bates, T. and Bell, E. (2016) 'Molecular specification of germ layers in vertebrate embryos', *Cell Mol Life Sci,* 73(5), pp. 923-47.

Kimelman, D. (2006) 'Mesoderm induction: from caps to chips', *Nat Rev Genet,* 7(5), pp. 360-72.

Kimmel, C. B., Ballard, W. W., Kimmel, S. R., Ullmann, B. and Schilling, T. F. (1995) 'Stages of embryonic development of the zebrafish', *Dev Dyn,* 203(3), pp. 253-310.

Kitamura, K., Miura, H., Miyagawa-Tomita, S., Yanazawa, M., Katoh-Fukui, Y., Suzuki, R., Ohuchi, H., Suehiro, A., Motegi, Y., Nakahara, Y., Kondo, S. and Yokoyama, M. (1999) 'Mouse Pitx2 deficiency leads to anomalies of the ventral body wall, heart, extra- and periocular mesoderm and right pulmonary isomerism', *Development,* 126(24), pp. 5749-58.

Kondo, T., Furuta, T., Mitsunaga, K., Ebersole, T. A., Shichiri, M., Wu, J., Artzt, K., Yamamura, K. and Abe, K. (1999) 'Genomic organization and expression analysis of the mouse qkI locus', *Mamm Genome,* 10(7), pp. 662-9.

Kozomara, A. and Griffiths-Jones, S. (2014) 'miRBase: annotating high confidence microRNAs using deep sequencing data', *Nucleic Acids Res,* 42(Database issue), pp. D68-73.

Kramer-Zucker, A. G., Olale, F., Haycraft, C. J., Yoder, B. K., Schier, A. F. and Drummond, I. A. (2005) 'Cilia-driven fluid flow in the zebrafish pronephros, brain and Kupffer's vesicle is required for normal organogenesis', *Development,* 132(8), pp. 1907-21.

Kreiling, J. A., Williams, G., Creton, R. and Prabhat (2007) 'Analysis of Kupffer's vesicle in zebrafish embryos using a cave automated virtual environment', *Dev Dyn,* 236(7), pp. 1963-9.

Krol, A. J., Roellig, D., Dequéant, M. L., Tassy, O., Glynn, E., Hattem, G., Mushegian, A., Oates, A. C. and Pourquié, O. (2011) 'Evolutionary plasticity of segmentation clock networks', *Development,* 138(13), pp. 2783-92.

Kuersten, S. and Goodwin, E. B. (2003) 'The power of the 3' UTR: translational control and development', *Nat Rev Genet,* 4(8), pp. 626-37.

Kumano, G., Ezal, C. and Smith, W. C. (2001) 'Boundaries and functional domains in the animal/vegetal axis of Xenopus gastrula mesoderm', *Dev Biol,* 236(2), pp. 465-77.

Kumano, G. and Smith, W. C. (2000) 'FGF signaling restricts the primary blood islands to ventral mesoderm', *Dev Biol,* 228(2), pp. 304-14.

Kumano, G. and Smith, W. C. (2002) 'The nodal target gene Xmenf is a component of an FGF-independent pathway of ventral mesoderm induction in Xenopus', *Mech Dev,* 118(1-2), pp. 45-56.

Kurpios, N. A., Ibañes, M., Davis, N. M., Lui, W., Katz, T., Martin, J. F., Izpisúa Belmonte, J. C. and Tabin, C. J. (2008) 'The direction of gut looping is established by changes in the extracellular matrix and in cell:cell adhesion', *Proc Natl Acad Sci U S A,* 105(25), pp. 8499-506.

Kuscu, C., Arslan, S., Singh, R., Thorpe, J. and Adli, M. (2014) 'Genome-wide analysis reveals characteristics of off-target sites bound by the Cas9 endonuclease', *Nat Biotechnol,* 32(7), pp. 677-83.

LaBonne, C. and Whitman, M. (1994) 'Mesoderm induction by activin requires FGF-mediated intracellular signals', *Development,* 120(2), pp. 463-72.

Ladher, R. K. (2017) 'Changing shape and shaping change: Inducing the inner ear', *Semin Cell Dev Biol,* 65, pp. 39-46.

Ladher, R. K., Wright, T. J., Moon, A. M., Mansour, S. L. and Schoenwolf, G. C. (2005) 'FGF8 initiates inner ear induction in chick and mouse', *Genes Dev,* 19(5), pp. 603-13.

Lakiza, O., Frater, L., Yoo, Y., Villavicencio, E., Walterhouse, D., Goodwin, E. B. and Iannaccone, P. (2005) 'STAR proteins quaking-6 and GLD-1 regulate translation of the homologues GLI1 and tra-1 through a conserved RNA 3'UTR-based mechanism', *Dev Biol,* 287(1), pp. 98-110.

Langley, A. R., Smith, J. C., Stemple, D. L. and Harvey, S. A. (2014) 'New insights into the maternal to zygotic transition', *Development,* 141(20), pp. 3834-41.

Larocque, D., Galarneau, A., Liu, H. N., Scott, M., Almazan, G. and Richard, S. (2005) 'Protection of p27(Kip1) mRNA by quaking RNA binding proteins promotes oligodendrocyte differentiation', *Nat Neurosci,* 8(1), pp. 27-33.

Larocque, D., Pilotte, J., Chen, T., Cloutier, F., Massie, B., Pedraza, L., Couture, R., Lasko, P., Almazan, G. and Richard, S. (2002) 'Nuclear retention of MBP mRNAs in the quaking viable mice', *Neuron,* 36(5), pp. 815-29.

Latimer, A. and Jessen, J. R. (2010) 'Extracellular matrix assembly and organization during zebrafish gastrulation', *Matrix Biol,* 29(2), pp. 89-96.

Lavine, K. J., White, A. C., Park, C., Smith, C. S., Choi, K., Long, F., Hui, C. C. and Ornitz, D. M. (2006) 'Fibroblast growth factor signals regulate a wave of Hedgehog activation that is essential for coronary vascular development', *Genes Dev,* 20(12), pp. 1651-66.

Lawton, A. K., Nandi, A., Stulberg, M. J., Dray, N., Sneddon, M. W., Pontius, W., Emonet, T. and Holley, S. A. (2013) 'Regulated tissue fluidity steers zebrafish body elongation', *Development,* 140(3), pp. 573-82.

Lee, J. D. and Anderson, K. V. (2008) 'Morphogenesis of the node and notochord: the cellular basis for the establishment and maintenance of left-right asymmetry in the mouse', *Dev Dyn,* 237(12), pp. 3464-76.

Lee, J. D., Migeotte, I. and Anderson, K. V. (2010) 'Left-right patterning in the mouse requires Epb4.1l5-dependent morphogenesis of the node and midline', *Dev Biol,* 346(2), pp. 237-46.

Lee, S. H., Schloss, D. J. and Swain, J. L. (2000) 'Maintenance of vascular integrity in the embryo requires signaling through the fibroblast growth factor receptor', *J Biol Chem,* 275(43), pp. 33679-87.

Lee, Y., Grill, S., Sanchez, A., Murphy-Ryan, M. and Poss, K. D. (2005) 'Fgf signaling instructs position-dependent growth rate during zebrafish fin regeneration', *Development,* 132(23), pp. 5173-83.

Lewis, B. P., Burge, C. B. and Bartel, D. P. (2005) 'Conserved seed pairing, often flanked by adenosines, indicates that thousands of human genes are microRNA targets', *Cell,* 120(1), pp. 15-20.

Lewis, J. (2003) 'Autoinhibition with transcriptional delay: a simple mechanism for the zebrafish somitogenesis oscillator', *Curr Biol,* 13(16), pp. 1398-408.

Li, Y., Fenger, U., Niehrs, C. and Pollet, N. (2003a) 'Cyclic expression of esr9 gene in Xenopus presomitic mesoderm', *Differentiation,* 71(1), pp. 83-9.

Li, Y., Sun, Y., Fu, Y., Li, M., Huang, G., Zhang, C., Liang, J., Huang, S., Shen, G., Yuan, S., Chen, L., Chen, S. and Xu, A. (2012) 'Dynamic landscape of tandem 3' UTRs during zebrafish development', *Genome Res,* 22(10), pp. 1899-906.

Li, Z., Takakura, N., Oike, Y., Imanaka, T., Araki, K., Suda, T., Kaname, T., Kondo, T., Abe, K. and Yamamura, K. (2003b) 'Defective smooth muscle development in qkI-deficient mice', *Dev Growth Differ,* 45(5-6), pp. 449-62.

Li, Z., Zhang, Y., Li, D. and Feng, Y. (2000) 'Destabilization and mislocalization of myelin basic protein mRNAs in quaking dysmyelination lacking the QKI RNA-binding proteins', *J Neurosci,* 20(13), pp. 4944-53.

Lianoglou, S., Garg, V., Yang, J. L., Leslie, C. S. and Mayr, C. (2013) 'Ubiquitously transcribed genes use alternative polyadenylation to achieve tissue-specific expression', *Genes Dev,* 27(21), pp. 2380-96.

Lin, C. R., Kioussi, C., O'Connell, S., Briata, P., Szeto, D., Liu, F., Izpisúa-Belmonte, J. C. and Rosenfeld, M. G. (1999) 'Pitx2 regulates lung asymmetry, cardiac positioning and pituitary and tooth morphogenesis', *Nature,* 401(6750), pp. 279-82.

Lin, Q., Taylor, S. J. and Shalloway, D. (1997) 'Specificity and determinants of Sam68 RNA binding. Implications for the biological function of K homology domains', *J Biol Chem,* 272(43), pp. 27274-80.

Liu, D., Chu, H., Maves, L., Yan, Y. L., Morcos, P. A., Postlethwait, J. H. and Westerfield, M. (2003) 'Fgf3 and Fgf8 dependent and independent transcription factors are required for otic placode specification', *Development,* 130(10), pp. 2213-24.

Liu, X., Homma, A., Sayadi, J., Yang, S., Ohashi, J. and Takumi, T. (2016) 'Sequence features associated with the cleavage efficiency of CRISPR/Cas9 system', *Sci Rep,* 6, pp. 19675.

Liu, Z., Luyten, I., Bottomley, M. J., Messias, A. C., Houngninou-Molango, S., Sprangers, R., Zanier, K., Krämer, A. and Sattler, M. (2001) 'Structural basis for recognition of the intron branch site RNA by splicing factor 1', *Science,* 294(5544), pp. 1098-102.

Lobbardi, R., Lambert, G., Zhao, J., Geisler, R., Kim, H. R. and Rosa, F. M. (2011) 'Fine-tuning of Hh signaling by the RNA-binding protein Quaking to control muscle development', *Development,* 138(9), pp. 1783-94.

Long, S., Ahmad, N. and Rebagliati, M. (2003) 'The zebrafish nodal-related gene southpaw is required for visceral and diencephalic left-right asymmetry', *Development,* 130(11), pp. 2303-16.

Lopes, S. S., Lourenço, R., Pacheco, L., Moreno, N., Kreiling, J. and Saúde, L. (2010) 'Notch signalling regulates left-right asymmetry through ciliary length control', *Development,* 137(21), pp. 3625-32.

Lu, M. F., Pressman, C., Dyer, R., Johnson, R. L. and Martin, J. F. (1999) 'Function of Rieger syndrome gene in left-right asymmetry and craniofacial development', *Nature,* 401(6750), pp. 276-8.

Léger, S. and Brand, M. (2002) 'Fgf8 and Fgf3 are required for zebrafish ear placode induction, maintenance and inner ear patterning', *Mech Dev,* 119(1), pp. 91-108.

Mangone, M., Manoharan, A. P., Thierry-Mieg, D., Thierry-Mieg, J., Han, T., Mackowiak, S. D., Mis, E., Zegar, C., Gutwein, M. R., Khivansara, V., Attie, O., Chen, K., Salehi-Ashtiani, K., Vidal, M., Harkins, T. T., Bouffard, P., Suzuki, Y., Sugano, S., Kohara, Y., Rajewsky, N., Piano, F., Gunsalus, K. C. and Kim, J. K. (2010) 'The landscape of C. elegans 3'UTRs', *Science,* 329(5990), pp. 432-5.

Mara, A., Schroeder, J., Chalouni, C. and Holley, S. A. (2007) 'Priming, initiation and synchronization of the segmentation clock by deltaD and deltaC', *Nat Cell Biol,* 9(5), pp. 523-30.

Marjoram, L. and Wright, C. (2011) 'Rapid differential transport of Nodal and Lefty on sulfated proteoglycan-rich extracellular matrix regulates left-right asymmetry in Xenopus', *Development,* 138(3), pp. 475-85.

Maroon, H., Walshe, J., Mahmood, R., Kiefer, P., Dickson, C. and Mason, I. (2002) 'Fgf3 and Fgf8 are required together for formation of the otic placode and vesicle', *Development,* 129(9), pp. 2099-108.

Marques, S., Borges, A. C., Silva, A. C., Freitas, S., Cordenonsi, M. and Belo, J. A. (2004) 'The activity of the Nodal antagonist Cerl-2 in the mouse node is required for correct L/R body axis', *Genes Dev,* 18(19), pp. 2342-7.

Martinez-Morales, J. R., Del Bene, F., Nica, G., Hammerschmidt, M., Bovolenta, P. and Wittbrodt, J. (2005) 'Differentiation of the vertebrate retina is coordinated by an FGF signaling center', *Dev Cell,* 8(4), pp. 565-74.

Mathieu, J., Griffin, K., Herbomel, P., Dickmeis, T., Strähle, U., Kimelman, D., Rosa, F. M. and Peyriéras, N. (2004) 'Nodal and Fgf pathways interact through a positive regulatory loop and synergize to maintain mesodermal cell populations', *Development,* 131(3), pp. 629-41.

Mathis, L., Kulesa, P. M. and Fraser, S. E. (2001) 'FGF receptor signalling is required to maintain neural progenitors during Hensen's node progression', *Nat Cell Biol,* 3(6), pp. 559-66.

Matoulkova, E., Michalova, E., Vojtesek, B. and Hrstka, R. (2012) 'The role of the 3' untranslated region in post-transcriptional regulation of protein expression in mammalian cells', *RNA Biol,* 9(5), pp. 563-76.

Matsui, T., Thitamadee, S., Murata, T., Kakinuma, H., Nabetani, T., Hirabayashi, Y., Hirate, Y., Okamoto, H. and Bessho, Y. (2011) 'Canopy1, a positive feedback regulator of FGF

signaling, controls progenitor cell clustering during Kupffer's vesicle organogenesis', *Proc Natl Acad Sci U S A,* 108(24), pp. 9881-6.

McGrath, J., Somlo, S., Makova, S., Tian, X. and Brueckner, M. (2003) 'Two populations of node monocilia initiate left-right asymmetry in the mouse', *Cell,* 114(1), pp. 61-73.

McMahon, A. P. and Bradley, A. (1990) 'The Wnt-1 (int-1) proto-oncogene is required for development of a large region of the mouse brain', *Cell,* 62(6), pp. 1073-85.

McMillen, P. and Holley, S. A. (2015) 'The tissue mechanics of vertebrate body elongation and segmentation', *Curr Opin Genet Dev,* 32, pp. 106-11.

Medioni, C., Astier, M., Zmojdzian, M., Jagla, K. and Sémériva, M. (2008) 'Genetic control of cell morphogenesis during Drosophila melanogaster cardiac tube formation', *J Cell Biol,* 182(2), pp. 249-61.

Meeker, N. D., Hutchinson, S. A., Ho, L. and Trede, N. S. (2007) 'Method for isolation of PCR-ready genomic DNA from zebrafish tissues', *Biotechniques,* 43(5), pp. 610, 612, 614.

Meno, C., Shimono, A., Saijoh, Y., Yashiro, K., Mochida, K., Ohishi, S., Noji, S., Kondoh, H. and Hamada, H. (1998) 'lefty-1 is required for left-right determination as a regulator of lefty-2 and nodal', *Cell,* 94(3), pp. 287-97.

Meyer, N. H., Tripsianes, K., Vincendeau, M., Madl, T., Kateb, F., Brack-Werner, R. and Sattler, M. (2010) 'Structural basis for homodimerization of the Src-associated during mitosis, 68-kDa protein (Sam68) Qua1 domain', *J Biol Chem,* 285(37), pp. 28893-901.

Migeotte, I., Grego-Bessa, J. and Anderson, K. V. (2011) 'Rac1 mediates morphogenetic responses to intercellular signals in the gastrulating mouse embryo', *Development,* 138(14), pp. 3011-20.

Milo, R. and Phillips, R. (2016) *Cell biology by the numbers.* New York, NY: Garland Science.

Mitrani, E., Gruenbaum, Y., Shohat, H. and Ziv, T. (1990) 'Fibroblast growth factor during mesoderm induction in the early chick embryo', *Development,* 109(2), pp. 387-93.

Miura, P., Shenker, S., Andreu-Agullo, C., Westholm, J. O. and Lai, E. C. (2013) 'Widespread and extensive lengthening of 3' UTRs in the mammalian brain', *Genome Res,* 23(5), pp. 812-25.

Moreno, T. A. and Kintner, C. (2004) 'Regulation of segmental patterning by retinoic acid signaling during Xenopus somitogenesis', *Dev Cell,* 6(2), pp. 205-18.

Murakami, M. and Simons, M. (2008) 'Fibroblast growth factor regulation of neovascularization', *Curr Opin Hematol,* 15(3), pp. 215-20.

Müller, M., von Weizsäcker, E. and Campos-Ortega, J. A. (1996) 'Transcription of a zebrafish gene of the hairy-Enhancer of split family delineates the midbrain anlage in the neural plate', *Dev Genes Evol,* 206(2), pp. 153-60.

Nabel-Rosen, H., Dorevitch, N., Reuveny, A. and Volk, T. (1999) 'The balance between two isoforms of the Drosophila RNA-binding protein how controls tendon cell differentiation', *Mol Cell,* 4(4), pp. 573-84.

Nabel-Rosen, H., Toledano-Katchalski, H., Volohonsky, G. and Volk, T. (2005) 'Cell divisions in the drosophila embryonic mesoderm are repressed via posttranscriptional regulation of string/cdc25 by HOW', *Curr Biol,* 15(4), pp. 295-302.

Nabel-Rosen, H., Volohonsky, G., Reuveny, A., Zaidel-Bar, R. and Volk, T. (2002) 'Two isoforms of the Drosophila RNA binding protein, how, act in opposing directions to regulate tendon cell differentiation', *Dev Cell,* 2(2), pp. 183-93.

Naiche, L. A., Holder, N. and Lewandoski, M. (2011) 'FGF4 and FGF8 comprise the wavefront activity that controls somitogenesis', *Proc Natl Acad Sci U S A,* 108(10), pp. 4018-23.

Najib, S., Martín-Romero, C., González-Yanes, C. and Sánchez-Margalet, V. (2005) 'Role of Sam68 as an adaptor protein in signal transduction', *Cell Mol Life Sci,* 62(1), pp. 36-43.

Nakamura, T., Mine, N., Nakaguchi, E., Mochizuki, A., Yamamoto, M., Yashiro, K., Meno, C. and Hamada, H. (2006) 'Generation of robust left-right asymmetry in the mouse embryo requires a self-enhancement and lateral-inhibition system', *Dev Cell,* 11(4), pp. 495-504.

Nakamura, T., Saito, D., Kawasumi, A., Shinohara, K., Asai, Y., Takaoka, K., Dong, F., Takamatsu, A., Belo, J. A., Mochizuki, A. and Hamada, H. (2012) 'Fluid flow and interlinked feedback loops establish left-right asymmetric decay of Cerl2 mRNA', *Nat Commun,* 3, pp. 1322.

Nimura, K., Yamamoto, M., Takeichi, M., Saga, K., Takaoka, K., Kawamura, N., Nitta, H., Nagano, H., Ishino, S., Tanaka, T., Schwartz, R. J., Aburatani, H. and Kaneda, Y. (2016) 'Regulation of alternative polyadenylation by Nkx2-5 and Xrn2 during mouse heart development', *Elife,* 5.

Nir, R., Grossman, R., Paroush, Z. and Volk, T. (2012) 'Phosphorylation of the Drosophila melanogaster RNA-binding protein HOW by MAPK/ERK enhances its dimerization and activity', *PLoS Genet,* 8(3), pp. e1002632.

Nonaka, S., Tanaka, Y., Okada, Y., Takeda, S., Harada, A., Kanai, Y., Kido, M. and Hirokawa, N. (1998) 'Randomization of left-right asymmetry due to loss of nodal cilia generating leftward flow of extraembryonic fluid in mice lacking KIF3B motor protein', *Cell,* 95(6), pp. 829-37.

Nonaka, S., Yoshiba, S., Watanabe, D., Ikeuchi, S., Goto, T., Marshall, W. F. and Hamada, H. (2005) 'De novo formation of left-right asymmetry by posterior tilt of nodal cilia', *PLoS Biol,* 3(8), pp. e268.

Norris, D. P. and Robertson, E. J. (1999) 'Asymmetric and node-specific nodal expression patterns are controlled by two distinct cis-acting regulatory elements', *Genes Dev,* 13(12), pp. 1575-88.

Noveroske, J. K., Lai, L., Gaussin, V., Northrop, J. L., Nakamura, H., Hirschi, K. K. and Justice, M. J. (2002) 'Quaking is essential for blood vessel development', *Genesis,* 32(3), pp. 218-30.

Noël, E. S., Verhoeven, M., Lagendijk, A. K., Tessadori, F., Smith, K., Choorapoikayil, S., den Hertog, J. and Bakkers, J. (2013) 'A Nodal-independent and tissue-intrinsic mechanism controls heart-looping chirality', *Nat Commun,* 4, pp. 2754.

Oates, A. C. and Ho, R. K. (2002) 'Hairy/E(spl)-related (Her) genes are central components of the segmentation oscillator and display redundancy with the Delta/Notch signaling

pathway in the formation of anterior segmental boundaries in the zebrafish', *Development,* 129(12), pp. 2929-46.

Odenthal, J. and Nüsslein-Volhard, C. (1998) 'fork head domain genes in zebrafish', *Dev Genes Evol,* 208(5), pp. 245-58.

Ohkubo, Y., Chiang, C. and Rubenstein, J. L. (2002) 'Coordinate regulation and synergistic actions of BMP4, SHH and FGF8 in the rostral prosencephalon regulate morphogenesis of the telencephalic and optic vesicles', *Neuroscience,* 111(1), pp. 1-17.

Okabe, N., Xu, B. and Burdine, R. D. (2008) 'Fluid dynamics in zebrafish Kupffer's vesicle', *Dev Dyn,* 237(12), pp. 3602-12.

Okada, Y., Takeda, S., Tanaka, Y., Belmonte, J. I. and Hirokawa, N. (2005) 'Mechanism of nodal flow: a conserved symmetry breaking event in left-right axis determination', *Cell,* 121(4), pp. 633-644.

Oki, S., Hashimoto, R., Okui, Y., Shen, M. M., Mekada, E., Otani, H., Saijoh, Y. and Hamada, H. (2007) 'Sulfated glycosaminoglycans are necessary for Nodal signal transmission from the node to the left lateral plate in the mouse embryo', *Development,* 134(21), pp. 3893-904.

Ornitz, D. M. and Itoh, N. (2015) 'The Fibroblast Growth Factor signaling pathway', *Wiley Interdiscip Rev Dev Biol,* 4(3), pp. 215-66.

Oteiza, P., Köppen, M., Krieg, M., Pulgar, E., Farias, C., Melo, C., Preibisch, S., Müller, D., Tada, M., Hartel, S., Heisenberg, C. P. and Concha, M. L. (2010) 'Planar cell polarity signalling regulates cell adhesion properties in progenitors of the zebrafish laterality organ', *Development,* 137(20), pp. 3459-68.

Pais-de-Azevedo, T., Magno, R., Duarte, I. and Palmeirim, I. (2018) 'Recent advances in understanding vertebrate segmentation', *F1000Res,* 7, pp. 97.

Palmeirim, I., Henrique, D., Ish-Horowicz, D. and Pourquié, O. (1997) 'Avian hairy gene expression identifies a molecular clock linked to vertebrate segmentation and somitogenesis', *Cell,* 91(5), pp. 639-48.

Pearce, J. J., Penny, G. and Rossant, J. (1999) 'A mouse cerberus/Dan-related gene family', *Dev Biol,* 209(1), pp. 98-110.

Peled-Zehavi, H., Berglund, J. A., Rosbash, M. and Frankel, A. D. (2001) 'Recognition of RNA branch point sequences by the KH domain of splicing factor 1 (mammalian branch point binding protein) in a splicing factor complex', *Mol Cell Biol,* 21(15), pp. 5232-41.

Perrimon, N., Pitsouli, C. and Shilo, B. Z. (2012) 'Signaling mechanisms controlling cell fate and embryonic patterning', *Cold Spring Harb Perspect Biol,* 4(8), pp. a005975.

Pfaffl, M. W. (2001) 'A new mathematical model for relative quantification in real-time RT-PCR', *Nucleic Acids Res,* 29(9), pp. e45.

Phillips, B. T., Bolding, K. and Riley, B. B. (2001) 'Zebrafish fgf3 and fgf8 encode redundant functions required for otic placode induction', *Dev Biol,* 235(2), pp. 351-65.

Picker, A. and Brand, M. (2005) 'Fgf signals from a novel signaling center determine axial patterning of the prospective neural retina', *Development,* 132(22), pp. 4951-62.

Picker, A., Brennan, C., Reifers, F., Clarke, J. D., Holder, N. and Brand, M. (1999) 'Requirement for the zebrafish mid-hindbrain boundary in midbrain polarisation, mapping and confinement of the retinotectal projection', *Development,* 126(13), pp. 2967-78.

Picker, A., Cavodeassi, F., Machate, A., Bernauer, S., Hans, S., Abe, G., Kawakami, K., Wilson, S. W. and Brand, M. (2009) 'Dynamic coupling of pattern formation and morphogenesis in the developing vertebrate retina', *PLoS Biol,* 7(10), pp. e1000214.

Pinto, P. A., Henriques, T., Freitas, M. O., Martins, T., Domingues, R. G., Wyrzykowska, P. S., Coelho, P. A., Carmo, A. M., Sunkel, C. E., Proudfoot, N. J. and Moreira, A. (2011) 'RNA polymerase II kinetics in polo polyadenylation signal selection', *EMBO J,* 30(12), pp. 2431-44.

Pinto, R. A., Almeida-Santos, J., Lourenço, R. and Saúde, L. (2018) 'Identification of Dmrt2a downstream genes during zebrafish early development using a timely controlled approach', *BMC developmental biology,* in press.

Pownall, M. E. and Isaacs, H. V. (2010) *FGF signalling in vertebrate development. Developmental biology* San Rafael, Calif.: Morgan & Claypool Life Sciences.

Presta, M., Dell'Era, P., Mitola, S., Moroni, E., Ronca, R. and Rusnati, M. (2005) 'Fibroblast growth factor/fibroblast growth factor receptor system in angiogenesis', *Cytokine Growth Factor Rev,* 16(2), pp. 159-78.

Pulina, M. V., Hou, S. Y., Mittal, A., Julich, D., Whittaker, C. A., Holley, S. A., Hynes, R. O. and Astrof, S. (2011) 'Essential roles of fibronectin in the development of the left-right embryonic body plan', *Dev Biol,* 354(2), pp. 208-20.

Pánek, J., Kolář, M., Herrmannová, A. and Valášek, L. S. (2016) 'A systematic computational analysis of the rRNA-3' UTR sequence complementarity suggests a regulatory mechanism influencing post-termination events in metazoan translation', *RNA,* 22(7), pp. 957-67.

Reifers, F., Böhli, H., Walsh, E. C., Crossley, P. H., Stainier, D. Y. and Brand, M. (1998) 'Fgf8 is mutated in zebrafish acerebellar (ace) mutants and is required for maintenance of midbrain-hindbrain boundary development and somitogenesis', *Development,* 125(13), pp. 2381-95.

Reyon, D., Tsai, S. Q., Khayter, C., Foden, J. A., Sander, J. D. and Joung, J. K. (2012) 'FLASH assembly of TALENs for high-throughput genome editing', *Nat Biotechnol,* 30(5), pp. 460-5.

Rhinn, M. and Brand, M. (2001) 'The midbrain--hindbrain boundary organizer', *Curr Opin Neurobiol,* 11(1), pp. 34-42.

Ribatti, D. and Presta, M. (2002) 'The role of fibroblast growth factor-2 in the vascularization of the chick embryo chorioallantoic membrane', *J Cell Mol Med,* 6(3), pp. 439-46.

Ribeiro, A., Monteiro, J. F., Certal, A. C., Cristovão, A. M. and Saúde, L. (2017) 'Foxj1a is expressed in ependymal precursors, controls central canal position and is activated in new ependymal cells during regeneration in zebrafish', *Open Biol,* 7(11).

Richard, S., Torabi, N., Franco, G. V., Tremblay, G. A., Chen, T., Vogel, G., Morel, M., Cléroux, P., Forget-Richard, A., Komarova, S., Tremblay, M. L., Li, W., Li, A., Gao, Y. J. and Henderson, J. E. (2005) 'Ablation of the Sam68 RNA binding protein protects mice from age-related bone loss', *PLoS Genet,* 1(6), pp. e74.

Riley, M. F., Bochter, M. S., Wahi, K., Nuovo, G. J. and Cole, S. E. (2013) 'Mir-125a-5p-mediated regulation of Lfng is essential for the avian segmentation clock', *Dev Cell,* 24(5), pp. 554-61.

Roehl, H. and Nüsslein-Volhard, C. (2001) 'Zebrafish pea3 and erm are general targets of FGF8 signaling', *Curr Biol,* 11(7), pp. 503-7.

Rossant, J., Zirngibl, R., Cado, D., Shago, M. and Giguère, V. (1991) 'Expression of a retinoic acid response element-hsplacZ transgene defines specific domains of transcriptional activity during mouse embryogenesis', *Genes Dev,* 5(8), pp. 1333-44.

Rossi, A., Kontarakis, Z., Gerri, C., Nolte, H., Hölper, S., Krüger, M. and Stainier, D. Y. (2015) 'Genetic compensation induced by deleterious mutations but not gene knockdowns', *Nature,* 524(7564), pp. 230-3.

Rousseau, B., Larrieu-Lahargue, F., Bikfalvi, A. and Javerzat, S. (2003) 'Involvement of fibroblast growth factors in choroidal angiogenesis and retinal vascularization', *Exp Eye Res,* 77(2), pp. 147-56.

Ruvinsky, I., Silver, L. M. and Ho, R. K. (1998) 'Characterization of the zebrafish tbx16 gene and evolution of the vertebrate T-box family', *Dev Genes Evol,* 208(2), pp. 94-9.

Ryder, S. P., Frater, L. A., Abramovitz, D. L., Goodwin, E. B. and Williamson, J. R. (2004) 'RNA target specificity of the STAR/GSG domain post-transcriptional regulatory protein GLD-1', *Nat Struct Mol Biol,* 11(1), pp. 20-8.

Ryder, S. P. and Massi, F. (2010) 'Insights into the structural basis of RNA recognition by STAR domain proteins', *Adv Exp Med Biol,* 693, pp. 37-53.

Ryder, S. P. and Williamson, J. R. (2004) 'Specificity of the STAR/GSG domain protein Qk1: implications for the regulation of myelination', *RNA,* 10(9), pp. 1449-58.

Rymond, B. C. (2010) 'The branchpoint binding protein: in and out of the spliceosome cycle', *Adv Exp Med Biol,* 693, pp. 123-41.

Saccomanno, L., Loushin, C., Jan, E., Punkay, E., Artzt, K. and Goodwin, E. B. (1999) 'The STAR protein QKI-6 is a translational repressor', *Proc Natl Acad Sci U S A,* 96(22), pp. 12605-10.

Sahara, S., Kawakami, Y., Izpisua Belmonte, J. C. and O'Leary, D. D. (2007) 'Sp8 exhibits reciprocal induction with Fgf8 but has an opposing effect on anterior-posterior cortical area patterning', *Neural Dev,* 2, pp. 10.

Sai, X. and Ladher, R. K. (2008) 'FGF signaling regulates cytoskeletal remodeling during epithelial morphogenesis', *Curr Biol,* 18(13), pp. 976-81.

Saijoh, Y., Adachi, H., Sakuma, R., Yeo, C. Y., Yashiro, K., Watanabe, M., Hashiguchi, H., Mochida, K., Ohishi, S., Kawabata, M., Miyazono, K., Whitman, M. and Hamada, H. (2000) 'Left-right asymmetric expression of lefty2 and nodal is induced by a signaling pathway that includes the transcription factor FAST2', *Mol Cell,* 5(1), pp. 35-47.

Saijoh, Y., Oki, S., Tanaka, C., Nakamura, T., Adachi, H., Yan, Y. T., Shen, M. M. and Hamada, H. (2005) 'Two nodal-responsive enhancers control left-right asymmetric expression of Nodal', *Dev Dyn,* 232(4), pp. 1031-6.

Sanfilippo, P., Wen, J. and Lai, E. C. (2017) 'Landscape and evolution of tissue-specific alternative polyadenylation across Drosophila species', *Genome Biol,* 18(1), pp. 229.

Sasado, T., Kondoh, H., Furutani-Seiki, M. and Naruse, K. (2017) 'Mutation in cpsf6/CFIm68 (Cleavage and Polyadenylation Specificity Factor Subunit 6) causes short 3'UTRs and disturbs gene expression in developing embryos, as revealed by an analysis of primordial germ cell migration using the medaka mutant naruto', *PLoS One,* 12(3), pp. e0172467.

Sawada, A., Shinya, M., Jiang, Y. J., Kawakami, A., Kuroiwa, A. and Takeda, H. (2001) 'Fgf/MAPK signalling is a crucial positional cue in somite boundary formation', *Development,* 128(23), pp. 4873-80.

Schier, A. F. (2009) 'Nodal morphogens', *Cold Spring Harb Perspect Biol,* 1(5), pp. a003459.

Schneider, C. A., Rasband, W. S. and Eliceiri, K. W. (2012) 'NIH Image to ImageJ: 25 years of image analysis', *Nat Methods,* 9(7), pp. 671-5.

Schnorrer, F., Schönbauer, C., Langer, C. C., Dietzl, G., Novatchkova, M., Schernhuber, K., Fellner, M., Azaryan, A., Radolf, M., Stark, A., Keleman, K. and Dickson, B. J. (2010) 'Systematic genetic analysis of muscle morphogenesis and function in Drosophila', *Nature,* 464(7286), pp. 287-91.

Schulte-Merker, S. and Smith, J. C. (1995) 'Mesoderm formation in response to Brachyury requires FGF signalling', *Curr Biol,* 5(1), pp. 62-7.

Schweickert, A., Weber, T., Beyer, T., Vick, P., Bogusch, S., Feistel, K. and Blum, M. (2007) 'Cilia-driven leftward flow determines laterality in Xenopus', *Curr Biol,* 17(1), pp. 60-6.

Shanmugalingam, S., Houart, C., Picker, A., Reifers, F., Macdonald, R., Barth, A., Griffin, K., Brand, M. and Wilson, S. W. (2000) 'Ace/Fgf8 is required for forebrain commissure formation and patterning of the telencephalon', *Development,* 127(12), pp. 2549-61.

Shen, M. M. (2007) 'Nodal signaling: developmental roles and regulation', *Development,* 134(6), pp. 1023-34.

Shepard, P. J., Choi, E. A., Lu, J., Flanagan, L. A., Hertel, K. J. and Shi, Y. (2011) 'Complex and dynamic landscape of RNA polyadenylation revealed by PAS-Seq', *RNA,* 17(4), pp. 761-72.

Shimogori, T., Banuchi, V., Ng, H. Y., Strauss, J. B. and Grove, E. A. (2004) 'Embryonic signaling centers expressing BMP, WNT and FGF proteins interact to pattern the cerebral cortex', *Development,* 131(22), pp. 5639-47.

Shimozono, S., Iimura, T., Kitaguchi, T., Higashijima, S. and Miyawaki, A. (2013) 'Visualization of an endogenous retinoic acid gradient across embryonic development', *Nature,* 496(7445), pp. 363-6.

Shiratori, H. and Hamada, H. (2014) 'TGFβ signaling in establishing left-right asymmetry', *Semin Cell Dev Biol,* 32, pp. 80-4.

Shiratori, H., Sakuma, R., Watanabe, M., Hashiguchi, H., Mochida, K., Sakai, Y., Nishino, J., Saijoh, Y., Whitman, M. and Hamada, H. (2001) 'Two-step regulation of left-right asymmetric expression of Pitx2: initiation by nodal signaling and maintenance by Nkx2', *Mol Cell,* 7(1), pp. 137-49.

Shiratori, H., Yashiro, K., Shen, M. M. and Hamada, H. (2006) 'Conserved regulation and role of Pitx2 in situs-specific morphogenesis of visceral organs', *Development,* 133(15), pp. 3015-25.

Shook, D. R., Majer, C. and Keller, R. (2004) 'Pattern and morphogenesis of presumptive superficial mesoderm in two closely related species, Xenopus laevis and Xenopus tropicalis', *Dev Biol,* 270(1), pp. 163-85.

Sirbu, I. O. and Duester, G. (2006) 'Retinoic-acid signalling in node ectoderm and posterior neural plate directs left-right patterning of somitic mesoderm', *Nat Cell Biol,* 8(3), pp. 271-7.

Slack, J. M., Darlington, B. G., Heath, J. K. and Godsave, S. F. (1987) 'Mesoderm induction in early Xenopus embryos by heparin-binding growth factors', *Nature,* 326(6109), pp. 197-200.

Smibert, P., Miura, P., Westholm, J. O., Shenker, S., May, G., Duff, M. O., Zhang, D., Eads, B. D., Carlson, J., Brown, J. B., Eisman, R. C., Andrews, J., Kaufman, T., Cherbas, P., Celniker, S. E., Graveley, B. R. and Lai, E. C. (2012) 'Global patterns of tissue-specific alternative polyadenylation in Drosophila', *Cell Rep,* 1(3), pp. 277-89.

Smith, K. M., Ohkubo, Y., Maragnoli, M. E., Rasin, M. R., Schwartz, M. L., Sestan, N. and Vaccarino, F. M. (2006) 'Midline radial glia translocation and corpus callosum formation require FGF signaling', *Nat Neurosci,* 9(6), pp. 787-97.

Solnica-Krezel, L. (2005) 'Conserved patterns of cell movements during vertebrate gastrulation', *Curr Biol,* 15(6), pp. R213-28.

Solnica-Krezel, L. (2006) 'Gastrulation in zebrafish -- all just about adhesion?', *Curr Opin Genet Dev,* 16(4), pp. 433-41.

Spies, N., Burge, C. B. and Bartel, D. P. (2013) '3' UTR-isoform choice has limited influence on the stability and translational efficiency of most mRNAs in mouse fibroblasts', *Genome Res,* 23(12), pp. 2078-90.

Staton, A. A., Knaut, H. and Giraldez, A. J. (2011) 'miRNA regulation of Sdf1 chemokine signaling provides genetic robustness to germ cell migration', *Nat Genet,* 43(3), pp. 204-11.

Steventon, B., Duarte, F., Lagadec, R., Mazan, S., Nicolas, J. F. and Hirsinger, E. (2016) 'Species-specific contribution of volumetric growth and tissue convergence to posterior body elongation in vertebrates', *Development,* 143(10), pp. 1732-41.

Storm, E. E., Garel, S., Borello, U., Hebert, J. M., Martinez, S., McConnell, S. K., Martin, G. R. and Rubenstein, J. L. (2006) 'Dose-dependent functions of Fgf8 in regulating telencephalic patterning centers', *Development,* 133(9), pp. 1831-44.

Sun, X., Meyers, E. N., Lewandoski, M. and Martin, G. R. (1999) 'Targeted disruption of Fgf8 causes failure of cell migration in the gastrulating mouse embryo', *Genes Dev,* 13(14), pp. 1834-46.

Sutherland, M. J., Wang, S., Quinn, M. E., Haaning, A. and Ware, S. M. (2013) 'Zic3 is required in the migrating primitive streak for node morphogenesis and left-right patterning', *Hum Mol Genet,* 22(10), pp. 1913-23.

Suárez, R., Gobius, I. and Richards, L. J. (2014) 'Evolution and development of interhemispheric connections in the vertebrate forebrain', *Front Hum Neurosci,* 8, pp. 497.

Tadros, W. and Lipshitz, H. D. (2009) 'The maternal-to-zygotic transition: a play in two acts', *Development,* 136(18), pp. 3033-42.

Talbot, J. C. and Amacher, S. L. (2014) 'A streamlined CRISPR pipeline to reliably generate zebrafish frameshifting alleles', *Zebrafish,* 11(6), pp. 583-5.

Tanaka, H., Abe, K. and Kim, C. H. (1997) 'Cloning and expression of the quaking gene in the zebrafish embryo', *Mech Dev,* 69(1-2), pp. 209-13.

Tanaka, Y., Okada, Y. and Hirokawa, N. (2005) 'FGF-induced vesicular release of Sonic hedgehog and retinoic acid in leftward nodal flow is critical for left-right determination', *Nature,* 435(7039), pp. 172-7.

Tavares, B., Jacinto, R., Sampaio, P., Pestana, S., Pinto, A., Vaz, A., Roxo-Rosa, M., Gardner, R., Lopes, T., Schilling, B., Henry, I., Saúde, L. and Lopes, S. S. (2017) 'Notch/Her12 signalling modulates, motile/immotile cilia ratio downstream of Foxj1a in zebrafish left-right organizer', *Elife,* 6.

Teplova, M., Hafner, M., Teplov, D., Essig, K., Tuschl, T. and Patel, D. J. (2013) 'Structure-function studies of STAR family Quaking proteins bound to their in vivo RNA target sites', *Genes Dev,* 27(8), pp. 928-40.

Thisse, B., Pflumio, S., Fürthauer, M., Loppin, B., Heyer, V., Degrave, A, Woehl, R., Lux, A., Steffan, T., Charbonnier, X. Q. and Thisse, C. (2001) 'Expression of the zebrafish genome during embryogenesis (NIH R01 RR15402)', ZFIN Direct Data Submission.

Thisse, C. and Thisse, B. (2008) 'High-resolution in situ hybridization to whole-mount zebrafish embryos', *Nat Protoc,* 3(1), pp. 59-69.

Thisse, C., Thisse, B., Halpern, M. E. and Postlethwait, J. H. (1994) 'Goosecoid expression in neurectoderm and mesendoderm is disrupted in zebrafish cyclops gastrulas', *Dev Biol,* 164(2), pp. 420-9.

Thomas, J. D., Sznajder, Ł., Bardhi, O., Aslam, F. N., Anastasiadis, Z. P., Scotti, M. M., Nishino, I., Nakamori, M., Wang, E. T. and Swanson, M. S. (2017) 'Disrupted prenatal RNA processing and myogenesis in congenital myotonic dystrophy', *Genes Dev,* 31(11), pp. 1122-1133.

Thomas, J. L., Ochocinska, M. J., Hitchcock, P. F. and Thummel, R. (2012) 'Using the Tg(nrd:egfp)/albino zebrafish line to characterize in vivo expression of neurod', *PLoS One,* 7(1), pp. e29128.

Thomsen, S., Azzam, G., Kaschula, R., Williams, L. S. and Alonso, C. R. (2010) 'Developmental RNA processing of 3'UTRs in Hox mRNAs as a context-dependent mechanism modulating visibility to microRNAs', *Development,* 137(17), pp. 2951-60.

Tian, B., Hu, J., Zhang, H. and Lutz, C. S. (2005) 'A large-scale analysis of mRNA polyadenylation of human and mouse genes', *Nucleic Acids Res,* 33(1), pp. 201-12.

Tian, B. and Manley, J. L. (2017) 'Alternative polyadenylation of mRNA precursors', *Nat Rev Mol Cell Biol,* 18(1), pp. 18-30.

Tole, S., Gutin, G., Bhatnagar, L., Remedios, R. and Hébert, J. M. (2006) 'Development of midline cell types and commissural axon tracts requires Fgfr1 in the cerebrum', *Dev Biol,* 289(1), pp. 141-51.

Toledano-Katchalski, H., Nir, R., Volohonsky, G. and Volk, T. (2007) 'Post-transcriptional repression of the Drosophila midkine and pleiotrophin homolog miple by HOW is essential for correct mesoderm spreading', *Development,* 134(19), pp. 3473-81.

Ulitsky, I., Shkumatava, A., Jan, C. H., Subtelny, A. O., Koppstein, D., Bell, G. W., Sive, H. and Bartel, D. P. (2012) 'Extensive alternative polyadenylation during zebrafish development', *Genome Res,* 22(10), pp. 2054-66.

Vemaraju, S., Kantarci, H., Padanad, M. S. and Riley, B. B. (2012) 'A spatial and temporal gradient of Fgf differentially regulates distinct stages of neural development in the zebrafish inner ear', *PLoS Genet,* 8(11), pp. e1003068.

Vermot, J., Gallego Llamas, J., Fraulob, V., Niederreither, K., Chambon, P. and Dollé, P. (2005) 'Retinoic acid controls the bilateral symmetry of somite formation in the mouse embryo', *Science,* 308(5721), pp. 563-6.

Vermot, J. and Pourquié, O. (2005) 'Retinoic acid coordinates somitogenesis and left-right patterning in vertebrate embryos', *Nature,* 435(7039), pp. 215-20.

Vinothkumar, S., Rastegar, S., Takamiya, M., Ertzer, R. and Strähle, U. (2008) 'Sequential and cooperative action of Fgfs and Shh in the zebrafish retina', *Dev Biol,* 314(1), pp. 200-14.

Volk, T. (1999) 'Singling out Drosophila tendon cells: a dialogue between two distinct cell types', *Trends Genet,* 15(11), pp. 448-53.

Volk, T. (2010) 'Drosophila star proteins: what can be learned from flies?', *Adv Exp Med Biol,* 693, pp. 93-105.

Volk, T. and Artzt, K. J. (2010) *Post-transcriptional regulation by STAR proteins : control of RNA metabolism in development and disease. Advances in experimental medicine and biology* New York Austin, Tex.: Springer Science+Business Media Landes Bioscience.

Volohonsky, G., Edenfeld, G., Klämbt, C. and Volk, T. (2007) 'Muscle-dependent maturation of tendon cells is induced by post-transcriptional regulation of stripeA', *Development,* 134(2), pp. 347-56.

Wahi, K., Friesen, S., Coppola, V. and Cole, S. E. (2017) 'Putative binding sites for mir-125 family miRNAs in the mouse Lfng 3'UTR affect transcript expression in the segmentation clock, but mir-125a-5p is dispensable for normal somitogenesis', *Dev Dyn,* 246(10), pp. 740-748.

Wahl, M. B., Deng, C., Lewandoski, M. and Pourquié, O. (2007) 'FGF signaling acts upstream of the NOTCH and WNT signaling pathways to control segmentation clock oscillations in mouse somitogenesis', *Development,* 134(22), pp. 4033-41.

Walshe, J. and Mason, I. (2003) 'Unique and combinatorial functions of Fgf3 and Fgf8 during zebrafish forebrain development', *Development,* 130(18), pp. 4337-49.

Wang, G., Cadwallader, A. B., Jang, D. S., Tsang, M., Yost, H. J. and Amack, J. D. (2011) 'The Rho kinase Rock2b establishes anteroposterior asymmetry of the ciliated Kupffer's vesicle in zebrafish', *Development,* 138(1), pp. 45-54.

Wang, G., Manning, M. L. and Amack, J. D. (2012) 'Regional cell shape changes control form and function of Kupffer's vesicle in the zebrafish embryo', *Dev Biol,* 370(1), pp. 52-62.

Wang, T., Wei, J. J., Sabatini, D. M. and Lander, E. S. (2014) 'Genetic screens in human cells using the CRISPR-Cas9 system', *Science,* 343(6166), pp. 80-4.

Weinberg, E. S., Allende, M. L., Kelly, C. S., Abdelhamid, A., Murakami, T., Andermann, P., Doerre, O. G., Grunwald, D. J. and Riggleman, B. (1996) 'Developmental regulation of zebrafish MyoD in wild-type, no tail and spadetail embryos', *Development,* 122(1), pp. 271-80.

Weiss, O., Kaufman, R., Mishani, E. and Inbal, A. (2017) 'Ocular vessel patterning in zebrafish is indirectly regulated by Hedgehog signaling', *Int J Dev Biol,* 61(3-4-5), pp. 277-284.

Westerfield, M. (2000) *The zebrafish book : a guide for the laboratory use of zebrafish (danio rerio).* Eugene, Or.: Univ. of Oregon Press.

Wolpert, L. (2002) *Principles of development.* 2nd ed. edn. Oxford: Oxford University Press.

Wright, T. J. and Mansour, S. L. (2003) 'Fgf3 and Fgf10 are required for mouse otic placode induction', *Development,* 130(15), pp. 3379-90.

Wu, J., Zhou, L., Tonissen, K., Tee, R. and Artzt, K. (1999) 'The quaking I-5 protein (QKI-5) has a novel nuclear localization signal and shuttles between the nucleus and the cytoplasm', *J Biol Chem,* 274(41), pp. 29202-10.

Wu, J. I., Reed, R. B., Grabowski, P. J. and Artzt, K. (2002) 'Function of quaking in myelination: regulation of alternative splicing', *Proc Natl Acad Sci U S A,* 99(7), pp. 4233-8.

Wu, X., Scott, D. A., Kriz, A. J., Chiu, A. C., Hsu, P. D., Dadon, D. B., Cheng, A. W., Trevino, A. E., Konermann, S., Chen, S., Jaenisch, R., Zhang, F. and Sharp, P. A. (2014) 'Genome-wide binding of the CRISPR endonuclease Cas9 in mammalian cells', *Nat Biotechnol,* 32(7), pp. 670-6.

Yabe, T. and Takada, S. (2016) 'Molecular mechanism for cyclic generation of somites: Lessons from mice and zebrafish', *Dev Growth Differ,* 58(1), pp. 31-42.

Yamaguchi, T. P., Harpal, K., Henkemeyer, M. and Rossant, J. (1994) 'fgfr-1 is required for embryonic growth and mesodermal patterning during mouse gastrulation', *Genes Dev,* 8(24), pp. 3032-44.

Yamamoto, M., Mine, N., Mochida, K., Sakai, Y., Saijoh, Y., Meno, C. and Hamada, H. (2003) 'Nodal signaling induces the midline barrier by activating Nodal expression in the lateral plate', *Development,* 130(9), pp. 1795-804.

Yang, X., Dormann, D., Münsterberg, A. E. and Weijer, C. J. (2002) 'Cell movement patterns during gastrulation in the chick are controlled by positive and negative chemotaxis mediated by FGF4 and FGF8', *Dev Cell,* 3(3), pp. 425-37.

Yelon, D., Horne, S. A. and Stainier, D. Y. (1999) 'Restricted expression of cardiac myosin genes reveals regulated aspects of heart tube assembly in zebrafish', *Dev Biol,* 214(1), pp. 23-37.

Yin, C., Ciruna, B. and Solnica-Krezel, L. (2009) 'Convergence and extension movements during vertebrate gastrulation', *Curr Top Dev Biol,* 89, pp. 163-92.

You, L., Wu, J., Feng, Y., Fu, Y., Guo, Y., Long, L., Zhang, H., Luan, Y., Tian, P., Chen, L., Huang, G., Huang, S., Li, Y., Li, J., Chen, C., Zhang, Y., Chen, S. and Xu, A. (2015)

'APASdb: a database describing alternative poly(A) sites and selection of heterogeneous cleavage sites downstream of poly(A) signals', *Nucleic Acids Res,* 43(Database issue), pp. D59-67.

Yu, X., St Amand, T. R., Wang, S., Li, G., Zhang, Y., Hu, Y. P., Nguyen, L., Qiu, M. S. and Chen, Y. P. (2001) 'Differential expression and functional analysis of Pitx2 isoforms in regulation of heart looping in the chick', *Development,* 128(6), pp. 1005-13.

Zaffran, S., Astier, M., Gratecos, D. and Sémériva, M. (1997) 'The held out wings (how) Drosophila gene encodes a putative RNA-binding protein involved in the control of muscular and cardiac activity', *Development,* 124(10), pp. 2087-98.

Zelarayan, L. C., Vendrell, V., Alvarez, Y., Domínguez-Frutos, E., Theil, T., Alonso, M. T., Maconochie, M. and Schimmang, T. (2007) 'Differential requirements for FGF3, FGF8 and FGF10 during inner ear development', *Dev Biol,* 308(2), pp. 379-91.

Zhang, Y. and Feng, Y. (2001) 'Distinct molecular mechanisms lead to diminished myelin basic protein and 2',3'-cyclic nucleotide 3'-phosphodiesterase in qk(v) dysmyelination', *J Neurochem,* 77(1), pp. 165-72.

Zhao, L., Ku, L., Chen, Y., Xia, M., LoPresti, P. and Feng, Y. (2006) 'QKI binds MAP1B mRNA and enhances MAP1B expression during oligodendrocyte development', *Mol Biol Cell,* 17(10), pp. 4179-86.

Zorn, A. M. and Krieg, P. A. (1997) 'The KH domain protein encoded by quaking functions as a dimer and is essential for notochord development in Xenopus embryos', *Genes Dev,* 11(17), pp. 2176-90.

CHAPTER VI

Appendix – Publication *facsimile*

Sara F. Fernandes, Rita Fior, Francisco Pinto, Margarida Gama-Carvalho and Leonor Saúde

Fine-tuning of *fgf8a* expression through alternative polyadenylation has a selective impact on Fgf-associated developmental processes

Biochimica et Biophysica Acta (BBA) - Gene Regulatory Mechanisms

Volume 1861, Issue 9, September 2018, Pages 783-793

BBA - Gene Regulatory Mechanisms 1861 (2018) 783–793

Contents lists available at ScienceDirect

BBA - Gene Regulatory Mechanisms

journal homepage: www.elsevier.com/locate/bbagrm

Fine-tuning of *fgf8a* expression through alternative polyadenylation has a selective impact on Fgf-associated developmental processes

Sara F. Fernandes[a,c], Rita Fior[a,1], Francisco Pinto[c], Margarida Gama-Carvalho[c,2], Leonor Saúde[a,b,*,2]

[a] Instituto de Medicina Molecular, Faculdade de Medicina da Universidade de Lisboa, 1649-028 Lisboa, Portugal
[b] Instituto de Histologia e Biologia do Desenvolvimento, Faculdade de Medicina da Universidade de Lisboa, 1649-028 Lisboa, Portugal
[c] University of Lisboa, Faculty of Sciences, BioISI – Biosystems & Integrative Sciences Institute, Campo Grande, 1749-016 Lisboa, Portugal

ARTICLE INFO

Keywords:
Fgf8a
Alternative polyadenylation
3′UTR
Ocular vasculature
Embryonic development

ABSTRACT

The formation of distinct 3′UTRs through alternative polyadenylation is a mechanism of gene expression regulation that has been implicated in many physiological and pathological processes. However, its functions in the context of vertebrate embryonic development have been largely unaddressed, in particular with a gene-specific focus. Here we show that the most abundant 3′UTR for the zebrafish *fgf8a* gene in the developing embryo mediates a strong translational repression, when compared to a more sparsely used alternative 3′UTR, which supports a higher translation efficiency. By inducing a shift in the selection efficiency of the associated polyadenylation sites, we show a temporally and spatially specific impact of *fgf8a* 3′UTR usage on embryogenesis, in particular at late stages during sensory system development. In addition, we identified a previously undescribed role for Fgf signalling in the initial stages of superficial retinal vascularization. These results reveal a critical functional importance of gene-specific alternative 3′UTRs in vertebrate embryonic development.

1. Introduction

Alternative polyadenylation (APA) is a mechanism of gene expression regulation that involves the formation of alternative mRNA 3′ ends through pre-mRNA cleavage and polyadenylation at different sites. It results from the use of different polyadenylation signals (PASs) and, in the 3′ untranslated region (UTR), leads to the formation of alternative 3′UTRs (alt3′UTRs). The presence of longer 3′UTRs formed through APA can provide additional binding sites for microRNAs (miRs) and RNA binding proteins (RBPs), enabling more complex forms of post-transcriptional regulation [1].

APA is a widespread phenomenon, having been associated with both physiological and disease contexts [1, 2]. In particular, genome-wide studies have revealed that high levels of APA occur throughout embryonic development. Widespread 3′UTR lengthening and shortening events have been shown to take place during early zebrafish development [3, 4] and a 3′UTR lengthening trend accompanies the progression of mouse embryogenesis [5]. In addition, several mouse and *Drosophila* genes undergo neural-specific 3′UTR elongation during development [6, 7]. These studies provide evidence of a tight temporal and spatial control of APA dynamics throughout embryogenesis. However, the functional importance of gene-specific APA events to embryonic development has been largely unaddressed.

Fibroblast growth factors (FGFs) represent a large family of secreted signalling molecules that has been implicated in the regulation of multiple processes of embryonic development [8]. Evidence that the post-transcriptional regulation of *Fgf* genes has a critical role during development comes from a study done in chick and mouse embryos, where the authors showed that *Fgf8* mRNA stability is crucial for the establishment of a signalling gradient required for somite formation [9, 10]. For the zebrafish *Fgf8* orthologue – the *fgf8a* gene – seven distinct alt3′UTRs have been reported, a number paralleled only by *fgf12b* among the other 32 *fgf* genes of the fish [3, 11]. However, the post-transcriptional regulatory events mediated by these *fgf8a* alt3′UTRs and

Abbreviations: APA, alternative polyadenylation; PAS, polyadenylation signal; alt3′UTR, alternative 3′ untranslated region; RBP, RNA binding protein; miR, microRNA; MHB, midbrain-hindbrain boundary; PSM, presomitic mesoderm; MM, minimal motif; SAV, superficial annular vessel

* Corresponding author at: Instituto de Medicina Molecular, Faculdade de Medicina da Universidade de Lisboa, 1649-028 Lisboa, Portugal.
E-mail addresses: saramfernandes@medicina.ulisboa.pt (S.F. Fernandes), rita.fior@neuro.fchampalimaud.org (R. Fior), frpinto@fc.ul.pt (F. Pinto), mhcarvalho@fc.ul.pt (M. Gama-Carvalho), msaude@medicina.ulisboa.pt (L. Saúde).
[1] Present address: Champalimaud Research, Champalimaud Centre for the Unknown, 1400-038 Lisboa, Portugal.
[2] MG-C and LS are joint senior authors.

https://doi.org/10.1016/j.bbagrm.2018.07.012
Received 5 March 2018; Received in revised form 24 July 2018; Accepted 27 July 2018
Available online 31 July 2018

their functional importance to different aspects of embryonic development have, thus far, remained unaddressed.

During embryonic development, multiple processes are known to be regulated by Fgf8a [8]. For instance, in tail and trunk development, *fgf8a* contributes to mesodermal progenitor specification [12–15] and somite formation [16, 17]. In anterior regions *fgf8a* is required for midbrain-hindbrain boundary (MHB) patterning [18] and contributes to several aspects of sensory organ development. These include neurogenesis in the statoacoustic ganglion [19], anterior and postoptic commissure formation [20], neuronal differentiation and nasal-temporal patterning in the retina [21, 22].

Here we perform the first functional characterization of the *fgf8a* alt3′UTRs. Our results show that the *fgf8a* alt3′UTR with the highest reported abundance mediates a strong translational repression, in contrast with the second most abundant alt3′UTR, which is much more sparsely used, but supports a higher translation efficiency. By inducing a shift in the usage of the two corresponding PASs we observed a specific impact on late developmental processes associated with the sensory system. Furthermore, this modulation of Fgf signalling enabled the identification of a previously undescribed role for this pathway in the early stages of superficial retinal vascularization.

2. Results

2.1. *fgf8a alt3′UTRs mediate distinct effects on translation efficiency*

To address the significance of APA to the regulation of *fgf8a* expression during embryonic development, we began by analysing the usage patterns of its alternative PASs. Data from two independent genome-wide poly(A) event profiling studies of embryonic development revealed seven alternative PASs for the zebrafish *fgf8a* gene [3, 11] (Table S1, altUTRs 1 to 7). A predominant PAS is used in 65.9–74.3% of *fgf8a* transcripts and generates a 3′UTR with 797 nucleotides (nt) which we termed *fgf8aM* (altUTR-4). The PAS with the second highest usage frequency, considering the data obtained in both studies, is used in 12.5–18.7% of transcripts. The resulting 3′UTR is 728 nt long and was named *fgf8aS* (altUTR-3). Three additional PASs (altUTR-5, -6 and -7) were identified distal to the *fgf8aM* PAS, with a reported combined usage frequency of 4.5–7.4%. The remaining two PASs (altUTR-1 and -2) are proximal to *fgf8aS* PAS and have a combined usage frequency of 2.5–14.2% [3, 11] (Table S1).

Given the distinctive expression patterns of the *fgf8a* gene during embryogenesis (Fig. S1a) [23], we set out to determine if the *fgf8a* alternative PASs displayed different usage preferences in different embryonic tissues and developmental timepoints. We considered two developmental stages, 8-somite stage (8 ss) and 24 h post fertilization (24 hpf), and performed microdissections to isolate the head, somites/anterior presomitic mesoderm (PSM) and posterior PSM at the 8 ss, along with the anterior-half and posterior-half of 24 hpf embryos (Fig. S1b). All samples were analysed by RT-qPCR using primers that specifically recognize different subsets of *fgf8a* alt3′UTRs (Fig. S2a). We observed no significant variations in relative alt3′UTR abundance between these conditions (Fig. S2b–d), indicating that *fgf8a* PAS usage preferences are largely conserved across the embryonic tissues and developmental stages analysed. Therefore, we focused on the alt3′UTRs with the highest reported abundance - *fgf8aM* and *fgf8aS*.

To assess the impact of the *fgf8aM* and *fgf8aS* 3′UTRs on translation efficiency and mRNA stability, we generated a set of reporters in which the eGFP coding sequence was fused to each 3′UTR. Reporter constructs were *in vitro* transcribed, and the resulting mRNAs were co-injected with control mCherry mRNA into wildtype 1-cell stage embryos. mCherry was used, in this context, to account for microinjection variability. eGFP-3′UTR fluorescence intensities and mRNA abundances were quantified 24 h post injection, normalized to mCherry, and compared to those obtained with control eGFP mRNA. (Fig. 1a). We found that the *fgf8aM* 3′UTR induced a 72% reduction in reporter fluorescence (Fig. 1b,d) in contrast to the *fgf8aS* 3′UTR which had a mild effect on reporter fluorescence (10% reduction) (Fig. 1b,d). No clear tissue-specific variations in reporter fluorescence were identified in these assays (Fig. 1d), suggesting that the effect of these 3′UTRs on reporter expression is spatially conserved. Furthermore, both 3′UTRs mediated a reduction in reporter mRNA levels, of 45% and 29% for *fgf8aM* and *fgf8aS*, respectively (Fig. 1c). Taken together, these results indicate that, while both 3′UTRs have a moderate impact on mRNA stability, the *fgf8aM* 3′UTR mediates a strong translational repression when compared to the *fgf8aS* 3′UTR.

To gain a better understanding of the *fgf8a* post-transcriptional regulation dynamics, we established a system of differential equations to simulate the translation and decay of the eGFP-*fgf8aS* and eGFP-*fgf8aM* reporters during a 24 h period and estimate their respective rate constants based on the observed mRNA and protein abundances. To account for the experimental observations, the best fitting model parameters require a 3 fold lower translation rate for the eGFP-*fgf8aM* mRNA than for the eGPF-*fgf8aS* mRNA, and a relatively small difference in the respective mRNA decay constants (k_M-k_S = 0.010 h^{-1}) (Supplemental Text - Analysis of the reporter system).

Interestingly, the *fgf8aM* and *fgf8aS* 3′UTRs differ only in a 71 nt sequence (Figs. 1a and 2a). To assess the relative importance of this sequence to the *fgf8aM*-mediated regulation of transcript stability and translation efficiency, we compared the fluorescence intensities and relative transcript levels of an eGFP reporter fused to this sequence to those obtained with the eGFP-*fgf8aM* reporter. We found that both the fluorescence intensities and the relative transcript levels of the eGFP reporter fused to this sequence were equivalent to those obtained with the eGFP-*fgf8aM* reporter (Fig. 2b,c,d). Therefore, this 71 nt sequence, which we termed Minimal Motif (MM), appears to be both necessary and sufficient to mediate the post-transcriptional regulation associated with the *fgf8aM* 3′UTR.

To understand the mechanisms underlying this regulation, we analysed the MM sequence for the presence of post-transcriptional regulatory elements. The TargetScanFish6.2 database reports a binding site for dre-miR-2187 in the central region of the MM (Fig. 2a) [3, 24, 25]. Furthermore, the available miRBase expression data indicates that this miR is expressed during development, in particular at 24 hpf [26]. This prediction therefore suggests that the dre-miR-2187 could be involved in the MM-mediated post-transcriptional regulation.

In conclusion, our results reveal a significant impact of the presence of the MM sequence on mRNA expression. Therefore, even though the endogenous levels of the *fgf8aS* 3′UTR are much lower than those of the *fgf8aM* 3′UTR, transcripts with the *fgf8aS* 3′UTR are likely to contribute significantly to Fgf8a protein synthesis due to the absence of the MM.

2.2. *Interference with alternative PAS usage potentiates Fgf signalling*

To investigate the functions of the *fgf8aS* and *fgf8aM* 3′UTRs, we used TALEN and CRISPR/Cas9 technologies, to modify relevant sequences in the MM, with no success (Supplemental Methods). We believe this was due to the low GC-content of this genomic region, a sequence feature which has been previously shown to be associated with ineffective mutagenesis [27–30].

Therefore, to address the functional relevance of the *fgf8aS* and *fgf8aM* 3′UTRs we designed a morpholino oligo against the central region of the MM, which we termed *fgf8a* alt3′UTR interference morpholino (*fa3ut*i^{MO}) (Fig. 2a). By targeting the MM, our aim was to disrupt either the post-transcriptional regulation mediated by the *fgf8aM* 3′UTR or the alternative PAS selection process.

Morpholino oligonucleotides have been previously used, as target protector molecules, to disrupt post-transcriptional regulation events. In their capacity as target protectors, morpholinos bind to regulatory RNA elements blocking their interaction with post-transcriptional regulators (e.g. miRs or RBPs), and thus protect the transcript from the resulting regulation of mRNA stability and/or translation efficiency

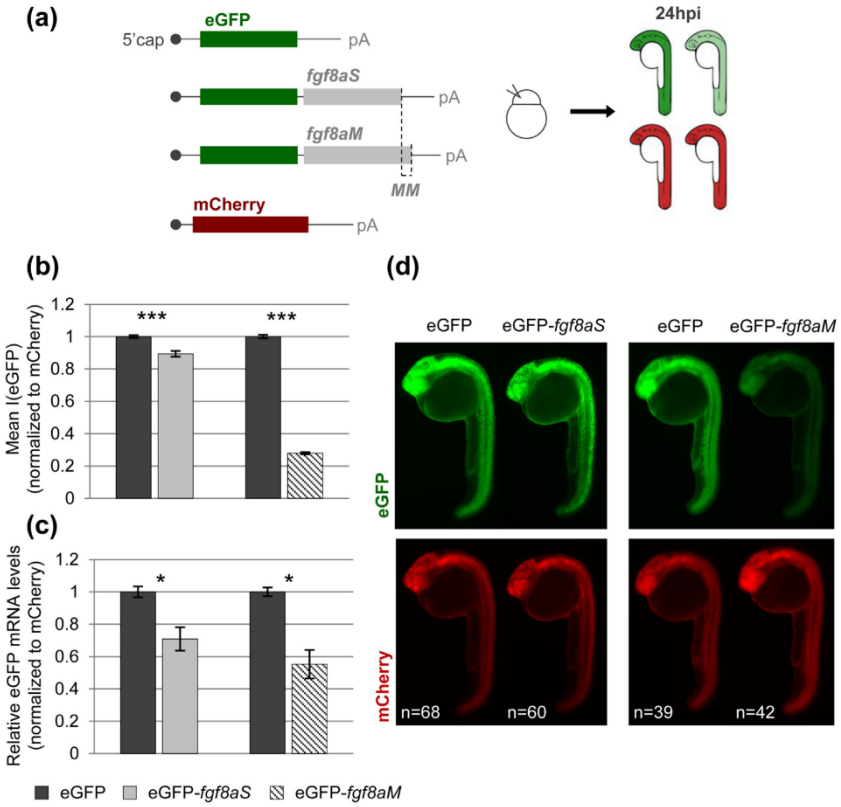

Fig. 1. Alt3′UTRs *fgf8aM* and *fgf8aS* mediate different effects on post-transcriptional regulation.
(a) Schematic representation of the experimental setup. *eGFP* mRNAs with and without the *fgf8aS* or *fgf8aM* 3′UTRs were co-injected with *mCherry* mRNA at the 1-cell stage. At 24 h post-injection (hpi) fluorescence intensities were measured and relative reporter mRNA levels determined by RT-qPCR. pA, SV40 polyadenylation signal; MM, Minimal Motif. (b) Mean eGFP fluorescence intensities, normalized to mCherry fluorescence intensities, obtained for the indicated reporters. (c) Relative eGFP mRNA levels, normalized to mCherry mRNA levels, obtained for the indicated reporters. (d) Representative images of embryos injected with each reporter. (b,c) Data show mean ± SEM (*p < 0.05; ***p < 0.001).

[31–33].

The *fa3ui*^{MO} was designed to protect the predicted miR-2187 target site (Fig. 2a) and its effect on the *fgf8aM*-mediated post-transcriptional regulation was assessed by co-injecting the *fa3ui*^{MO} with eGFP-*fgf8aM* mRNA and analysing the resulting effects on reporter fluorescence and relative reporter mRNA levels. We would expect that if the predicted miR-2187-*fgf8aM* interaction had a significant contribution to the post-transcriptional repression mediated by this 3′UTR, the *fa3ui*^{MO} would disrupt this interaction and thus bring about an increase in eGFP-*fgf8aM* reporter fluorescence and/or relative transcript levels. However, we found that the presence of the *fa3ui*^{MO} had a minor effect on eGFP-*fgf8aM* reporter fluorescence (9% reduction) (Fig. 2e,f) and did not affect the relative transcript levels of the eGFP-*fgf8aM* reporter (Fig. 2e,g). These results therefore argue against a role for the miR-2187 in the regulation of *fgf8a* expression.

In addition, the observation that the *fa3ui*^{MO} had a negligible impact on eGFP-*fgf8aM* reporter expression, both at the mRNA and at the protein level (Fig. 2f,g), indicates that this morpholino does not interfere substantially with either the stability or with the translation efficiency of transcripts with the *fgf8aM* 3′UTR. Therefore, we conclude that the *fa3ui*^{MO} does not effectively disrupt these post-transcriptional regulation mechanisms.

Considering that the *fa3ui*^{MO} target sequence is directly upstream of the *fgf8aM* polyadenylation signal (Fig. 2a), we next sought to determine if the *fa3ui*^{MO} could be used to interfere with the endogenous *fgf8a* alternative PAS selection process.

To address this question, we assessed the impact of *fa3ui*^{MO} injection on the endogenous *fgf8a* transcript and alt3′UTR levels, using the previously described RT-qPCR approach (Fig. S2a). At 24 hpf, using primers that target the coding sequence we observed that the presence of the *fa3ui*^{MO} led to a 2.5 fold increase in total *fgf8a* mRNA levels, (Fig. 3a, pCDS2). A similar increase (2.7 fold) was observed when using primers that detect both the *fgf8aS* and *fgf8aM* 3′UTRs (Fig. 3a, pUTRs3-7). However, when using primers that detect the *fgf8aM* 3′UTR, but not the *fgf8aS* 3′UTR, we observed a smaller increase in transcript levels (1.8 fold) in *fa3ui*^{MO} morphants (Fig. 3a, pUTRs4-7). A similar trend was observed in *fa3ui*^{MO} morphants at the 8 ss (Fig. 3b), albeit with less pronounced fold changes in transcript levels when using the pCDS2 (1.3 fold) and pUTRs3-7 (1.4 fold) primers and no significant difference in relative transcript levels when using the pUTRs4-7 primers.

Furthermore, while the relative abundance of the longer 3′UTRs (altUTRs-5 to -7) did not change at 24 hpf (Fig. 3a, pUTRs5-7), a significant reduction was detected at the 8 ss in *fa3ui*^{MO} morphants

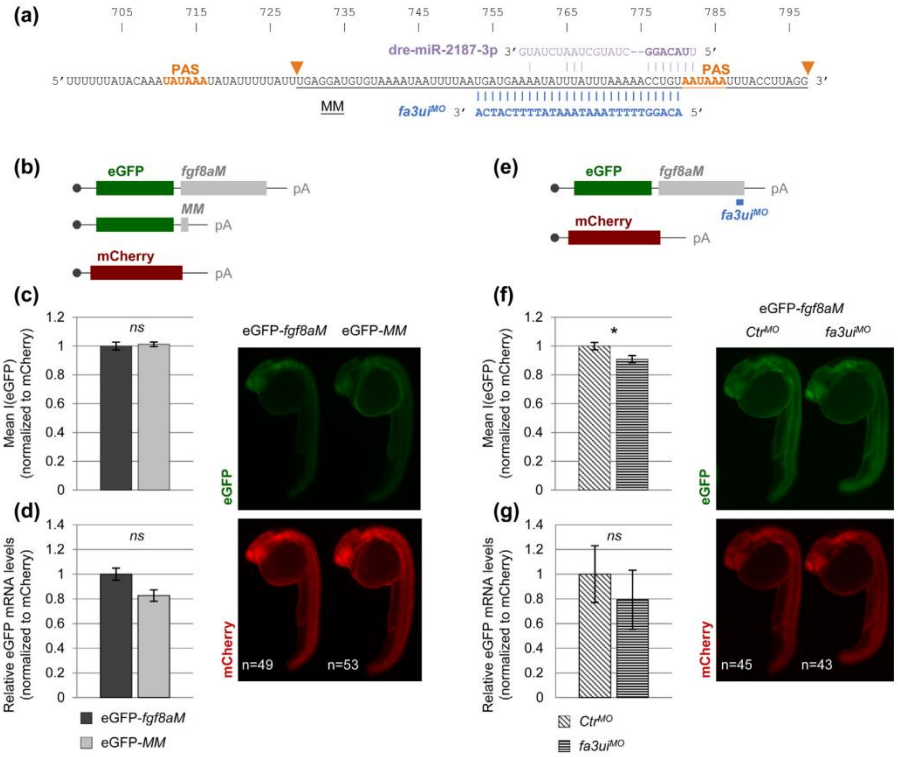

Fig. 2. The *MM* is necessary and sufficient to mediate the *fgf8aM*-associated post-transcriptional regulation and this regulation is not substantially affected by the *fa3ui*^{MO}.

(a) Illustration of the MM sequence, the *fgf8aS* and *fgf8aM* PASs and polyadenylation sites (arrowheads), the predicted miR-2187 binding site and the *fa3ui*^{MO} binding site. (b) Schematic representation of the experimental setup. *eGFP* mRNAs with either *fgf8aM* or *MM* were co-injected with *mCherry* mRNA at the 1-cell stage. At 24 hpi (c) fluorescence intensities were measured and (d) relative reporter mRNA levels determined by RT-qPCR. (e) Schematic representation of the experimental setup. eGFP-*fgf8aM* mRNA was co-injected with *mCherry* mRNA and either *Ctr*^{MO} or *fa3ui*^{MO} at the 1-cell stage. At 24 hpi (f) fluorescence intensities were measured and (g) relative reporter mRNA levels determined by RT-qPCR. (c,f) Mean eGFP fluorescence intensities, normalized to mCherry fluorescence intensities. (d,g) Relative eGFP mRNA levels normalized to mCherry mRNA levels. (c,d,f,g) Data show mean ± SEM (*p < 0.05). Representative images of embryos for each condition are shown.

(Fig. 3b, pUTRs5-7). However, given the low abundance of these longer 3′UTRs in the developing embryo (4.5–7.4%, Table S1), their contribution to the system is negligible and therefore we did not consider them in the global analysis of *fgf8* expression.

From these results we conclude that there is a differential increase in the relative levels of the *fgf8aS* 3′UTR compared to the *fgf8aM* 3′UTR in the presence of *fa3ui*^{MO} (pUTRs3-7 and pUTRs4-7 in Fig. 3a,b). The simplest explanation for these observations is that the *fa3ui*^{MO} interferes with the endogenous PAS selection process, leading to a more pronounced usage of the *fgf8aS* PAS. However, this intuitive interpretation is limited by the fact that we are only quantifying the change in transcript abundance between the control and *fa3ui*^{MO} injected embryos for each primer pair, and the fact that the signal from the primer pair pUTRs3-7 represents the sum of both the *fgf8aS* and *fgf8aM* 3′ UTRs. Furthermore, these results reveal an overall increase in total *fgf8a* transcript levels (pCDS2 in Fig. 3a,b), which was not expected to emerge from the proposed shift in PAS usage.

Therefore, to gain a better understanding of the *fa3ui*^{MO}-mediated interference with PAS selection and address the nature of the observed increase in total *fgf8a* transcript levels, we resorted to mathematical modelling of the kinetics of *fgf8a* expression (Supplemental Text). The data obtained in the fluorescent reporter assays (Fig. 1) were used to estimate the mRNA decay and translation rate constants imposed by the *fgf8aS* and *fgf8aM* 3′UTRs (Supplemental Text – Analysis of the Reporter system). In addition, the model incorporates the RT-qPCR data assessing the impact of the *fa3ui*^{MO} on the endogenous target expression (Fig. 3a,b and Supplemental Text - Model of endogenous *fgf8a* expression). This approach allowed us to integrate the results obtained using the reporter constructs and endogenous targets, into a comprehensive model of the endogenous *fgf8a* gene-to-protein pathway (Fig. 3c).

We began by using the mathematical model to calculate the relative fractions of transcripts produced with each 3′UTR in control and *fa3ui*^{MO} conditions. This analysis estimates that in control conditions 11–19% of transcripts are produced with the *fgf8aS* 3′UTR, whereas in the presence of the *fa3ui*^{MO} this percentage increases to 36–46% at 24 hpf and 31–42% at the 8 ss (Supplemental Text, Fig. 3c). The model can simulate this change in UTR abundance by altering the parameter defining the selection of the polyadenylation site (Supplemental Text). This supports the conclusion that the presence of the *fa3ui*^{MO} stimulates the usage of the *fgf8aS* PAS. Furthermore, the similarity between the values obtained for 24 hpf and 8 ss indicates that the effect of the *fa3ui*^{MO} on PAS usage is consistent between both developmental stages.

Interestingly, since the *fgf8aS* 3′UTR supports a higher translation efficiency (Fig. 1b), the model predicts that the *fa3ui*^{MO}-induced

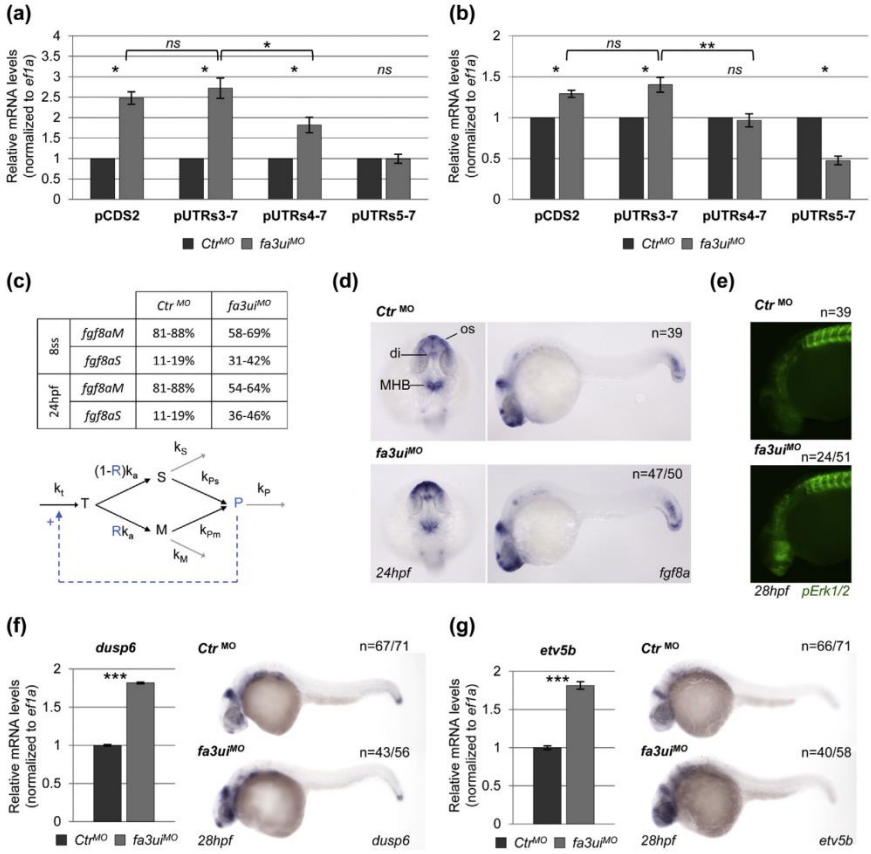

Fig. 3. *fa3ui*^{MO} morphants display a shift in PAS usage preferences and an increase in Fgf signalling.
(a,b) RT-qPCR quantification of the relative endogenous *fgf8a* transcript and indicated alt3′UTR levels in *Ctr*^{MO} and *fa3ui*^{MO} morphants (a) at 24 hpf and (b) at the 8 ss. (a,b) The pCDS2 primer pair recognizes the *fgf8a* coding sequence. The pUTRs3-7 primer pair recognizes transcripts with the *fgf8aS* UTR, the *fgf8aM* UTR and the longer alt3′UTRs -5 to -7. The pUTRs4-7 primer pair recognizes transcripts with the *fgf8aM* UTR and the longer alt3′UTRs -5 to -7, but not transcripts with the *fgf8aS* UTR. The pUTRs5-7 primer pair only recognizes transcripts with the longer alt3′UTRs -5 to -7. (c) Estimated relative percentages of the *fgf8aM* and *fgf8aS* 3′UTRs under *Ctr*^{MO} and *fa3ui*^{MO} morphant conditions at the 8 ss and at 24 hpf and schematic representation of the mathematical model. Black arrows represent transcription, APA and translation. Grey arrows represent mRNA and protein decay. Parameters in blue highlight key points of the *fa3ui*^{MO}-mediated interference. For more details see Supplemental text. (d) WISH for the coding sequence of *fgf8a* at 24 hpf in *Ctr*^{MO} and *fa3ui*^{MO} morphants. os, optic stalks; di, diencephalon; MHB, midbrain-hindbrain boundary. (e) Immunohistochemistry for pErk1/2 (Phospho-p44/42MAPK) at 28 hpf in *Ctr*^{MO} and *fa3ui*^{MO} morphants. (f,g) WISH (28 hpf) and RT-qPCR quantification (24 hpf) of the relative mRNA levels of (f) *dusp6* and (g) *etv5b* in *Ctr*^{MO} and *fa3ui*^{MO} morphants. (a,b,f,g) Data show mean ± SEM (*$p < 0.05$; **$p < 0.01$;***$p < 0.001$).

increase in *fgf8aS* PAS usage would lead to a 40–60% increase in Fgf8a protein levels (Supplemental Text).

Furthermore, our model revealed that this shift in PAS usage, on its own, would not be sufficient to account for the observed increase in total *fgf8a* transcript levels in *fa3ui*^{MO} morphants. The simplest way to mathematically account for this increase is to accompany the shift in PAS usage with an increase in *fgf8a* transcription (Supplemental Text). To address this increase in *fgf8a* transcription, we propose the presence of a direct or indirect positive feedback element. In essence, the enhanced production of the *fgf8aS* 3′UTR is predicted to lead to an increase in Fgf8a protein levels (Supplemental Text and Fig. 1b), which in turn is expected to induce an overactivation of Fgf signalling. By introducing a feedback element whereby this overactivation of Fgf signalling leads to a positive modulation of the transcription of the *fgf8a* gene, we were able to accurately reproduce the observed increase in *fgf8a* mRNA levels in the mathematical model as an indirect response to the shift in PAS usage (Supplemental Text, Fig. 3c).

Taken together, our results indicate that the *fa3ui*^{MO} induces a shift in PAS selection preferences, favouring *fgf8aS* PAS usage, along with an increase in total *fgf8a* transcript levels which could emerge from feedback-based mechanisms.

We next evaluated if the increase in *fgf8a* mRNA levels in the presence of the *fa3ui*^{MO} was spatially uniform in the embryo. Using whole-mount *in situ* hybridization (WISH), we observed a greater increase in *fgf8a* mRNA levels in the optic stalks and diencephalon than in the MHB (Fig. 3d). Additionally, using RT-qPCR, we showed that in *fa3ui*^{MO} morphants the increase in total *fgf8a* transcript levels was more pronounced in anterior (2.4 fold) than in posterior (2.0 fold) tissues (Fig. S3). These results reveal the presence of tissue-specific responses to the *fa3ui*^{MO}. Since the Fgf pathway interacts with varied signalling

pathways in different tissues [8], these tissue-specific responses could arise from tissue-specific differences in the mechanisms underlying the previously proposed feedback element.

To determine if the overall effects of the *fa3ui*^{MO} on *fgf8a* at the transcript level effectively led to a modulation of Fgf signalling we analysed the phosphorylation of Erk1/2, an effector of Fgf signalling, and the expression of the Fgf downstream targets *dusp6* and *etv5b* in *fa3ui*^{MO} morphants. We found an increase in the activated forms of Erk1/2, primarily in the eye-field (Fig. 3e) and, using RT-qPCR and WISH, we observed an increase in the expression levels of *dusp6* and *etv5b* (Fig. 3f,g). These results show that the *fa3ui*^{MO} mediates an activation of Fgf signalling.

2.3. Interference with fgf8a PAS usage selectively affects sensory system development

We next took advantage of the *fa3ui*^{MO}-induced shift in *fgf8a* PAS usage to address the impact of interfering with this process on embryonic development. We began by focusing on developmental processes that are known to be dependent on, or affected by, Fgf8a.

In the otic vesicle, we observed that *fa3ui*^{MO} morphants showed a downregulation of *neurog1* in the statoacoustic ganglion, indicating an impairment of neuroblast specification (Fig. 4a). Furthermore, we observed a reduction in *isl1* expression, which suggests an inhibition of neuronal maturation (Fig. 4b). Both observations are consistent with previous studies conducted in the context of a strong activation of *fgf8a* expression at 24 hpf using a heat-shock promoter [19].

In the forebrain, *fa3ui*^{MO} morphants presented defects in axon guidance in the anterior commissure (Fig. 4c). This is consistent with the defects observed in commissure formation in *ace* and *aus* mutants, which display a depletion and overexpression of *fgf8a*, respectively [20, 34].

Interestingly, earlier developmental processes known to involve Fgf8a, were not compromised in *fa3ui*^{MO} morphants. Namely, we did not observe alterations in the tailbud mesodermal progenitor population (Fig. 4d) or defects in somite formation (Fig. 4e). Furthermore, MHB patterning also appeared to be unaffected in *fa3ui*^{MO} morphants (Fig. 4f,g).

These results reveal that the *fa3ui*^{MO} mediated interference with *fgf8a* PAS selection affects primarily developmental processes taking place at later stages of development and in more anterior tissues associated with the sensory system. This is in line with our observation that *fgf8* transcript levels were more substantially affected by the *fa3ui*^{MO} at later (24 hpf) than earlier stages (8 ss), with different tissues displaying different magnitudes of this effect (Fig. 3a,b,d and Fig. S3). These spatially and temporally specific responses to the *fa3ui*^{MO} likely reflect the distinct mechanisms involved in the different functions of Fgf8a throughout development [8].

We additionally observed abnormalities in *fa3ui*^{MO} morphants regarding the formation of the superficial ocular vasculature [35]. Using a *kdrl*:mCherry transgenic line, which labels endothelial cells, we found that *fa3ui*^{MO} morphants displayed an increased number of superficial ocular radial vessels when compared to control embryos (Fig. 5a,c). This increase was partially rescued by a mild activation of the dominant-negative form of Fgfr1 (Fig. 5b,c), suggesting an involvement of Fgf signalling in superficial ocular vascularization.

To determine the effect of Fgf signalling depletion on the formation of this vascular system, we analysed the ocular vasculature of *ace* mutant embryos and embryos expressing the hs:*dnfgfr1* transgene. We found no noticeable difference in the number of radial vessels formed in these conditions, relative to controls. However, both *ace* mutants and hs:*dnfgfr1*+/− embryos showed a delay in the formation of the superficial annular vessel (SAV) at 48 hpf (Fig. 5f,i, arrows in Fig. 5d,g). By 72 hpf, *ace* mutants recovered from this delay while hs:*dnfgfr1*+/− embryos still presented an incomplete SAV (Fig. 5f,i,e, arrow in Fig. 5h). Furthermore, we detected morphological abnormalities, primarily an increase in the width of the SAV vessel, in hs:*dnfgfr1*+/− embryos but not in *ace* mutants (Fig. 5i, arrowheads in Fig. 5g,h).

Taken together these results reveal a previously undescribed role for Fgf signalling in the early stages of superficial ocular vascularization.

3. Discussion

Alternative polyadenylation in the 3′UTR is remarkably prevalent during embryonic development, with studies in zebrafish revealing that approximately half of all expressed protein-coding genes undergo 3′UTR APA during embryogenesis [3, 4]. However, the functional relevance of individual APA events has remained largely unaddressed. While investigating the 3′UTR-dependent regulation of *fgf8a* expression during embryonic development we came across multiple alternative 3′UTRs reported in different databases and transcriptome profiling datasets (Table S1). This study was focused on assessing the impact of the two most abundant *fgf8a* alt3′UTRs on gene expression, and addressing their functional relevance to embryonic development.

The emerging picture for the post-transcriptional regulation of *fgf8a* expression is somewhat distinct from the trends reported by large scale studies of gene expression control and alternative polyadenylation. Firstly, the impact of alternative 3′UTRs in mRNA stability and protein translation tends to be quite limited (i.e. < 20%) [36]. Here we demonstrate that the most abundant alt3′UTR - *fgf8aM* - is associated with a strong inhibition of protein synthesis (Fig. 1b,d), with the source of this differential post-transcriptional regulation residing in a 71 nt sequence motif, termed minimal motif (MM) (Fig. 2b,c,d). Furthermore, we observed that a shift from distal to proximal PAS usage has a significant impact on Fgf signalling levels (Fig. 3). Secondly, genome wide studies report that average 3′UTR lengths tend to vary throughout the progression of embryonic development [3–5, 37, 38], with several genes also displaying tissue-specific alternative PAS usage preferences [3, 6, 7, 37]. In contrast, our results indicate that, for the *fgf8a* gene, endogenous alternative PAS usage seems to remain relatively stable across the tissues and developmental stages analysed (Fig. S2). Therefore, we propose that in this specific case, APA can act to fine-tune overall protein levels within each cell.

To address the functions of the *fgf8aS* and *fgf8aM* 3′UTRs we initially resorted to TALEN and CRISPR/Cas9 technologies, to modify relevant sequences in the MM, with no success (Supplemental Methods). Both CRISPR/Cas9 and TALEN technologies have been previously used successfully in our lab [39, 40]. We believe that in this case, site directed mutagenesis was unsuccessful due to the very low G/C content of the MM sequence. As previously shown, mutagenesis efficiency is dependent on the G/C content of the target sequence, with guide RNAs targeting regions with either very low or very high G/C contents, being less efficient [27–30]. An additional sequence-specific factor, known to influence mutagenesis efficiency, which could have contributed to our inability to generate a stable mutant line is the local chromatin structure [41–43]. The *fa3ui*^{MO} was therefore used in this study, to address the functional importance of the *fgf8a* alt3′UTRs.

Sequence analysis of the *fgf8aM* alt3′UTR using the TargetScanFish algorithm revealed a predicted binding site for dre-miR-2187 in the MM region (Fig. 2a). miRs have well-established roles in the post-transcriptional regulation of gene expression, through the modulation of translation efficiency and mRNA decay, in several model organisms [44, 45]. In this study, the *fa3ui*^{MO}, which directly targets the predicted miR-2187 binding site, was used as a target protector morpholino, to address the potential significance of this predicted miR-MM interaction. However, as shown in Fig. 2e,f,g, the expression levels of the eGFP reporter containing the *fgf8aM* alt3′UTR were not restored by co-injection of the *fa3ui*^{MO}. This result indicates that the dre-miR-2187 is unlikely to be involved in the MM-associated regulation, and consequently, that this predicted miR-MM interaction does not have a meaningful role in the regulation of *fgf8a* expression *in vivo*. Therefore, the mechanism that underlies the post-transcriptional regulation

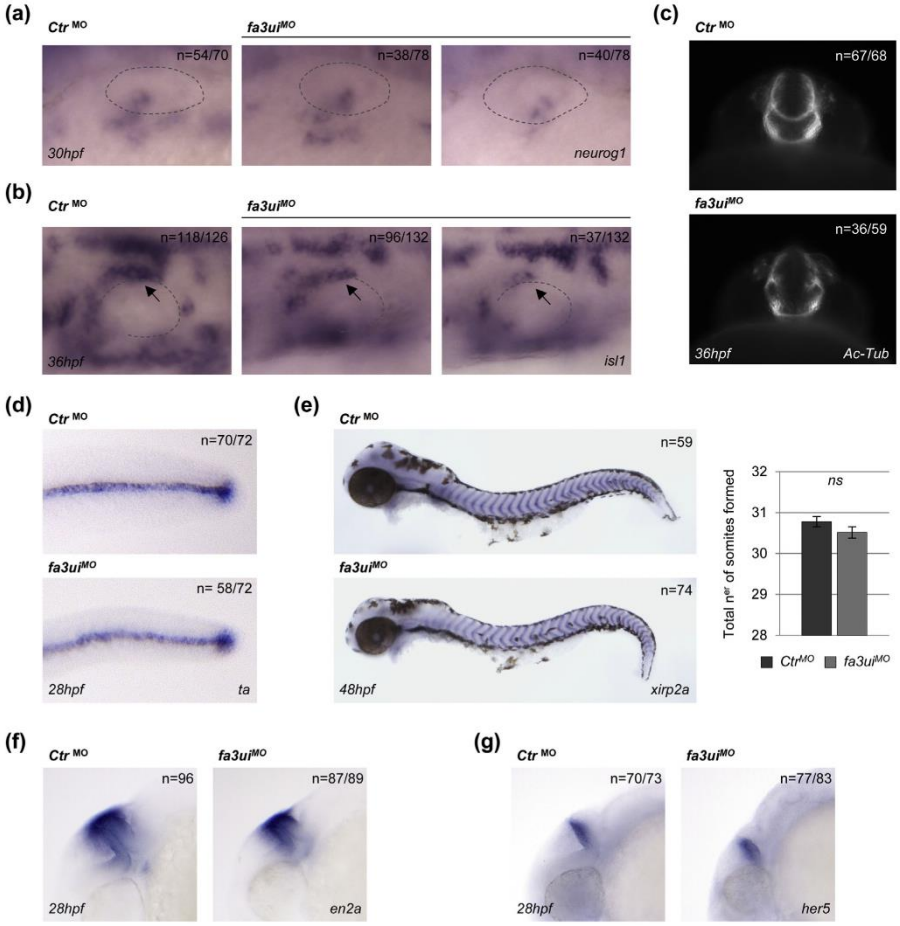

Fig. 4. Assessment of *fgf8a*-associated developmental processes in *fa3ui*^{MO} morphants.
(a) WISH for *neurog1* at 30 hpf in *Ctr*^{MO} and *fa3ui*^{MO} morphants. (b) WISH for *isl1* at 36 hpf in *Ctr*^{MO} and *fa3ui*^{MO} morphants. Arrows indicate the mature neuronal population of the statoacoustic ganglion. (a,b) Dorsolateral views, anterior to the left. The otic vesicle is outlined. (c) Immunohistochemistry for acetylated-tubulin at 36 hpf in *Ctr*^{MO} and *fa3ui*^{MO} morphants. (d–g) WISH in *Ctr*^{MO} and *fa3ui*^{MO} morphants for (d) the tailbud progenitor marker *ta*, (e) the somite boundary marker *xirp2a*, mean ± SEM number of somites for each condition, (f) the MHB markers *en2a* and (g) *her5*, (d,f,g) at 28 hpf, (e) at 48 hpf.

associated with the *fgf8aM* 3′UTR remains to be elucidated.

Furthermore, the observation that the *fa3ui*^{MO} had a negligible impact on the expression of the eGFP-*fgf8aM* reporter, both at the mRNA and at the protein levels (Fig. 2e,f,g), indicates that this morpholino does not interfere markedly with the regulation of *fgf8a* expression at the post-transcriptional level (e.g. mRNA stability and translation efficiency). Therefore, we set out to determine if the *fa3ui*^{MO} could be used to interfere with the regulation of *fgf8a* expression at the co-transcriptional level (e.g. APA).

In particular, the *fa3ui*^{MO} targets the sequence directly upstream of the *fgf8aM* polyadenylation signal (Fig. 2a), thus raising the possibility that it could interfere with the endogenous *fgf8a* polyadenylation. In agreement with this, we observed that the *fa3ui*^{MO} induced a shift in PAS selection, favouring *fgf8aS* PAS usage (Fig. 3a,b). The increase in *fgf8aS* PAS usage was accompanied by an increase in total *fgf8a* transcript levels, which seemed difficult to explain considering the small differences in transcript stability conferred by the two alt3′UTRs (Figs. 3a,b and 1c). To address this issue, we built a mathematical model that integrates the distinct kinetic parameters of *fgf8a* gene expression, from transcription to protein turn-over (Supplemental Text). The aim of this modelling approach was to understand if, given the dynamics of the process underlying the biogenesis of transcripts with the *fgf8aS* and *fgf8aM* 3′UTRs and the actual experimental measurements obtained in our system, the observed results could be explained by a shift in polyadenylation efficiency between the *fgf8aS* and *fgf8aM* PASs. Furthermore, such a modelling approach allowed us to estimate the relative abundance of each mRNA species.

Analysis of this model confirmed that our experimental observations imply a 2 to 4 fold increase in the selection of the proximal PAS in the presence of the *fa3ui*^{MO}, whereas the observed increase of total mRNA levels could only be efficiently reproduced with the inclusion of a feedback-based mechanism in the mathematical model (Supplemental Text, Fig. 3c). In conclusion, this modelling approach demonstrates that our experimental observations are well described by a simple model

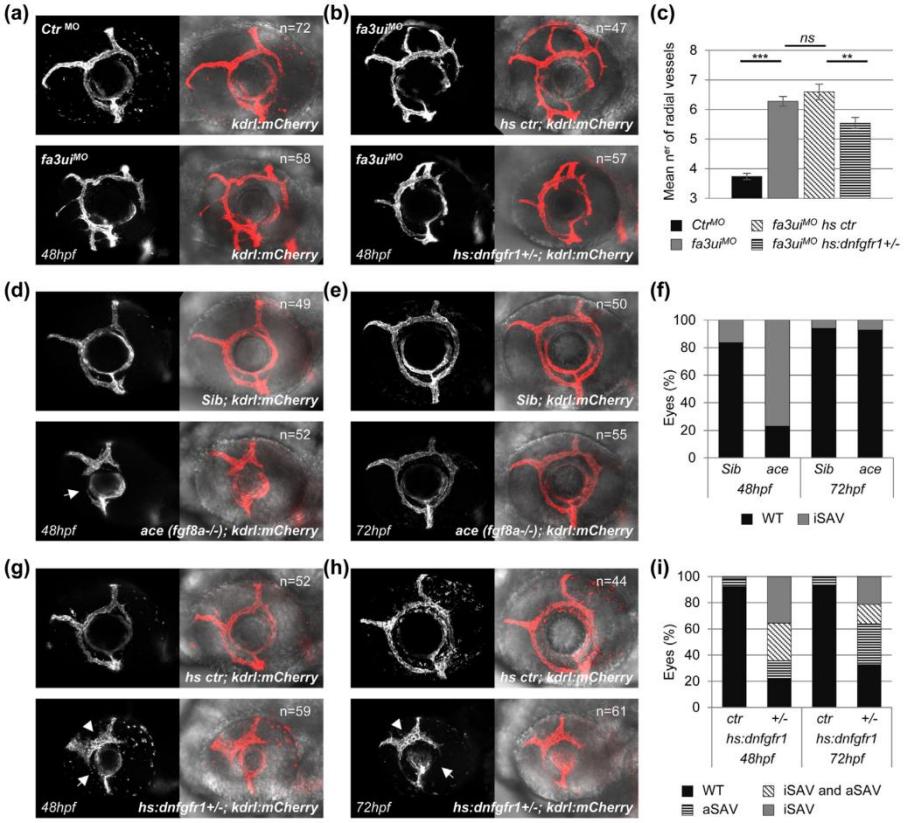

Fig. 5. Fgf signalling is involved in the early stages of superficial retinal vascularization.
(a–c) Superficial ocular vasculature of 48 hpf *kdrl*:mCherry embryos (a) injected with Ctr^{MO} or $fa3ui^{MO}$ (b) injected with $fa3ui^{MO}$ with and without the hs:*dnfgfr1* +/− transgene, under mild heat-shock conditions. (c) Mean number of ocular radial vessels ± SEM(**p < 0.01; ***p < 0.001). (d–i) Superficial ocular vasculature of (d,e) *ace*(*fgf8a* −/−), *kdrl*:mCherry embryos and siblings (g,h) hs:*dnfgfr1* +/−, *kdrl*:mCherry embryos and siblings under strong heat-shock conditions (d,g) at 48 hpf (e,h) at 72 hpf (f,i) Percentage of embryos with wildtype SAV, incomplete SAV formation (iSAV, Arrows) and abnormal SAV morphology (aSAV, Arrowheads).

where the sequence targeted by the $fa3ui^{MO}$ is important for polyadenylation site selection and an overactivation of Fgf signalling can, directly or indirectly, positively regulate *fgf8a* transcription. The presence of such feedback mechanisms fits into a model of regulation of *fgf8a* gene expression in which alternative polyadenylation is part of a fine-tuning system that coordinates protein expression levels with cellular needs.

The shift in PAS usage preferences brought about a spatially and temporally specific impact on embryonic development (Fig. 4). These responses to the $fa3ui^{MO}$ likely reflect the complex mechanisms and inter-pathway crosstalk events involved in the different functions of Fgf8a during development [8]. For instance, previous work done in mouse has shown that, during commissural plate patterning, a reciprocal induction loop is present between Fgf8 and Sp8 in the forebrain, with Sp8 acting as a transcriptional activator of *Fgf8* [46]. Therefore, the presence of an analogous positive feedback element in the zebrafish forebrain, could underlie the enhanced response to the $fa3ui^{MO}$ observed in these tissues at 24 hpf (Fig. 3d), and the subsequent disruption of commissure formation (Fig. 4c).

In addition, by targeting this mechanism of *fgf8a* expression fine-tuning, we generated a late-onset overexpression of *fgf8a* without inducing *fgf8a* missexpression, which enabled the identification of a previously undescribed Fgf signalling function in the early stages of superficial ocular vascularization (Fig. 5). In this context, the greater severity of the vascular phenotype observed in hs:*dnfgfr1* +/− embryos, when compared to *ace* mutants (Fig. 5d–i), indicates that Fgf8a has a non-essential role in the process, with other Fgfs being likely involved. Indeed, concerted actions between Fgf ligands were previously reported in the context of zebrafish ocular development. In particular, Fgf8 and Fgf3 are both necessary and sufficient to initiate neuronal differentiation in the retina [21], and the combined action of Fgf8, Fgf3 and Fgf24 is required to fully control nasal-temporal patterning of the neural retina [22]. A potential role for these Fgfs in the vascularization of the zebrafish retina remains to be explored.

The morphological abnormalities observed in the SAV vessels of hs:*dnfgfr1* +/− embryos (Fig. 5i and arrowheads in Fig. 5g,h) might derive from an impaired capacity to maintain vessel integrity. In fact, Fgf signalling has been shown to play an important role in the maintenance of intersomitic vascular integrity in zebrafish embryos [47]. In addition, a study done in mouse described a role for FGF signalling at later stages of superficial ocular vascularization, specifically during choroidal angiogenesis [48]. In light of this, our results are strongly indicative of an earlier requirement for Fgf signalling, specifically in the initial stages of superficial retinal vasculature assembly, with this

pathway appearing to contribute, not only to the timely induction of superficial vessel formation, but also to the structural integrity of this vascular system (Fig. 5g–i).

Interestingly, the Vascular Endothelial Growth Factor (VEGF) and Hedgehog signalling pathways have also been implicated in the formation of the superficial ocular vasculature in the zebrafish embryo [49]. Various synergistic effects and pathway crosstalk events have been described, between the FGF and VEGF pathways, in multiple angiogenic contexts [50]. Therefore, a potential synergy between these pathways may underlie the especially enhanced response to the *fa3ui*^{MO} observed in the eye field (Fig. 3e) and contribute to the observed vascular phenotype (Fig. 5a,c). Future studies are required to determine if FGF-VEGF crosstalk mechanisms are present in this context.

4. Conclusions

In conclusion, to the extent of our knowledge, this is the first study to address the functional impact of the 3′UTR APA of a regulator of vertebrate embryonic development.

By inducing a shift in *fgf8a* PAS usage preferences we brought about a spatially and temporally specific impact on embryonic development. In addition, this approach enabled the identification of a previously undescribed role for Fgf signalling in the early stages of zebrafish ocular vascularization.

These findings highlight the importance of addressing gene expression fine-tuning mechanisms, and 3′UTR APA in particular, to fully understand gene and pathway functions in embryonic development.

5. Materials and methods

The fibroblast growth factor 8a gene is listed in the National Center for Biotechnology Information (NCBI) under the Gene ID 30538, and in the Zebrafish Information Network (ZFIN) under the identifier ZFIN:ZDB-GENE-990415-72.

5.1. Zebrafish lines and heat-shock experiments

Zebrafish lines used in this study: Tg(hsp70l:*dnfgfr1*-eGFP) [51]; Tg (*kdrl*:Hsa.HRAS-mCherry) [52]; fgf8a^{ti282a} (*ace*) [18].

For the heat-shock experiments performed on *fa3ui*^{MO} morphants, embryos were raised at 28 °C and heat-shocked at 24 hpf at 38 °C for 5 min. For the remaining heat-shock experiments, embryos were raised at 28 °C and heat-shocked at 20 hpf at 39 °C for 5 min.

Imaging of transgenic embryos was done using Zeiss LSM 880 and Zeiss LSM 710 confocal point-scanning microscopes. Representative images are maximum intensity projections of confocal z-stacks.

5.2. Real-time quantitative PCR

Embryos were dechorionated prior to RNA extraction and microdissections were performed in Leibovitz's L-15 medium (Invitrogen) using a fine pointed scalpel and tungsten needle.

RNA extractions were done using TRIzol (Invitrogen) followed by DNAseI digestion and RNA Clean & Concentrator™-5 column purification (Zymo Reseach).

cDNA was synthetized using either the DyNAmo cDNA Synthesis Kit (Thermo) or the ProtoScript® II First Strand cDNA Synthesis Kit (NEB).

RT-qPCR reactions were performed using Power SYBR® Green PCR Master Mix (Applied Biosystems). Relative fold changes in transcript levels were determined using the standard curve method [53].

The primers used for RT-qPCR are listed in Table S2. For the fluorescent reporter experiments (Figs. 1c and 2d,g), the primers used were designed to specifically target the coding sequences of eGFP and mCherry. For the pUTR and pCDS primer sets, primer design was done as illustrated in Fig. S2a and detailed in the corresponding figure legend. For this set of primers, primer concentrations and annealing temperatures were optimized using 24 hpf and 8 ss whole embryo cDNA.

For the experiments done using wildtype whole embryo and microdissected tissue samples (Fig. S2b–d), the standard curves were done using serial dilutions of a DNA template amplified from wildtype genomic DNA with the following primers F: 5′-ATT GGC AAG AAA AAT GGT CTG GGA AAA GAC TG-3′ and R: 5′-ATC TTG GCT TTC GGC TCC TT-3′. In this set of experiments quantities were normalized to pCDS2. The results shown are relative to the whole embryo condition, except in comparisons between 8 ss whole embryo and 24 hpf whole embryo (Fig. S2d) where values are relative to the 24 hpf whole embryo condition.

For the experiments done with *fa3ui*^{MO} and *Ctr*^{MO} injected whole embryo and microdissected tissue samples (Fig. 3a,b,f,g and Fig. S3), the standard curves were done using serial dilutions of wildtype cDNA from the respective tissue sources. In this set of experiments quantities were normalized to *ef1a*, and the results shown are relative to the *Ctr*^{MO} condition.

For the fluorescent reporter experiments shown in Figs. 1c and 2d, the standard curves were done using serial dilutions of cDNA obtained from wildtype embryos injected with eGFP and mCherry mRNA. For the experiment shown in Fig. 2g, standard curves were done using serial dilutions of cDNA from the indicated control condition. In this set of experiments (Figs. 1c and 2d,g) quantities were normalized to mCherry, and the results shown are relative to the indicated control condition.

For each experimental condition, the results shown represent the mean of three biological replicates, with the exception of the results shown in Fig. 2g which represent the mean of five biological replicates per experimental condition. Each biological replicate was obtained from a pool of 20 to 70 embryos.

5.3. Fluorescent reporter assays

The 3′UTR and MM sequences were amplified from wildtype genomic DNA using the primers indicated in Table S2 and cloned into a pCS2 + eGFP vector downstream of the eGFP stop codon. Following plasmid linearization with *Not*I (NEB), *in vitro* transcription was done using the Message machine kit (Ambion).

mCherry mRNA was co-injected with mRNA from each of the eGFP reporters in a 1:1 molar ratio, into 1-cell stage zebrafish embryos. mRNAs from each reporter were microinjected at 0.3fmol/embryo for the experiments shown in Figs. 1 and 2b,c,d, and at 0.15fmol/embryo when co-injected with the *fa3ui*^{MO} or *Ctr*^{MO} (Fig. 2e,f,g), injection volume 1.4 nL/embryo. In the latter set of experiments these quantities equate to a 1:4267 molar ratio of reporter mRNA to *fa3ui*^{MO}.

Average fluorescence intensities were measured at 24 h post-injection in a circular section adjacent to the MHB. Following subtraction of background intensity, the values obtained for eGFP were normalized to those obtained for mCherry in each embryo. Means of normalized fluorescence intensities are shown for each condition, relative to the indicated controls. Image acquisition was done with a Zeiss Axiovert 200 M widefield fluorescence microscope and measurements were done using ImageJ 1.44p.

5.4. Morpholinos

The following antisense morpholino oligonucleotides were obtained from Gene Tools,

fa3ui^{MO}: 5′-ACAGGTTTTTAAATAAATATTTTCATCA-3′.

Ctr^{MO}: 5′-CCTCTTACCTCAGTTACAATTTATA-3′.

and injected at 6 ng/embryo at the one-cell stage, injection volume 1.4 nL/embryo.

5.5. Whole-mount in situ hybridization and immunohistochemistry

WISHs were done as described in [54] and Immunohistochemistry experiments were done as described in [55]. Acetylated tubulin staining

was done using a monoclonal anti-acetylated tubulin, clone 6-11B-1 primary antibody (Sigma), at 1:400 working dilution. p-ERK1/2 staining was done using Phospho-p44/42 MAPK (Erk1/2) (Thr202/Tyr204) primary antibody (Cell Signalling Technology), at 1:150 working dilution.

5.6. Statistical analysis

Statistical analysis were done using two-tailed *t*-test, for all the results shown, with the exception of the RT-qPCR results shown in Fig. 3a,b and Fig. S3 where statistical analysis was done using both two-tailed *t*-test and 2-way ANOVA.

For the RT-qPCR experiments, three biological replicates were used per experimental condition, with the exception of the experiment shown in Fig. 2g in which five biological replicates were used per experimental condition. Each biological replicate was obtained from a pool of 20 to 70 embryos.

For the remaining experiments, the number of biological replicates considered per experimental condition is indicated in the corresponding figure panel.

5.7. Ethics statement

This project was approved by the Centro Hospitalar Lisboa Norte – Centro Académico de Medicina de Lisboa (CHLN-CAML) Ethics Committee. Adult zebrafish were used only as breeders and all the experimental procedures were done in larvae with less than five days post fertilization, considered non-protected animals according to the European Council Directive 86/609/EEC updated and replaced by Directive 2010/63/EU of the European Parliament and of the Council of 22 September 2010.

All the procedures performed in zebrafish were done at the IMM fish facility, licensed by the national General Directorate authority (DGAV - Direcção Geral de Alimentação e Veterinária) complying with the Directive 2010/63/EC (transposed to the Portuguese legislation by Decreto-Lei 113/2013) and following the Federation of European Laboratory Animal Science Associations (FELASA) guidelines and recommendations concerning laboratory animal welfare, scientific use and proper education/training of all personnel performing animal work.

Availability of data and material

The data that support the findings of this study, and the materials produced in this study (i.e. DNA constructs), are available from the corresponding author upon reasonable request.

Author contributions

S.F.F. performed the experiments and analysed the data. F.P. built the mathematical model and performed its analysis. S.F.F., R.F., M.G.-C. and L.S. conceived the project and contributed to the analysis and interpretation of the data. All the authors wrote and approved the final version of the manuscript.

Transparency document

The Transparency document associated with this article can be found, in online version.

Acknowledgements

We thank Aida Barros and Lara Carvalho from the IMM Fish Facility for the technical support. We are grateful to Filipa Marques and Rita Pinto for the helpful scientific discussions and to the Bioimaging Unit of the IMM for technical assistance. We thank Filipa Dias, Noélia Custódio, and once more Lara Carvalho, for their contributions to the manuscript revision process and would like to particularly acknowledge the assistance provided by Evguenia Bekman and Pedro Prudêncio during this revision.

This research was supported by the grant PTDC/BIA-BCM/101282/2008 awarded to LS and MG-C from Fundação para a Ciência e a Tecnologia (FCT). Work in MG-C lab was supported by the grant UID/MULTI/04046/2013 given to BioISI from FCT/MCTES/PIDDAC. SFF was supported by the grant SFRH/BD/86371/2012 from FCT. RF was supported by the grant SFRH/BPD/28586/2006 from FCT. LS was supported by an IF contract from FCT. This work was developed with the support of the research infrastructure Congento, project LISBOA-01-0145-FEDER-022170 co-financed by Lisboa Regional Operational Programme (Lisboa 2020), under the Portugal 2020 Partnership Agreement, through the European Regional Development Fund (ERDF) and Fundação para a Ciência e a Tecnologia (FCT). Publication was sponsored by the LISBOA-01-0145-FEDER-007391 project co-funded by FEDER through POR Lisboa 2020 - Programa Operacional Regional de Lisboa, PORTUGAL 2020 and by Fundação para a Ciência e a Tecnologia (FCT).

The funding agency had no role in study design, data collection, data analysis, data interpretation, manuscript writing or in the decision to submit the manuscript for publication.

Conflict of interest

The authors declare that there is no conflict of interest.

Appendix A. Supplementary data

Supplementary data to this article can be found online at https://doi.org/10.1016/j.bbagrm.2018.07.012.

References

[1] B. Tian, J.L. Manley, Alternative polyadenylation of mRNA precursors, Nat. Rev. Mol. Cell Biol. 18 (2017) 18–30.
[2] W. Chen, Q. Jia, Y. Song, H. Fu, G. Wei, T. Ni, Alternative polyadenylation: methods, findings, and impacts, Genomics Proteomics Bioinformatics 15 (2017) 287–300.
[3] I. Ulitsky, A. Shkumatava, C.H. Jan, A.O. Subtelny, D. Koppstein, G.W. Bell, H. Sive, D.P. Bartel, Extensive alternative polyadenylation during zebrafish development, Genome Res. 22 (2012) 2054–2066.
[4] Y. Li, Y. Sun, Y. Fu, M. Li, G. Huang, C. Zhang, J. Liang, S. Huang, G. Shen, S. Yuan, L. Chen, S. Chen, A. Xu, Dynamic landscape of tandem 3′ UTRs during zebrafish development, Genome Res. 22 (2012) 1899–1906.
[5] Z. Ji, J.Y. Lee, Z. Pan, B. Jiang, B. Tian, Progressive lengthening of 3′ untranslated regions of mRNAs by alternative polyadenylation during mouse embryonic development, Proc. Natl. Acad. Sci. U. S. A. 106 (2009) 7028–7033.
[6] P. Miura, S. Shenker, C. Andreu-Agullo, J.O. Westholm, E.C. Lai, Widespread and extensive lengthening of 3′ UTRs in the mammalian brain, Genome Res. 23 (2013) 812–825.
[7] V. Hilgers, M.W. Perry, D. Hendrix, A. Stark, M. Levine, B. Haley, Neural-specific elongation of 3′ UTRs during Drosophila development, Proc. Natl. Acad. Sci. U. S. A. 108 (2011) 15864–15869.
[8] M.E. Pownall, H.V. Isaacs, FGF Signalling in Vertebrate Development, San Rafael, Calif., Morgan & Claypool Life Sciences, 2010 (p viii, 75 p.).
[9] J. Dubrulle, O. Pourquié, fgf8 mRNA decay establishes a gradient that couples axial elongation to patterning in the vertebrate embryo, Nature 427 (2004) 419–422.
[10] J. Dubrulle, M.J. McGrew, O. Pourquié, FGF signaling controls somite boundary position and regulates segmentation clock control of spatiotemporal Hox gene activation, Cell 106 (2001) 219–232.
[11] L. You, J. Wu, Y. Feng, Y. Fu, Y. Guo, L. Long, H. Zhang, Y. Luan, P. Tian, L. Chen, G. Huang, S. Huang, Y. Li, J. Li, C. Chen, Y. Zhang, S. Chen, A. Xu, APASdb: a database describing alternative poly(A) sites and selection of heterogeneous cleavage sites downstream of poly(A) signals, Nucleic Acids Res. 43 (2015) D59–D67.
[12] K. Griffin, R. Patient, N. Holder, Analysis of FGF function in normal and no tail zebrafish embryos reveals separate mechanisms for formation of the trunk and the tail, Development 121 (1995) 2983–2994.
[13] J. Mathieu, K. Griffin, P. Herbomel, T. Dickmeis, U. Strähle, D. Kimelman, F.M. Rosa, N. Peyriéras, Nodal and Fgf pathways interact through a positive regulatory loop and synergize to maintain mesodermal cell populations, Development 131 (2004) 629–641.
[14] H. Goto, S.C. Kimmey, R.H. Row, D.Q. Matus, B.L. Martin, FGF and canonical Wnt signaling cooperate to induce paraxial mesoderm from tailbud neuromesodermal

progenitors through regulation of a two-step epithelial to mesenchymal transition, Development 144 (2017) 1412–1424.
[15] B.W. Draper, D.W. Stock, C.B. Kimmel, Zebrafish fgf24 functions with fgf8 to promote posterior mesodermal development, Development 130 (2003) 4639–4654.
[16] R. Akiyama, M. Masuda, S. Tsuge, Y. Bessho, T. Matsui, An anterior limit of FGF/Erk signal activity marks the earliest future somite boundary in zebrafish, Development 141 (2014) 1104–1109.
[17] A. Sawada, M. Shinya, Y.J. Jiang, A. Kawakami, A. Kuroiwa, H. Takeda, Fgf/MAPK signalling is a crucial positional cue in somite boundary formation, Development 128 (2001) 4873–4880.
[18] F. Reifers, H. Böhli, E.C. Walsh, P.H. Crossley, D.Y. Stainier, M. Brand, Fgf8 is mutated in zebrafish acerebellar (ace) mutants and is required for maintenance of midbrain-hindbrain boundary development and somitogenesis, Development 125 (1998) 2381–2395.
[19] S. Vemaraju, H. Kantarci, M.S. Padanad, B.B. Riley, A spatial and temporal gradient of Fgf differentially regulates distinct stages of neural development in the zebrafish inner ear, PLoS Genet. 8 (2012) e1003068.
[20] S. Shanmugalingam, C. Houart, A. Picker, F. Reifers, R. MacDonald, A. Barth, K. Griffin, M. Brand, S.W. Wilson, Ace/Fgf8 is required for forebrain commissure formation and patterning of the telencephalon, Development 127 (2000) 2549–2561.
[21] J.R. Martinez-Morales, F. Del Bene, G. Nica, M. Hammerschmidt, P. Bovolenta, J. Wittbrodt, Differentiation of the vertebrate retina is coordinated by an FGF signaling center, Dev. Cell 8 (2005) 565–574.
[22] A. Picker, F. Cavodeassi, A. Machate, S. Bernauer, S. Hans, G. Abe, K. Kawakami, S.W. Wilson, M. Brand, Dynamic coupling of pattern formation and morphogenesis in the developing vertebrate retina, PLoS Biol. 7 (2009) e1000214.
[23] **B. Thisse, S. Pflumio, M. Fürthauer, B. Loppin, V. Heyer, A. Degrave, R. Woehl, A. Lux, T. Steffan, X.Q. Charbonnier, C. Thisse, Expression of the zebrafish genome during embryogenesis (NIH R01 RR15402), In ZFIN Direct Data Submission, 2001.** http://zfin.org.
[24] B.P. Lewis, C.B. Burge, D.P. Bartel, Conserved seed pairing, often flanked by adenosines, indicates that thousands of human genes are microRNA targets, Cell 120 (2005) 15–20.
[25] A. Grimson, K.K. Farh, W.K. Johnston, P. Garrett-Engele, L.P. Lim, D.P. Bartel, MicroRNA targeting specificity in mammals: determinants beyond seed pairing, Mol. Cell 27 (2007) 91–105.
[26] A. Kozomara, S. Griffiths-Jones, miRBase: annotating high confidence microRNAs using deep sequencing data, Nucleic Acids Res. 42 (2014) D68–D73.
[27] X. Liu, A. Homma, J. Sayadi, S. Yang, J. Ohashi, T. Takumi, Sequence features associated with the cleavage efficiency of CRISPR/Cas9 system, Sci. Rep. 6 (2016) 19675.
[28] T. Wang, J.J. Wei, D.M. Sabatini, E.S. Lander, Genetic screens in human cells using the CRISPR-Cas9 system, Science 343 (2014) 80–84.
[29] J.G. Doench, E. Hartenian, D.B. Graham, Z. Tothova, M. Hegde, I. Smith, M. Sullender, B.L. Ebert, R.J. Xavier, D.E. Root, Rational design of highly active sgRNAs for CRISPR-Cas9-mediated gene inactivation, Nat. Biotechnol. 32 (2014) 1262–1267.
[30] J.A. Gagnon, E. Valen, S.B. Thyme, P. Huang, L. Akhmetova, L. Ahkmetova, A. Pauli, T.G. Montague, S. Zimmerman, C. Richter, A.F. Schier, Efficient mutagenesis by Cas9 protein-mediated oligonucleotide insertion and large-scale assessment of single-guide RNAs, PLoS One 9 (2014) e98186.
[31] W.Y. Choi, A.J. Giraldez, A.F. Schier, Target protectors reveal dampening and balancing of Nodal agonist and antagonist by miR-430, Science 318 (2007) 271–274.
[32] A.A. Staton, H. Knaut, A.J. Giraldez, miRNA regulation of Sdf1 chemokine signaling provides genetic robustness to germ cell migration, Nat. Genet. 43 (2011) 204–211.
[33] M. Cibois, C. Gautier-Courteille, A. Vallée, L. Paillard, A strategy to analyze the phenotypic consequences of inhibiting the association of an RNA-binding protein with a specific RNA, RNA 16 (2010) 10–15.
[34] C.P. Heisenberg, C. Brennan, S.W. Wilson, Zebrafish aussicht mutant embryos exhibit widespread overexpression of ace (fgf8) and coincident defects in CNS development, Development 126 (1999) 2129–2140.
[35] R. Kaufman, O. Weiss, M. Sebbagh, R. Ravid, L. Gibbs-Bar, K. Yaniv, A. Inbal, Development and origins of zebrafish ocular vasculature, BMC Dev. Biol. 15 (2015) 18.
[36] N. Spies, C.B. Burge, D.P. Bartel, 3′ UTR-isoform choice has limited influence on the stability and translational efficiency of most mRNAs in mouse fibroblasts, Genome Res. 23 (2013) 2078–2090.
[37] P. Sanfilippo, J. Wen, E.C. Lai, Landscape and evolution of tissue-specific alternative polyadenylation across Drosophila species, Genome Biol. 18 (2017) 229.
[38] M. Mangone, A.P. Manoharan, D. Thierry-Mieg, J. Thierry-Mieg, T. Han, S.D. Mackowiak, E. Mis, C. Zegar, M.R. Gutwein, V. Khivansara, O. Attie, K. Chen, K. Salehi-Ashtiani, M. Vidal, T.T. Harkins, P. Bouffard, Y. Suzuki, S. Sugano, Y. Kohara, N. Rajewsky, F. Piano, K.C. Gunsalus, J.K. Kim, The landscape of *C. elegans* 3′UTRs, Science 329 (2010) 432–435.
[39] A. Ribeiro, J.F. Monteiro, A.C. Certal, A.M. Cristovão, L. Saúde, Foxj1a is expressed in ependymal precursors, controls central canal position and is activated in new ependymal cells during regeneration in zebrafish, Open Biol. 7 (2017).
[40] R.A. Pinto, J. Almeida-Santos, R. Lourenço, L. Saúde, Identification of Dmrt2a downstream genes during zebrafish early development using a timely controlled approach, BMC Dev. Biol. 18 (2018) 14.
[41] X. Chen, J. Liu, J.M. Janssen, M.A.F.V. Gonçalves, The chromatin structure differentially impacts high-specificity CRISPR-Cas9 nuclease strategies, Mol. Ther.–Nucleic Acids 8 (2017) 558–563.
[42] X. Wu, D.A. Scott, A.J. Kriz, A.C. Chiu, P.D. Hsu, D.B. Dadon, A.W. Cheng, A.E. Trevino, S. Konermann, S. Chen, R. Jaenisch, F. Zhang, P.A. Sharp, Genome-wide binding of the CRISPR endonuclease Cas9 in mammalian cells, Nat. Biotechnol. 32 (2014) 670–676.
[43] C. Kuscu, S. Arslan, R. Singh, J. Thorpe, M. Adli, Genome-wide analysis reveals characteristics of off-target sites bound by the Cas9 endonuclease, Nat. Biotechnol. 32 (2014) 677–683.
[44] M.R. Fabian, N. Sonenberg, W. Filipowicz, Regulation of mRNA translation and stability by microRNAs, Annu. Rev. Biochem. 79 (2010) 351–379.
[45] I. Alvarez-Garcia, E.A. Miska, MicroRNA functions in animal development and human disease, Development 132 (2005) 4653–4662.
[46] S. Sahara, Y. Kawakami, J.C. Izpisua Belmonte, D.D. O'Leary, Sp8 exhibits reciprocal induction with Fgf8 but has an opposing effect on anterior-posterior cortical area patterning, Neural Dev. 2 (2007) 10.
[47] F. De Smet, B. Tembuyser, A. Lenard, F. Claes, J. Zhang, C. Michielsen, A. Van Schepdael, J.M. Herbert, F. Bono, M. Affolter, M. Dewerchin, P. Carmeliet, Fibroblast growth factor signaling affects vascular outgrowth and is required for the maintenance of blood vessel integrity, Chem. Biol. 21 (2014) 1310–1317.
[48] B. Rousseau, F. Larrieu-Lahargue, A. Bikfalvi, S. Javerzat, Involvement of fibroblast growth factors in choroidal angiogenesis and retinal vascularization, Exp. Eye Res. 77 (2003) 147–156.
[49] O. Weiss, R. Kaufman, E. Mishani, A. Inbal, Ocular vessel patterning in zebrafish is indirectly regulated by Hedgehog signaling, Int. J. Dev. Biol. 61 (2017) 277–284.
[50] M. Presta, P. Dell'Era, S. Mitola, E. Moroni, R. Ronca, M. Rusnati, Fibroblast growth factor/fibroblast growth factor receptor system in angiogenesis, Cytokine Growth Factor Rev. 16 (2005) 159–178.
[51] Y. Lee, S. Grill, A. Sanchez, M. Murphy-Ryan, K.D. Poss, Fgf signaling instructs position-dependent growth rate during zebrafish fin regeneration, Development 132 (2005) 5173–5183.
[52] N.C. Chi, R.M. Shaw, S. De Val, G. Kang, L.Y. Jan, B.L. Black, D.Y. Stainier, Foxn4 directly regulates tbx2b expression and atrioventricular canal formation, Genes Dev. 22 (2008) 734–739.
[53] M.W. Pfaffl, A new mathematical model for relative quantification in real-time RT–PCR, Nucleic Acids Res. 29 (2001) e45.
[54] C. Thisse, B. Thisse, High-resolution in situ hybridization to whole-mount zebrafish embryos, Nat. Protoc. 3 (2008) 59–69.
[55] T. Matsui, S. Thitamadee, T. Murata, H. Kakinuma, T. Nabetani, Y. Hirabayashi, Y. Hirate, H. Okamoto, Y. Bessho, Canopy1, a positive feedback regulator of FGF signaling, controls progenitor cell clustering during Kupffer's vesicle organogenesis, Proc. Natl. Acad. Sci. U. S. A. 108 (2011) 9881–9886.

Supplemental Data

Table S1 – **Reported alt3'UTRs for the *fgf8a* gene.** Also shown are the relative abundances of each alt3'UTR reported in the indicated studies.

Alternative 3'UTRs	3'UTR length (nts)	Relative polyadenylation site usage (%) [(a)]	Relative polyadenylation site usage (%) [(b)]
altUTR-1	654	-	1.6
altUTR-2	680	14.2	0.9
altUTR-3 *(fgf8aS)*	728	12.5	18.7
altUTR-4 *(fgf8aM)*	797	65.9	74.3
altUTR-5	1242	-	3.7
altUTR-6	1667	5.4	0.8
altUTR-7	1829	2.0	-

[(a)] Pooled data obtained for the following developmental stages: 0hpf; 4hpf; 6hpf; 12hpf; 24hpf; 48hpf; 72hpf; 120hpf. Adapted from L. You, J. Wu, Y. Feng, Y. Fu, Y. Guo, L. Long, H. Zhang, Y. Luan, P. Tian, L. Chen, G. Huang, S. Huang, Y. Li, J. Li, C. Chen, Y. Zhang, S. Chen and A. Xu, APASdb: a database describing alternative poly(A) sites and selection of heterogeneous cleavage sites downstream of poly(A) signals, Nucleic Acids Res. 43, 2015, D59–D67.

[(b)] Pooled data obtained for the following samples: Embryos:1.5–2hpf; 4.5–5.5hpf; 24hpf; 72 hpf; Mixed gender adults; Adult tissues: brain, testes, and ovaries. Adapted from I. Ulitsky, A. Shkumatava, C.H. Jan, A.O. Subtelny, D. Koppstein, G.W. Bell, H. Sive and D.P. Bartel, Extensive alternative polyadenylation during zebrafish development, Genome Res. 22, 2012, 2054–2066.

Figure S1

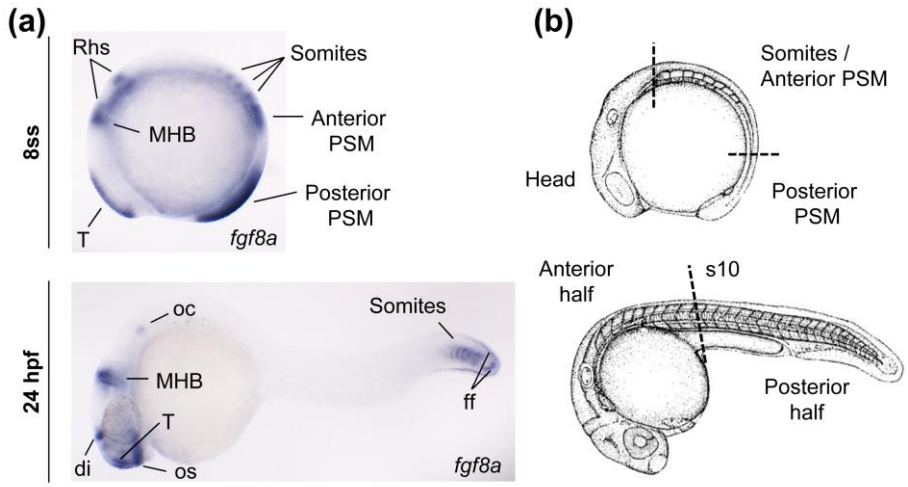

Fig. S1 – Wildtype *fgf8a* expression pattern and illustration of microdissection procedures.

(a) Representative images of the wildtype expression pattern of the zebrafish *fgf8a* gene at the 8 somite stage (8 ss) and at 24 h post fertilization (hpf). Images obtained following Whole Mount *In Situ* Hybridization (WISH) for the coding sequence of *fgf8a*. T, telencephalon; Rhs, rhombomeres 2 and 4; MHB, midbrain-hindbrain boundary; PSM, presomitic mesoderm; oc, otic capsule; os, optic stalks; di, diencephalon; ff, dorsal and caudal fin fold. **(b)** Illustration of the microdissection procedures performed on 8 ss and 24 hpf zebrafish embryos. s10, position of the 10th somite.

Figure S2

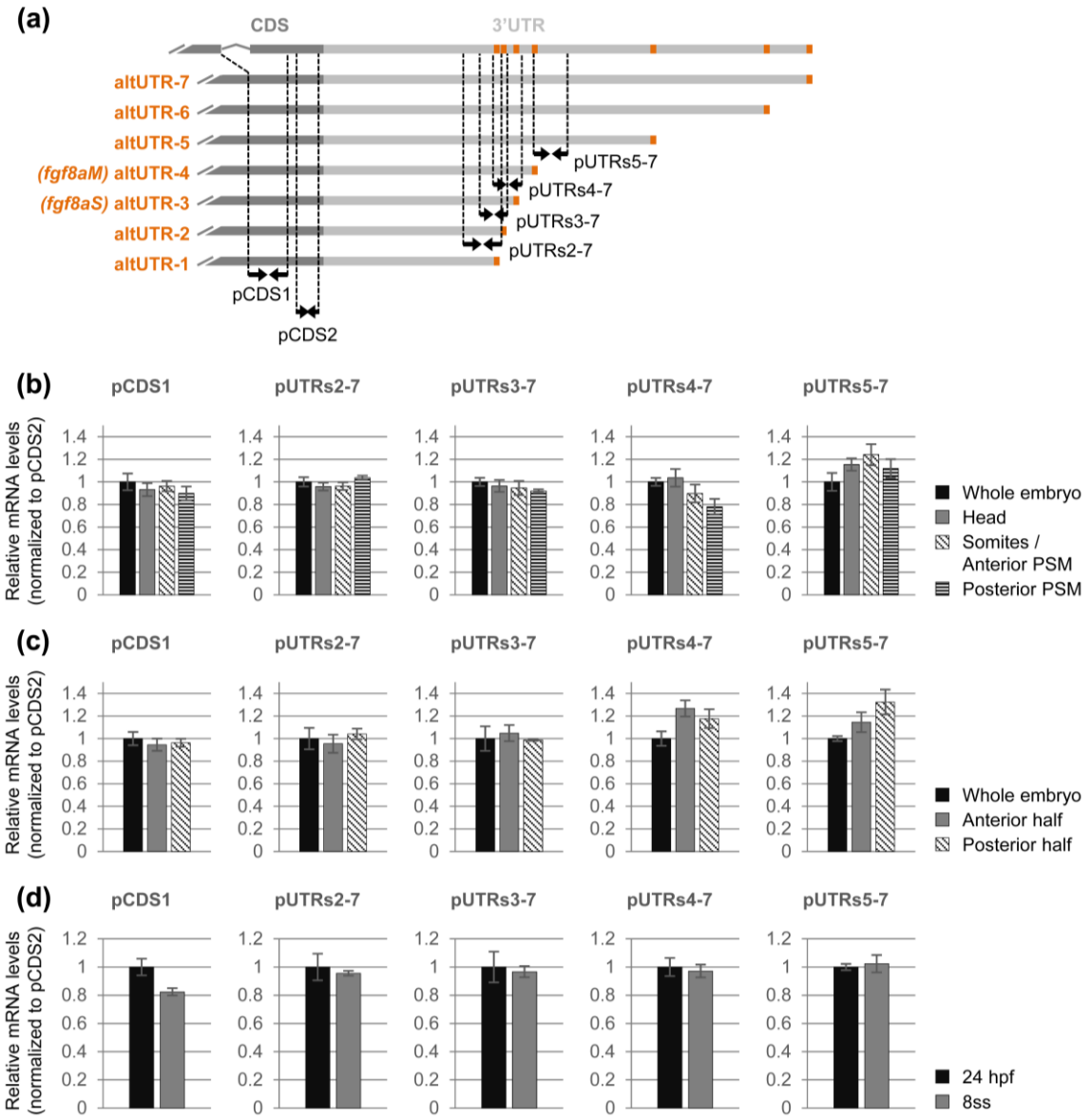

Fig. S2 – Alternative *fgf8a* 3'UTR usage in the developing embryo.

(a) Schematic representation of the alt3'UTRs previously reported for *fgf8a*. Primers used for RT-qPCR (pUTRs, pCDS). The alt3'UTRs amplified by each primer pair are indicated by the dashed lines. The pCDS1 and pCDS2 primer pairs both recognize the *fgf8a* coding sequence, with pCDS1 targeting the exon4-exon5 junction. The pUTRs2-7 primer pair recognizes all *fgf8a* transcripts, except those with the altUTR-1. The pUTRs3-7 primer pair recognizes transcripts with the *fgf8aS* UTR, the *fgf8aM* UTR and the longer alt3'UTRs-5 to 7. The pUTRs4-7 primer pair recognizes transcripts with the *fgf8aM* UTR and the longer alt3'UTRs-5 to 7. The pUTRs5-7 primer pair only recognizes transcripts with the longer alt3'UTRs-5 to 7. **(b-d)** Relative RT-qPCR quantification of the endogenous levels of *fgf8a* transcript and indicated alt3'UTRs **(b)** in 8 ss whole embryos and microdissected tissue

(Fig. S2 cont.) samples, **(c)** in 24 hpf whole embryos and microdissected tissue samples, **(d)** in 24 hpf and 8 ss whole embryos. **(b-d)** All the results shown are relative to the indicated control conditions, namely, **(b,c)** the whole embryo condition, **(d)** the 24 hpf condition. **(b-d)** Data show mean ± SEM. Statistical analysis was done using two-tailed t-test, and all comparisons were deemed not statistically significant ($p>0.05$). For an illustration of the microdissection procedures performed see Fig. S1b.

Figure S3

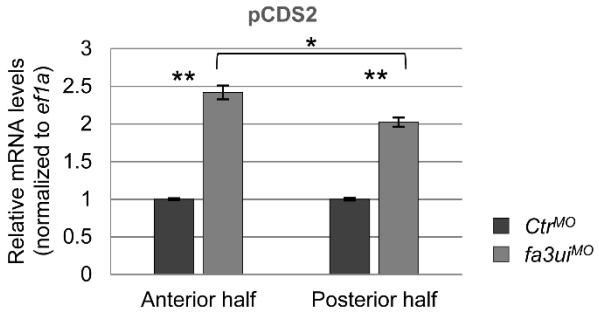

Fig. S3 - *fa3ui*^{MO} morphants display a differential increase in *fgf8a* transcript levels at 24 hpf in anterior and posterior tissues.

RT-qPCR quantification of the endogenous relative *fgf8a* transcript levels in microdissected anterior and posterior tissues of 24 hpf *Ctr*^{MO} and *fa3ui*^{MO} injected embryos. For an Illustration of the microdissection procedures performed see Fig. S1b. Statistical analysis was done using two-tailed t-test and 2-way ANOVA. Data show mean ± SEM (*p<0.05; **p<0.01).

Supplemental Text

Analysis of the reporter system

24 hours-post-injection eGFP-*fgf8aS* mRNA is approximately 1.3 times more abundant than eGFP-*fgf8aM* mRNA (Fig. 1c). As both molecular species are not produced endogenously, we can assume that they both decay exponentially (equation 1).

$$N(t) = N_0 e^{-k_d t} \quad (1)$$

Therefore, we can compute the ratio between the two quantities for a given time point (equation 2).

$$\frac{N_S}{N_M} = \frac{N_{S0}}{N_{M0}} e^{(k_M - k_S)t} \quad (2)$$

Considering equal initial quantities, we can determine the difference between degradation rate constants k_M and k_S through equation 3.

$$(k_M - k_S) = \ln\left(\frac{N_S}{N_M}\right)/t \quad (3)$$

Applying equation 3 for t=24h we get (k_M-k_S)=0.01 h^{-1}.

The absolute rate constant values vary with the baseline degradation rate constant of one of the forms. Considering that most transcripts have half-lives of between 1 and 30 hours [1], in the fastest degradation scenario k_S=0.68 h^{-1} and k_M=0.69 h^{-1} while for the more stable scenario k_S=0.02 h^{-1} and k_M=0.03 h^{-1}.

Additionally, we also observed that, 24 hours-post-injection, the ratio of protein produced by eGFP-*fgf8aS* vs eGFP-*fgf8aM* is approximately 3.4 (Fig. 1b). To explain this variation, we analysed a simple dynamical model of protein synthesis including mRNA degradation (but not synthesis, since mRNA was exogenous), protein synthesis and protein degradation (equation 4).

$$\frac{dS}{dt} = -k_S S$$

$$\frac{dM}{dt} = -k_M M$$

$$\frac{dPs}{dt} = k_{Ps} S - k_P Ps$$

$$\frac{dPm}{dt} = k_{Pm} M - k_P Pm \quad (4)$$

S represents eGFP-*fgf8aS* while M is eGFP-*fgf8aM*, the two variant transcripts that code for the proteins Ps and Pm respectively. Although it is the same protein (eGFP), each variant is expressed in a different reporter system, so two different variables are modelled. Being the same protein, both Ps and Pm have the same degradation rate constant k_P. eGFP in zebrafish has an approximate half-life of 24 hours [2], therefore we considered k_P=0.03 h^{-1}.

We simulated the model until 24 hours and computed the ratios Ps/Pm and M/S.

The initial M and S values were 1 (varying these initial values did not change the ratios). All other variables were absent in the beginning of the simulation.

We started by considering k_{Pm}=1 h^{-1} and increased k_{Ps} until Ps/Pm was around 3.4, as observed experimentally. We could reproduce the 3.4 ratio with k_{Ps}=3.15 h^{-1}. If we changed k_{Pm} and k_{Ps} maintaining their ratio (k_{Ps}/k_{Pm}=3.15), both Ps/Pm and M/S values were not affected.

Similarly, we could change k_S and k_P constants, but, if their difference was kept at 0.01 h^{-1}, both Ps/Pm and M/S ratios were constant.

Changing k_P (protein degradation constant) has a slight effect on the ratio P_S/P_M. But even considering k_P=0.7 h^{-1} (half-life of 1h) k_{Ps}/k_{Pm} would have to be 2.75 to reproduce the 3.4 ratio of Ps/Pm.

In conclusion, although we are uncertain about absolute parameter values, having k_M-k_S=0.010 h^{-1} and k_{Ps}/k_{Pm} around 3 are sufficient conditions to support the experimental observations made with the reporter system.

Model of endogenous *fgf8a* expression

Quantification of endogenous expression of different transcript variants in the presence of *fa3ui*^{MO} (Fig. 3a,b) showed that this morpholino induces a global increase in total transcript (1.4 times increase at 8 ss and 2.7 times at 24 hpf) that is not proportionately distributed among the two main transcript variants.

To enhance the understanding of this system, we developed a dynamical model of endogenous *fgf8a* expression, including the two main transcript variants and the capacity of Fgf signalling to, directly or indirectly, activate *fgf8a* transcription. This feedback element was necessary to allow the model to replicate the increase in total transcript observed in presence of the morpholino.

The model is defined as a set of ordinary differential equations (equation 5).

$$\frac{dT}{dt} = k_t + k_{tP}H(P,P_T) - k_aT \text{ where } H(P,P_T) = \begin{cases} 0 \; if \; P \leq P_T \\ 1 \; if \; P > P_T \end{cases}$$

$$\frac{dS}{dt} = k_a(1-R)T - k_SS$$

$$\frac{dM}{dt} = k_aRT - k_MM$$

$$\frac{dP}{dt} = k_{Ps}S + k_{Pm}M - k_PP \qquad (5)$$

In this model, T is a common transcript precursor, S is *fgf8aS*, M is *fgf8aM* and P is Fgf8a. k_t is a basal transcription rate constant, k_{tP} is the transcription rate constant associated with the positive feedback, and P_T is the Fgf8a concentration threshold above which this feedback is effective. k_a is the polyadenylation rate constant, while R is the fraction of transcripts that originate the M transcript after polyadenylation. Considering the system evolves to a steady state we can deduce the relation between the ratio M/S, R and $f=k_M/k_S$ (equation 6).

$$\frac{M}{S} = \frac{R}{(1-R)f} \qquad (6)$$

According to previous observations (Table S1), M/S should be between 4 and 5. According to our analysis of the reporter system, and allowing for large variations in mRNA stability, f can vary between 1.1 and 1.5. This implies that R should vary between 81 and 88%.

When the morpholino is present, we assume that R changes to a lower value R', giving rise to new steady state values of T', M', S' and P'. As we know the observed values of M'/M and of (M'+S')/(M+S), we can deduce the experimental values of M'/S'. Given our uncertainty in the M/S value (that can vary between 4 and 5), at 8 ss M'/S' is between 1.3 and 1.5, while at 24 hpf it is between 1.1 and 1.2. Using equation 6, we can predict that, at 8 ss, R' is between 58 and 69%, while at 24 hpf it is between 54 and 64%.

If there is no positive feedback (k_{tP}=0) and if k_M-k_S=0.010 h^{-1}, k_{Ps}/k_{Pm}= 3 and the previously estimated R and R' were used, the model predicts a ratio P'/P between 1.4 and 1.6, but the ratio (M'+S')/(M+S) is never higher than 1.1. Since the increase in protein levels is significant (between 40 and 60%), the hypothesis that this extra protein can lead to a positive regulation of *fgf8a* expression (positive feedback element) could explain the experimentally observed increase of total transcript in the presence of the morpholino.

Considering the positive feedback and simulating the model until it reached a steady state (keeping k_M-k_S=0.010 h^{-1}, k_{Ps}/k_{Pm}= 3, R between 81-88% and R' between 54-69%), it was possible to vary the remaining parameters and still replicate the observed M/S, (M'+S')/(M+S) and M'/M ratios. This was easily achieved by tuning the values of P_T and k_{TP}. ratios. Several successful parameter sets are presented in the Parameter Table below.

In conclusion, this analysis demonstrates that our experimental observations are well described by a simple model where the sequence targeted by the morpholino is important for polyadenylation site selection and an overactivation of Fgf signalling can, directly or indirectly, positively regulate *fgf8a* expression.

Parameter Table – Sets of parameters that make the dynamical model compatible with the experimental observations.

Parameters	**Set 1**	**Set 2**	**Set 3**	**Set 4**	**Set 5**	**Set 6**	**Set 7**	**Experimental observations**	
k_T (h^{-1})	0.50	0.50	0.50	0.50	0.50	0.50	0.50		
k_{TP} (h^{-1})	0.25	0.25	0.25	0.75	0.75	0.75	0.75		
P_T (A.U.)	10	250	40	40	250	10	10		
k_a (h^{-1})	0.50	0.50	0.50	0.50	0.50	0.50	0.50		
R (%)	85	85	85	85	85	85	85		
R' (%)	63	63	59	59	59	59	63		
k_M (h^{-1})	0.12	0.12	0.03	0.03	0.12	0.12	0.12		
k_S (h^{-1})	0.11	0.11	0.02	0.02	0.11	0.11	0.11		
k_{Pm} (h^{-1})	1.00	1.00	1.00	1.00	1.00	1.00	1.00		
k_{Ps} (h^{-1})	3.00	3.00	3.00	3.00	3.00	3.00	3.00		
k_P (h^{-1})	0.70	0.03	0.70	0.70	0.03	0.70	0.70		
Ratios								**8 ss**	**24 hpf**
M/S	5.19	5.19	3.78	3.78	5.19	5.19	5.19	4-5	
M'/S'	1.56	1.56	0.96	0.96	1.32	1.32	1.56	1.3-1.5	1.1-1.2
(M'+S')/(M/S)	1.53	1.53	1.68	2.79	2.56	2.56	2.55	1.4	2.7
M'/M	1.10	1.10	1.00	1.73	1.73	1.73	1.85	1.0	1.8

Table S2 - **Primers used for RT-qPCR and for the amplification of the alt3'UTR and MM sequences.**

RT-qPCR primers		
Target	Forward primer (5'->3')	Reverse primer (5'->3')
pCDS1	TGGCAAGAAAAATGGTCTGGGA	GCCTGGTTTTGGAGCCCTTG
pCDS2	GCCCAAGGGACACCAAATC	GGTGCGTTTAGTCCGTCTGTT
pUTRs2-7	ACACGGTTAAAGCAAACAGAGC	AGCTTTTTCCTACAGTCCATACAA
pUTRs3-7	ATTATCGCAGGTTTCCTACCG	CAAAATGCAACAAAGAACAAAAGC
pUTRs4-7	TGCATTGTATGGACTGTAGG	TATTTTACACATCCTCAAATAAAAAT
pUTRs5-7	CTTAGGATACTGATGTCTTTTGCTT	ACCCCATAGACTTTCATTGTGTTT
eGFP	GGACGACGGCAACTACAAGA	TTCAGCTCGATGCGGTTCA
mCherry	GCCGACATCCCCGACTACTT	GTAGATGAACTCGCCGTCCT
dusp6	GTTCGAGAATGCCGGGGAG	GTCCACGGGCCTCATCAATAAA
etv5b	TGGTGAGGGTTTTGGGTATGA	CCTTCGCTGATATGGAGGGC
ef1a [3]	ACGCCCTCCTGGCTTTCACCC	TGGGACGAAGGCAACACTGGC
alt3'UTR and MM amplification primers		
Amplicon	Forward primer (5'->3')	Reverse primer (5'->3')
fgf8S	TGTAATCGATAGAGTGAAGCCAGAGAAAAG	TGTTCTCGAGTCAAATAAAAATATATTTATATTTGTATAA
fgf8M	TGTAATCGATAGAGTGAAGCCAGAGAAAAG	TGTTCTCGAGATCCTAAGGTAAATTTATTACA
MM	GAGGATGTGTAAAATAATTT	TGTTCTCGAGATCCTAAGGTAAATTTATTACA

Supplemental Methods

CRISP/Cas9 and TALEN mutagenesis

We designed two CRISPR guide RNAs and one TALEN pair against the *fgf8aM* PAS. An additional TALEN pair was produced against the *fgf8aS* PAS, and lastly, two TALEN pairs were designed against the *fgf8aS and fgf8aM* polyadenylation sites which flank the MM sequence. The last two TALEN pairs were used in conjunction with the aim of excising the full MM sequence.

CRISPR guide RNA design was done as described in [4] and *pCS2nCas9n* was a gift from Wenbiao Chen (Addgene plasmid # 47929) [5]. Guide RNA and Cas9 mRNA production was done as described in [6].

TALEN design was done using the TAL Effector Nucleotide Targeter 2.0 and Paired Target Finder web tools as described in [7]. TALEN construct assembly and TALEN mRNA production was done using the golden gate approach described in [8, 9].

Microinjection procedures were done at the 1-cell stage using wildtype zebrafish embryos and an injection volume of 1.4nL/embryo. Each guide RNA was co-injected with Cas9 mRNA, and for each TALEN pair a 1:1 molar ratio of each TALEN mRNA in the pair was used. Several RNA concentrations were tested for each mutagenesis strategy.

Mutagenesis efficiencies were assessed following genomic DNA extraction and PCR amplification of the relevant genomic region. The presence of mutations was evaluated using the T7 Endonuclease I method [10] and by sanger sequencing (Stabvida). All the mutagenesis strategies carried out in this study were inefficient.

Supplemental Data References

[1] R. Milo and R. Phillips, Cell Biology by the Numbers, 2016, Garland Science; New York, NY, (p xlii, 356 pages).

[2] J.L. Thomas, M.J. Ochocinska, P.F. Hitchcock and R. Thummel, Using the Tg(nrd:egfp)/albino zebrafish line to characterize in vivo expression of neurod, PLoS One 7, 2012, e29128.

[3] A.S. Azevedo, B. Grotek, A. Jacinto, G. Weidinger and L. Saúde, The regenerative capacity of the zebrafish caudal fin is not affected by repeated amputations, PLoS One 6, 2011, e22820.

[4] J.C. Talbot and S.L. Amacher, A streamlined CRISPR pipeline to reliably generate zebrafish frameshifting alleles, Zebrafish 11, 2014, 583–585.

[5] L.E. Jao, S.R. Wente and W. Chen, Efficient multiplex biallelic zebrafish genome editing using a CRISPR nuclease system, Proc. Natl. Acad. Sci. U. S. A. 110, 2013, 13904–13909.

[6] J.A. Gagnon, E. Valen, S.B. Thyme, P. Huang, L. Akhmetova, L. Ahkmetova, A. Pauli, T.G. Montague, S. Zimmerman, C. Richter and A.F. Schier, Efficient mutagenesis by Cas9 protein-mediated oligonucleotide insertion and large-scale assessment of single-guide RNAs, PLoS One 9, 2014, e98186.

[7] E.L. Doyle, N.J. Booher, D.S. Standage, D.F. Voytas, V.P. Brendel, J.K. Vandyk and A.J. Bogdanove, TAL Effector-Nucleotide Targeter (TALE-NT) 2.0: tools for TAL effector design and target prediction, Nucleic Acids Res. 40, 2012, W117–W122.

[8] T. Cermak, E.L. Doyle, M. Christian, L. Wang, Y. Zhang, C. Schmidt, J.A. Baller, N.V. Somia, A.J. Bogdanove and D.F. Voytas, Efficient design and assembly of custom TALEN and other TAL effector-based constructs for DNA targeting, Nucleic Acids Res. 39, 2011, e82.

[9] T.J. Dahlem, K. Hoshijima, M.J. Jurynec, D. Gunther, C.G. Starker, A.S. Locke, A.M. Weis, D.F. Voytas and D.J. Grunwald, Simple methods for generating and detecting locus-specific mutations induced with TALENs in the zebrafish genome, PLoS Genet. 8, 2012, e1002861.

[10] D. Reyon, S.Q. Tsai, C. Khayter, J.A. Foden, J.D. Sander and J.K. Joung, FLASH assembly of TALENs for high-throughput genome editing, Nat. Biotechnol. 30, 2012, 460–465.